Syed Tanweer Iqbal

Systematic studies of hyperfine structure of neutral praseodymium based on a Fourier transform spectrum and laser induced fluorescence

DOCTORAL THESIS

For obtaining the academic degree of

Doktor der technischen Wissenschaften

Doctoral Programme of Technical Sciences
Technical Physics

Graz University of Technology

Supervisor:

Univ.-Prof. Dipl.-Ing. Dr.techn. Laurentius Windholz

Institute of Experimental Physics, Graz, Austria

January 2012

Deutsche Fassung:
Beschluss der Curricula-Kommission für Bachelor-, Master- und Diplomstudien vom 10.11.2008
Genehmigung des Senates am 1.12.2008

EIDESSTATTLICHE ERKLÄRUNG

Ich erkläre an Eides statt, dass ich die vorliegende Arbeit selbstständig verfasst, andere als die angegebenen Quellen/Hilfsmittel nicht benutzt, und die den benutzten Quellen wörtlich und inhaltlich entnommene Stellen als solche kenntlich gemacht habe.

Graz, am ....
(Unterschrift)

Englische Fassung:

STATUTORY DECLARATION

I declare that I have authored this thesis independently, that I have not used other than the declared sources / resources, and that I have explicitly marked all material which has been quoted either literally or by content from the used sources.

....
date (signature)

To My Parents, Sisters, Brothers, Brothers in Law
My Wife, Rakhshind
and
Kids, Duaa, Tihaam, Eshaal

Abstract

The atomic nucleus creates the central field in which the electrons are not only bound but they also move inside an atom. The interaction of magnetic moments due to spin and orbital motion of the electrons gives rise to the fine structure splitting in an atom. The interaction of the electromagnetic multipole nuclear moments with the electric and magnetic field due to spin and orbital motion of electrons causes hyperfine structure splitting of fine structure levels. The understanding of electronic levels is essentially needed for the classification of an atomic spectrum.

The measurement of a hyperfine structure of the spectral lines requires an especially high spectral resolution. This thesis is solely concerned with laser spectroscopic investigations of spectral lines of praseodymium atoms using laser induced fluorescence (LIF) detection in a hollow cathode discharge lamp. A cloud of free Pr atoms and ions is produced in a hollow cathode discharge lamp, not only in the respective ground states but also in high lying excited states, which is one of the advantages of using a hollow cathode lamp as a source of free atoms and ions. In order to investigate spectral lines in the region from 4200 to 7600 Å, various laser dyes are used such as Stilbene 3, Rhodamine 6G, Sulforhodamine (Kiton Red), DCM, and Rhodamine 700 (LD700). For pumping the dye laser a solid state, diode-pumped, frequency doubled Nd: Vanadate Nd:YVO_4 Verdi V-18 laser, or an Ar-ion or a Kr-ion laser is used. Laser induced fluorescence technique is unique in a sense that it is not only helpful in studying the hyperfine structures but also allows one to resolve situations where two or more hyperfine structures overlap. The LIF technique was used in this work to classify spectral lines, to find the hyperfine constants of the levels involved in the transitions, to resolve the blend situations found in the Fourier transform spectrum of praseodymium, and to find the missing levels of the transitions.

During the course of this study more than 125 new levels were found, unfortunately only 100 levels were confirmed via at least one second excitation. 99 out of these 100 levels are upper levels and one is a lower level. 54 new levels are odd and 46 are even parity levels. From the observed hyperfine patterns, J quantum numbers and A-values,

describing the magnetic dipole interaction for the combining levels, have been determined. By using J and A values, known levels involved in the transitions have been identified. Then energies of new levels have been determined by using excitation wave numbers. The new levels must then explain all observed fluorescence lines. The excitation wavelengths have been taken from a Fourier transform (FT) spectrum.

Using these newly discovered levels, 631 lines were classified by means of laser spectroscopy, 231 of them by laser excitation and 400 via laser-induced fluorescence. In addition, 39 lines, observed in a Fourier transform spectrum, were classified by means of their wave numbers and their hyperfine patterns. Furthermore, laser excitation of 12 already known energy levels was performed. These levels were previously not investigated by LIF techniques. 13 spectral lines were classified as a result of these investigations and also thereby ameliorating the accuracy of their hf structure constants.

Kurzfassung

Der Atomkern erzeugt das Zentralfeld, in dem die Elektronen eines Atoms gebunden sind und sich bewegen. Die Wechselwirkung zwischen den magnetischen Momenten der Bahnbewegung der Elektronen und des Spins gibt Anlaß zur Feinstrukturaufspaltung der atomaren Niveaus. Die Wechselwirkung der elektromagnetischen Multipolmomente des Kerns mit den elektrischen magnetischen Feldern aufgrund von Spin und Bahndrehimpuls führt zur Hyperfeinaufspaltung der Feinstruktur-Niveaus. Das Verständnis der elektronischen Niveaus ist unerläßlich für die Klassifizierung des atomaren Spektrums.

Die Messung der Hyperfeinstruktur der Spektrallinien benötigt eine besonders hohe spektrale Auflösung. Diese Arbeit beschäftigt sich mit laser-spektroskopischen Untersuchungen von Spektrallinien des Praseodym-Atoms unter Anwendung der Detektion laser-induzierter Fluoreszenz in einer Hohlkathoden-Entladungslampe. Eine Wolke freier Pr-Atome und -Ionen wird in einer Hohlkathoden-Entladungslampe erzeugt, wobei nicht nur die entsprechenden Grundzustände, sondern auch höhere angeregte Zustände besetzt werden, was einer der Vorteile der Hohlkathodenlampe als Quelle freier Atome und Ionen ist.

Um Spektrallinien im Bereich von 4200 bis 7600 Å zu untersuchen, wurden verschiedene Laserfarbstoffe wie Stilben 3, Rhodamin 6G, Sulforhodamin B (Kiton red), DCM und Rhodamin 700 (LD700) verwendet. Der Farbstofflaser wurde mit einem frequenzverdoppelten dioden-gepumpten Nd:Vanadat (Nd:YVO4) Verdi V 18 Festkörper-Laser, oder einem Ar- oder Kr-Ionen-Laser gepumpt. Die Methode der laser-induzierten Fluoreszenz ist sehr hilfreich beim Studium der Hyperfeinstruktur und erlaubt zusätzlich, Situationen zu untersuchen, bei denen zwei oder mehr Hyperfeinstrukturen überlappen.

Laser-induzierte Fluoreszenz wurde in dieser Arbeit benutzt, um Spektrallinien zu klassifizieren, die Hyperfeinkonstanten der beteiligten Energieniveaus zu bestimmen,

überlappende Strukturen, wie sie im Fourier-Transformations-Spektrum zu finden sind, zu trennen, und noch unbekannte am Übergang beteiligte Niveaus zu finden.

Im Rahmen dieser Studie wurden mehr als 125 neue Energieniveaus entdeckt, davon konnten leider nur 100 durch zumindest eine zweite Anregung bestätigt werden. 99 dieser Niveaus sind obere Niveaus des Übergangs, eines ist ein unteres. 54 Niveaus haben ungerade und 46 gerade Parität.

Aus der beobachteten Hyperfeinstruktur wurden die Quantenzahlen J und die A-Faktoren (zur Beschreibung der magnetischen Wechselwirkung der Atomkerne mit der Hülle) der am Übergang beteiligten Niveaus bestimmt. Aufgrund von J und A konnten bereits bekannte Niveaus als ein am Übergang beteiligtes Niveau gefunden werden. Die Energien der zweiten, neuen Niveaus wurden dann aufgrund der Anregungswellenzahl errechnet. Die neuen Niveaus müssen alle beobachteten Fluoreszenzlinien erklären. Die Anregungswellenlängen wurden dem Fourier-Spektrum entnommen.

Mit Hilfe der neu entdeckten Niveaus konnten 631 Linien klassifiziert werden, 231 durch Laseranregung und 400 als Fluoreszenzlinien. Zusätzlich wurden 39 Linien des Fourier-Spektrums aufgrund ihrer Wellenzahl und ihrer Hyperfeinstruktur klassifiziert. Weiters wurden 12 bereits bekannte Energieniveaus angeregt, die vorher nicht mit Hilfe laserinduzierter Fluoreszenz untersucht waren. Damit konnte die Genauigkeit ihrer Hyperfeinstrukturkonstanten A verbessert und 13 Spektrallinien klassifiziert werden.

Declaration

This dissertation is submitted to the Institute of Experimental Physics, Graz University of Technology, Graz, Austria, in partial fulfillment of the requirement for the degree of Doctor of Technical Sciences.

The thesis is entitled:

Systematic studies of hyperfine structure of neutral praseodymium based on a Fourier transform spectrum and laser induced fluorescence

written by Syed Tanweer Iqbal and has been approved by the Institute of Experimental Physics, Graz University of Technology, Graz, Austria.

The final copy of this thesis has been examined by the under signed authority, and find that both the content and the form meet acceptable presentation standards of scholarly work in the above mentioned discipline.

_____

Univ.-Prof. Dipl.-Ing. Dr.techn. Laurentius Windholz

Date _____

Acknowledgements

First of all I would like to thank the Almighty ALLAH for His Support and Blessings which made me able to complete this research work. I pay deep respect to the Holy Prophet Muhammad peace be upon him who is like a beacon in every aspect of life.

Without the help and support of many persons, it would be quite difficult to complete this work. I am indebted to many persons and would like to express my sincerest gratitude in the following lines.

I want to thank my supervisor Prof. Dr. Laurentius Windholz for supervising this research work. During my research I found him very knowledgeable, cooperative, polite, sincere and caring person.

I am very much thankful to the head of the institute, Prof. W. E. Ernst for giving me this opportunity to work here as a research student. I am thankful to the members of the institute and people from machine workshop for their cooperation.

I am also thankful to my colleagues, Shamim khan, Imran Siddiqui, Nadeem Akhtar, Naveed Anjum, Muhammad Faisal and Betina Gamper at Graz University of Technology for companionship and a nice working atmosphere. Special thanks to Imran Siddiqui, Nadeem Akhtar, Syed Khuram Shahzad, Zaheer uddin, Muhammad Naeem, Muhammad Janhangir and Kashif Nadeem for their discussions and supports.

In hostel, I found many caring and respecting Pakistani scholars in Graz, especially my gratitude goes to Mudassir Abbas, Zahid Abro, Rizwan Alam, Khurram Shahzad, Farhan Hayder, Farrukh Shahzad and members of C15 and D12.

Thanks also to my colleagues, Mazher Mehmood and Shahid Iqbal in Pakistan for their cooperation and support.

Finally, I would like to thank my loving and caring parents and all family members (sisters, brothers and in law relatives) for their knowledge, wisdom, support and prayers in every sense of the word. They continuously encouraged me to achieve my goals.I would especially like to mention names of my sister Sultana Naheed and my brother Syed Zeshan. Their key contributions, for providing me constant insistence, motivation and financial support, made my Ph D studies possible. This will not be complete without mentioning Rakhshinda (my wife) for her immense sacrifice and patience involved in raising our beloved kids: Duaa, Tihaam and Eshaal, alone for past many years. I would like to convey my deep sense gratitude to my wife and kids for their understanding.

Syed Tanweer Iqbal,

Graz, January 2012.

CONTENTS

1 INTRODUCTION

1.1 Preface

The interaction of the nuclear magnetic moment with the magnetic field due to spin and orbital motion of electrons causes hyperfine (hf) structure splitting of fine structure levels [1]. Due to mass ratio of electron and proton the hyperfine interaction energy is three orders of magnitude smaller than the fine structure energy, therefore the name hyperfine structure is given. The interaction is due to coupling of the total electronic angular momentum (quantum number J) of electron and the total nuclear spin (quantum number I) resulting a new total angular momentum (quantum number F) for an atom. The number of levels into which hyperfine level splits depends on number of values of F. This in turn depends on coupling of I and J. So, the fine structure level is split into $(2I+1)$ number of hyperfine structure levels for $I \leq J$. Whereas the fine structure level is split into $(2J+1)$ number of hyperfine structure levels for $J \leq I$. In 1935, anomalies in the spacing of the hf structure components of some elements led to the discovery of an electrostatic interaction due to deviation of the nuclear charge distribution from spherical symmetry which can be expressed by a quadrupole moment Q [2].

Main objective of this research is to explore a complex atom in terms of energy levels by exploiting spectroscopic techniques. There are five electrons in the outer most shell of praseodymium atom which increase the level density; therefore its spectrum is quite complicated. This complexity makes praseodymium atom to be a most suitable candidate for our investigation. Also there exist very precise hyperfine data of not only low lying levels but also for relatively high lying levels of lower configuration. So employing the LIF technique in a hollow cathode discharge we can extend the knowledge of the Pr atom. This work may be small part of the mapping of Pr I levels.

Measurements of the hf structure of praseodymium are very useful for astrophysics since Pr lines are found in the optical spectra of many chemical peculiar (CP) stars. Laboratory measurements are helpful in giving the abundance of Pr in such stars. From

the view of basic research, the study of the spectrum of Pr is helpful in further theoretical understanding of its electronic structure.

1.2 Praseodymium: An Element

Z=59

59 electrons

Ground state ($1s^2\ 2s^2\ 2p^6\ 3s^2\ 3p^6\ 3d^{10}\ 4s^2\ 4p^6\ 4d^{10}\ 5s^2\ 5p^6$) $4f^3 6s^2\ {}^4I^o_{9/2}$

Identified even configurations $4f^2 5d 6s^2$, $4f^2 5d^2 6s$, $4f^3 6s 6p$, $4f^3 5d 6p$

Identified odd configurations $4f^3 6s^2$, $4f^3 5d 6s$, $4f^2 6s^2 6p$, $4f^2 5d 6s 6p$, $4f^2 5d^2 6p$

In 1885, the Austrian chemist C F Auer von Welsbach was first scientist who discovered the chemical element Praseodymium. It was separated from a material known as didymium. The name Praseodymium is derived from the Greek words "prasios didymos″ meaning "green twin". It is a soft, silvery, malleable, ductile rare-earth element. The Rare Earth Elements are divided into the Lanthanide and Actinide series. Praseodymium is classified as an element in the Lanthanide series.

Praseodymium is primarily obtained through an ion exchange process from Monazite sand, a material rich in rare earth elements. Praseodymium has only one stable isotope $^{141}Pr_{59}$ which occurs naturally. Most of the radioisotopes of Pr have half lives either less than few minutes or less than few seconds but two of the them are relatively stable; one is ^{143}Pr with a half life of 13.57 hours and other is ^{142}Pr with a half life of about 19 hours.

The naturally occurring isotope ^{141}Pr has atomic mass of 140.907647 amu, 100% natural abundance, its nuclear spin is 5/2 and magnetic moment is 4.2754 μ_N (μ_N is known as nuclear magneton). The table 1.1 below shows some important information about naturally occurring and artificial radioactive isotopes.

Table 1.1: Some of radioisotopes of Praseodymium.

Isotope	Atomic mass (amu)	Half life	Nuclear spin (I)
^{135}Pr	134.913112	24 min	3/2
^{136}Pr	135.912692	13.1 min	2
^{137}Pr	136.91068	1.28 h	5/2
^{138}Pr	137.91075	1.45 m	1
^{139}Pr	138.90893	4.41 h	5/2
^{140}Pr	139.90907	3.39 m	1
^{142}Pr	141.910041	19.12 h	- 2
^{143}Pr	142.910813	13.57 h	7/2+
^{144}Pr	143.913301	17.28 m	0
^{145}Pr	144.91451	5.98 h	7/2
^{146}Pr	145.91764	24.15 min	-2
^{147}Pr	146.918996	13.4 min	3/2
^{148}Pr	147.922135	2.29 min	-1

Praseodymium is vulnerable to corrosion; however it is more resistant to corrosion in air than other members of the Lanthanide series. However it develops a green oxide coating due to exposure to air making it corrosion. A sample of size about one centimeter of Pr completely oxidizes in the period of one year. For this reason, praseodymium is usually stored under a light mineral oil or filled under noble gas e.g. Ar in glass.

The most important utilization of praseodymium is that it serves as alloying agent with magnesium to form high-strength metals that are used in aircraft engines. Misch metal which contains 5% of praseodymium is used to make cigarette lighters. Along with other rare earth elements, praseodymium forms the core of carbon arc lights which are used in the motion picture industry for studio lighting and projector lights. In fiber optic cables it is added as a doping agent so that it acts as a signal amplifier. Praseodymium forms a number of salts; few of them are used to give glasses and enamel a yellow color.

Particular types of welder's and glass blower's goggles are made of didymium glass where praseodymium is one of an important component.

Table 1.2: Some of the chemical and physical properties of ^{141}Pr are given here[3].

Symbol	Pr
Period	6
Atomic weight	140.90765(2)
Standard state	Solid at 298K
Ground state electronic configuration	[Xe] $4f^3 6s^2$
Color	Silvery white
Classification	Metallic
Structure	Hexagonal close packed
Melting point	931 °C
Boiling point	3320 °C
Thermal conductivity	13 W m^{-1} K^{-1}
Coefficient of linear thermal expansion	6.7 x 10^{-6} K^{-1}
Density of solid	6.67 g cm^{-3}
Electrical resistivity	70 x 10-8 Ω m
Atomic radius	267pm
1^{st} Ionization energy	5.464 ± 0.005 eV or 44070 ± 40cm^{-1}

1.3 History of investigation of fine and hyperfine structure of neutral atom (Pr I), singly ionized (Pr II) and doubly ionized (Pr III) of Praseodymium

The praseodymium was investigated by spectroscopists intensively in last century. Physicists and chemists investigated the fine and the hyperfine structure of the praseodymium atom and ions. In 1928 A S King [4] reported for the first time the investigation of hf structure of Pr. He investigated the spectra of cerium, praseodymium, neodymium and samarium as produced in the furnace at various temperature, as well as in the arc and the spark. He classified the 1018 lines for Pr I and Pr II in the region 3111 - 6828 Å. He observed that the large proportion of praseodymium spectrum was highly complex lines. H E White [5] studied the fine structure components of 173 spectral lines in Pr II in the region 3920 - 4860Å in 1929. During the investigation he discovered spin quantum number I = 5/2 to the nucleus of the praseodymium atom because he found that the fine structure components of 100 spectral lines out of 173 were completely resolved into 6 components. Rosen et al. [6] published the investigation of Zeeman Effect of Pr lines in the region 2400 - 7100 Å in 1941. They observed the most strong lines displaying hyperfine structure of the $f^3 s$ configuration and found $f^3(4I^o)\, s - {}^5I^o_4$ as the lowest term of Pr II. They also calculated g and J values for 74 Pr II levels from resolved Zeeman patterns of 141 lines. An important contribution towards establishing $4f^3 6s^2$ as the ground configuration of Pr I was done by H Lew in 1953 [7]. He determined J value and very accurate Landé factor g values for the ${}^4I^o_{9/2}$ level using the atomic beam magnetic resonance method. In 1953 P Brix [8] determined the magnetic hyperfine interaction constant $a_{6s} = 0.416 \pm 0.015$ cm^{-1} for the 6s electron in the configuration $4f^3({}^4I)\, 6s$. He also calculated the magnetic moment μ (^{141}Pr) = 3.9±0.3 nuclear magnetons) of Pr.

In 1955, J M Baker and B Bleany [9] determined the hyperfine structure constants of the level involved when investigating the hyperfine structure of Pr lines.

K Murakawa [10] in 1960 analyzed the spectrum of Pr I and classified a strong line at 4951.37 Å. Although he classified three lines of Pr I.

In 1961, B R Judd and I Lindgren [11] made a number of corrections to the simple Landé formula for the g values of levels belonging to the configuration of the type $4f^n$ by theoretical calculations using existing experimental data.

In 1962, B G Wybourne [12] investigated hyperfine structure of rare earth elements and examined the effect of intermediate coupling on the calculation of nuclear moments for them. He found that the coupling depends strongly on the interaction of the electron spin moments of 4f electrons with the nuclear magnetic moment.

In 1962, Y C Amado et al. [13] studied the hyperfine structure of the short living (19 hours) isotope (^{142}Pr) of praseodymium. They used atomic beam magnetic resonance spectroscopic method to investigate the ground state $^4I_{9/2}$. They determined the splitting factor, nuclear spin, electric quadrupole and magnetic dipole hyperfine constants, and nuclear moment and quadrupole moment for this isotope of Pr.

In 1964, N J Spector [14] studied the $4f^2$6s and $4f^2$6p electronic configurations and determined energy parameters for these configurations of Pr III.

In 1965 J Reader and J Sugar [15] studied the hyperfine structure of doubly ionized ^{141}Pr and the found nuclear moment of ^{141}Pr using Goudsmit-Fermi-Segrè formula as 4.09 ± 0.06 μ_N. They measured the magnetic hyperfine interaction constant a_{6s} = 0.63 09 ± 0.007 cm^{-1} for the 6s electron. They also studied the configurations $4f^2$ 6s and $4f^2$ 7s to calculate the quantum difference and the probability density of the 6s electron.

In 1965, R Zalubas and M Wilson [16] gave a list of 3532 lines of Pr I which were obtained in absorption in the range 1741 - 5839 Å. A Ginibre and S Gerstenkorn [17] in 1970 at Orsay began the theoretical and experimental work on the hf structure of spectrum of Pr I.

In 1973, R Zalubas and B R Borchardt [18] discovered about 60 upper even levels and three lowest levels of the odd configuration $4f^3 6s^2\ {}^4I^o$ ground term of Pr I.

J Blaise et al. [19] in 1973, and J Blaise and A Ginibre [20] in 1976 studied the effect of hf structure on Zeeman pattern and found that it resulted in lowering of the accuracy of the derived *g* values.

In 1974, J F Wyart et al. [21] presented the interpretation of the $4f^N(5d + 6s)$ in the lanthanides using the methods of Racah. They improved the energies of seven spectra and found the new energy levels for Pr II and Pr III.

In 1975, W F Meggers et al. [22] published a list of 1460 lines of Pr I and Pr II in the region 2558 - 8715 Å.

All available data on Pr energy levels were summarized in 1978 by W C Martin et al. [23].

In 1981, A Ginibre [24] and W J Childs and L S Goodman identified a number of atomic levels via their hyperfine structure constants, the technique used by both groups was different. Ginibre's work was based on Fourier transform spectroscopy, whereas W J Childs and L S Goodman [25] work was based on a technique of laser-rf double-resonance. Childs and Goodman also classified many lines in the region $5746 < \lambda < 6148$ Å.

In 1982, R M Macfarlane et al. [26] studied the nuclear magnetic moment of ^{141}Pr. He determined the new value for nuclear magnetic moment μ_{nucl} (^{141}Pr) = 4.2754(5) μ_N which is two orders magnitude better than previous.

In 1985, K T Cheng and W J Childs [27] investigated the quadrupole moment values in neutral rare-earth atoms and found the quadrupole moment value of ^{141}Pr Q = -0.066b (1 barn = 10^{-24} cm^{-2}).

In 1988, M N Reddy and G N Rao [28] studied atomic and ionic spectra of Pr using optogalvanic spectroscopy. They identified about 78 atomic transitions of Pr I and 43 transitions of Pr II in the spectral range 5760 - 6250 Å and also used the laser

optogalvanic spectroscopy to record the hyperfine structure of the 5779.28 Å, 5821.36 Å and 605513 Å transitions in Pr I.

In 1988 - 89, A Ginibre [29-30] published two papers. In first paper she studied the fine and hyperfine structure of singly ionized Pr by Fourier transforms spectroscopy. Based on her high resolution data in the range 2783 - 27920 cm^{-1}, she found new energy levels of the odd configuration $4f^{2}5d6p$ and of the mixed even configurations $4f^{2}5d^{2}+ 4f^{2}5d\,6s + 4f^{3}6p$. She also found the energy, J value and hyperfine structure splitting for these levels. In second paper she presented a parametric interpretation of the fine and hyperfine structure of the even levels of Pr II on the basis of the 3 mixed even configurations $4f^{2}5d^{2}+4f^{2}5d6s+ 4f^{3}6p$.

In 1990, H Iimura et al. [31] studied the hyperfine structure of Pr ion (Pr II) by means of collinear laser ion beam spectroscopy. They measured the magnetic dipole and electric quadrupole constants for the levels involved in their investigation.

In 1991, M K Kim and R Kachru [32] studied the hyperfine structure of doubly ionized Pr using stimulated-photon-echo modulation.

In 1994, H Iimura et al. [33] measured the magnetic moment and electric quadrupole moment of a Pr isotope (^{143}Pr) by means of laser ion beam spectroscopy.

In 1996, T Kuwamoto et al. [34] studied the hf structure of 34 Pr I transitions with high resolution by laser-atomic beam fluorescence spectroscopy in the region 5440 - 5960 Å. They measured the electric quadrupole and magnetic dipole hyperfine constants for 57 levels. They also found 18 new transitions and determined the energies and electronic total angular momenta for 11 levels.

In 1997, A Krzykowski et al. [35] studied the configuration $4f^{3}5d6s$ of the Pr I via the laser induced fluorescence **(**LIF) method on an atomic beam. They measured the values of the hyperfine structure constants of the lower levels related to this configuration.

In 1998, M Song et al. [36] measured the fourteen new lifetimes of Pr I low lying states using thermal atomic beam with single-step pulsed laser excitation.

In 2000, Li Maosheng et al. [37] published two papers. In first paper they studied the atomic spectra of singly ionized Pr and neodymium by means of collinear laser ion beam spectroscopy. They investigated the hyperfine structure of 19 atomic transitions in the wavelength range 5600 - 5900 Å and also measured hyperfine interaction constant for 28 levels. In second paper they measured the hyperfine structure in the lines 5787.7 Å and 5870.4 Å of Pr II via collinear laser ion beam spectroscopy and also determine the magnetic dipole constant and the electric quadrupole constant of the involved levels.

In 2001, S Ivarsson et al. [38] observed the spectra of Pr I and Pr II via Fourier transform spectroscopy in the region 2800 - 8000 Å. They ameliorated the wavelengths for 49 lines, analyzed the hyperfine structure patters for 44 lines and determined the magnetic dipole constants for 8 odd and 18 even levels in Pr II. They also measured the accurate wavelengths for 15 strong transitions in Pr III and discussed the solar abundance of praseodymium.

In 2001, B Furmann et al. [39] studied the hyperfine structure of Pr II using the method of laser induced fluorescence in a hollow cathode discharge and discovered three new low-lying levels in Pr II.

In 2002, Ma Hong-Liang [40] investigated the hyperfine structure of single ionized lanthanum and praseodymium by means of collinear fast ion beam laser spectroscopy. They improved the accuracy of the magnetic dipole constants by one order of magnitude compared with published data.

In 2002, R C Rivest et al. [41] measured the hyperfine structure of 36 transitions in Pr II in tge region 4200 - 4600 Å using collinear fast ion beam laser spectroscopy.

In 2002, M W Glenn [42] investigated the lanthanide elements in stellar and laboratory spectra. He used the synthetic spectrum program SYNTHE and model atmospheres generated by the program ATLAS9 to analyze the effective temperature dependence for strong lines Pr I λ = 5227.967 Å, Pr II λ = 5220.108 Å and Pr III λ = 5299.969 Å.

In 2003, Ruczkowski et al. [43] made a parametric study of the hyperfine structure of even configuration system $4f^2 5d\ 6s^2 + 4f^2\ 5d^2\ 6s + 4f^3 6s6p + 4f^2 5d^3$ of Pr I. They used the known level energies to adapt calculated ones using wavefunctions in intermediate coupling. After this procedure they used the best wavefunctions for a calculation of the hyperfine interaction constants A and B, which could be compared with the measured constants.

In 2005, B Furmann et al. [44] discovered 42 new levels in Pr II by using LIF technique and also determine the magnetic dipole constant and the electric quadrupole constant for all levels.

In 2006, B Furmann et al.[45] presented fifty seven new levels of odd parity in neutral praseodymium by using LIF technique.

The group of G H Guthöhrlein [46] in Hamburg has been involving in studies of the hf structure of the Pr I since 1996 and L Windholz et al. [47] have been studying hyperfine structure of Praseodymium using laser induced fluorescence spectroscopy since 2005.

In 2010, S Oppel et al. [48] published the achievement for the active frequency stabilization of a diode laser using several neutral praseodymium lines between 11050 and 11230Å for eliminating the frequency drift of the unlocked laser more than 30 MHz/h and laser stabilized to within 1.4(1) MHz for a average times > 0.2 s.

In 2011, B Gamper et al. [49] presented the recording of new highly resolved Fourier transform spectrum of the Pr I and Pr II. FT spectrum covered greater wavelength range from 2380 - 12500 Å. They discovered twenty three new atomic energy levels of odd parity and one of even parity. They also classified 1194 lines as transition between energy levels of the Pr I and 19 lines as transition of the Pr II.

2 ATOMIC STRUCTURE

Spectroscopy is an important branch of Physics. It is direct consequence of a classic experiment of Newton in which he allowed sunlight to pass through a glass prism and observed a regular series of colors onto a screen. These series of colors he called a spectrum. The light emitted or absorbed by matter (atoms or molecule) is usually termed as spectrum when analyzed via its frequency or wavelength. After the discovery of the dark absorption lines of the sun's spectrum and sharp emission lines in spectra of sparks, flames and arcs, the physicists of the 19 century regarded spectroscopy as a most important tool for qualitative chemical analysis. From middle of 19 century to the beginning of 20 century simple spectroscopic observation demonstrated that hydrogen does not emit light of a continuous distribution of wavelengths but of only discrete values, known as spectral lines. Experimentally observed hydrogen wavelengths were 3970 Å, 4102 Å, 4341 Å, 4861 Å and 6563 Å. The atomic spectra of all elements could be studied and one important point was noted that atoms emitted light at discrete wavelengths which were characteristic for each atom. It was generally accepted that the atomic spectra could play an important role in the understanding of the structure of atom and that of electrons which were considered somehow responsible for producing the emitted light. Nobody had an ideal to relate them precisely at that time. In 1911 Ernest Rutherford performed the historical experiment of scattering of alpha particles with a thin gold foil. He interpreted this classic experiment that the positively charge of the atom was densely concentrated at the center of the atom surrounded by electrons and it was responsible for most of the mass of atom. His brilliant interpretation led him to the discovery of atomic nucleus. He led the foundation of atomic and nuclear physics. But he could not explain the discrete wavelengths of hydrogen atom (atomic spectra of any element) and the stability of an atom. This problem is resolved by Niels Bohr in 1913. He began a new era in spectroscopy and atomic physics by relating line spectra to the quantum ideas recently proposed by M Planck's quantization concept and A Einstein's photon concept. He adopted the theory of Rutherford and made some assumption that electrons in an atom can exist in stable states of constant energy

(without radiating) and only change energy by undergoing a transition from one stable state to another stable state. Electron in an atom either emits or absorbs an amount of energy which is exactly equal to the energy difference between two states when it moves from one state to another. The electron in a permitted orbit must have an angular momentum which is an integral multiple of ħ (ħ = h/2π). Bohr not only explained the spectrum of hydrogen atom and ionized helium but also calculated the Rydberg constant. Bohr's theory did not justify stationary state and explain the spectral lines of the complex atoms. But perhaps more important was the unsatisfying nature of the Bohr's theory which used classical mechanics along with quantization of the angular momentum to explain the spectrum of the hydrogen atom. Scientists initiated to search for a more universal theory to describe matter. Finally Physicists succeeded to develop the Quantum mechanics. It is the most unified theory of atomic physics which we owe to de Broglie, Heisenberg, Schrödinger, Dirac and others. It explained all problems related to Bohr's theory.

2.1 Schrödinger's equation for Hydrogen atom and Hydrogen-like ions

Hydrogen atom consists of one electron and nucleus (one proton) and hydrogen like ions (He^{+}, Li^{++}, Be^{+++}, etc.) consist of one electron and nucleus (more than one proton). In hydrogen atom and hydrogen like ions one electron (charge = -*e*) moves around the nucleus of charge '+*Ze*' at a distance 'r' in a Coulomb field and its potential energy is given by

$$V(r) = -\frac{Ze^2}{4\pi\varepsilon_o r} \qquad \textit{Equation 2.1}$$

In order to explain more precisely the spectrum of the hydrogen atom and hydrogen like ions than Bohr atomic theory, one needs to apply the time independent Schrödinger equation. This equation is given by

$$\hat{H}\Psi = E\Psi$$ *Equation 2.2*

where E is a definite energy value (eigenvalue) of the stationary state

Ψ is the wavefunction which is solution of this equation. $\hat{H}$ is the Hamiltonian operator of the system and it can be written as

$$\hat{H} = -\frac{h^2\nabla^2}{2m} + V(r)$$ *Equation 2.3*

m = reduced mass

$$m = \frac{m_e M}{m_e + M}$$

m_e = mass of an electron

M = mass of nucleus

where ∇^2 is Laplace operator

$-\frac{h^2\nabla^2}{2m}$ is the kinetic energy operator and it is in polar coordinates

$$-\frac{h^2\nabla^2}{2m} = -\frac{h^2}{2m}\frac{1}{r^2}\frac{\partial}{\partial r}\left(r^2\frac{\partial}{\partial r}\right) + \frac{1}{2mr^2}\hat{l}^2$$ *Equation 2.4*

with $\hat{l}^2$ is square of the angular momentum operator

$$\hat{l}^2 = -\hbar^2\left[\frac{1}{\sin\theta}\frac{\partial}{\partial\theta}\left(\sin\theta\frac{\partial}{\partial\theta}\right) + \frac{1}{\sin^2\theta}\frac{\partial^2}{\partial\phi^2}\right]$$ *Equation 2.5*

From equation (2.1) it is clear that potential energy depends only on the magnitude of position vector. Therefore it is possible to separate angular and radial functions in a wavefunction, so

$$\Psi(r,\theta,\phi) = R(r)F_{lm}(\theta,\phi)$$ *Equation 2.6*

Now putting the value of equation (2.6), and equation (2.3) in equation (2.2), we get

$$\left[-\frac{\hbar^2\nabla^2}{2m}+V(r)\right]R(r)F_{lm}(\theta,\phi)=ER(r)F_{lm}(\theta,\phi) \qquad \textit{Equation 2.7}$$

Now putting equation (2.4) in equation (2.7), we have

$$F_{lm}(\theta,\phi)\left[-\frac{\hbar^2}{2m}\frac{1}{r^2}\frac{\partial}{\partial r}\left(r^2\frac{\partial}{\partial r}\right)+V(r)\right]R(r)+\frac{R(r)}{2mr^2}\hat{l}^2F_{lm}(\theta,\phi)=ER(r)F_{lm}(\theta,\phi)$$

Equation 2.8

The wavefunction of stationary states are eigenfunctions of operators $\hat{l}^2$ and $\hat{l}_z$ and must satisfy the following equations

$$\hat{l}^2F(\theta,\phi)=\hbar^2l(l+1)F(\theta,\phi) \qquad \textit{Equation 2.9}$$

$$\hat{l}_zF(\theta,\phi)=\hbar m_lF(\theta,\phi) \qquad \textit{Equation 2.10}$$

From the eigenvalues of the square of the angular momentum $\hat{l}^2$ are $\hbar^2l(l+1)$, so the magnitude of angular momentum may take only the values

$$L=\left|\vec{L}^2\right|=\sqrt{l(l+1)}\hbar \qquad (l=0,\ 1,\ 2,\ 3,\ldots\ldots) \qquad \textit{Equation 2.11}$$

where l is known as orbital quantum number

From the eigenvalues of the z-component of the angular momentum $\hat{l}_z$ are $m_l\hbar$ that is z-component of the angular momentum can only take the values

$$L_z=m_l\hbar, \qquad (m_l=0,\ \pm1,\ \pm2,\ \pm3,\ \ldots\ldots\ \pm l.) \qquad \textit{Equation 2.12}$$

m_l is known as magnetic quantum number

Now putting the value of equation 2.9 in equation 2.8 and we obtain an equation for radial part *R(r)* alone

$$\left[-\frac{\hbar^2}{2m}\frac{1}{r^2}\frac{\partial}{\partial r}\left(r^2\frac{\partial}{\partial r}\right)+V(r)+\frac{\hbar^2 l(l+1)}{2mr^2}\right]R(r)=ER(r) \qquad \textit{Equation 2.13}$$

Since an electron is bound in an atom, therefore energy must be negative ($E < 0$) and only at certain discrete negative values of energy are possible for solutions of equation (2.13), so

$$E_n=-\frac{mZ^2e^4}{2\hbar^2(4\pi\varepsilon_o)^2}\frac{1}{n^2} \qquad \textit{Equation 2.14}$$

where n is integer and is known as principle quantum number (third quantum number). It is related with l as $n \geq l+1.$

In an atom, electron in any state is characterized by n, l, m_l. For each value of l, there are $2l+1$ values of m_l ($m_l = l, l-1, \quad 0, \quad , -l$).

From equation (2.14) it is clear that the energy of electron in hydrogen atom and hydrogen like ions in the state (n, l *and* m_l) is independent of l and m_l but it depends upon n only. For n >1 each energy level E_n contains some different wavefunctions, so these levels are called degenerate. Due to Coulomb potential this degeneracy problem is exist in the hydrogen atom. This l degeneracy is removed by including relativistic effects and spin orbit interaction.

For l values states are characterized as

l = 0 1 2 3 4

s p d f g

2.2 Spin orbit interaction

Here the dipole moment $\vec{\mu}_s$ is due to the electron's intrinsic spin and magnetic field B_l due to orbital motion of electron. The orientation energy of a intrinsic magnetic dipole moment $\vec{\mu}_s$ in a magnetic field B_l is given by

$$E_{l,s} = -\vec{\mu}_s \cdot \vec{B}_l$$ *Equation 2.15*

We know that

$$\vec{\mu}_s = -\frac{g_s e}{2m_e}\vec{s}$$

$$\vec{\mu}_s = -\frac{2e}{2m_e}\vec{s}$$ *Equation 2.16*

where $\vec{s}$ is spin angular momentum of an electron.

The relative motion of the nucleus and electron produce the magnetic field and it is given by

$$\vec{B}_l = \frac{Ze\mu_o}{8\pi r^3 m_e}\vec{l}$$ *Equation 2.17*

where $\vec{l}$ is orbital angular momentum of an electron

therefore equation (2.15) becomes

$$E_{l,s} = \frac{Ze^2\mu_o}{8\pi m_e{}^2 r^3}\left(\vec{s}\cdot\vec{l}\right)$$ *Equation 2.18*

$$E_{l,s} = \frac{a}{\hbar^2}\left(\vec{l}\cdot\vec{s}\right)$$ *Equation 2.19*

where

$$\frac{Ze^2\mu_o\hbar^2}{8\pi r^3 m_e} = a$$ *Equation 2.20*

where constant ‘a’ which is called as the spin orbit coupling constant

We have

$$\left(\vec{l}+\vec{s}\right)\cdot\left(\vec{l}+\vec{s}\right) = \vec{j}\cdot\vec{j}$$

$$\vec{l}\cdot\vec{l}+\vec{s}\cdot\vec{s}+2\vec{l}\cdot\vec{s}=\left|\vec{j}\right|^2$$

$$\left|\vec{l}\right|^2+\left|\vec{s}\right|^2+2\vec{l}\cdot\vec{s}=\left|\vec{j}\right|^2$$

$$\vec{l}\cdot\vec{s}=\frac{\left[\left|\vec{j}\right|^2-\left|\vec{l}\right|^2-\left|\vec{s}\right|^2\right]}{2} \qquad \textit{Equation 2.21}$$

Therefore equation (2.19) becomes

$$E_{l,s}=\frac{a}{2\hbar^2}\left[\left|\vec{j}\right|^2-\left|\vec{l}\right|^2-\left|\vec{s}\right|^2\right]$$

$$=\frac{a}{2\hbar^2}\left[\hbar^2 j(j+1)-\hbar^2 l(l+1)-\hbar^2 s(s+1)\right]$$

$$E_{l,s}=\frac{a}{2}\left[j(j+1)-l(l+1)-s(s+1)\right] \qquad \textit{Equation 2.22}$$

where *j* is total angular momentum quantum number and *s* is spin quantum number of electron

Equation (2.22) represents spin orbit coupling energy in terms of quantum numbers *j*, *l*, *s* and constant 'a' for hydrogen atom and hydrogen like ions (one electron system).

2.3 Fine Structure in the Hydrogen atom and Hydrogen-like ions

We used non-relativistic Schrödinger equation to solve the problem of the hydrogen atom and hydrogen like ions. This treatment we obtained one important result such as the energy states E_n. Here we want to include both relativistic effects and spin orbit interaction. Both corrections provide the energies smaller than E_n. But both corrections which are related with electron mass velocity dependence and with electron spin have same order of magnitude. In addition to E_n total correction to the energy is given by

$$E_{n,l,j}=E_n+E_{rel}+E_{l,s} \qquad \textit{Equation 2.23}$$

where

E_{rel} is the energy due to relativistic correction (relativistic mass change)

$E_{l,s}$ is the energy due to spin orbit interaction correction

$$E_{rel} + E_{l,s} = E_{FS} \qquad \textit{Equation 2.24}$$

where E_{FS} is the fine structure energy

The complete calculation for fine structure energy E_{FS} was done by Dirac and result of this calculation is given by

$$E_{FS} = -\frac{E_n \alpha^2}{n}\left(\frac{1}{j+\frac{1}{2}} - \frac{3}{4n}\right) \qquad \textit{Equation 2.25}$$

where α is known as Sommerfeld fine structure constant and its mathematical expression is given by

$$\alpha = \frac{e^2}{4\pi\varepsilon_o \hbar c}$$

It is one of the fundamental dimensionless constants of physics. In case of defining the scale of the splitting for fine structure, then α is called fine-structure constant.

$$\alpha^2 = \left(\frac{1}{137}\right)^2 \qquad \textit{Equation 2.26}$$

From equation (2.17) it is clear that E_{FS} of hydrogen atom and hydrogen like ions is independent of *l* but depends upon *n* and *j*.

2.4 Lamb Shift

Lamb and Retherford performed the experiment in 1947 and they discovered that even the relativistic Dirac theory was not complete theory in describing the hydrogen atom.

They observed 0.03 cm^{-1}energy difference between same *j* terms $2^2S_{1/2}$ and $2^2P_{1/2}$. This small difference in energy (as compare to fine structure splitting) is called Lamb shift. Quantum electrodynamics (QED) explains this discrepancy between Dirac theory and experiment in such a way that the quantum mechanical zero-point fluctuations (vacuum fluctuations) of the electromagnetic field act statistically on the electrons and thus cause a shift of their potential energy.

2.5 Many Electron Systems

It is very difficult to obtain the exact solution of Schrödinger's equation for an atom containing more than one electron. The Hamiltonian of an N electrons system is approximately given by

$$H = \sum\left[-\frac{\hbar^2}{2m}\nabla^2 i - \frac{Ze^2}{4\pi\varepsilon_o r_i}\right] + \sum_{i<j}\frac{e^2}{4\pi\varepsilon_o r_{ij}} + \sum_i \xi_i(r_i)\vec{l}_i \cdot \vec{s}_i \qquad \textit{Equation 2.27}$$

Where r_i is the position of the electron *i* with respect to nucleus. r_{ij} is the distance between the electrons *i* and *j*. First term within the bracket represents the single particle Hamiltonian; second term in summation repulsive interaction, $+Ze^2/4\pi\varepsilon_o r_{ij}$, between each pairs of electrons and last term in summation is spin orbit interaction. Here it is assumed that nucleus creates the electric field which depends upon only '*r*' and this field is called central field approximation. Every electron moves in this central field independently of the other electrons. The electrostatic repulsion between the electrons must be taken into account. This repulsion causes non central field i.e. it becomes non-symmetrical interaction. For multi-electron atom Schrödinger equation is more complicated than in case of hydrogen atom where radial and angular part can be treated separately. So it is very difficult to solve Schrödinger equation for multi-electron atom and to calculate the exact eigenfunctions and energy eigenvalues. In this situation some approximations methods are used, e.g. Hartree-Fock method so on, to get approximation solution for Schrödinger equation for many electrons system.

2.6 Angular Momentum Coupling

In one-electron system, orbital angular momentum $\vec{l}$ and spin angular momentum $\vec{s}$ couple to give a resultant angular momentum $\vec{j}$ of an electron. The angular momenta are coupled by means of magnetic and electric interactions between the electrons in the atom. There are two types of angular momentum coupling.

2.6.1 LS Coupling (Russell-Saunders Coupling)

Total orbital angular momentum $\vec{L}$ is vector sum of the individual orbital angular momentum of electrons. Total spin $\vec{S}$ is vector sum of the individual spins of electrons. It is because the mutual interactions of the orbital or spin angular momenta of different electrons are much greater than the interactions between the orbital and spin angular momenta of the individual electrons. Therefore total angular momentum $\vec{J}$ is resultant of $\vec{L}$ and $\vec{S}$ and it is known as Russell-Saunders Coupling. It is given by

$$\vec{J} = \vec{L} + \vec{S} \qquad \textit{Equation 2.28}$$

$$\left|\vec{J}\right| = \sqrt{j(j+1)}\hbar \qquad \textit{Equation 2.29}$$

where *J* is quantum number can take the following values

$$J = |L+S|,.....|L-S| \qquad \textit{Equation 2.30}$$

For $L \geq S$, so number of possible values of *J* is (2*S*+1). It can be said that the term splits into (2*S*+1) different components. (2*S*+1) is called the multiplicity of the term. In case of $L \leq S$, so the number of components is equal to (2*L*+1).

Similar to the one electron system, the spin-orbit interaction energy for many electrons is given by

$$E_{LS} = \frac{1}{2}A[J(J+1) - L(L+1) - S(S+1)] \qquad \textit{Equation 2.31}$$

where A is constant.

2.6.2 *jj* Coupling

The spin-orbit coupling for each electron depends upon nuclear charge *Z* and it increases rapidly with increasing Z. So *jj* coupling takes place only in heavy atoms. In *jj* coupling the mutual interactions of the orbital or spin angular momenta of different electrons are much smaller than the interactions between the orbital and spin angular momenta of the individual electrons.

Suppose that an atom contains N electrons, and then according to the *jj* coupling, angular momenta of individual electrons are given by

$$\vec{j}_1 = \vec{l}_1 + \vec{s}_1, \vec{j}_2 = \vec{l}_2 + \vec{s}_2, \ldots\ldots\ldots\ldots.., \vec{j}_N = \vec{l}_N + \vec{s}_N$$

Total angular momentum $\vec{J}$ of the atom is

$$\vec{J} = \sum \vec{j}_i \qquad \textit{Equation 2.32}$$

2.7 Electron Configuration

There two basic rules for determining the structure of atoms containing N electrons:

I. Total energy of N electrons system should be minimum.
II. Pauli Exclusion Principle i.e. No two electrons can have all same quantum numbers (n, l, m_l and m_s).

If electrons having the same principle quantum number *n* occupy the same atomic shell i.e.

Principle quantum number *n* =1 2 3 4…….

Atomic shells K L M N…..……..

The energy of electron in any atomic shell depends upon *n* and *l*. An electron having small *l* is more likely to be found near the nucleus and the result is a lower total energy for electron. Therefore electrons are distributed in each shell accordingly increase in energy with increasing *l*. Each sub-shell is characterized by *n* followed by letter corresponding to its *l*. A superscript after the letter shows the number of electron in that

sub-shell. Let us give an example of the electron configuration of sodium i.e.$1s^2\ 2s^2\ 2p^6\ 3s^1$ (ground state configuration). For 1*s* ($n = 1$, $l = 0$), sub-shell contain two electrons and for 2*p* ($n = 2$, $l = 1$), sub-shell contain six electrons. According to the Pauli Exclusion Principle, the maximum number of electrons in each sub-shell is $2(2l + 1)$. $2n^2$ gives the maximum number of electrons in each shell. One of the excited configurations of sodium is given by $1s^2\ 2s^2\ 2p^6\ 3p$. When highly excited states begin to overlap each other, then such situation is term as configuration mixing or configuration interaction. Since parity is good quantum number, thus configuration interaction takes place only within configurations of same parity.

3 HYPERFINE STRUCTURE

The nucleus as being composed of protons and neutrons is much heavier than an electron. The comparison of weight of nuclei with that of electron allows us to consider in good approximation the nuclei to be point charges of infinite mass. The most important interaction between a nucleus of charge *Ze* and an electron in an atom is the Coulomb interaction. All other interactions between the nucleus and the electrons of the atom are classified as HYPERFINE EFFECTS. These effects were first observed by A Michelson in 1891, C Fabry and A Perot in 1897, and O Lummer and E Gehrcke in 1903.

The hyperfine effects fall into two main categories,

I. Slight shifting of energy levels (Isotope effect): The isotope effect is related to the shift the energy levels but no splitting. There are two main features for isotope shifts in atom which are mass effect and field or volume effect. There are two types of mass effect, normal and specific mass effect. The normal mass effect arises due to movement of the nucleus which is not considered to be infinitely heavy. The interactions between the different outer electrons contribute the specific mass effect. The distribution of a nuclear charge over a finite volume also shifts of the energy levels; it is called field effect. Electrons in a low-lying ‘s’ states are most sensitive to volume effect.

II. Splitting of electronic energy states (Hyperfine structure): Hyperfine structure is the splitting of electronic levels. The hyperfine structure effect results from the fact that nucleus may possess electromagnetic multipole moments.

3.1 The nuclear moments

In hyperfine interaction, the splitting of the energy levels of the atoms ranges from 10^{-3} to 1 cm^{-1}, the properties of nucleus which differs from its charge play the role to explain this splitting. Each nucleon possesses an intrinsic spin 1/2 and it is regarded that up to some extent each nucleon also involves in orbital motion of the nucleus. Pauli

[1] was first physicist who suggested the existence of spins and magnetic moments of the nucleus. Nuclear angular momentum I is known as nuclear spin which is the resultant of spins and angular momenta of the nucleons. The nuclear spin quantum number I may be integer or half integer. I-values of the stable atomic nuclei are between 0 and 15/2. There are a large number of nuclei with I = 0 because nuclei have even number of nucleons and atoms of these nuclei do not exhibit the hyperfine structure.

The nucleus possesses electromagnetic multipole moments; these multipole moments can interact with the electromagnetic field produced at the nucleus by the electron/electrons. There is a restriction on the number of possible multipole (2^p poles); the only non-vanishing nuclear multipole moments are the magnetic moments for the odd p and electric moments for even p where p > 0. A nucleus spin quantum number I cannot have a multipole moment of order 2p where p > 2I. The most important of these moments are the magnetic dipole moment (p = 1) and electric quadrupole moment (p = 2).

3.2 Hyperfine interaction

The hyperfine interaction results from the interaction of motions of electron and nucleons. The nucleus possesses multipole moments, these moments may be magnetic or electric, and hence the nucleus has electric as well as magnetic moments. These moments when interact with the electronic motion give rise to two types of interactions

I. Magnetic dipole interaction
II. Electric quadrupole interaction

3.2.1 Magnetic Dipole Hyperfine Structure

The nucleus has spin that leads to the nuclear magnetic moment; this nuclear magnetic moment interacts with the magnetic field $\overrightarrow{B_J}$ produced by the orbital motion and the spin of the electrons. This magnetic interaction between the nucleus and the moving

electron of the atom gives rise to magnetic dipole hyperfine structure effect; it depends upon the orientation of the nuclear spin.

Atomic nuclei acquire a mechanical angular momentum $\vec{I}$ and magnitude of nuclear angular momentum is given by

$$\left|\vec{I}\right| = \sqrt{I(I+1)}\hbar \qquad \textit{Equation 3.1}$$

where $\left|\vec{I}\right|$ = magnitude of nuclear angular momentum

I = the nuclear spin quantum number

The z-component of nuclear angular momentum is given by

$$(I)_z = m_I\hbar \text{ with } m_I = I, I\text{-}1, \ldots\ldots\ldots\text{-}I \qquad \textit{Equation 3.2}$$

A nuclear magnetic moment $\overrightarrow{\mu_I}$ is associated with nuclear angular momentum i.e.

$$\overrightarrow{\mu_I} = \gamma\vec{I} \qquad \textit{Equation 3.3}$$

where γ is the nuclear gyromagnetic ratio

The nuclear magnetic moment can be written as

$$\overrightarrow{\mu_I} = \frac{g_I\mu_N}{\hbar}\vec{I} \qquad \textit{Equation 3.4}$$

Where μ_N is nuclear magneton and it is unit of nuclear magnetic moment and it is related with Bohr magneton $\mu_B = \frac{e\hbar}{2m_e} = 9.27x10^{-24}\frac{Joules}{Tesla}$ as

$$\mu_N = \frac{\mu_B}{1836} = 5.05082X10^{-27}\frac{Joules}{Tesla} \qquad \textit{Equation 3.5}$$

The dimensionless number $g_I = \frac{\gamma\hbar}{\mu_N}$ is known as nuclear g factor.

The component of the nuclear magnetic moment in z direction is given by

$$(\mu_I)_Z = \gamma(I)_z = \gamma m_I \hbar$$

$$= g_I \mu_N m_I \qquad \textit{Equation 3.6}$$

The maximum observable value of nuclear magnetic moment is

$$\mu_I = (\mu_I)_z \text{ max} = g_I \mu_N I \text{ (since max. value of } m_I = I\text{)} \qquad \textit{Equation 3.7}$$

Therefore $\overrightarrow{\mu_I}$ in the direction of $\vec{I}$ can be written as

$$\overrightarrow{\mu_I} = \frac{\mu_I \vec{I}}{I\hbar} \qquad \textit{Equation 3.8}$$

The time average magnetic field due to orbital motion and the spin of the electrons in the direction of $\vec{J}$ at the position of nucleus is given by

$$\left\langle \vec{B}_J \right\rangle = \frac{\langle B_J \rangle \vec{J}}{J\hbar} \qquad \textit{Equation 3.9}$$

The magnetic energy E_{μ_I} due to hyperfine interaction is

$$E_{\mu_I} = -\overrightarrow{\mu_I} \cdot \left\langle \overrightarrow{B_J} \right\rangle$$

$$= -\mu_I \langle B_J \rangle \frac{\vec{I} \cdot \vec{J}}{IJ\hbar^2}$$

$$= -g_I \mu_N I \langle B_J \rangle \frac{\vec{I} \cdot \vec{J}}{IJ\hbar^2}$$

$$= -\frac{g_I \mu_B \langle B_J \rangle \vec{I} \cdot \vec{J}}{1836 J\hbar^2} \qquad \textit{Equation 3.10}$$

This magnetic interaction is a coupling of the total angular momenta of the electron $\vec{J}$ and the nucleus $\vec{I}$ to a total angular momentum of the atom $\vec{F}$ i.e.

$$\vec{F} = \vec{I} + \vec{J}$$ *Equation 3.11*

$$\vec{F} \cdot \vec{F} = F^2 = \left(\vec{I} + \vec{J}\right) \cdot \left(\vec{I} + \vec{J}\right)$$ *Equation 3.12*

$$F^2 = I^2 + J^2 + 2\vec{I} \cdot \vec{J}$$

$$\vec{I} \cdot \vec{J} = \left(\frac{F^2 - I^2 - J^2}{2} \right)$$ *Equation 3.13*

E_{μ_I} can be written as

$$E_{\mu_I} = -\frac{g_I \mu_B \langle B_J \rangle \left(F^2 - I^2 - J^2\right)}{2 \times 1836 J \hbar^2}$$ *Equation 3.14*

$$= -\frac{g_I \mu_B \langle B_J \rangle \left[F(F+1)\hbar^2 - I(I+1)\hbar^2 - J(J+1)\hbar^2\right]}{2 \times 1836 J \hbar^2}$$

$$= -\frac{g_I \mu_B \langle B_J \rangle \left[F(F+1) - I(I+1) - J(J+1)\right]}{2 \times 1836 J}$$

$$E_{\mu_I} = \frac{A\left[F(F+1) - I(I+1) - J(J+1)\right]}{2} = \frac{AC}{2}$$ *Equation 3.15*

where

$$A = -\frac{g_I \mu_B \langle B_J \rangle}{1836 J}$$ *Equation 3.16*

A is known as as magnetic dipole hyperfine constant. Physically it determines the spitting of hyperfine levels.

$$C = F(F+1) - I(I+1) - J(J+1)$$ *Equation 3.17*

3.2.1.1 Interval Rule and Properties for Magnetic Dipole Hyperfine Structure

I. The Landé interval rule for fine structure also holds for the magnetic hyperfine structure. The separation between two consecutive levels is proportional to the larger of the F values i.e.

$$\Delta E_{\mu_I} = E_{\mu_I}(F+1) - E_{\mu_I}(F)$$

$$= \frac{A}{2}[(F+1)(F+1+1) - F(F+1)]$$

$$\Delta E_{\mu_I} = A(F+1) \qquad \textit{Equation 3.18}$$

II. The number of levels into which hyperfine level splits depends on number of values of F. This in turn depends on coupling of I & J. So, the fine structure level is split into (2I+1) number of hyperfine structure levels for $I \leq J$ whereas the fine structure level is split into (2J+1) number of hyperfine structure levels for $J \leq I$.

III. The values of F will be in this range $|I - j| \leq F \leq I + J$

IV. If $E(F) > E(F-1)$ the splitting is called normal splitting, if $E(F) < E(F-1)$ the splitting is called inverted splitting. Both depend on sign of magnetic dipole interaction constant "A". In case of normal splitting, gI is positive and A is also positive. While in the case of inverted splitting, gI is negative and A is also negative.

V. The total width of splitting between levels $|I-J|$ and $|I+J|$ is

$$\Delta W = \begin{cases} AI(2J+1) \, for J \geq I \\ AJ(2I+1) \, for J \leq I \end{cases} \qquad \textit{Equation 3.19}$$

VI. For unpaired's' electrons, total width of splitting is largest.

VII. The electric dipole selection rule for F is, $\Delta F = 0, \pm 1$ but transition between $F = 0 \; to \; F = 0$ is forbidden.

VIII. The hyperfine levels are (2F+1) fold degenerate and independent of quantum number m_F. The degeneracy can be removed by the application of external magnetic field which is called the Zeeman Effect in hyperfine structure.

3.2.2 Electric Quadrupole Hyperfine Structure

In 1935 Schüler and Schmidt [2] found that the optical spectra of the isotopes of Europium (Eu) do not follow the interval rule and cannot be explained by magnetic hyperfine structure but by the existence of electrical quadrupole moments in nuclei. For all nuclei with spin $I \geq 1$, the electric potential of a homogeneously charged is no longer spherically symmetry but similar to ellipsoid of rotation i.e. electrical quadrupole moments. The Electric quadrupole moment is an important property of the nucleus; it is a measure of deviation of charge distribution in the nucleus from spherical symmetry and is denoted by Q. The quadrupole moment Q = 0 indicates that the charge distribution is spherically symmetric. By convention, the value of Q is taken to be positive if the ellipsoid is prolate and negative if it is oblate. If the nuclear charge distribution is elongated along the direction of *I*, a configuration is called prolate and Q > 0. For flattened nuclei a configuration is called oblate and Q < 0.

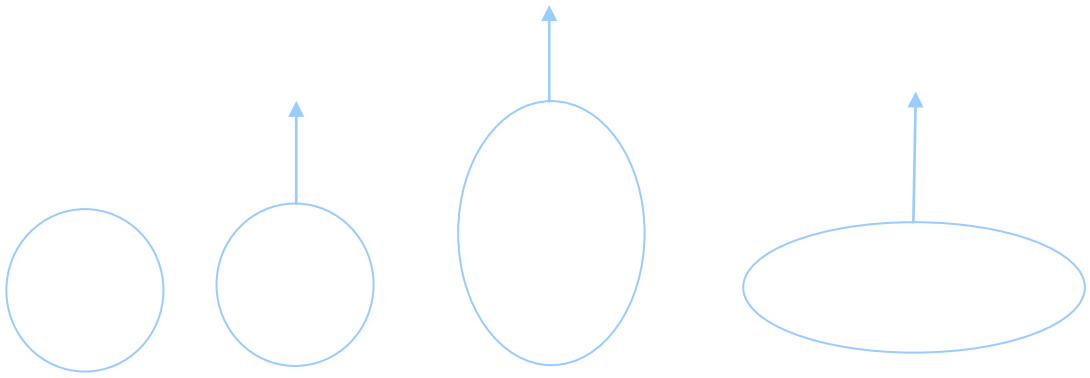

Figure 3.1:The charge distribution of nuclei for different nuclear spin.

The interaction energy between the electric quadrupole moment of the nucleus and the electrostatic potential V created by an electron at the nucleus is known as quadrupole interaction and energy shift due to electric quadrupole interaction is

$$E_Q = \frac{B}{4}\left[\frac{\frac{3}{2}C(C+1) - 2I(I+1)J(J+1)}{IJ(2J-1)(2I-1)}\right] \qquad \textit{Equation 3.20}$$

where

$$C = F(F+1) - I(I+1) - J(J+1)$$

$$B = eQ\left[\frac{\partial^2 V}{\partial Z^2}\right]$$

V = the electrostatic potential created by all electron at the nucleus

Q = electric quadrupole moment of the nucleus

B = is called the quadrupole coupling constant or electric quadrupole hyperfine constant

(i) The term $\frac{\partial^2 V}{\partial Z^2} = 0$ for's' electron. Therefore for's' terms the electric hyperfine constant B is zero.

(ii) B is zero for I < 1 and for J = 1/2.

(iii) B is zero for atoms having even number of protons and even number of neutrons.

The total energy of the hyperfine structure level with quantum number *F* can be determined by adding the two magnetic dipole and electric quadrupole interaction i.e.

$$\Delta E = E_{\mu_I} + E_Q$$

$$\Delta E = \frac{hAC}{2} + \frac{hB}{4}\left[\frac{\frac{3}{2}C(C+1) - 2I(I+1)J(J+1)}{IJ(2J-1)(2I-1)}\right] \qquad \textit{Equation 3.21}$$

By inspection of above equation we note that the quadrupole interaction and magnetic dipole interaction have different dependence on F and hence quadrupole interaction is responsible for the violation of interval rule, especially when electric quadrupole hyperfine constant B is comparable in magnitude with magnetic dipole hyperfine constant A.

3.3 Experimental Determination of Hyperfine Constants

The equation (3.21) can be interpreted as the hyperfine interaction includes magnetic dipole interaction and electric quadrupole interactions, both of these interactions modify the energy levels, the magnetic hyperfine interaction gives rise to splitting of hyperfine levels and quadrupole interaction gives rise to shifting of hyperfine level. So equation (3.21) can also be written as

$$\Delta E = \alpha hA + \beta hB$$ *Equation 3.22*

where α and β are called Casimir factors and are functions of F and J for a given atom of nuclear angular momentum I, and are given by the following equations

$$\alpha = \frac{1}{2}[F(F+1) - I(I+1) - J(J+1)] = \frac{C}{2}$$ *Equation 3.23*

$$\beta = \frac{\frac{3}{2}[C(C+1) - 2I(I+1)J(J+1)]}{4IJ(2J-1)(2I-1)}$$ *Equation 3.24*

I. The selection rules $\Delta F = 0, \pm 1$ and $\Delta J = 0, \pm 1$ for electrical dipole transition between two different fine structure levels containing hyperfine splitting energy ΔE.

II. The transition between two hyperfine levels each having F = 0 is forbidden.

III. The electrical dipole transition can only take place between combining fine structure levels of opposite parity.

IV. Each allowed transition represents a component of hyperfine structure pattern of a spectral line. Each component position can be determined by the following relation

$$\nu = \nu_C + \alpha_o(F_o, J_o, I)A_o + \beta_o(F_o, J_o, I)B_o - \alpha_u(F_u, J_u, I)A_u - \beta_u(F_u, J_u, I)B_u$$

Equation 3.25

where ν_C is the center of gravity of the frequency which corresponds to the energy difference between fine structure levels.

The letter 'o' and 'u' are denoted for upper and lower levels respectively. The constants Ao, Bo, Au and Bu are hyperfine interaction constants of upper and lower levels respectively. They have unique value for a level. The level can be identified by its hyperfine constants, they are characteristic of the levels.

From above equation it is clear that it contains Ao, Bo, Au and Bu as unknown quantities excluding the ν_C. In order to experimental determination of hf constants from recorded hyperfine pattern, it is as essential to identify the quantum numbers of at least

5 hf components and to measure their (absolute or relative) positions. Using above equation, first of all we make 5 linear equations and solve them. In this way one can identify more than 5 components, a least square method has to be used to fit the experimental recorded hf structure.

3.4 The Line Intensity

Electromagnetic interaction between atomic nucleus and electrons can be written in term of the matrix element of the scalar product of two tensor operators i.e.

$$H_{hfs} = \sum_{p\geq 1} < JIF \left| T^{(p)} . U^{(p)} \right| JIF >$$

Where both T(p) and U(p) are irreducible tensor operators, former gives the effect of the electron and later gives the effect of nucleus. By using above equation, the relative intensities of the individual hyperfine components for electric dipole transition are given by

$$I\left(F_o \rightarrow F_u\right) = \frac{\left(2F_o+1\right)\left(2F_u+1\right)}{2I+1} \begin{Bmatrix} J_o & F_o & I \\ F_u & J_u & I \end{Bmatrix}^2 \qquad \textit{Equation 3.26}$$

where J_o and J_u are total electronic angular momentum involved in the transition and I is nuclear spin.

The term in the curly bracket is a 6j symbol. This equation is valid for cases where interactions between neighboring levels are weak, so that J_o and J_u are good quantum numbers. If I is smaller than the other the 4 quantum numbers in the 6j symbol, then strongest components of hyperfine structure multiplet are those for $\Delta F = \Delta J$, such components are called diagonal components. The line intensity or strength of diagonal lines increases with increasing F. The components for which $\Delta F \neq \Delta J$ are called off-diagonal components, these are the weaker components. Physical significance of $\Delta F = \Delta J$ is that since the nuclear spin interacts very weakly to the total angular momenta electrons, therefore it does not influence the total electromagnetic radiation of the atom with a given J. However by forcing J into a particular orientation with regard

to F it changes the statistical weight of the level and causes a certain distribution of radiation over the hyperfine structure components [50].

4 LASER SPECTROSCOPY

4.1 Line Broadening Mechanisms

Study of broadening of spectral lines is very important especially in the investigation of hyperfine structure because sometimes the smaller hyperfine spitting and large Doppler width of the spectral lines cause very difficult accurate spectroscopic measurements. It is impossible to observe the spectral lines absorbed and emitted by an atom or molecule strictly monochromatic because of some physical processes are responsible for broadening the spectral line. Even with the help of high resolving power instruments one observes a spectral distribution of the emitted or absorbed intensity around the center frequency corresponding to a transition between the combining levels. The finite life time of the excited state, random motions of atoms, and collisions mainly contribute to the line broadening. Line broadening can be homogeneous or inhomogeneous.

Homogeneous line broadening

If all atoms which are in a particular level E_i in a sample (for example collimated ionic beam), have an equal probability of absorption or emission of radiation with frequency v causing a transition $E_i \rightarrow E_f$, then the broadening is called homogeneous broadening. The homogeneous broadening leads to Lorentzian profile of emitting frequencies. Natural broadening is an example of homogeneous broadening.

Inhomogeneous line broadening

If all atoms in a sample (discharge) have not an equal probability of absorption or emission of radiation, then this leads to inhomogeneous broadening. In such sample there are different velocity groups and each velocity group has a certain Doppler shift from resonance frequency hence broaden the line. This line broadening is called inhomogeneous line broadening. The inhomogeneous broadening leads to Gaussian profile of emitting frequencies. The Doppler broadenings is an example of inhomogeneous broadening.

Accurate measurement of intensity and wavelength requires knowledge of the profiles of the spectral lines and the distribution of intensity about the center frequency ν_o. The spectral distribution function I(ν) of absorbed or emitted radiation in the vicinity of ν_o is called the line profile. The figure 4.1 gives the line profile of a transition around the central frequency ν_o. The importance of any line broadening is measured by its full width at half maximum (FWHM) and is called line width or half width of spectral line.

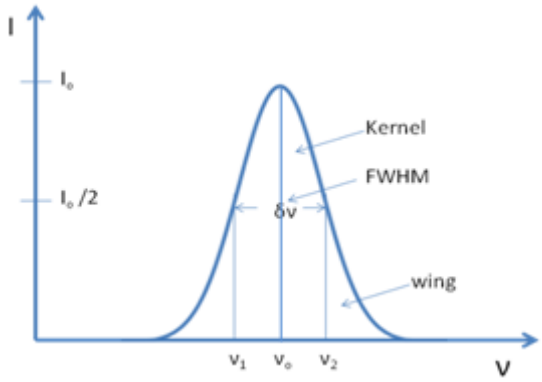

Figure 4.1: The line profile of a transition about the central frequency ν_o.
The region within half width is called kernel and outside region is called wing.

4.1.1 Natural Broadening

All atoms have naturally finite lifetime of an excited state, this finite life time of the state leads to the broadening of the line, which is known as natural broadening. This natural broadening is associated with the characteristic decay time of the radiating levels. The width caused by this mechanism is determined using Heisenberg uncertainty principle

$$\Delta E \cdot \Delta t \approx \hbar = \frac{h}{2\pi} \qquad \textit{Equation 4.1}$$

The population of the excited state at any time is given by

$$n_i(t) = n_i(0)e^{\frac{t}{\tau}} \qquad \textit{Equation 4.2}$$

Where 'n_i (t)' is number of atoms in excited state 'i' at time 't' second, 'n_i (0)' is number of atoms in excited state at 't' = 0 and 'τ' is called mean natural life time of the

state and it depends on the transition rate (transition probability) for spontaneous emission. The life time 'τ_i' in the excited state '*i*' is given by

$$\tau_i = \sum_j \frac{1}{A_{ij}} \qquad \textit{Equation 4.3}$$

where 'A_{ij}' is the transition rate for spontaneous emission from state with energy E_i to state E_j.

The levels cannot be narrowed to zero; this is the requirement of uncertainty principle. The spread in energy is given by

$$\Delta E = \frac{\hbar}{\Delta t} = \frac{\hbar}{\tau_i} \qquad \textit{Equation 4.4}$$

where 'Δt' is the uncertainty in time associated with finding the atom in that particular state and it is equal to mean life time 'τ_i' of the state. The frequency of the decay from state with energy 'E_i' to the stable ground state with energy 'E_j' is given by $\omega_{ij} = \frac{E_i - E_j}{\hbar} = \frac{\Delta E}{\hbar}$. The corresponding uncertainty in energy of level 'E_i' is given by

$$\Delta E_i = \hbar \Delta \omega_i = \frac{\hbar}{\tau_i} \qquad \textit{Equation 4.5}$$

This gives uncertainty in frequency of the excited state

$$\Delta \omega_i = \frac{1}{\tau_i} \qquad \textit{Equation 4.6}$$

It is just the reciprocal of mean life time of that state. In some cases the life time of high lying excited state is shorter than the low lying states. The life time of the ground state is infinitely long, so $\Delta\omega_i$ is negligible for ground and metastable states.

If the terminating state 'E_j'is not the ground state but also an excited state with a life time 'τ_j', then uncertainties in 'E_i' and 'E_j' of the two levels both contribute to the line width. In this case the total uncertainty in energy is given by

$$\Delta E = \Delta E_i + \Delta E_j \qquad \textit{Equation 4.7}$$

and

$$\Delta\omega = \frac{1}{\tau_i} + \frac{1}{\tau_j} \qquad \textit{Equation 4.8}$$

The life time of excited states is of the order 10^{-6} to 10^{-9} sec. Therefore natural line width of 0.1 to 100 MHz is observed for transitions which take place from such state to the ground state. The transition rate is proportional to the cube of frequency, hence for infrared and microwave regions the natural line width is much smaller. The line profile function of a spectral line broadened by the natural broadening is given by

$$I(\nu) = \frac{\frac{1}{4\pi\tau}}{(\nu - \nu_o)^2 + (\frac{1}{4\pi\tau})^2} \qquad \textit{Equation 4.9}$$

ν_o is the central frequency corresponding to the peak intensity, the line profile shown above in figure 4.1 is Lorentzian profile or Lorentzian line shape function.

4.1.2 Doppler Broadening

In sample (for example vapor cell or discharge) atoms or molecules are in random motion, this random motion of molecules or atoms produce a net broadening of spectral lines. Such broadening of line is known as Doppler broadening. The Doppler broadening profile is a Gaussian profile.

The Doppler shift is not the same for all atoms because of random directions and magnitudes of motions of atoms. The atoms moving at non relativistic speed will emit the light of frequency

$$\nu = \left(1 + \frac{\upsilon_x}{\upsilon}\right)\nu_o \quad \text{(Atoms moving towards the spectrometer)} \qquad \textit{Equation 4.10}$$

$$\nu = \left(1 - \frac{\upsilon_x}{\upsilon}\right)\nu_o$$ *Equation 4.11*

(Atoms moving away from the spectrometer)

where υ_x is the component of velocity of atoms along the direction of laser, and ν_o is the resonant frequency. This Doppler Effect can be significant for gaseous state. Suppose that atoms are in thermal equilibrium at temperature T kelvin, then Doppler width '$\Delta\nu_D$' of the spectral line is given by

$$\Delta\nu_D = \left(7.1\text{X}10^{-7}\right)\nu_o\sqrt{\frac{T}{M}} \quad \text{(in Hz)}$$ *Equation 4.12*

where M is mass number of the element.

I. $\Delta\nu_D \propto \nu_o$, so Doppler width $\Delta\nu_D$ decreases with decreasing in central frequency ν_o. Doppler width $\Delta\nu_D$ is smaller for a red spectral line and $\Delta\nu_D$ is large for ultraviolet region.

II. $\Delta\nu_D \propto \sqrt{T}$, so Doppler width $\Delta\nu_D$ decreases with decreasing the square root of the temperature. For example in our experiment a hollow cathode discharge is cooled with liquid Nitrogen for investigation of the hyperfine structure of praseodymium.

III. $\Delta\nu_o \propto \frac{1}{\sqrt{M}}$, so Doppler width $\Delta\nu_D$ decreases with increasing the atomic or molecular mass number.

It is possible to reduce Doppler width $\Delta\nu_D$ by one to two orders of magnitude by using atomic and ion beam experiments, where a well collimated atomic or ionic beam interact perpendicular to the laser beam (this topic will be discussed in article 4.4.2.3).

4.1.3 Collisional Broadening

For high density of atoms, an atom in an excited state transfers its excitation to other atoms by nonradiative processes such as collisions with other atoms. These collisions

induce a decay of the excited state before spontaneous emission. The life time of the excited atom is therefore shortened and the line is broadened. By increasing pressure the collisions take place at faster rate and this type of broadening is known as collisional broadening or pressure broadening.

The collisional broadening can be divided into two types

I. Lorentz broadening: This occurs when collision takes place between different kinds of atoms.
II. Holtsmark broadening: This occurs when collision takes place between same kinds of atoms.

Due to long range Coulomb interaction between charged particles the collisional broadening takes place prominently in plasma (gas discharges). Collisional broadening is basically the result of elastics and inelastic collision between atoms and ions. The intensity of fluorescence remains constant in the elastic collisions but during the collision frequency shift occurs and correspondingly it changes the phase of oscillator. Where as intensity of fluorescence reduces during the inelastic collisions.

The collisional broadening is homogeneous type of broadening so it produces a Lorentzian profile same as natural broadening but it has relatively larger width as compared to natural broadening.

The pressure broadening can be avoided by keeping the pressure in the spectral source as low as possible. The information about the collisional broadening occurring in the gas can be obtained by changing the pressure and observing the corresponding change in line width. Observable line broadening and shifting in the center line can be obtained by using the large collisional impact parameters.

4.1.4 Stark Broadening

The degeneracy in the atomic and molecular levels can also be removed by external electric field. The level splits into a number of components depending upon the total angular momentum; this splitting in external electric field is called Stark effect. The line broadening also takes place due to strong electric field experienced by atoms

during collisions between ions and electrons in plasma (gas discharge). Such broadening of line is called Stark broadening.

4.1.5 Saturation Broadening

The noticeable change in population densities of the excited and lower levels can be obtained by applying an intense field of laser light operating at transition frequency of the combining levels. This interaction with a strong radiation field may result in an increase in the line width due to the saturation of population densities. This additional broadening due to the saturation effect is known as Saturation Broadening or power broadening.

Saturation broadening for homogeneously and inhomogenously broadened lines have different spectral line profiles. For example a homogeneously broadened spectral line is Lorentzian line profile and inhomogenously broadened spectral line is Gaussian line shape.

4.2 Combined Line Profile

In an experiment, for example the laser induced fluorescence investigation of atoms and ion, different broadening mechanisms cannot be studied separately. However, it is possible to reduce the effects of particular line broadening, for example:

I. reduced pressure: diminishes the pressure broadening
II. reduced temperature: diminishes the Doppler broadening, and
III. weakening the intensity of the laser light: diminishes the saturation broadening.

It is not possible to isolate a spectral line from all broadenings.

The total contribution of all types of broadenings can be represented by the single line profile which is the convolution of all type of line broadening profiles i.e.

$$I(\nu) = I_N(\nu) \cdot I_D(\nu) \cdot I_P(\nu) \cdot I_S(\nu) \qquad \textit{Equation 4.13}$$

Where

$I(\nu)$ = Total line broadening

$I_N(\nu)$= Natural broadening

$I_D(\nu)$= Doppler broadening

$I_P(\nu)$= Pressure broadening

$I_S(\nu)$ = Saturation broadening

4.3 Voigt Profile:

Since all these broadenings are not same, some are homogeneous and some are inhomogeneous, so the total line profile $I(\nu)$ is neither Lorentzian nor Gaussian because collisional broadening and natural broadening together give a Lorentzian line profile, while Doppler line broadening gives a Gaussian line profile. The resulting line profile is a convolution of Lorentzian and Gaussian functions, and is known as a Voigt profile. Figure 4.2 shows that the Voigt profile is the sum of individual groups of Lorentzian profiles over a Doppler distribution of velocities. So

$$I_\nu(\nu) = I_G(\nu) \cdot I_L(\nu) \qquad \textit{Equation 4.14}$$

where

$I_V(\nu)$ = Voigt profile

$I_G(\nu)$ = Gaussian profile

and

$I_L(\nu)$ = Lorentzian profile

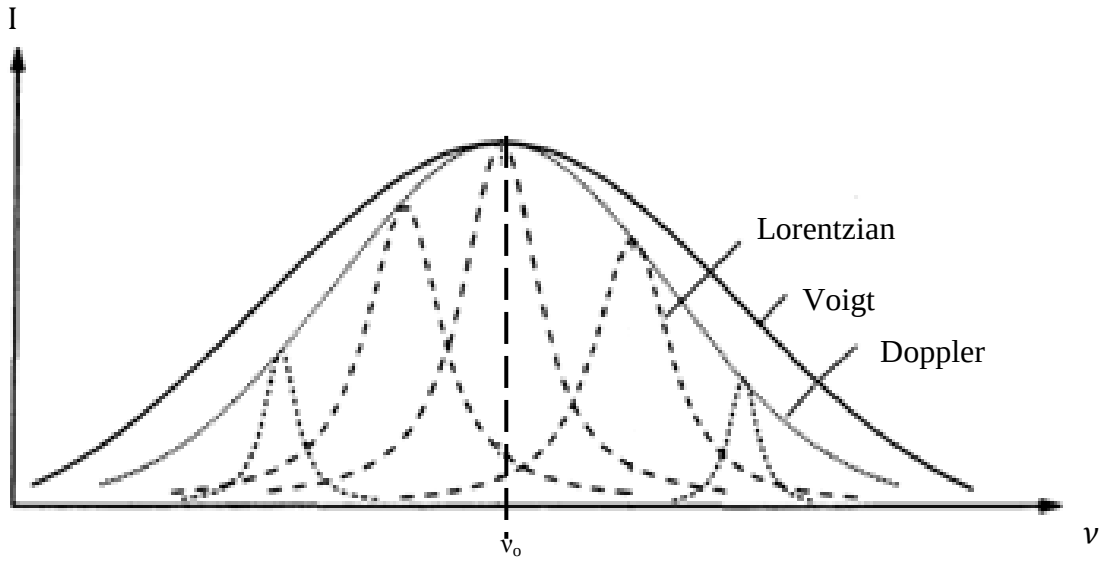

Figure 4.2 : Voigt profile [Demtroder W, "Laser Spectroscopy", Springer (1982)].

Most of the times during our investigations of the hyperfine structure of praseodymium (atoms and ions), we observe the line profile as Gaussian line profile. Because no saturation broadening is observed as the excitation probability is less then what is required for saturation effect. On the other hand, where the excitation probability of a transition is very high, saturation effects may play their role and line profile is observed as a Voigt profile. In our experiment Doppler width of about 800 MHz is observed.

4.4 Laser spectroscopy

Spectroscopy is one of the branches of Physics, in which we study the interaction of radiation with matter. The electromagnetic radiation interacts with the matter in three different ways:

I. Absorption of electromagnetic radiation by the sample: This type of interaction is called Absorption spectroscopy.
II. Emission of electromagnetic radiation by the sample: This type of interaction is called Emission spectroscopy.
III. The scattering of electromagnetic radiation by the sample: This type of interaction is called Scattering Spectroscopy.

Conventional absorption spectroscopy prefers radiation sources with a continuous broad emission spectrum (for example high pressure Hg arc, Xe flash lamps so on). A collimated electromagnetic radiation is divided into two beams, one as a reference beam and second beam is passed through the absorption cell. Behind the absorption cell a dispersing element is placed for wavelength selection (for example spectrometer or interferometer). The intensity $I_T(\lambda)$ of transmitted light is measured as a function of frequency or wavelength. By taking the difference between reference intensity $I_R(\lambda)$ and transmitted intensity $I_T(\lambda)$, the absorption spectrum is recorded. The spectral resolution is restricted by the resolving power of the dispersing element. The detection sensitivity is defined as minimum absorbed power can be detected within limitation of detector noise and intensity fluctuation of the radiation source.

The invention of laser revolutionalised almost every branch of science, including spectroscopy. In absorption spectroscopy conventional light source has been replaced by tunable laser because it is a highly coherent intense light source with extremely narrow linewidth and its spectral energy density is several orders of magnitude greater than conventional light source. The tunable laser covers a wide wavelength (spectral) region from Ultra violet (UV) to Infrared (IR). Another important feature of laser spectroscopy is that the laser covers a wide wavelength (spectral) range extending from the far-infrared to the hard X-UV domain. Following are the main advantages of Lasers over conventional radiation sources.

I. The absorption coefficient α(v) which is function of frequency can be measured directly from difference ΔI(v) =a[IR(v) - IT(v)] between intensity of reference beam IR(v) and transmitted intensity IT(v) (where "a" is sum of losses). Therefore a monochromator is not required. Tunable single mode laser provides higher spectral resolution than in conventional spectroscopy. Spectral resolution is only restricted by the line width of the absorbing transition.

II. It is possible to have laser with high power, this not only increase the signal to noise ratio, but also overcomes the detector noises and increases the sensitivity.

III. Less divergence in laser radiation makes it possible to increase the interaction path length of the sample and radiations. Hence with laser radiations, transitions with less absorption probabilities can also be studied effectively.

IV. A long Fabry Perot interferometer (FPI) can be used as frequency marker. An FPI consists of two mirrors which are separated by a distance "d". Small part of the laser beam (output) with frequency v_L is guided to pass through Fabry Perot interferometer, a photodetector receives intensity peaks each time the laser frequency is tuned to a transmission maximum at v = c/2d, 2c/2d , 3c/2d, 4c/2d, …. The separation between two consecutive transmission maxima is known as free spectral range (FSR) of Fabry Perot interferometer which is equal to c/2d. These equally spaced maxima serve as accurate wavelength markers which allow measurement of adjacent absorption lines.

V. In tunable laser a large range of radiation spectrum is available so it is possible to tune the laser frequency over the desired spectral region.

VI. The high intensity and narrow line width of laser light make it possible to achieve appreciable population in excited state this also gives a good signal to noise ratio.

VII. It is possible to measure the line profiles of absorbing atomic transitions with high accuracy in absorption spectroscopy with tunable single mode laser.

The above discussion supports the use of lasers as radiation source for absorption spectroscopy, natural line width and Doppler broadening of the investigated spectral line limits the resolution of the experimental measurements. However, there are some techniques through which either we can limit or remove almost completely the Doppler broadening, hence the laser spectroscopy is further divided into two types.

4.4.1 Doppler Limited Spectroscopy

Here we discuss some experimental techniques where the spectral resolution is limited by the Doppler width of the atomic absorption lines. Few examples of Doppler limited laser absorption spectroscopy are: Optogalvanic spectroscopy, Photoacoustic

spectroscopy, Optothermal spectroscopy, Optical Double Resonance, Cavity Ring-down spectroscopy and Laser Lnduced Fluorescence spectroscopy.

4.4.1.1 Laser Induced Fluorescence Spectroscopy

In laser induced fluorescence spectroscopy laser light of suitable frequency is passed through plasma of atom and ions (the plasma in a hollow cathode gas discharge lamp). The atoms in the absorbing sample are excited if the laser wavelength exactly matches with the energy difference between lower and upper (excited) level of atoms. The excited atoms are de-excited spontaneously to lower levels by emitting light of various wavelengths known as fluorescence light or by collisional de-excitation (in case of high pressure discharge). At low pressure the collisional de-excitation is less likely to occur (in case of our experiment pressure of gas is about 0.5 mbar), it happens only when another atom has excited level of almost same energy. The fluorescence is most likely to occur, this method of studying the atomic and molecular structure is known as Laser induced fluorescence (LIF).

This absorption spectroscopy is known as excitation spectroscopy. The excitation spectrum provides information for both qualitative and quantitative measurements. It directly reveals the absorption spectrum of the investigated sample. Let us demonstrate how to detect LIF signal. The plasma in the hollow cathode lamp is irradiated by laser light. The intensity of the incoming laser beam is modulated by a mechanical chopper and the chopping frequency is fed to a lock-in amplifier as reference frequency. Selection and detection of fluorescence signals is performed by a grating monochromator (focal length: 0.5 m) and a photomultiplier tube (Hamamatsu R 955). In order to detect the LIF signal, the frequency of the laser light is tuned into resonance with the transition frequency of combining levels. Since the intensity of the incoming laser beam is modulated, also the populations of lower and upper level involved in the transition are modulated. Thus, the fluorescence intensity is also modulated with the chopper frequency which allows a phase sensitive detection of the LIF signal.

The population of the atoms in excited state is increased by irradiating laser light with resonance frequency, and the excited atoms decay to lower states giving rise to

fluorescence of different wavelengths which are monitored as a function of laser frequency. Our primary research assignment is to investigate the hf structure of Pr I to discover its energy levels. The energy levels are characterized by a set of parameters such as the hyperfine constants, energy, parity, total angular momentum of electron, nuclear spin quantum number I and the Lande 'g' factor. Laser light is used to excite atoms not only from ground state but also from high lying excited states, so numbers of fluorescence wavelengths are observed by decaying these excited levels to lower lying states according to dipole allowed transitions. The strength of a LIF signal depends upon the transition probability, laser intensity, number of excited atoms, and the branching ratio of the upper excited level. The hyperfine structure of the LIF lines does not play any role, since the monochromator selecting one LIF line does not resolve the hf structure of this line (monochromator with grating having 1200 lines/mm), but acts only as a filter to suppress other lines of the discharge.

4.4.1.1.1 Quantitative analysis of Laser induced fluorescence signal

Laser light of wavelength 'λ_L' is tuned to an absorption transition as shown in figure; the number of photons absorbed per second 'n_a' depends on

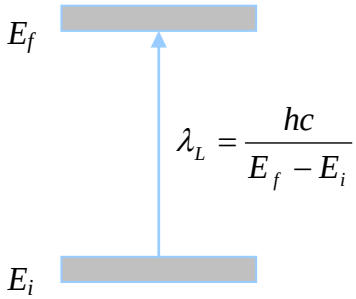

I. Absorption path length 'Δx'
II. Number of incident laser photons per second 'n_L'
III. The absorption cross section per atom *'σ_{if}'*
IV. Density of atoms in absorbing state E_i, *'N_i'*

Hence, this relation can be written as

$$n_a = N_i \sigma_{if} n_L \Delta x \qquad \textit{Equation 4.15}$$

The absorption cross section 'σ_{if}' is measure a of absorption probability and is related to absorption coefficient 'α_{if}' i.e.

$$\alpha_{if} = \sigma_{if}\left(N_i - N_f \frac{g_i}{g_f}\right)$$ *Equation 4.16*

The intensity of fluorescence signal depends on the number of fluorescence photons emitted per second from excited state n_{fl}, which is given by

$$n_{fl} = N_f A_f = n_a \eta_f$$ *Equation 4.17*

where

$A_f = \sum A_{fm}$ = sum of spontaneous probability for each decay channel from E_f to different lower states E_m

η_f = quantum efficiency of excited state

η_f is the ratio of the spontaneous transition rate of excited state to the total de-excitation rate which may also include radiation-less transitions.

Total fluorescence intensity 'I_{fl}' monitored as a function of wavelength λ_L i.e.

$$I_{fl}(\lambda) \propto n_L N_i \sigma_{if}$$ *Equation 4.18*

4.4.1.1.2 Characteristics of LIF

I. At very low pressure the excited atoms radiate before they collide with other atom, therefore $\eta_f = 1$ for all excited states.
II. The quantum efficiency of photomultiplier cathode should be constant over the whole spectral range.

4.4.1.1.3 Types of LIF Signals

There are following types of experimentally observed LIF signals:

Fluorescence with positive LIF signal

The fluorescence wavelengths which appear as decay from the upper level of the excited transition are known as positive fluorescence. The resonance laser light of wavelength λ_{23} is absorbed by the atoms in state E_2; the atoms are excited to energy level E_3, the population of lower level decreases and that of upper level increases. The

level then decays to the levels E_4 and E_5 by emitting positive fluorescence light of wavelengths λ_{34} and λ_{35}. The intensity of the incoming laser beam is modulated by a mechanical chopper and the chopping frequency is fed into a lock-in amplifier as the reference frequency. In order to observe the maximum LIF signal, the reference frequency and LIF signal should be in phase. Since the LIF signal increases when the laser is irradiated to sample, in this situation 'positive fluorescence' is obtained as shown in figure 4.3.

Negative Fluorescence

Some time it happens that lower level is high lying compared to very low lying levels, this level decays to the further low lying levels and also emit fluorescence light. This type of LIF signals is 180^o out of phase and is known as negative fluorescence. In the resonance excitation from lower level E_2 to upper level E_3, some of the atoms decay directly from E_2 to the ground state E_1 and emit fluorescence light of wavelength λ_{21} as shown in figure 4.3. The population of E_2 is diminished when the laser is irradiated to sample. This fluorescence is registered with 180^o phase shift as compared to positive fluorescence.

Impact or collision coupling

Some time probability of collision between two closely lying excited levels is high. In such a case during collision the atoms in excited state transfer their energy to the atoms of closely lying excited states, which then decay and emit fluorescence light. The excited level E_3 lies very close to another excited state E_6 as shown in figure 4.3. Due to collision transfer of energy takes place from state E_3 to state E_6. Then atoms of excited state E_6 decay to the energy state E_7 by emitting fluorescence light of wavelength λ_{67}.

Self-absorption

A photon emitted by an atom may be re-absorbed by a different atom before it has a chance to escape from the source. This phenomenon is known as self-absorption. This

re-absorbed photon may take part either in radiative decay to a different lower level or through collisional de-excitation of the absorbing atom.

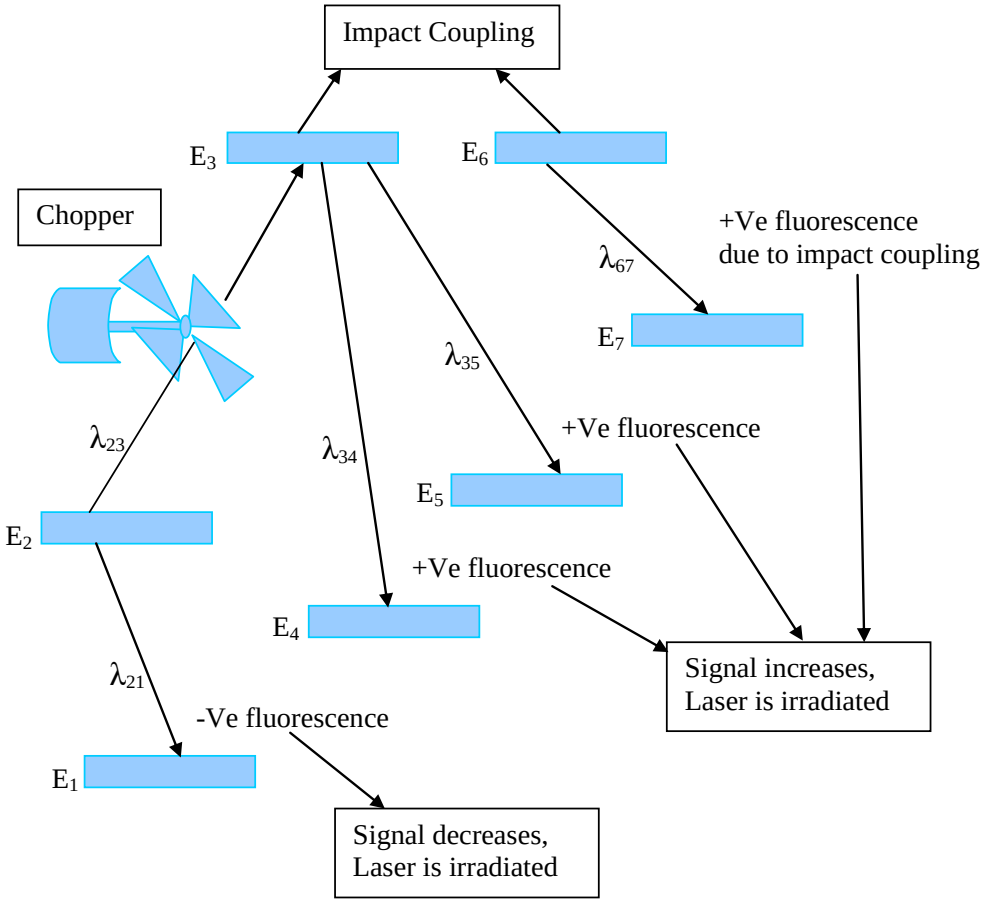

Figure 4.3: Types of Laser induced fluorescence signals.

Since probability of emission was greatest at the center of the line, the probability of absorption is also greatest at the center. Therefore result of this re-absorption within light source, the intensity of the spectrum line decreases more proportionately at the centre of the line than elsewhere, changes the line shape and makes it appearing broader. If the self-absorption is strong, then an minimum intensity is observed at the center of spectral line and the line is said to be self reversed. Self-absorption phenomenon generally occurs in the excitation between ground state and lowest excited states.

4.4.1.1.4 Advantages of LIF

Blend situation

It happens most of the cases where the line density is larger (for example praseodymium), the lines are very close and sometimes more than one level is excited simultaneously (both lines having almost the same cg of wavelength) in a single scan range of laser. In this way a large number of fluorescence lines are observed as both levels show LIF. This is known as blend situation. It is possible to detect two or more blend lines separately. The hyperfine structure of each line can be recorded separately by detecting the corresponding fluorescence line and energy of upper level is determined by using the information from recorded hyperfine structure, wave number of excitation line and known lower level.

LIF signal of free atoms

LIF signal of an atomic line of comparable intensity should be stronger than that of an ionic line, because one of advantages of a hollow cathode discharge is; it produces more free atoms than free ions depending upon the discharge conditions.

Increased sensitivity for Fluorescence Signal

Higher sensitivity for fluorescence signal can be achieved by using Lock-in techniques as compared to absorption measurements.

4.4.1.2 Optogalvanic Spectroscopy

The plasma in a hollow cathode lamp as a gas discharge is irradiated by laser light. When the laser frequency is tuned to an optical resonance transition, then a significant change in the population densities of lower and excited states takes place. The different ionization probabilities of these two levels causes in a change of discharge current. This change can be detected as a voltage change across the ballast resistor. This effect is considered as optogalvanic effect. This method opens new branch in spectroscopy namely Optogalvanic spectroscopy.

The Optogalvanic effect was first observed by F M Penning [51]. He observed a change in the electrical properties of a gas discharge caused by the light of a second discharge. Similar observations were made by C Kenty [52] and K W Meissner and W F Miller [53]. R B Green et al. [54] made first spectroscopic measurement using the optogalvanic effect with the tunable dye laser. Figure 4.4 is schematic lay out of an experimental set up for optogalvanic spectroscopy.

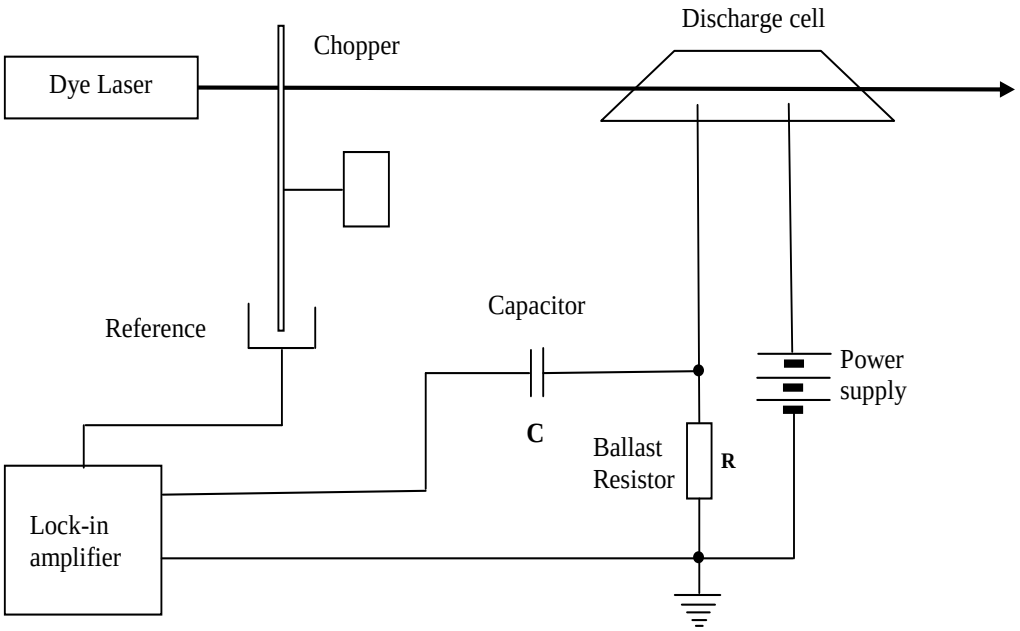

Figure 4.4: Experiment set up for optogalvanic spectroscopy.

Several processes may contribute to ionization of an atom. Some of them are following:

Direct ionization by electron impact on atom 'A':

$$A + e^- \rightarrow A^+ + 2e^-$$

This process dominates at low pressure.

Collisional ionization by metastable atoms:

$$A^* + B^* \rightarrow A^+ + B + e^-$$

Direct photoionization by laser:

$$A + h\nu \rightarrow A^+ + e^-$$

Two step or multistep ionization:

$$A + e^- \rightarrow A^*$$
$$A^* + e^- \rightarrow A^+ + 2e^-$$

This usually occurs in highly excited levels.

Application of Optogalvanic spectroscopy:

Excitation and ionization processes in flame, gas discharge and plasma [55] can be investigated by simple optogalvanic spectroscopy. The technique is specifically utilized to evaluate collissional/ionizational probabilities, wavelength calibration [56], Doppler free saturation spectroscopy [57], investigation of Rydberg states [58], diagnostic tool in atomic vapor laser isotope separation AVLIS, studies in autoionizing levels [59], laser frequency locking and stabilization [60-61], and for the investigation hf structure of atom or ion [62-63] through LIF spectroscopy.

4.4.2 Doppler Free Spectroscopy:

Single mode lasers with extremely narrow line width are used in Doppler free experiments. Some examples of Doppler free laser absorption spectroscopy are: Two Photon absorption spectroscopy, the Collimated Atomic Beam spectroscopy and Saturation spectroscopy.

4.4.2.1 Two Photon Spectroscopy

In an intense field of laser light, it is possible that an atom or molecule absorbs two photons. It is known as two photon absorption process. This process can be regarded as two consecutive one-photon absorptions. If two photons are in resonance with the consecutive absorptions, then two-photon absorption takes place either as intermediate step is real level or virtual level, undergoing a transition from initial state E_i to final state E_f.

Parity forbidden transition can be studied using two photon spectroscopy. Excited levels with same parity can be reached via two-photon excitation. These two photons

may either come from a single laser beam passing through the absorbing sample or they may come from two separate lasers.

An atom makes a transition from its ground state (energy E_i) to an excited state after absorbing a photon of frequency ν_1. In this excited state the atom may absorb another photon of frequency ν_2 to reach to further high lying excited state having energy E_f. The difference of energies of ground and final excited states is given by

$$E_f - E_i = h(\nu_2 + \nu_1) \qquad \textit{Equation 4.19}$$

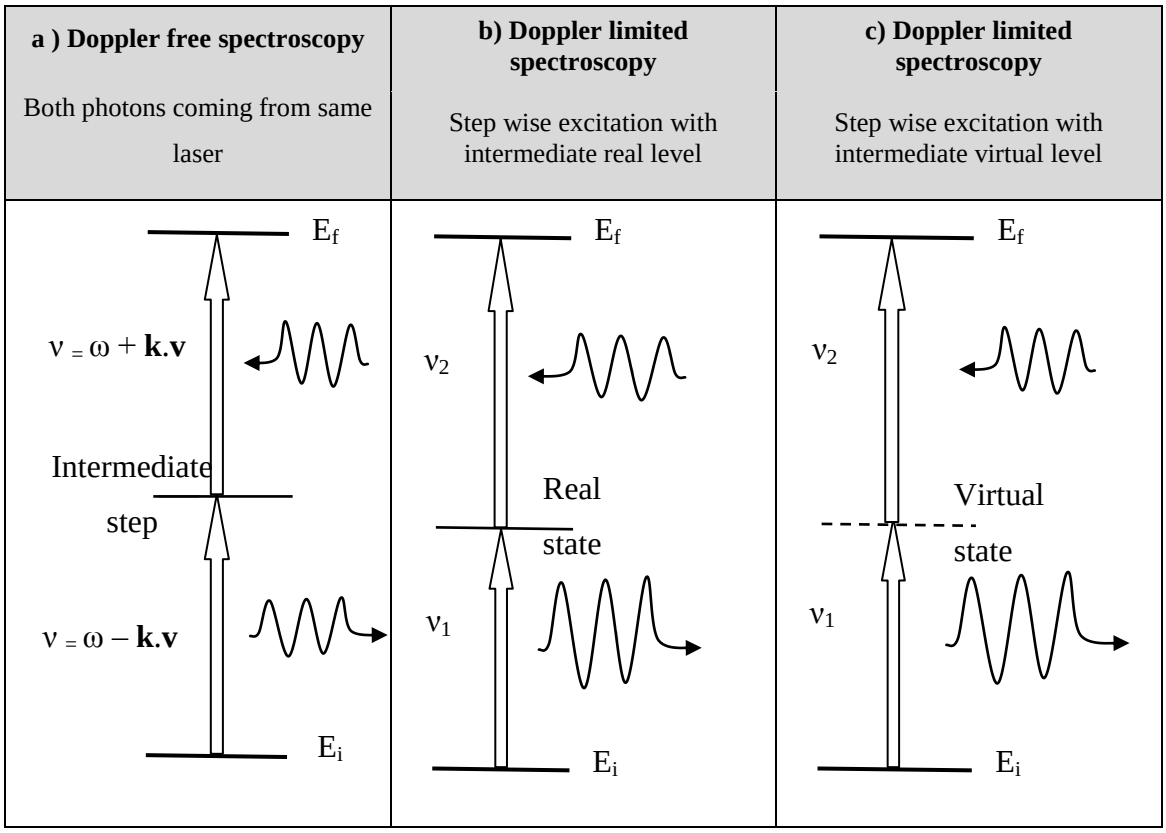

Figure 4.5: Two photon absorption.

If absorption takes place from two counter propagating beams such that $\nu_2 = \nu_1$ as in figure 4.5 (a), therefore the first order Doppler shift in one absorption is exactly cancelled by the corresponding shift in the second absorption. Hence

$$E_f - E_i = 2h\nu \qquad \textit{Equation 4.20}$$

From equation 4.20, it is clear that the two photon absorption is independent of the velocity of atoms or molecules. It is known as Doppler free spectroscopy for two photon absorption.

In order to observe the Doppler free two photon absorption laser induced fluorescence signals (LIF) is monitored.

Figure 4.6 shows a narrow peak in LIF signal at resonance frequency of the transition (produced by two photon having same energy propagating in opposite direction) and a Doppler broadening background produced is larger because both pairs of photons which are moving in same and opposite in directions, contribute this broadening. Since probability of two photons absorption is directly proportional to (laser intensity)^2, therefore probability of absorption of two photons from opposite beams is double as

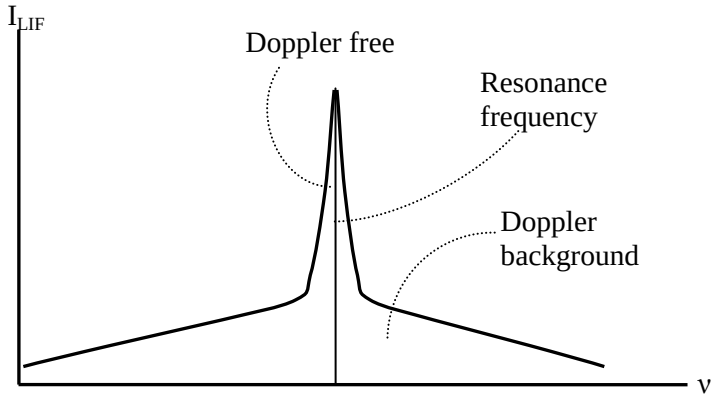

Figure 4.6: Doppler free line profile for two photon.

compare to that for two photons from same beam.

In figure 4.5 (b) and (c) even two photons moving in opposite direction but these are the examples of Doppler limited spectroscopy for two photons absorption because two photons have different energies, therefore in this case absorption of these photons cannot cancel Doppler shift completely.

It should be noted that two photons absorption can also take place for photons moving in the same direction.

Some properties of two photon spectroscopy

I. The selection rules for optical transitions of two photon absorption are $\Delta L = 0$ and ± 2.

II. Doppler free spectrum can be obtained by two photon absorption which is independent of the atomic or molecular velocity.

4.4.2.2 Saturation Spectroscopy

The saturation spectroscopy is Doppler free spectroscopy based on the following fact:

An intense laser beam with resonance frequency corresponding to transition between lower and excited state is passed through the sample, so excitation process takes place. Excitation process may take place faster than atoms of the sample decay to the lower state by spontaneous emission. Therefore lower state has significantly less number of atoms and excited state becomes saturated. The high resolution laser spectroscopy based on this process is called saturation laser spectroscopy.

Consider two laser beams moving an opposite in direction along same path and having same frequency interacting with the sample in the absorption cell. The laser beam is tuned to the center frequency of the absorption curve, both beams will be absorbed at the same position. Atoms moving perpendicular to the laser beam are only affected (perpendicular velocity group of atoms); atoms experience the double intensity for center frequency and the total absorption will decrease. An intense laser creates a narrow dip in the Maxwell velocity distribution of the lower state atoms and a peak in the excited state. The dip burnt by the intense laser is called Lamb dip [64-65]. It is an example of non linear laser spectroscopy [66].

Figure 4.7 is schematic lay out of an experimental set up for saturation spectroscopy. A beam of the tunable laser falls on beam splitter, which divides the incident laser beam into two parts, a strong pump beam and a probe beam (weak). Both beams are guided by two mirrors in such a way that after reflection both counter propagating beams pass through the absorption cell with overlapping path.

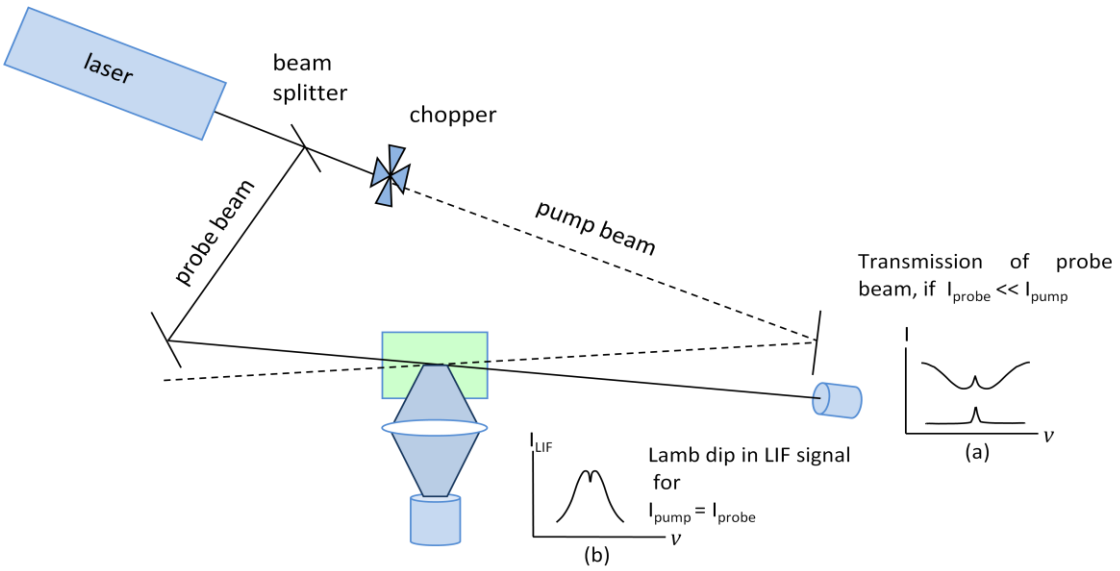

Figure 4.7: Experimental arrangement for Saturation Spectroscopy.

In order to monitor the Lamb peak (lamb dip) the intensity of transmitted probe beam as function of laser frequency is recorded by a detector. When the laser beam is tuned to the center frequency of a transition over Doppler broadened profile then the strong laser beam saturates the transitions for atoms in a particular velocity group and after it probe detects the hole. Therefore in this situation transmission signal of probe beam is increased i.e. the absorption profile shows a Lamp dip at center frequency in figure 4.8 (a) and a peak corresponding to Lamp dip appears in the transmitted intensity with Doppler background shown in upper part of figure 4.7 (a). In order to suppress the background the intensity of pump beam is modulated by a mechanical chopper and the frequency of the chopper wheel serves as reference frequency for the phase sensitive lock-in amplifier. Better signal is obtained as shown in lower part of figure 4.7 (a) and figure 4.8 (b).

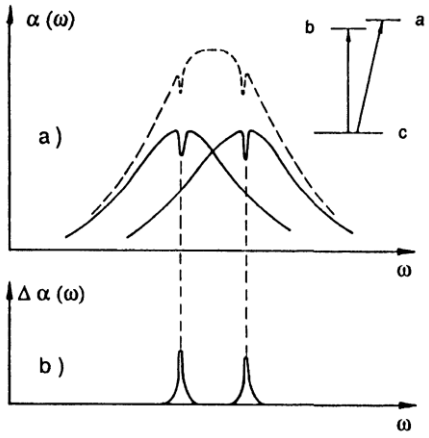

Figure 4.8: a) and b) Spectral resolution of the Lamb dips of two transition with overlapping Doppler profiles [Demtroder W, "Laser Spectroscopy", Springer (1982)].

The first saturation spectroscopy experiments using a tunable narrow band laser were performed by T W Hänsch et al. and M D Levenson and A L Schawlow [67-68] and by C Borde [69]. The saturation spectroscopy is discussed in detail in [70].

It is also possible to monitor the laser induced fluorescence signal for detection of Lamb dip. In order to observe better laser induced fluorescence signal (which is proportional to the absorbed laser power) experimentally in saturation spectroscopy, two counter propagating laser beams must have same intensity. When laser frequency is tuned exactly to center frequency of absorption profile, then due to saturation process probability of absorption and stimulated emission are equal and absorption cell becomes transparent to laser at this (resonance) frequency. Therefore fluorescence signal is deceased at resonance frequency of the transition and hence Lamb dip is easily observed as shown in figure 4.7 (b).

4.4.2.3 Collimated Atomic and Ionic Beams Spectroscopy

High resolution spectroscopy with collimated atomic and ionic beams is possible when a narrow band single mode laser interact perpendicular to the collimated atoms and ions. The Doppler width is reduced off by the collimation ratio defined by the following figure 4.9.

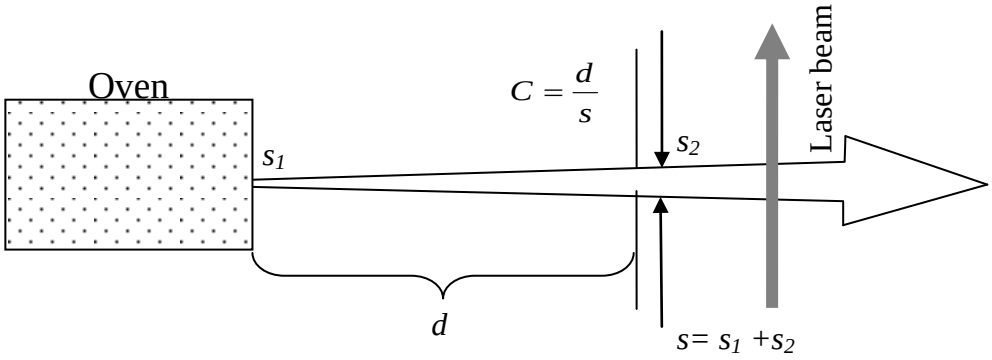

Figure 4.9: Definition of Collimation ratio.

Well collimated atoms and ions in beam do have only a small velocity component in perpendicular direction, high resolution spectroscopy can be performed by an exposing such beam at perpendicular to narrow band, single mode laser.

In well collimated atom and ion beam residual (reduced) Doppler width is given by

$$(\Delta\nu_D)_{\text{Res}} \approx \frac{\Delta\nu_D}{C} \qquad \textit{Equation 4.21}$$

Where $(\Delta\nu_D)_{\text{Res}}$ = residual (reduced) Doppler width

$\Delta\nu_D$ = normal Doppler width

C = collimation ratio

A Jackson and H Kuhn [71] had already made the use of atomic beam spectroscopy using a high resolution Fabry-Perot interferometer before the invention of lasers. The first application of atomic or molecular beams in laser spectroscopy was described S. Ezekiel and R. Weiss [72].

Main characteristics of atomic beam spectroscopy:

I. An atomic beam can be produced essentially for any element.
II. The Doppler width is almost eliminated reduced appreciably. With a collimation ratio of 100 a typical residual broadening of 5 MHz is obtained. For example see figure 4.10.

III. Since all atoms have almost same velocity, collisions rate is smaller than in the gas at equivalent pressure (pressure of gas is about 5 - 10 mbar). Hence the collissional broadening is reduced.

IV. Fluorescence light radiates in all direction (4π steradians) and very few of them reach the photodetector. So, in order to each atom interacts with the laser, laser beam is deflected many times using the pair of corner mirrors (corner mirror is consist of a pair of mirror joined perpendicular to each other) and hence a resulting in higher fluorescence signal is obtained.

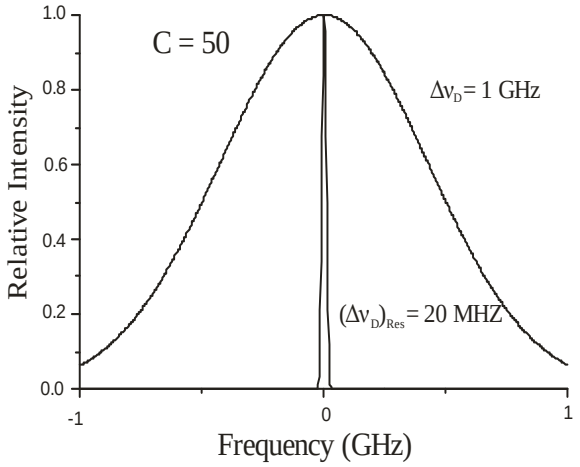

Figure 4.10: Residual (reduced) Doppler width $(\Delta\nu_D)_{\text{Res}}$ *is obtained 20 MHz for Doppler width* $\Delta\nu_D$ *= 1 GHz and collimation ratio C = 50[Experimental 4].*

Interaction Detection methods:

Following are the Detection methods for the interaction of an atomic beam with a laser beam.

4.4.2.3.1 Detection by Photoionisation:

Two laser beams one with a narrow band laser and other an intense laser interact simultaneously with the atomic beam. The narrow band laser involves in the process of excitation and intense beam involves in the process of photoionization. The intense beam has sufficient energy to ionize the atoms in excited states, where as the ground state atoms cannot be ionized. The photoelectrons or the ions are detected in an electron detector [73].

4.4.2.3.2 Detection by Fluorescence:

The investigation of the optical resonance is directly possible by making the arrangement to observe fluorescence light which is emitted by atom or molecule in de-excitation process. This process has been demonstrated for isotopes separation [74].

4.4.2.3.3 Detection of the Recoil Effect:

An atom is deflected from the beam (usually deflection is very small) by absorbing a photon which transfers the momentum to the atom. In the de-excitation process the recoil momentum transferred either is cancelled (stimulated emission) or is transferred to the atomic beam (spontaneous emission). The spontaneous emission results in spread and broadening of atomic beam. The deflection of an atomic beam was first experimently observed by R Frisch in 1933 [75]. A Ashkin [76] proposed an idea to use this method for isotopes separation. P Jacquinet et al. [77] first time recorded the hyperfine structure by beam deflection for the sodium D lines.

4.4.2.3.4 Detection by Magnetic Deflection:

In 1938 I I Rabi et al. [78] introduced atomic beam magnetic resonance (ABMR) technique, this method works on the principle of magnetic resonance. They observed that an atom (in metastable state) in the atomic beam with a magnetic moment passing through an inhomogeneous magnetic field is deflected in the direction of the field gradient (change in an inhoinmogeneous magnetic field with respect to position). In 1952 I I Rabi [79] proposed an idea that this method could be used in the investigation of excited states if atoms are exposed resonantly in the interaction region. He also predicted that this technique could be used to study isotope shifts. In 1965 Marrus used Rabi's idea to detect and measure [80].

5 EXPERIMENT

5.1 Ring dye laser

In our experiment a cw-ring dye laser cavity has the ring geometry as shown in the figure 5.1 [81]. The lasing medium is a dye dissolved in a viscous medium, like ethyleneglycole that flows continuously in the flowing jet. The orientation of dye jet at Brewster angle makes sure for nearly 100 % transmission of a proper polarized component of the laser light. Population inversion in the dye can be achieved by shinning of an intense laser beam from a pump laser (Argon ion laser) on it. This pump beam is focused by a spherical mirror (pump mirror) Mp onto the dye jet and excites the dye molecules in the jet. The combination of mirrors M1, M2, M3 and M4 produce a resonator cavity for the lasing and an optical diode in combination with quartz plate make it possible for the laser to run in one direction. Optical diode consists of a Faraday rotator and a birefringent crystal, which allows the laser light to pass in one direction with fewer losses. So, optical diode prevents the formation of standing wave in the laser cavity and within the dye medium. Therefore the process of spatial-hole-burning is avoided in this way. Because of this single mode operation becomes easier and higher output power can be reached.

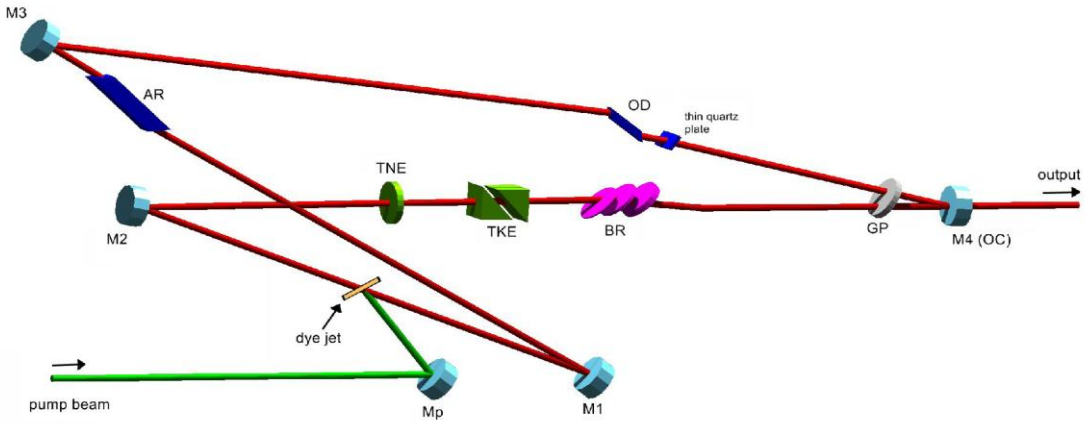

Mp	=	*Pump Mirror*	*OD*	=	*Optical Diode with Thin Quartz Plate*
M1	=	*Lower Folding Mirror*	*TNE*	=	*Thin Etalon*
M3	=	*Upper Folding Mirror*	*TKE*	=	*Thick Etalon*
M2	=	*Tweeter with piezo electric transducer (PZT)*	*BR*	=	*Birefringent Filter*
M4	=	*Output Coupler*	*AR*	=	*Astigmatism Compensation Rhomb*
GP	=	*Galvo (Brewster) Plate*			

Figure 5.1: Optical lay out of a cw-Ring Dye Laser.

In order to achieve a single longitudinal mode (emission of one light frequence) several essential frequency selective elements are introduced to select one resonantor mode. This is done by the combination of:

I. Birefringent filter (BRF): A birefringent filter is a Lyot type filter consisting of one to three quartz-plates, each plate being four times the thickness of the previous one and inserted at Brewster angle in the cavity. The FSR and the width of the transmission peak depend upon the thinnest and thickest plates. The Birefringent filter has low finesse and an FSR of the order of THz [81].

II. Thin etalon: It is a 0.5 mm thick quartz plate placed almost perpendicular to incidence and has a FSR of the order of 200 GHz.

III. Thick etalon (scanning etalon): It is a 10 mm thick solid prism-etalon placed at almost perpendicular to incidence and has a FSR of the order of 10 GHz. A scanning piezo which is attached to one of the prisms is responsible for changing the distance between the prisms.

Since in a dye laser a large number of modes of oscillations are possible in the cavity, BRF and thick and thin etalons select one of these modes and cause a single mode operation. A Galvo plate which is controlled with an applied current is placed at Brewster angle near to the output coupler mirror M4 so that it causes a frequency shift of the selected mode when it is tilted, changing in this way the optical cavity length. 20% reflectivity of thin and thick etalons makes sure a single mode selection across the entire gain region of the dye. The figure 5.2 shows longitudinal modes generated by laser cavity with the transmission curves of the optical elements like, thick etalon, thin etalon and birefringent filter in order of decreasing resolution and in this way the single mode operation is achieved.

Misalignment of etalons, thermal fluctuations, turbulence in the dye jet, presence of micro bubbles in the dye etc may cause instability in laser frequency. This is known as mode hopping. This problem can be overcome by developing of a temperature stabilized confocal external reference cavity. In case of mode hopping reference cavity produces error signals which change the length of resonance cavity. In order to obtain active stabilization the mirror M2 is mounted on a piezo electric transducer (PZT). Error signals generated by reference cavity are divided into low and high frequency parts. Low frequency part is used to drive the laser cavity Galvo plate and high frequency parts drives to PZT attached to the tweeter mirror (M2). Both tweeter PZT and Galvo plate are responsible for changing the length of cavity. In this way a single mode laser frequency with a width of 1MHz can be achieved, which is sufficient for our investigation.

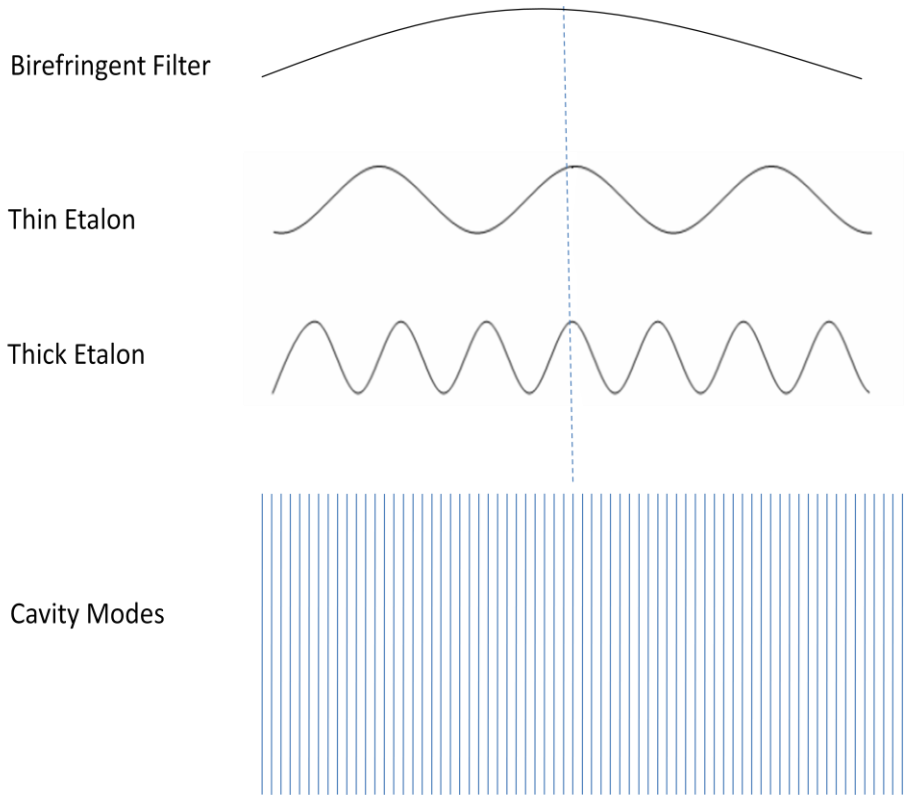

Figure 5.2: Transmission curves of the optical elements in tunable dye laser.

5.2 Experimental Setup

Similar to the any spectroscopy experiment, our experimental setup for investigation of the hf structure of Pr lines by using LIF technique requires three essential components which are following

I. Spectroscopic light source (Laser)
II. Free atoms to be investigated (produced in a hollow cathode lamp)
III. Detection and Measurement of LIF signal

5.2.1 Spectroscopic Light Source

In order to investigate the hf structure of Pr, a suitable light source is needed for observing absorption processes. Here the spectroscopic light source is the dye laser (figure 5.1). The excitation sources (light sources) are operated with Rhodamine 6G or Kiton red, DCM, Rhodamine 700 (LD700) and Stilbene 3 in cw-single mode tunable

ring-dye laser pumped by a solid state diode-pumped, frequency doubled Nd:Vanadate Nd:YVO4 Verdi V-18 laser system, Argon-ion or Krypton-ion.

Different dyes were employed as lasing medium in the ring-dye laser system for different areas of investigation. We used the following pump lasers and dye lasers in our experiment:

Table 5.1.

	Pump laser	**Pumping region**	**Power of pump laser**
1	Verdi V-18	532 nm	7.5 watts
2	Argon-ion Ar^+	514 nm	7.5 watts
3	Argon-ion Ar^+	Multi-line UV	7 watts
4	Krypton-ion Kr^+	Multi-line Red	4.5 watts

Table 5.2.

Dyes for lasing	**Range/ nm**	**Pumped by**
Rhodamine 6G	560 - 595	1
Kiton red (Sulforhodamine B)	598 - 650	1
DCM	630 - 690	2
Rhodamine 700 (LD700)	700 - 780	4
Stilbene 3	410 - 465	3

5.2.2 Free atoms to be investigated (produced in a hollow cathode lamp)

One widely used conventional source of narrow lines is a hollow cathode (HK) lamp. A number of scientists contributed towards the development of HK lamp. History began with H Schüler [82-83] who made the first hollow cathode lamp with one anode. F Paschen modified Schüler's model a hollow cathode with the cathode inside two anodes [84]. D Feldmann was the first who introduced a discharge with a clear path through the electrodes [85], K Miyazaki et al. modified discharge assembly by placing the hollow cathode between two hollow anodes [86]. A similar lamp was developed by H O Behrens et al. and H O Behrens and G H Guthöhrlem [87-88].

In our experiment, a hollow cathode lamp is made by fitting a hollow cylinder of praseodymium into another hollow copper cylinder. Our aim of research is to investigate the hyperfine structure of praseodymium. The length of hollow cathode lamp is 19.5 mm and inner diameter of praseodymium cathode was 3 mm with central bore as shown in figure 5.3. A hollow cathode is placed between two anodes. In order to prevent the contact of anodes and cathode, anodes are fixed in a ceramic holder. Anodes and cathode are kept at a distance of 0.75 mm. A coaxial hole of almost same diameter is present inside the anodes, the cathode and the ceramic parts. The whole arrangement is fitted in a brass tube, which is capsulated in a glass tube that extended to both ends and made the actual discharge container. Two circular quartz glass plates are used to close the ends of glass tube.

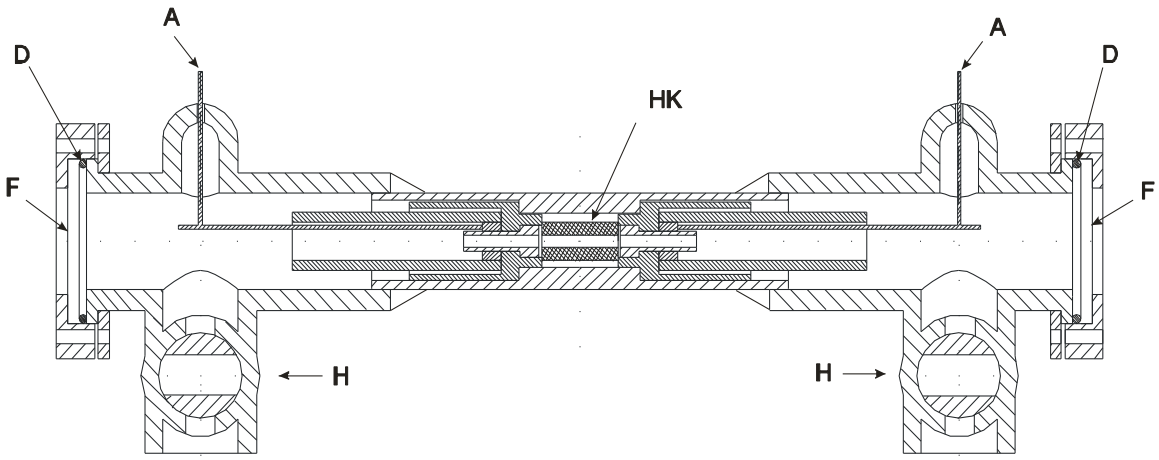

Figure 5.3: Cross sectional view for a hollow cathode lamp. HK= hollow cathode, A= anode current, F= quartz windows, D= o rings, H= glass stop cocks [87, 89].

The function of the quartz glass plates is to pass the fluorescence light to emerge from the cathode lamp and act as windows of the hollow cathode lamp. In this way the discharge is completely confined inside the cathode, the efficiency of the excitation is high. After the installation of cathode assembly, it is evacuated by switching on the rotary pump for at least for 10 hours to create a good vacuum. Figure 5.4 shows the assembly of vacuum system with hollow cathode lamp.

At the time of performing the experiment, Argon gas is filled in the cathode lamp at a typical gas pressure of 0.5 mbar to 0.8 mbar. The potential difference is applied across hollow cathode between 350 – 650V and cathode current (dc) is kept constant at a value between 55 – 65m A. The ionized gas is accelerated by the applied electric field between anode and cathode and strike with cathode material. This leads to the sputtering of praseodymium out of the cathode material. A cloud of free Pr atoms and ions is produced, not only in ground state but also in high lying excited states, which is one of the advantages of using a hollow cathode lamp as source of free atoms and ions.

The Doppler width of the hf components is reduced by cooling the discharge with liquid nitrogen. The typical broadening in the HK is of the order of 1GHz and by cooling with liquid nitrogen it could be reduced to about 600MHz.

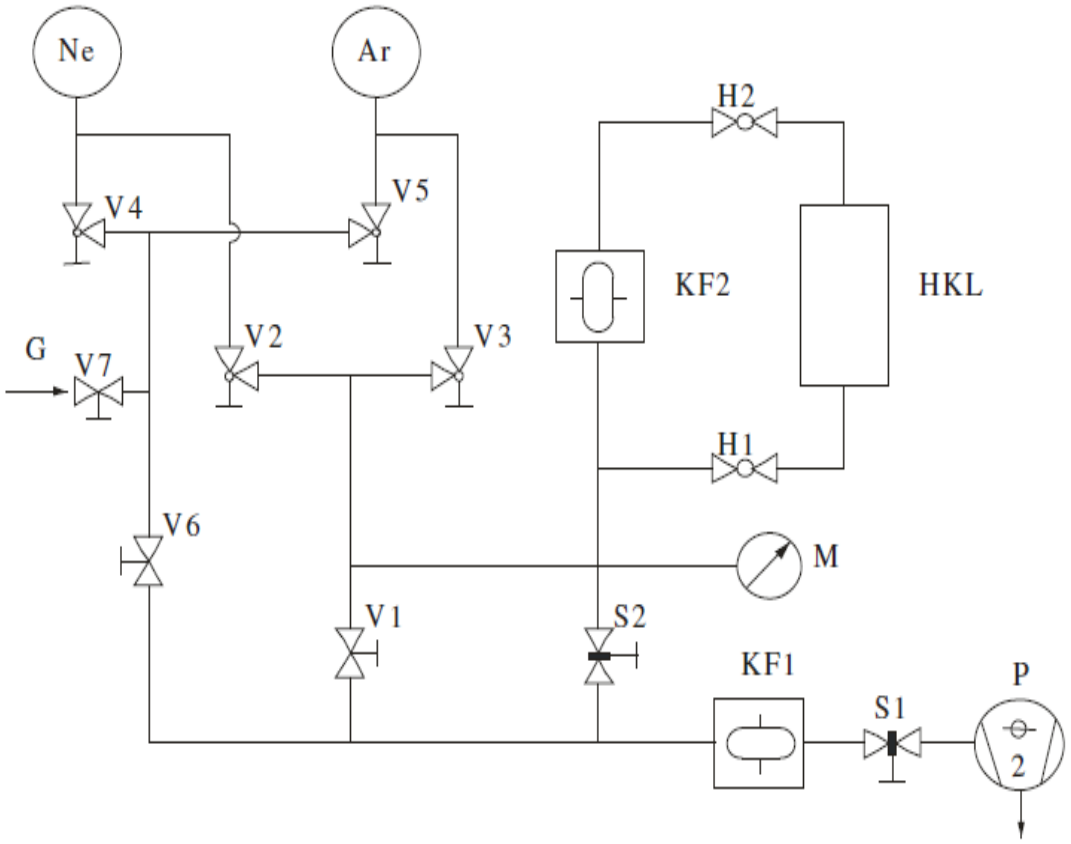

Figure 5.4: Assembly of vacuum system with hollow cathode lamp. Ne = reservoir for neon gas, Ar = reservoir for argon, G = gas inlet, V1-V7 = shut-off and gauge valves, M = manometer, HKL = hollow cathode lamp, H1, H2 = glass stop cocks, S1-S2 = slide valves, KF1, KF2 = cold traps, P = two-stage rotary vacuum pump[87, 90].

5.2.3 Detection and Measurement of Laser-Induced Fluorescence

The experimental setup employed for investigation of praseodymium is same as mentioned in [89] and is shown in figure 5.5. Two lasers were used in the experiment, the pump laser and dye laser. Single mode tunable laser radiation was achieved by the combination of pump laser and dye laser. A beam of the tunable laser falls on beam splitter BS1, which divides the incident laser beam into two parts, a strong beam (about 90%) and a weak beam (about 10%).

The weak beam laser falls on another beam splitter BS2, which further divides it into two parts. One part goes to mirror M1 which reflects it towards a lambda meter for

measuring the laser wavelength and another part goes to beam splitter BS3, which further divides into two parts. One beam falls on mirror M2, which reflects it towards a Marker etalon for making equidistant frequency markers (frequency scale). Another beam falls to an optical spectrum analyzer.

The strong beam passes through the chopper 1 and falls on mirror M3. The intensity of this laser beam is modulated by a mechanical chopper 1 and the frequency of the chopper wheel serves as reference frequency for the phase sensitive lock-in amplifier 1. After the reflection from mirror M3, the laser beam passes through the lenses L1 and L1 of a telescope. The telescope makes sure the laser beam to pass exactly through the central hole of hollow cathode lamp, where interaction between laser and plasma cathode takes place. The resonance condition is satisfied by choosing photon energy precisely equal to difference of energies of two levels involved in the transition, provided selection roles are not violated. The LIF signal is emitted by atoms relaxing to a lower state. With the help of mirror M6 and lenses L3 and L4, the LIF signal is guided towards the monochromator. Here the monochromator is a grating monochromator (focal length: 0.5 m) with 1200 lines/mm. A photomultiplier tube (Hamamatsu R 955) installed at the exit slit of the monochromator detects LIF signal and converts it into a photocurrent. This photocurrent is passing to the phase sensitive lock-in amplifier. The chopper frequency serves as reference frequency for phase sensitive lock-in amplifier. In this way detection of LIF signal is done.

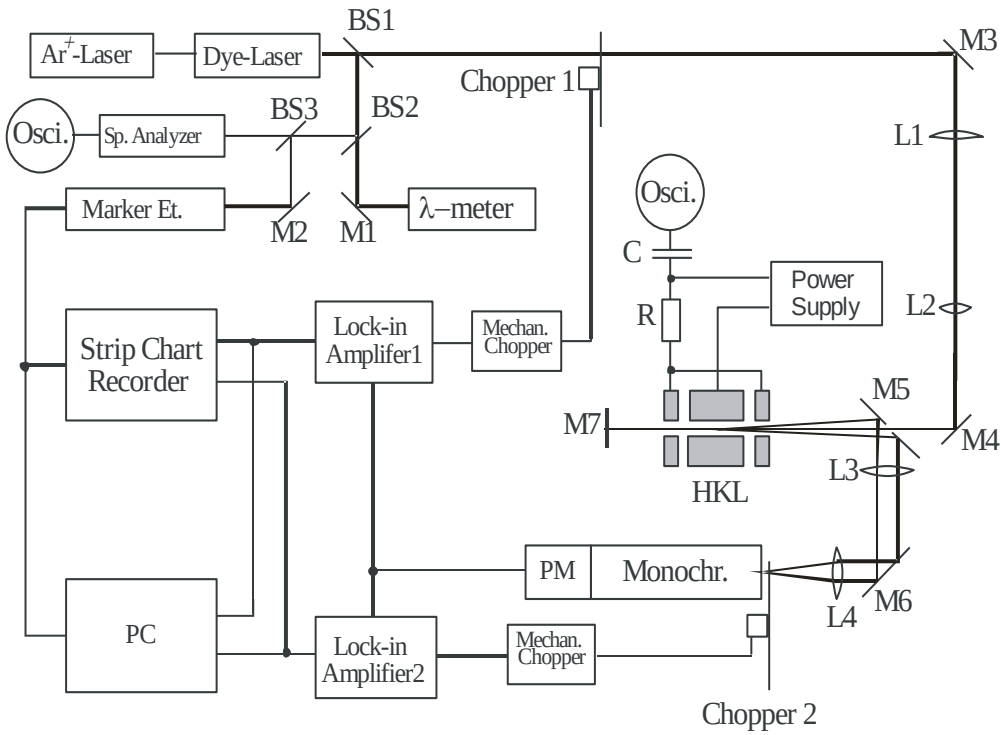

Figure 5.5: Experimental setup for investigation of the hyperfine structure of Pr I.
BS1, BS2, BS3 = beam splitters, M1-M4, M6, M7 = mirrors, M5 = mirror with central hole,
L1-L4 = lenses, Ar^+- Laser = pump laser, Dye-Laser= ring dye laser, Osz =oscilloscope,
Sp. Analyzer = spectrum-analyzer, Marker Et = marker etalon for measuring frequency markers,
λ −meter = wavemeter, Monochr = monochromatorPM = photomultiplier tube,
HKL = hollow cathodeLamp, R = ohmic resistance, C = capacitance of the capacitor.

For a systematical analysis of the hyperfine structure (spectrum) of a line, the frequency scaled distances between different hyperfine components must be known precisely. This problem is solved by using a marker etalon, which is a temperature stabilized Fabry-Perot interferometer. The marker etalon provides excellent equidistant frequency marks parallel to the hyperfine structure signal. The distance between two consecutive frequency marker peaks (transmission peaks) is called FSR and relies upon the distance of the interferometer mirrors. In different spectral regions we have used different interferometers. For example values of FSR of Marker Etalon in blue region, yellow and red regions and infrared region and in blue region are 150.3 MHz, 367.33 MHz, and 150.3 MHz respectively. Marker Etalon signals and LIF signals are recorded at

same time on a computer and on strip chart recorder for documentation, so that further evaluation can be done.

In some situations it is essential to measure the wavelength of the LIF light with greater accuracy than the reading precision of the monochromator (measuring the wavelength with an uncertainty of ±2 Å). This can be achieved with help of a second chopper wheel placed in front of the input window of the monochromator to modulate the light emitted by the hollow cathode lamp. The output signal of the photomultiplier is fed as input to a second lock-in amplifier, with the frequency of the second chopper wheel as its reference frequency. The frequency of laser light is set on the highest component of the excited transition, and the grating monochromator is scanned over several 10 Å and the output signals of both lock-in amplifier is recorded simultaneously on separate traces. On one trace one gets the emission spectrum of the discharge, on the other a peak when the monochromator wavelength is equal to the fluorescence wavelength. Comparison with FT spectrum gives the wavelength of LIF line with an accuracy of ±.05 Å although the relatively low resolution of the monochromator. This precise measurement wavelength of fluorescence lines helps to identify both unknown upper and lower levels involved in the transition.

5.3 Investigation of Spectrum

Investigation of spectral lines of an atom or ion provides an experimental method to determine energy levels of atom and ion. In order to observe the spectrum of an atom, it is necessary to excite the atom with the help of various energy sources like by absorption of photons, by heating, by electrical discharge and by impact with other energetic particle. The excited atom decays to lower level, so we observe the spectrum of atom. The cathode sputtering produces a cloud of free atoms of praseodymium which take part in the discharge, thus ground and excited states of Pr I and Pr II are populated. The praseodymium-argon plasma in the hollow cathode lamp is irradiated by laser light; the frequency of the laser light is tuned into resonance with the transition frequency. So absorption of photon takes place and excited states decay spontaneously

to lower states by emitting electromagnetic radiation with discrete frequencies. The emitted radiation can be resolved into components or discrete lines using a dispersion device. The lines are observed in the form of distribution of intensity as function of frequency or wavelength. The observed spectra are characteristic of element (praseodymium) and regarded as finger print of the atom. The knowledge of electronic levels is essentially needed for a description of the interactions in the atom and for the classification of an atomic spectrum. This goal can be achieved by experimental investigations of the numerous spectral lines. In order to investigate wide spectral regions, a high resolution Fourier transform (FT) spectrum is available in our laboratory. Our research group has been using FTS of praseodymium, tantalum and lanthanum for investigation of hf structure of their spectral lines.

5.4 Fourier Transform Spectrum

A Fourier transform (FT) spectrometer is an interferometer which is based on the principle of a Michelson interferometer. The FT spectroscopy is superior to other spectroscopic technique in some aspect, for example here in Doppler-limited environments it is possible to record large number of lines in one scan and covers a large wavelength range in each scan. FT spectrum is highly resolved and has a relatively low scan time.

The discovery of new levels helps in reducing the number of unclassified lines of Pr I and Pr II. In order to extract precise excitation wavelength for laser spectroscopic investigation of Pr lines, FT spectrum for praseodymium is used The FT Spectrum of praseodymium was recorded at the Institute of Quantum Optics at Leibniz University in Hannover with help of a continuously scanning high resolution FT-IR spectrometer (model number IFS 120 HR, Bruker Corporation). FTS covered greater wavelength range from 3260 to 9880 Å.

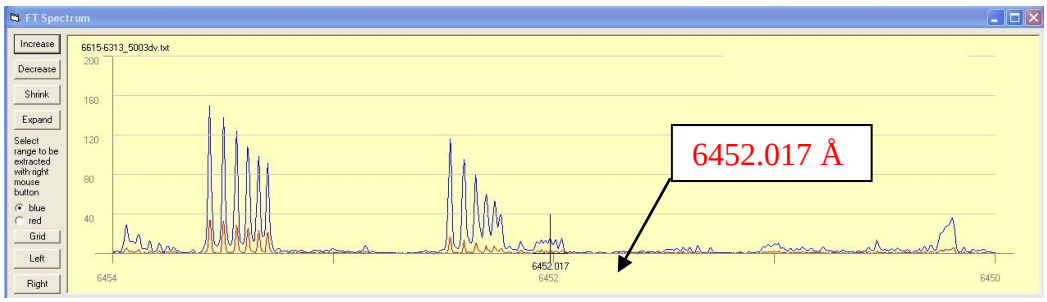

Figure 5.6: Part of FTS from 6450 to 6454 Å. Classification of line at λ = 6452.017 Å: transition between 29834.920$^{e}_{17/2}$ cm^{-1} and 14340.1743$^{o}_{17/2}$ cm^{-1}.

Resolution of FTS were different for different regions for example it was 0.025 cm^{-1} at 50000 cm^{-1} (0.001 Å at 2000 Å); 0.0125 cm^{-1} at 25000 cm^{-1} (0.002 Å at 4000 Å) and 0.005 cm^{-1} at 10000 cm^{-1} (0.005 Å at 10000 Å) [49]. The original data files of the FT spectrometer were recorded as intensity versus wave number but were converted to intensity versus air wavelength using the dispersion formula given by E R Peck and K Reader [91]. Then the files were combined to form one spectrum covering the mentioned large wavelength range. Due to the high line density of Pr**,** in most cases the FT spectrum shows hf components of a line which are overlapped with the hf components of other nearby located lines. So in general the hf components of a line are only partially resolved. Although the convolution of the Doppler width of the hf components and the instrumental profile of the FT spectrometer restricts the resolution of the spectrum to 0.03 cm^{-1} (on the average resolution due to multiple scan), but in some cases where the hf components of a line are visible and resolved in the FT spectrum, the line profile can be used to identify the line, provided that the combining levels and their hf constants are known. Wavelength calibrated FT spectrum of praseodymium will play a key role in our investigation. Figure 5.6 displays a small part of FT spectrum.

5.5 Computer Programs for Data Analysis

In order to analyze the recorded hf structures of praseodymium, we employed the following computer programs for data analysis:

5.5.1 Data Viewer

The recorded hf structures of praseodymium can be viewed with the help of this program.

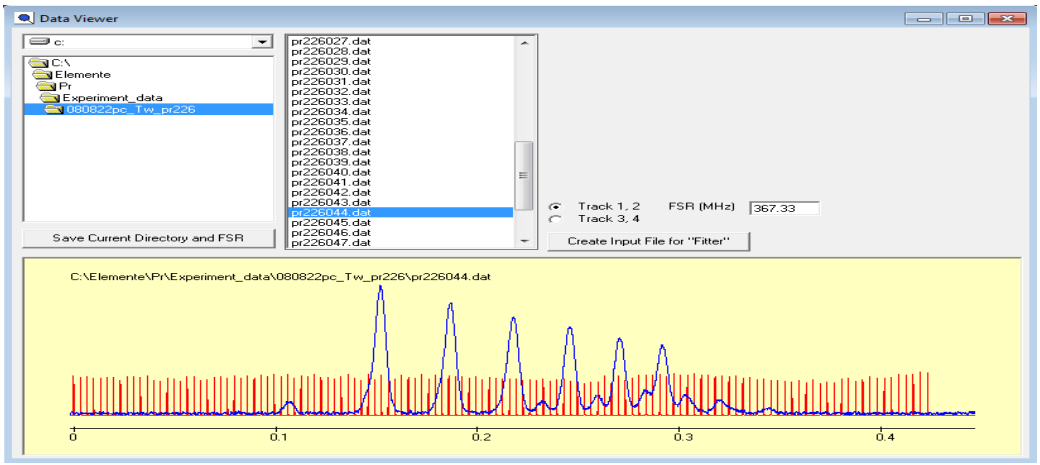

Figure 5.7: Data viewer displaying the recorded LIF Pr226044 data file.

Characteristics of this program are:

I. It enables us to choose best recorded file for data analysis.

II. It creates input "mes" file for fitter program.

III. It provides center of gravity of fluorescence line.

IV. It can convert wavelength into wave number and vice versa.

5.5.2 Classification Program

Presently our database contains ca. 2700 known energy levels of Pr I and ca. 350 known levels of Pr II. The wavelength table contains ca. 29000 spectral lines (Ar, Pr I, Pr II). For evaluating and predicting the hf structure of spectral lines of praseodymium contained in the database, a special computer program (classification program) has been developed by L Windholz (Institute of experimental physics, Graz, Austria) [90]. It is a comprehensive program for evaluating the spectrum of any element. The viewer version of this program is available on internet. This program has been developed in such a way that it uses three data files for particular element. These data files are following

I. A data file which provides the information of all known levels of an atom. In general name of this file as Level_symbol of element. dat for example our investigated element is praseodymium i.e. Level_pr.dat. Let us give an example of a level stored as one line in this file

8.5, o, 27405.036, 653(2),-,*Tw090819 pr411030 a6596.872 pr451010 a5669.049 f+5364 f5670

The first entry is angular momentum, next entries are parity, energy, A and B values of level and comment about the level.

II. A data file which presents all known levels of first ionic state of atom. Name of this file is given by Lev_prii.dat and its example is

7, e, 26445.09, 523.62, -, *Gi89 Tw100917 mK641 pr580039 a7451.729 f++4031

Here entries are in same order as mention in above (atomic level) example.

III. The wavelength table is a data file which give the information about all known spectral lines whether classified or unclassified. Example of a classified line is

5355.603, , , , , 29335.783, 6.5 , e, 581.12, , *Tw090131, 10668.96, 7.5, o, 951.310 ,-2.670, CG81 GrHi99, (PrI) Tw090131 pr322005 a5683.651 pr363003 a6248.315 pr441004 a6519.884 f3575 f+5355 f6247

The first entry is wavelength in Å in air, next four entries are for intensities from different sources. Since this line is classified, next entries are energy, angular momentum, parity, magnetic dipole constant A and electrical quadrupole constant B and comment about the upper level. Then it is turn for lower level for which entries are filled in a similar manner as did for upper level. In last, name of person/names of persons or group who discovered or investigated this line, file numbers, excitation wavelengths and fluorescence lines are mentioned in the comments.

Some modification has been done in classification program from time to time since 2003. Latest version of classification program displays three windows (left, middle and right windows) with menu bar at top and various buttons such as “Insert Line” and “Go to Lambda” for selected spectral line. The left side of window displays the center of

gravity (cg) wavelength and the wave numbers of current line and also shows the previous and next lines. For a classified line, energies, the angular momenta, parities, hf constants of upper and lower levels and comments with each level are displayed. Name of person/names of persons or group who discovered the levels are given in this comment lines. With the help of dispersion formula of E K Peck and K Reeder [91] the center of gravity wavelength of current line is changed into the wave number and, difference of center of gravity wave number and calculated the wave number (difference in wave numbers of upper and lower levels) are also displayed. This difference is a criteria to understand how accurately the energies of upper and lower levels and wave number of center of gravity are known. This window also shows the hf structure of this spectral line graphically (as shown in figure 5.8).

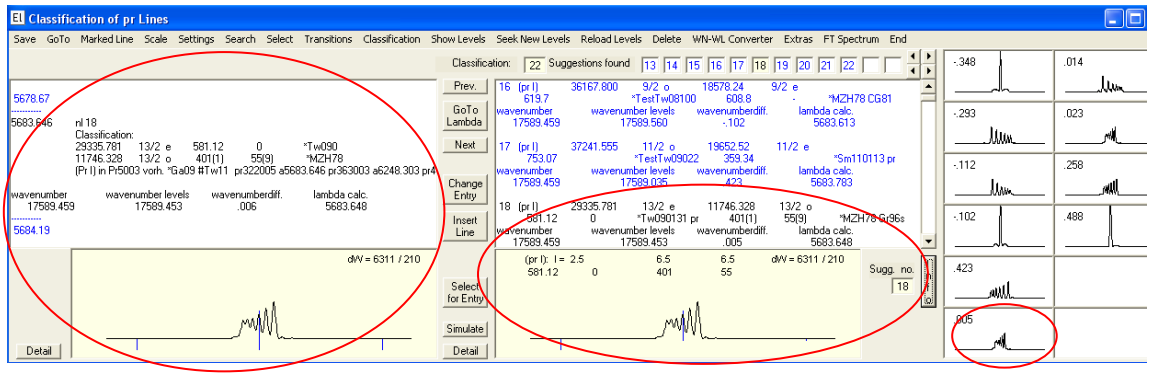

Figure 5.8: Classification program shows the left, middle and right windows for classified line λ= 5683.646 Å.

Middle window shows all possible suggestion for currently selected spectral line for both atomic and ionic transition within the setting of wave number difference limit ($0.5cm^{-1}$) provided transition rules ($\Delta J = \pm 1, 0$ and parity) are not violated. Here options are also available either to display only atomic transitions or ionic transitions or both. The graphic field of this window exhibits the hf structure of selected suggestion, if the hf constants of the involved levels are known.

Right window exhibits all hf structures for possible suggestion of selected line for both atomic and ionic transitions. Difference in wave number also appears in each graphic fields of hf structure. This difference in wave number indicates how the given hf

structure is near or far from currently selected spectral line. This serves to give a fast comparison between suggestions and observed hf pattern.

The classification program makes the life of researcher easier and salient features of classification program are good example of this statement i.e.

I. In order to save wavelength table after editing, it can be done by using the "Save" button in menu bar.

II. "Go To" button in menu bar allows us to navigating to any line for example go to lambda start, lambda (insert any wavelength), lambda min and lambda max.

III. "Marked line" button in menu bar serves as the option for marking two lines for after that to move on it.

IV. "Scale" button in menu bar allows us to change the size of graphic field of hf structure of selected suggestion.

V. "Setting" button in menu bar lays down the certain parameters for classification program. For example it imposes the boundary condition for following parameters: Wavelength difference limit, Wave number difference limit, Wavelength limit for fluorescence lines, Doppler width, nuclear spin quantum number, Ionization limit atom, Ionization limit ion, New levels wave number difference limit, New levels lowest wave number so on.

VI. "Search" button in menu bar sets the search criterion for seeking all possible suggestion for currently selected spectral line for both atomic and ionic transitions, and either only atomic transitions or ionic transitions provided transition rules are not violated ($\Delta J = \pm 1, 0$ and parity). If angular momentum J is not certain, then it searches all possible transitions for any arbitrary ΔJ.

VII. "Select" button in menu bar picks the lines with different option such as it chooses all lines in wavelength list or it prefers lines with a certain level energy and so on.

VIII. "Transition" button in menu bar gives options to select different transitions, for example it shows transition: from upper level (positive fluorescence lines),

from lower level (negative fluorescence lines), to upper level, and to lower level.

IX. "Classification" button in menu bar provides options for either using classification routine or deactivating classification routine.

X. "Show levels" button in menu bar exhibits the list of all atomic or ionic levels sorted by with respect to energy, J and energy, and J and A.

XI. "Seek New Levels" button in menu bar serves as option for searching a new level based on current line, on special level, on fluorescence lines and on A and J.

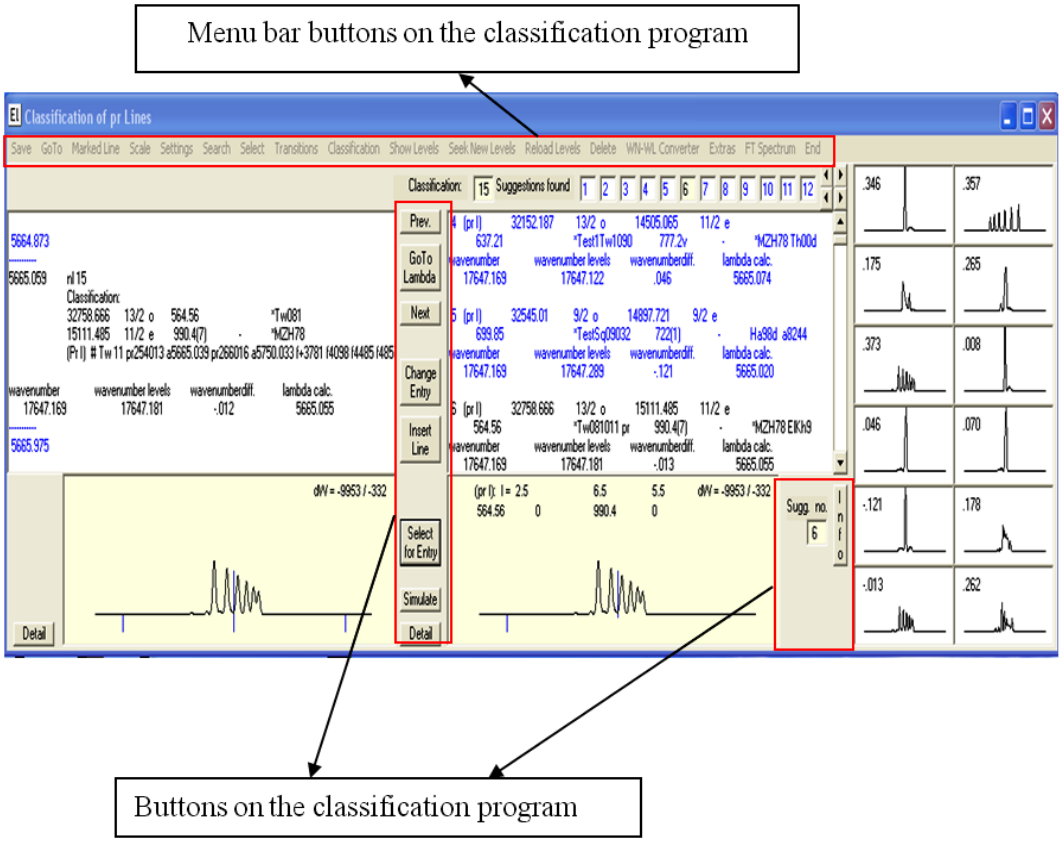

Figure 5.9: Keys function for the classification program.

XII. "Reload Levels" button in menu bar reloads the Level_pr.dat (atomic levels) and Lev_prii.dat (ionic levels) from up-to-date files.

XIII. "Delete" button in menu bar gives the option to delete the current line or classification.

XIV. "WN-WL Converter" button in menu bar opens a window which uses Peck and Reeder dispersion formula for either converting wavelength into wave number or vice versa. It also provides the difference between two wavelengths into wave number.

XV. "Extra" button in menu bar can be used to calculate all possible new atomic (even or odd levels) or ionic (even or odd levels). It also calculates atomic or ionic line wavelengths. It updates wavelength file.

XVI. "FT Spectrum" button in menu bar provides option either to open a window of FT Spectrum or to close it. Window shows the recorded FT spectrum of element (in our case for praseodymium), if FT Spectrum of element is available and window of FT Spectrum also contains some buttons, for example, the intensity and width of FT Spectrum can be changed by using these buttons. Also FT Spectrum can be moved either right or left by using these buttons. Clicking of mouse at any point of FT Spectrum gives the values of wave length in air, wave length in vacuum and SNR.

XVII. "End" button in menu bar terminates the classification program.

XVIII. We can select any classified line out of thousand lines. This can be done by using the buttons either "Go To Lambda".

XIX. With the help of "prev. or next" buttons we can scroll to previous or next spectral lines.

XX. We can edit the wavelength table having already entered line with the help of "Change Entry" button. Some essential data can be written down regarding to the spectral line in the window of wavelength table which is opened by using the "Change Entry" and "Insert Line".

XXI. We can add a new line in the wavelength file by using the button "Insert Line" without opening the actual file.

XXII. It is possible to choose any suggestion from the suggestion list of the selected line and add it to wavelength table for classification of line. This can be done by using "Select for Entry" button.

XXIII. “Simulation” button opens the window which not only shows information discussed in “Detail” button but also simulates the hf structure of the classified or unclassified line and some additional key functions. It will be discussed in more detail in particle 5.5.2.1.

XXIV. “Detail” button opens the window which shows two portions. Upper portion shows the wave length in air of selected spectral line and the transitions between hf levels of upper and lower levels. Lower portion displays the hf structure of selected suggestion regarding to current line. This window also shows the ‘finger print’ of the levels.

XXV. “Info” button provides the information about the transition for selected suggestion.

5.5.2.1 Simulation

The hf structure of a classified or unclassified line can be simulated with the help of the Simulation program. This program can be opened from main window of classification program because it is included in classification program. For classification of selected line, it loads the hf constants, angular momenta and parities of both levels involved in the transition from our database and shows the hf structure of line. If a line is selected from FT spectrum then classification program displays all possible suggestions regarding to the currently selected line. One of the suggestions can only be accepted, if well resolved hf structure related to selected line in FT spectrum, completely overlaps with the hypothetical hf structure generated by the simulation program. This simulation program can also be used to make a model for ‘Fitter Program’ because simulation program creates hypothetical hf structure to match with the experimentally recorded linearized hf structure for unclassified line by using A, B and J values. It can be used to calculate the accurate center gravity of line by overlapping of the hf structures of this line from FT spectrum and suggested by classification program.

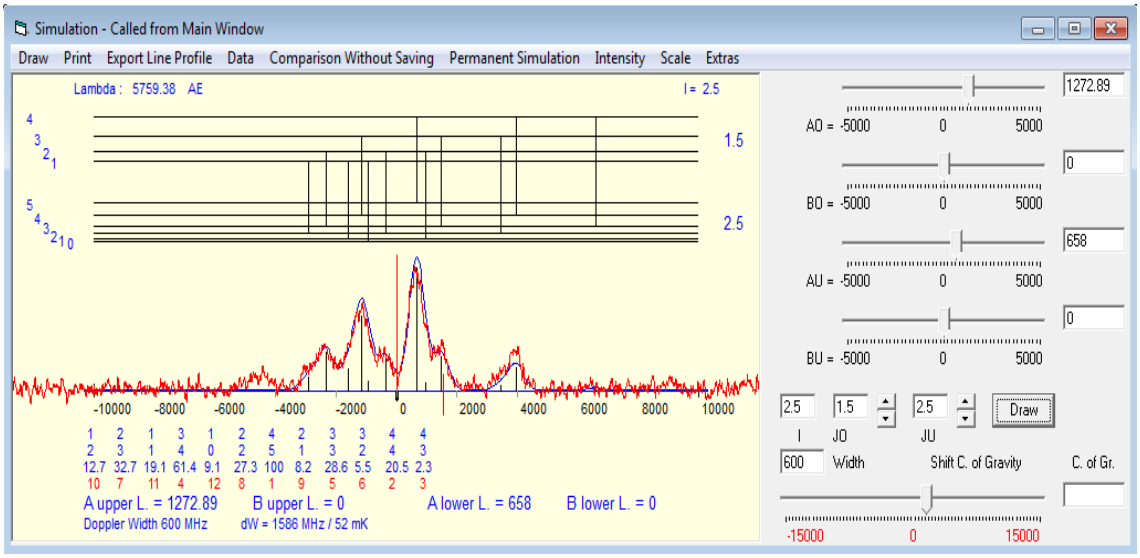

Figure 5.10: Simulation of the line λ = 5759.382 Å and its hf structure taken from experimentally recorded linearized file for unclassified line.

The Doppler width can be changed by using the buttons provided by simulation program. Simulation program warns for violation of Selection rules. Figure 5.10 displays the matching of simulated curve with the experimentally recorded linearized hf structure for unclassified line 5759.38 Å.

5.5.2.2 Classification of a Line by Means of its Hyperfine Structure for Known Levels

If an unclassified line is inserted in the classification program, then main window shows all possible suggestion related to currently selected spectral line. One of the suggestions can only be accepted, if well resolved hf structure related to selected line in FT spectrum completely overlaps with hf structure of this suggestion in the simulation program and their peak positions are also coinciding. In this situation this line can be classified. For example an unclassified line 4612.742 Å having SNR of 18 is inserted in the classification program. One of suggestion is completely matching with line in FT spectrum in terms of shape and peak positions. "Select" for Entry button serves as to select this suggestion for classification. This line is classified as transition between 24519.749 cm^{-1}, Jo = 11/2, even parity, Ao = 555.86 MHz and 2846.741 cm^{-1}, Ju = 13/2, odd parity, Au = 613.240 MHz, Bu = -12.850 MHz.

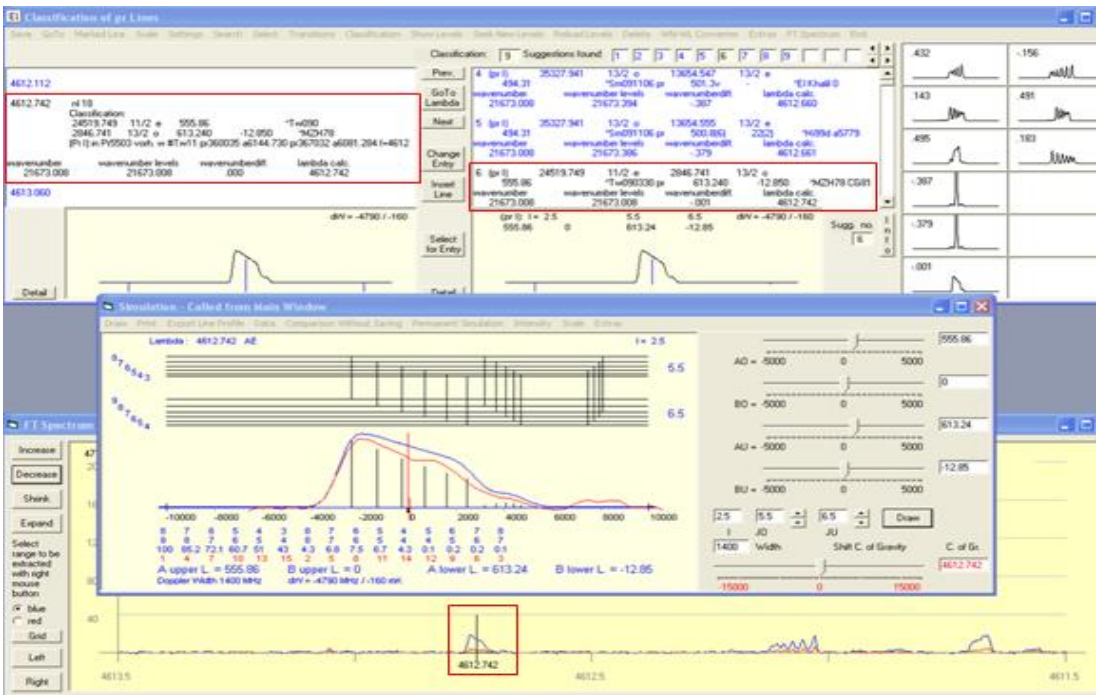

Figure 5.11: Classification of line at λ = 4612.742 Å which is the transition between 24519.749$^{e}_{11/2}$ cm^{-1} and 2846.741$^{o}_{13/2}$ cm^{-1}.

The wavelength table is saved by using the 'Save 'button in menu bar. Figure 5.11 displays the classification program 4612.742 Å with FT spectrum. This method is used by our group to classify large number of lines as transitions between already known levels.

5.5.2.3 Finding a New Level by Combination of the wave Numbers

This method is based on the Ritz combination principle [92]. This procedure has been adopted by our research group to discover the new levels of Ta I in 2003 [90]. This principle can be applied to any element but in case of praseodymium it is not feasible due to very high levels density. Let us see how this method works.

We introduce an unclassified line, in which at least one unknown level is involved in the transition, to our classification program. The classification program then does not display any suggestion for this currently selected spectral line. In order to find the new level by using the wave number of the unclassified line we have to take the following

steps. First of all we have to make an assumption about the parity of new level. Suppose parity is even, then we search for lowest known energy level of odd parity from list of known odd level energies. The energy of hypothetical new even level in wave number is obtained by adding the wave number of line and wave number of lowest level. Then the wave numbers of all other unclassified lines within line list are added to other odd level energies. If energy obtained in this procedure matches with the energy of hypothetical new even level within some uncertainty, then the wavelengths and odd lower levels are listed. Whole procedure is repeated again for next higher odd level and this process continuing till last lower level of odd parity is taken. In the result of this process yields the number of hypothetical new even levels. Selection rules provide the J value of new calculated levels. In order to determine the A and B values of new hypothetical level (only for possible simulation), we have to simulate hf structure of unclassified line by fixing the A and B values of lower level. For confirmation of this new level we simulate hf structure of other unclassified lines which appears as decaying from new level, with the corresponding hf structure in FT spectrum. If simulation of one or more hf structures of other unclassified lines is possible then this new level really does exist. If no new even level is satisfied above mentioned conditions, the whole procedure is repeated for seeking new level with odd parity.

5.5.2.4 Finding a New Level by Fluorescence Lines

This method is also based on the Ritz combination principle. In the result of laser excitation of unclassified line some fluorescence wavelengths are observed and then exact fluorescence wavelengths are measured by using the method which already discussed in the last paragraph of article 5.2.3. First of all we insert center-of-gravity (cg) wavelength of this unclassified line in the classification program. Next step is to open 'seek for new level based on fluorescence lines' button in menu bar of classification program and this button displays the window (subprogram) in which all observed fluorescence lines and excitation of line are fed into it. This program works almost in a same way as discussed in article 5.5.2.3 but uses the selected line

(excitation of line) and lines from data base within the wavelength around the observed fluorescece lines.

5.5.2.5 Finding a New Level by Analysis of Hyperfine Structure

Hyperfine constants (Magnetic dipole constant A and Electrical quadrupole B) are regarded as 'finger print' of a level because both A and B are characteristic of a level. Beyond any doubt the level energy can be identified by knowing the value of J (angular momentum) and pair A and B values. Therefore in this method a new level energy can be determined by analysis of hf structure i.e. by using the values of J, A and B. In the result of laser excitation of unclassified line some fluorescence wavelengths are observed and their hf structures are recorded. Simulation program can be used to create hypothetical hf structure to match with the experimentally recorded linearized hf structure for unclassified line. In practice simulation program gives start values for Fitter program which fits hf structure and calculates the hyperfine constants (better pairs of values of A and B) and center-of-gravity wavelength. But here we demonstrate how useful is the simulation program for evaluating J and hf constants and an identification of new level. For an example we performed the laser excitation of unclassified line at 5798.547 Å and observed the seven fluorescence wavelengths i.e. 3649 Å, 5122 Å, 5913 Å, 5993 Å , 6153 Å, 6285 Å and 6457 Å. On all observed fluorescence signals, the same hf structure was observed indicating that all seven lines belong to the same excited transition and this hf structure did not match with suggestions related to this unclassified line. Therefore we assumed that at least one of the combining levels was unknown. By analyzing the relative intensity and position of the components of the recorded hf structure, it was concluded that the transition was taking place between levels with the same J value ($\Delta J = 0$) and not with a large difference in the values of the hf constants (Ao, Au) of both levels, since the hf structure was not widely split. In order to obtain the pairs of J, A and B values for lower and upper levels we simulated the experimentally recorded linearized hf structure by using the simulation program. We found the Jo = 5/2, Ao = 465 MHz and Ju = 15/2, Au = 320 MHz for completely overlapping of hypothetical hf structure with the

experimentally recorded linearized hf structure shown in figure 5.12. In next step we assumed that upper level was unknown in this transition. We searched known lower level having J = 15/2 and A value for a close to 320 MHz with help of 'Seek New Levels based on A and J' button in menu bar in classification program in a following steps. It displayed a window 'possible new Pr I levels based on A and J' in which the A value of lower level, J values of both levels and accuracy of A value were fed. Program then searched for all possible known lower levels based on A and J values in the database of known levels and generated a transition list for all possible calculated new upper levels. Program displayed all these information into two windows in which left one for even atomic levels and right one for odd atomic levels. Here we assumed that parity of new level was even. We found all recorded fluorescence wavelengths in the first suggestion in the left window as shown in figure 5.13 and therefore,

Known lower energy level = 13002.02 cm^{-1}, Ju = 15/2, odd parity

Au = 316.6(14) MHz, Bu = 29(33) MHz

Wave number of line = 17240.92 cm^{-1}

The energy of new upper level was determined by adding the cg wave number of the investigated line to the energy of the lower level, which is

New Upper Energy Level = 30242.97 cm^{-1}, Jo = 15/2, Even parity.

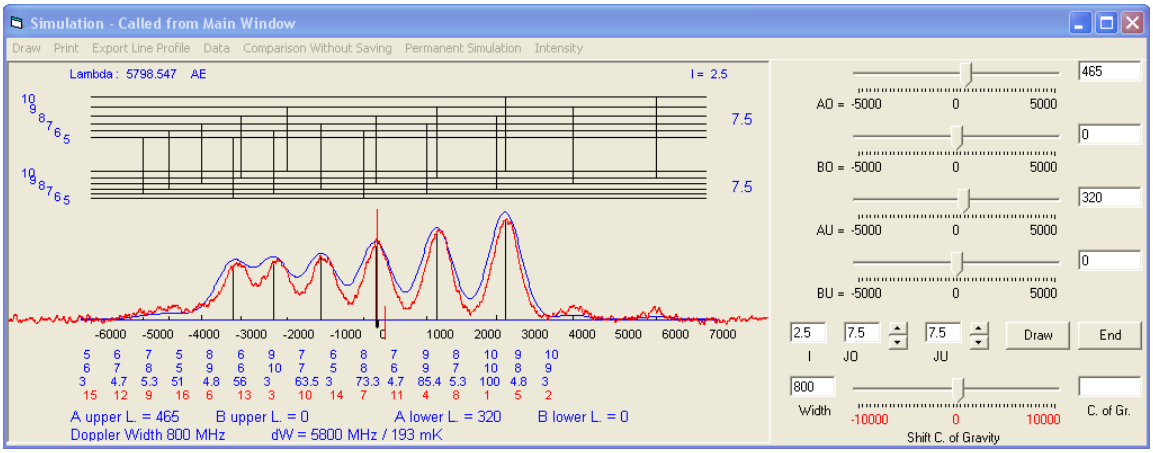

Figure 5.12: Simulation of the line at λ = 5798.547 Å and its hf structure taken from experimentally recorded linearized file for unclassified line.

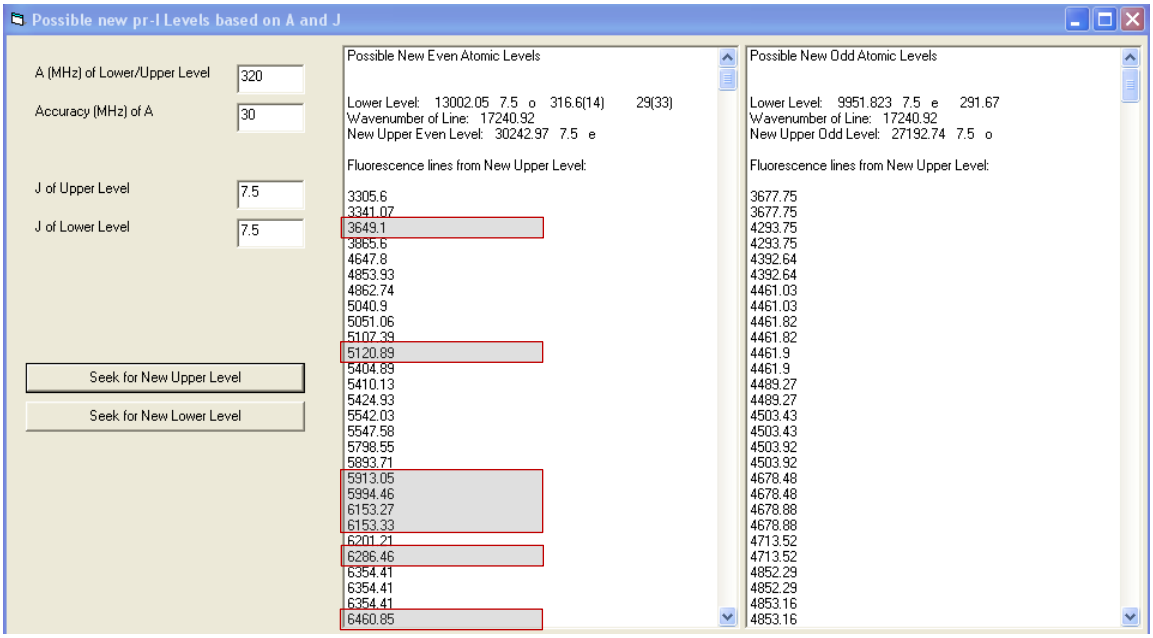

Figure 5.13: Possible new Pr-I upper levels based on A and J values for laser excitation of line at

$\lambda = 5798.547$ *Å.*

Next step was to find the now more accurate hf constants for new upper level (generally it is done using fitter program) and again this could be done by using the simulation program in such a way that we fixed pair of J values (both upper and lower levels) and hf constant for lower level and obtained the hf constants of upper level for overlapping of hypothetical hf structure and recorded linearized hf structure as shown in figure 5.14 i.e. Ao = 460.63 MHz and Bo = 0 MHz. This newly discovered level with energy 30242.97 cm^{-1}, even parity, J = 15/2 and A = 461 MHz was introduced in our level data base. This newly discovered level not only explained all observed fluorescence signals but also one other line of the FT spectrum with respect to its hf pattern and wave number.

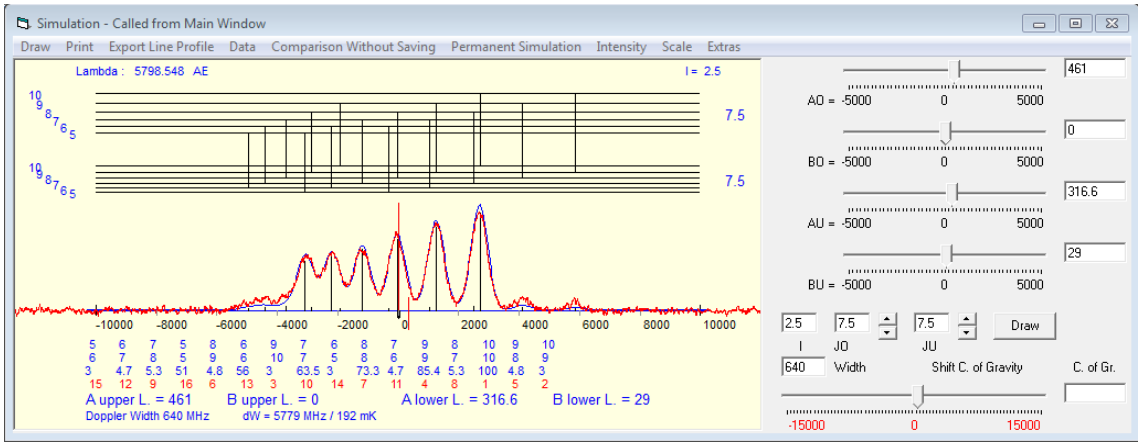

Figure 5.14: Simulation program of line at λ = 5798.547 Å after fixing the pair of J values and hf constant for lower level to obtain the hf constants of upper level.

In last step we made plan to confirm this new level at least one second laser excitation. The new level was then confirmed by two more laser excitations from other known levels, one from 13565.490 cm^{-1} (fluorescence line 5994.46 Å) and other from 15347.428 cm^{-1} (line 6711.57 Å) present in the transition list of the newly discovered level. Finally the newly discovered level with odd parity, J = 15/2, A = 462(5) and energy of 30242.928(25) cm^{-1} explains 10 lines in the visible region. Figure 5.15 displays the level diagram for newly discovered level $30242.928^{e}_{15/2}$ cm^{-1}.

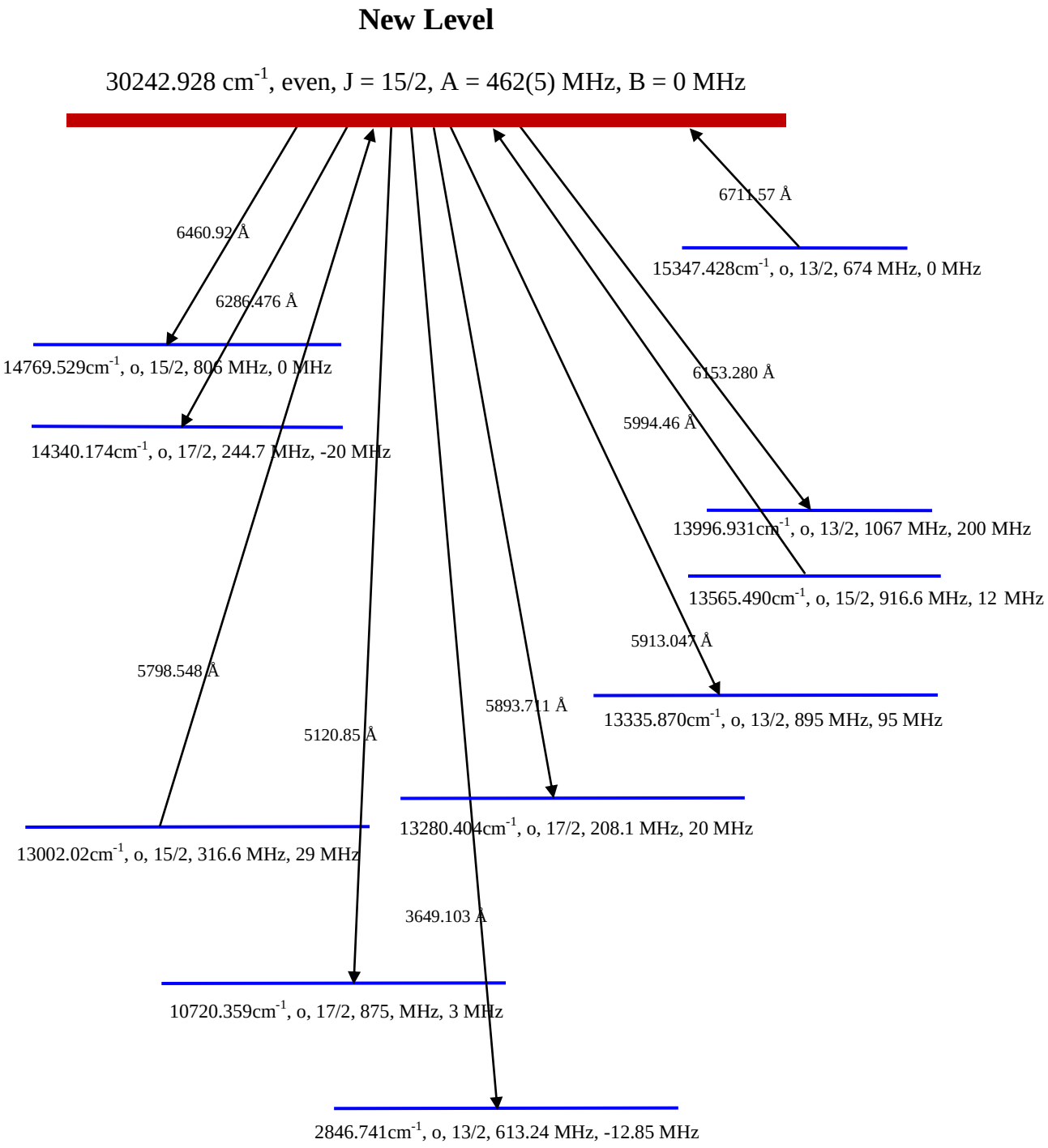

Figure 5.15: Level scheme for new level 30242.928$^{e}_{15/2}$ cm^{-1} at line λ = 5798.547 Å.

5.5.3 Fitter Program

It is an evident from article 5.5.2.5 that how helpful the analysis of hf structure is in determining J, A and B of the combining lower and upper levels involved in the excitation of line. Finger prints (A, B and J) of levels along with the center-of-gravity wave number of the excitation line and fluorescence wavelengths are used to find the energies of both levels involved in this transition. Naturally we are forced to have a comprehensive computer program for fitting of experimentally recorded hf structure of the excited line. This requirement is fulfilled by "Fitter Program" [93]. The fitter program was developed in University of Bundeswehr Hamburg, Germany. The fitter program fits experimentally recorded hf structure using least square method and determines the pairs A and B values of the levels involved in transition and cg wavelength of the excited line. This Least square method is an iteration process in which a curve is fitted to the recorded data points so as to minimize the sum of the square of the deviation of the points from the curve. This program is based on the principle of Least square or Gauss-Newton method. Before computer program is used for fitting the investigated hf structure of the excited line, the recorded file containing data points must be converted into a form readable to the fitter program. In our experimental investigation of the hf structure of a line, the investigated hf structure which is an intensity distribution I(t) profile, is recorded as function of regular time intervals (equidistant time intervals). Recorded data is stored digitally in a computer in the form of a file. Since laser frequency is scanned with time, so it does not vary linearly with time. Due to this fact intensity distribution of spectrum cannot be recorded as function of equidistant frequency spacing. Therefore we use the linearization process to overcome this problem i.e. linearization process converts the intensity distribution I(t) into the intensity distribution I(ν) (where I(ν) as function of frequency (ν)) using equal frequency marker etalon signal which is simultaneously recorded with LIF signals. Linearization process begins when free spectral range (FSR) of the marker etalon and the starting wavelength of the laser scan are fed into digitally recorded data file of LIF signals. The equidistant frequency spacing data points are required for the

fact that mathematical least square method has faster convergence towards the best fit situation with lowest sum of the squared errors (SSE) for data points.

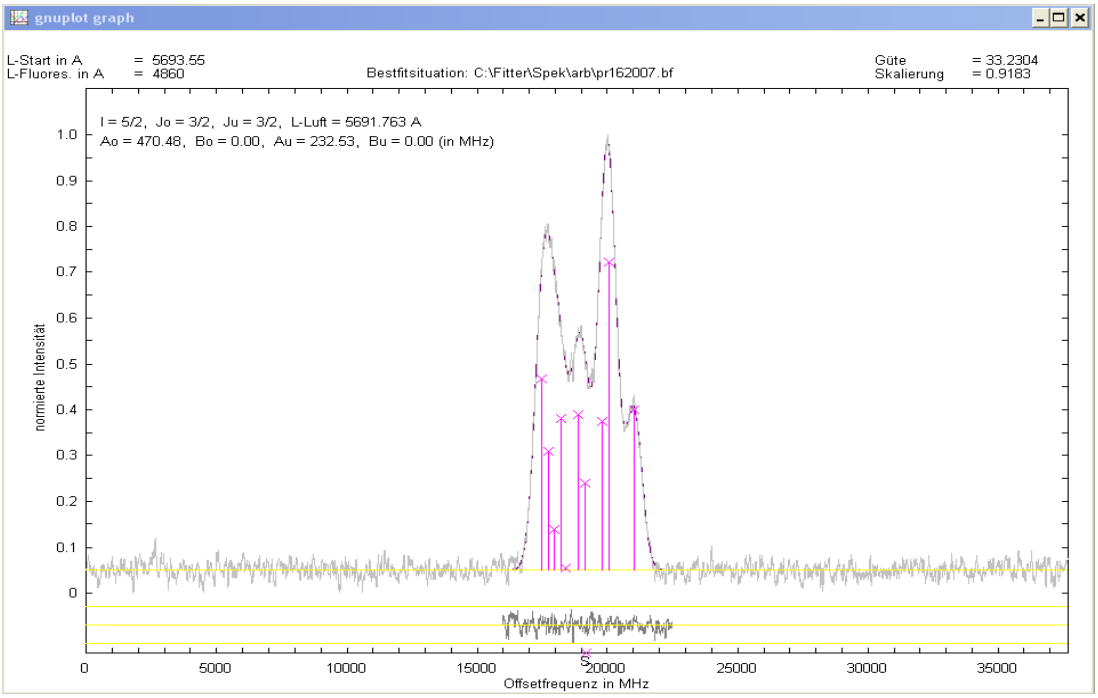

Figure 5.16: Fitting of single Pr I line at λ = 5691.753 Å.

Fitter program takes input parameters such as number of isotopes, angular momentum of lower level (Ju) and upper level (Jo), nuclear spin quantum number of investigated element, frequency position of the strongest diagonal hyperfine component, hf constants (A, B) for both levels, background intensity, the half width of components (hwb), underground intensity and function model (for example Gaussisan or Lorentzian line profile). These parameters can be reduced by keeping some parameters constant (in case of known values). For example if the hwb is known then the number of parameters is decreased by 1. If one of the levels involved in the transition is known then by keeping the hf constants of this level fixed the number of parameters are decreased by 2. Furthermore this can also be done by coupling the relative intensities of various components together. In this way the coupling parameters are decreased by 1. In case of saturation effects, which play the role in changing the relative intensity of some hf components, can be taken into account by coupling of these components together in the

fitting process. Fitter program determines the individual positions of components by using Casimir factors and hf constants for both levels involved in the transition. In addition to single line fitting, if hf structures of two or more are overlapped, then a multiline fitting procedure is used. Fitter program can also work for two or more isotopes simultaneously.

6 RESULTS AND DISCUSSION

The ground state configuration of Pr I is $4f^3\,6s^2$ and is spectroscopically designated as $4I^o_{9/2}$, odd parity. Due to the five valence electrons, praseodymium has a very large number of levels and consequently has a highly dense line spectrum. In recent years the spectrum of praseodymium has been investigated thoroughly by a number of groups [23-25, 29-30, 34-35, 39, 43]. Measurements of the hf structure of Pr I-lines have also been carried out in our group [47, 49, 89, 94].

This work is based on the experimental investigation of the spectrum of praseodymium with emphasis on its hyperfine structure. The investigations were performed in a low pressure hollow cathode discharge lamp by the method of Laser Induced Fluorescence (LIF) spectroscopy. The investigations were performed in the spectral region 4200 to 7500 Å. A high resolution Fourier transform (FT) spectrum for praseodymium was used to extract excitation wavelengths for the investigations of the spectral lines. The major portion of the work was devoted to the finding new fine structure (fs) levels using their hyperfine (hf) structure splitting and measuring their magnetic hyperfine interaction A and electric quadruple interaction B constants. Praseodymium has in most cases a normal hyperfine multiplet i.e. smallest hyperfine level lies deepest in terms of energy. This means that for praseodymium in most cases the magnetic hyperfine interaction A constant of fine structure levels is positive. In most cases the new levels discovered are the upper levels of the investigated lines having energies higher than 25000 cm^{-1}. Most of the low lying levels have already been discovered by previous investigations [24]. A large number of previously unclassified lines have also be classified either by unknown or already known levels using laser excitation. Furthermore, a large number of unclassified lines have also been classified with the help of the FT spectrum of praseodymium by shape position of the hf pattern. Some of the previously excited lines have again been excited in order to improve or correct the spectral parameters (angular momentum J, hyperfine interaction constant A and B) of

the combining lower and upper levels involved in the formation of the line. The chapter is organized in the following manner:

The first part contains some examples of the way how to find previously unknown levels whose investigations were performed during this work. The selection of examples is based on J values ranging from 3/2 to 17/2 of the newly discovered levels. The end of the chapter contains tables of the newly discovered even and odd parity levels, classification of the investigated lines belonging to newly discovered levels, classification of lines belonging to already known lower and upper levels and a table of lines involving already known levels whose hyperfine constants were improved

Table 6.1 contains the data of the newly discovered even and odd parity energy levels. Column 1 lists the angular momentum J values. For each J, the energies (in cm^{-1}) of the levels are given in ascending order in column 2. The hf interaction constants A (MHz) and B (MHz) are listed in columns 3 and 4 repectively. Column 5 contains excitation wavelengths (λ_{exc}) given in Å (in air) and column 6 gives observed fluorescence wavelengths (λ_{LIF}) in Å (in air). Column 7, marked as λ_{FT}, lists the wavelength of additional prominent lines in the FT spectrum which are explained by the newly discovered levels, both in terms of cg wave number and hyperfine pattern but were not experimentally observed as fluorescence lines. For these lines, located in the red or infrared region, the detection sensitivity of our monochromator and photomultiplier tube is not sufficient. Nevertheless, such lines strongly support the assumption that the new level really exists. For some of the new levels we obtained the favourable situation that for one of the combining lower levels the A- and B-values were known with radio-frequency accuracy from ref. [25]. In such cases, we had to determine from the observed pattern only the hf constants of the new upper level. Thus it was possible to determine even small values of B with reliable accuracy. For most of new levels the value of B is neglected because it was found to be very small as compared to the limits of error. In such cases a bar (-) is introduced in column 4. The new levels were confirmed by at least one additional laser excitation from another known lower level (all excitation wavelengths in column 5).

The accuracy of the energies of the new levels depends not only on the excitation and fluorescence lines appearing with good signal to noise ratio (SNR) in the FT spectrum, but also on the accuracy of the energies of already known levels involved in the transitions. These energies have been corrected using the high wavelength accuracy of our FT spectrum [49].

Lines investigated by laser excitation in the discovery or confirmation of newly found levels are given in table 6.2. In column 1 of this table the cg wavelengths are given in Å (in air). In column 2, the symbol ‘nl’ means ‘new line’ i.e. lines which were not known before these investigations and not contained in commonly used tables, e.g. [95]. Column 3 provides the information about the SNR of the lines taken from the FT spectrum of Pr.

When confirming the existence of a newly discovered level, we sometimes have set the laser wavelength to a calculated value (transition to a known level), even the corresponding line is not noticeable in the FT spectrum. Due to the high density of the laser light, excitation of the new level and observation of LIF signals was possible. For such lines we give SNR "-". The cg wavelength in such cases is the value measured with the help of our lambdameter (given with two digits after the decimal point, accuracy 0.01 Å).

If the hf structure of the line in the FT spectrum is in agreement with the hf structure pattern of the corresponding transition, regarding both position and shape, then the cg wavelength of the excited line is taken from the FT spectrum (given with three digits after the decimal point). The absolute accuracy in the cg wavelength for such lines is estimated to be 0.003 Å over the whole range of the FT spectrum. Columns 4 and 5 give the values of angular momentum J and energy of the even levels, where as columns 6 and 7 represent these values of the odd levels involved in the transition respectively.

Table 6.3 presents the classification of all observed fluorescence decay lines. Column 1 gives the fluorescence wavelengths given in Å (in air). Columns 2 to 6 correspond to the respective columns of table 6.2. For lines with SNR column containing "-", the cg

of the fluorescence wavelength has been calculated from the level energies and is given with two digits after decimal point. The hf pattern of such lines is not visible in the FT spectrum, either because of low intensity or because the line is completely masked by another, much stronger transition having approximately the same cg wavelength. Such blend situations are commonly observed in the FT spectrum of Pr due to high line density.

Table 6.4 lists additional lines which are obtained in the FT spectrum and classified based on their hf patterns and wave numbers, involving the newly found levels mentioned in table 6.1.

Table 6.5 gives a list of additional spectral lines, investigated in the frame of this work for the first time by laser excitation, classified as transitions between known levels. For some of the involved levels the values of hf interaction constants A and B could be improved. Table 6.6 lists in columns 1 to 3 the properties of the upper levels of the lines of Table 6.5 and in columns 4, 5 the A and B values determined in this work. Literature values are given in columns 6 and 7. Column 8 contains the reference and column 9 the excitation wavelength.

6.1 Discovery of a new energy level $28465.851^{o}_{3/2}\,cm^{-1}$

The spectral region in the neighborhood of 5759.38 Å (figure 6.1) was investigated which led to the discovery of a new level. The hf structure of the line is completely masked by the hf structure of other nearby lines. Therefore in order to classify the lines in this blend laser excitation was performed. This was done by setting the laser frequency successively to each peak appearing in the blend and searching for the fluorescence signals by varying the transmission wavelength of the monochromator.

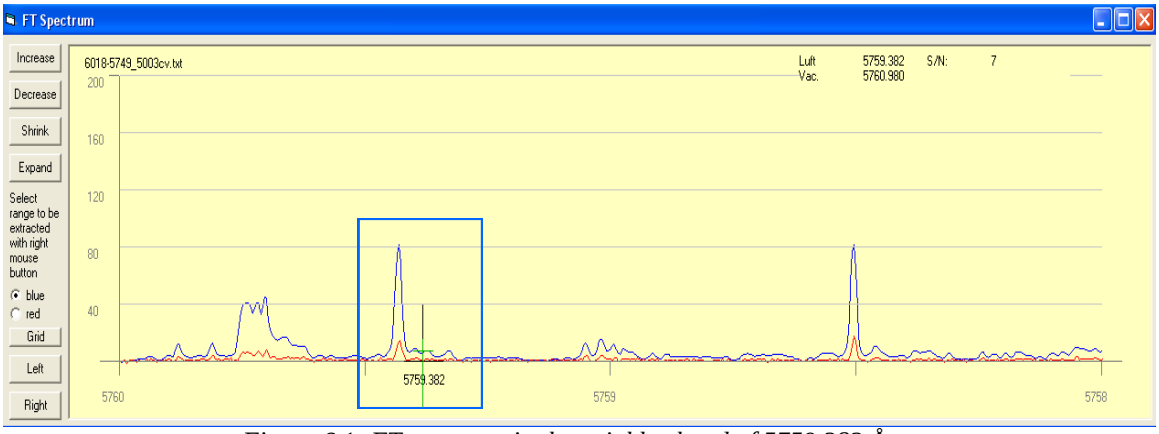

Figure 6.1: FT spectrum in the neighborhood of 5759.382 Å.

In this way we were able to classify a line at 5759.434 Å as a transition between $25721.903^{o}_{17/2}$ – $8363.901^{e}_{15/2}$ giving fluorescence signal at 6860 Å. At excitation wavelength 5759.37 Å a LIF signal was observed on 3255 Å, 4395 Å, 4451 Å, 4541 Å and 5313 Å. On all observed fluorescence lines the LIF signal was recorded by scanning the laser frequency across the investigated region (scan width 45 GHz). Three different hf structures were observed, one at fluorescence line 3255 Å, which allowed to identified the excited lines a transition between the already known levels $33563.151^{e}_{15/2}$ – $16205.041^{o}_{13/2}$ at cg wavelength 5759.40 Å. The hf structure at fluorescence lines 4395 Å, 4451 Å was identified belonging to an ionic transition between the known levels 31906.041^{e}_{2} – 1458.71^{o}_{2} with cg wavelength 5759.42 Å. The hf structure observed at fluorescence lines 4543 Å, 5313 Å (figure 6.2) could not be

identified from any of the listed suggestions for the line in the classification program. This implies that either one or both combining levels are not known and yet to be discovered.

Since the recorded hf structure contains only a small number of hf components, one can guess low values of angular momentum (J < I) of the combining levels. Furthermore, the off-diagonal components lie on the higher frequency side so the change in J is negative i.e. $\Delta J = Jo - Ju = -1$. The strongest diagonal component is on the higher frequency side which implies that magnetic hf constant for upper level is larger in magnitude as compared to that of lower level i.e. Ao > Au. Using these assumptions the recorded structure was fitted and a best fit with minimum SSE was obtained (figure 6.3) at spectral values Jo = 3/2, Ao = 1266.33MHz, Ju = 5/2 and Au = 649.95MHz.

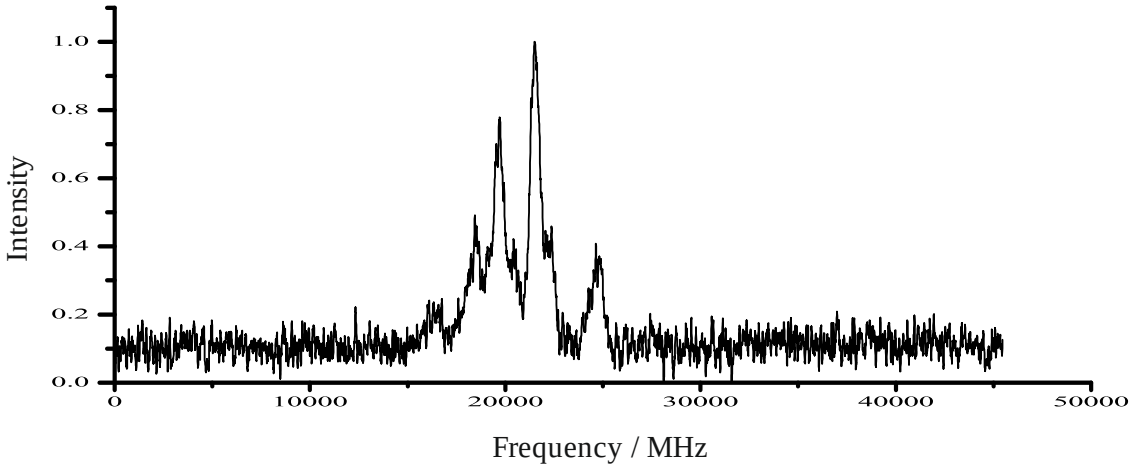

Figure 6.2: Recorded hf structure of the line at cg wavelength 5759.38 Å.

Assuming that the upper level of the excited transition is not known, a known lower level is searched in the data base of known levels based on best fit values of the spectral parameters of the combining levels. One of the suggestions for a possible new upper level explained both the observed fluorescence lines. The known lower level for this suggestion is 11107.690 cm^{-1}, even parity, Ju = 5/2 and Au = 658 MHz. The possible new upper level was calculated by adding the energy of the known lower level and cg wave number of the line obtained from the fitting process, this gives 28465.849 cm^{-1}, odd parity, Jo = 3/2 and Ao = 1266.33 MHz.

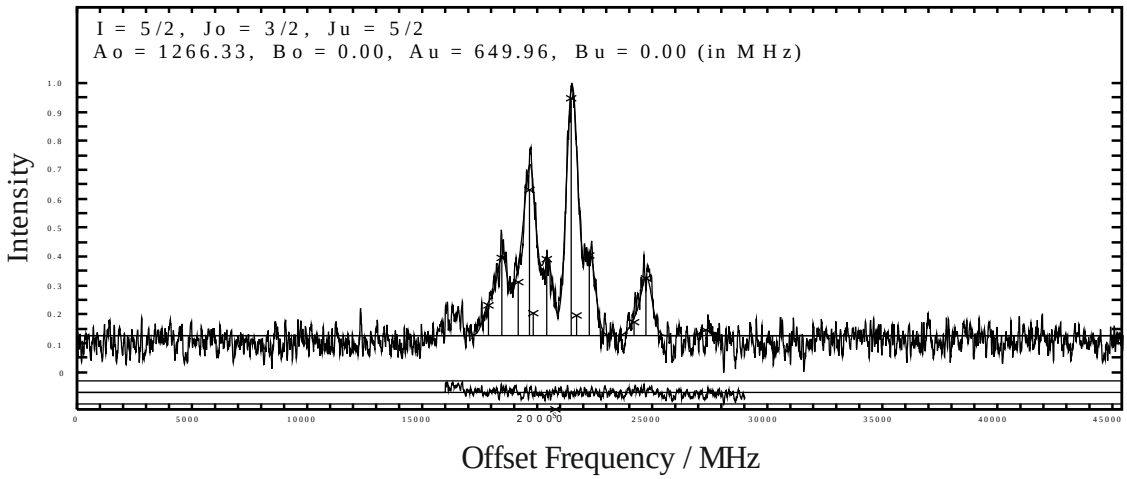

Figure 6.3: Best situation of the recorded hf structure of line 5759.38 Å.

The newly found level is introduced in the data base of known levels and was uploaded in the classification program. At both of the observed fluorescence wavelength 4541.258 Å and 5313.181 Å, good agreement both in terms of shape and position of hf components was observed between hf structure predicted by the classification program and FT Spectrum (figure 6.4). This not only confirms the existence of the newly found upper level but the energy of the newly found level could also be corrected.

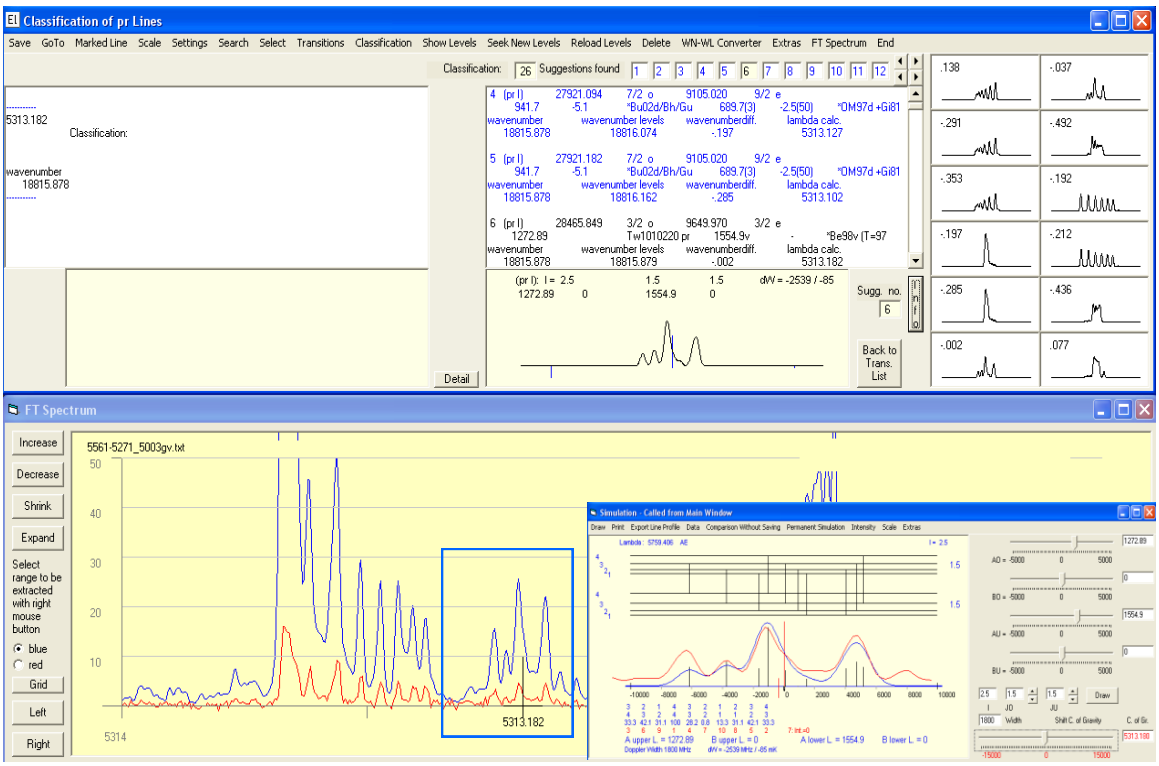

Figure 6.4: A good agreement between hf predicted by classification program and FT spectrum at 5313.182 Å.

In order to further consolidate the existence of the newly discovered level a second laser excitation was also performed at a line 5668.396 Å, appearing in the transition list of the newly discovered level. Although the hf structure of the line 5668.396 Å is completely hidden in underneath the hf structure of a line with much larger angular momentum (figure 6.5). Nevertheless the laser excitation was performed at this line number of fluorescence lines were observed including the fluorescence lines previously observed for the newly discovered level. The LIF signal was observed on 4541 Å, 5313 Å, 5525 Å, 5854 Å, 6321 Å and 6459 Å.

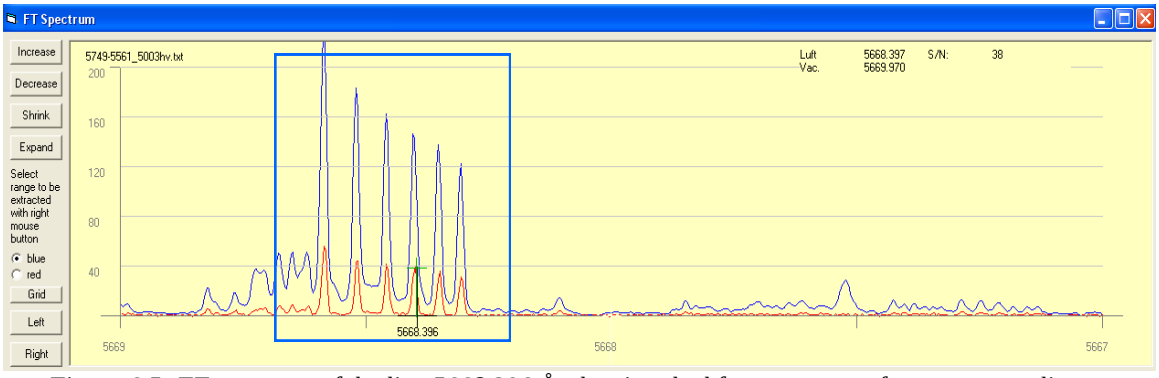

Figure 6.5: FT spectrum of the line 5668.396 Å, showing the hf components of a very strong line.

As expected a widely split hf structure was observed on fluorescence lines 5525 Å, 5854 Å, 6321 Å, 6459 Å belonging to the already known transition 302274.965$^{e}_{21/2}$ – 12638.359$^{o}_{21/2}$. Here we have a blend situation and predicted hf structure is basically overlapping with the 4th hf structure strong component of the line 5668.396 Å (figure 6.5). At fluorescence lines 4541.258 Å, 5313.180 Å, which were also observed previously at the first excitation 5759.434 Å, the hf structure was recorded (figure 6.6) with not good SNR. Nevertheless the observed hf pattern is in good agreement both in terms of shape and hf components with the predicted hf structure (figure 6.7) of the line 5668.396 Å.

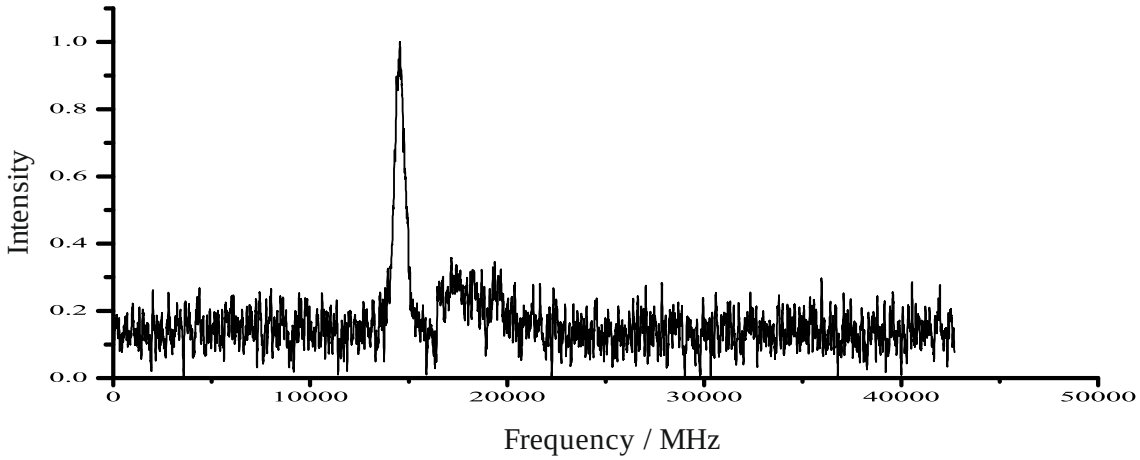

Figure 6.6: Recorded hf structure of line 5668.40 Å.

This confirmed beyond doubt the existence and energy of the newly discovered upper level. By using several recorded files for both excitations the statistical average of the A value of the newly determined level was calculated. The newly determined level 28465.851(20) cm^{-1}, odd parity, J = 3/2, A = 1274(6) MHz explained 4 lines in the

visible region. The excitation and the observed fluorescence lines were classified. The level scheme is shown in figure 6.8.

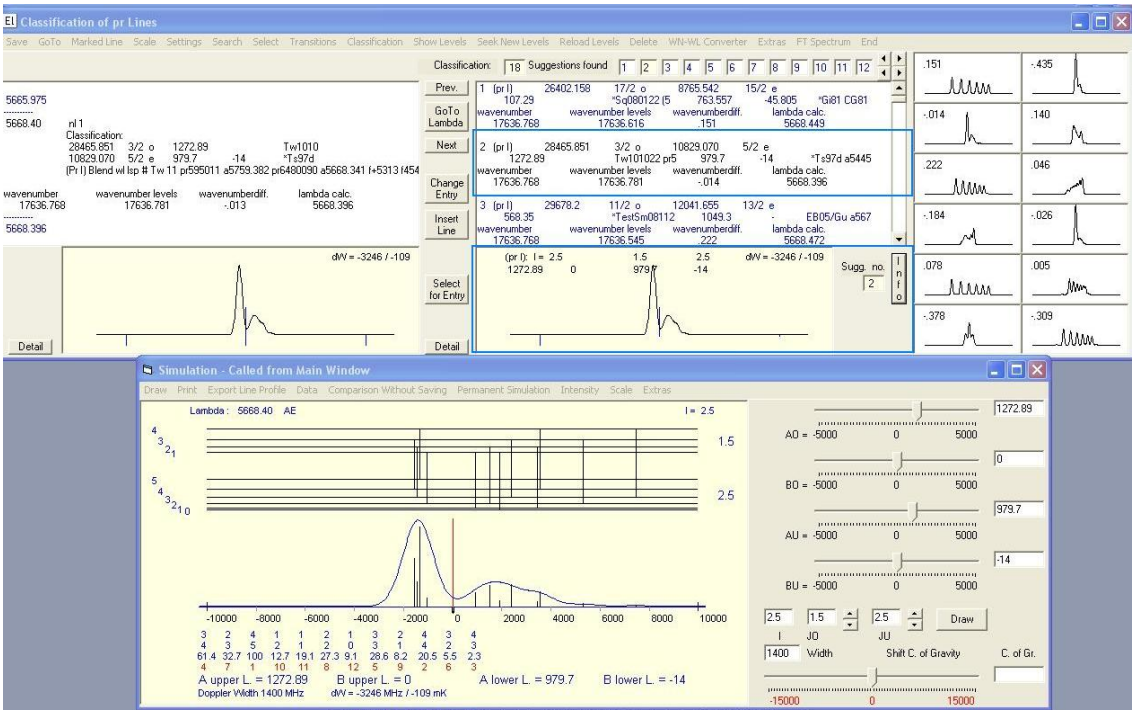

Figure 6.7: Hyperfine structure predicted by classification program for line 5668.40 Å.

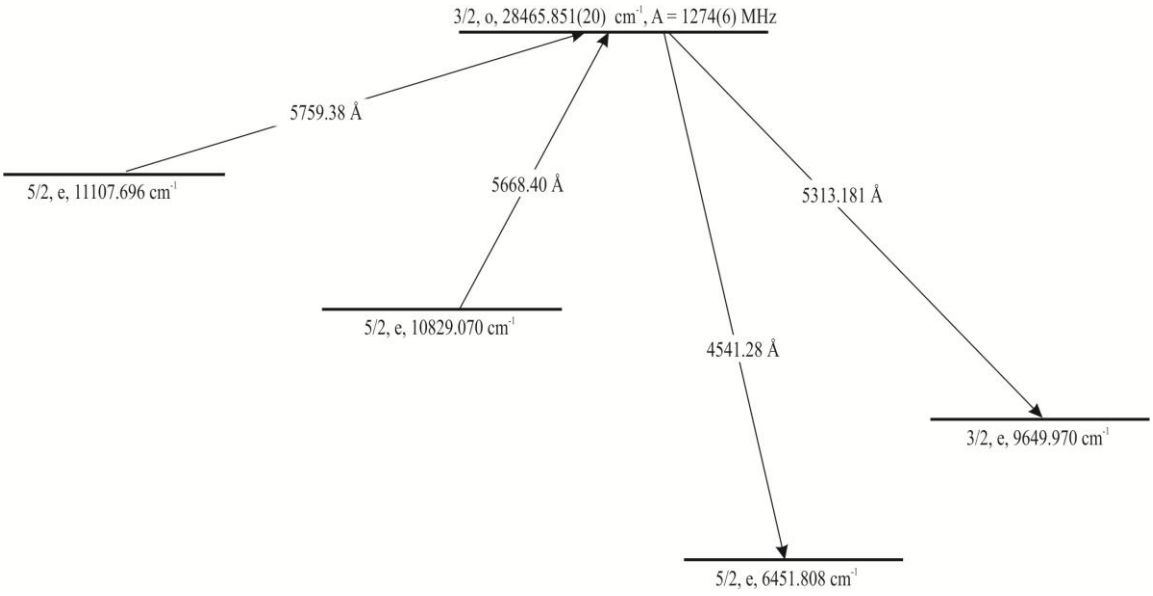

Figure 6.8: Energy level scheme for the newly discovered level 28465.851$^{o}_{3/2}$ cm^{-1}.

6.2 Discovery of a new energy level $30270.526^{o}_{5/2}$ cm^{-1}

The odd parity energy level 30270.526 cm^{-1} was discovered in an attempt to classify a line 5757.65 Å which appears to be a single peak hf structure or a blend of more than one lines. The said line could not be classified by any of the suggestions listed in the classification program, neither in terms of shape nor in terms of hf components positions. The line has a weak SNR with a relative strength of 7 (figure 6.9) but nevertheless laser excitation was performed.

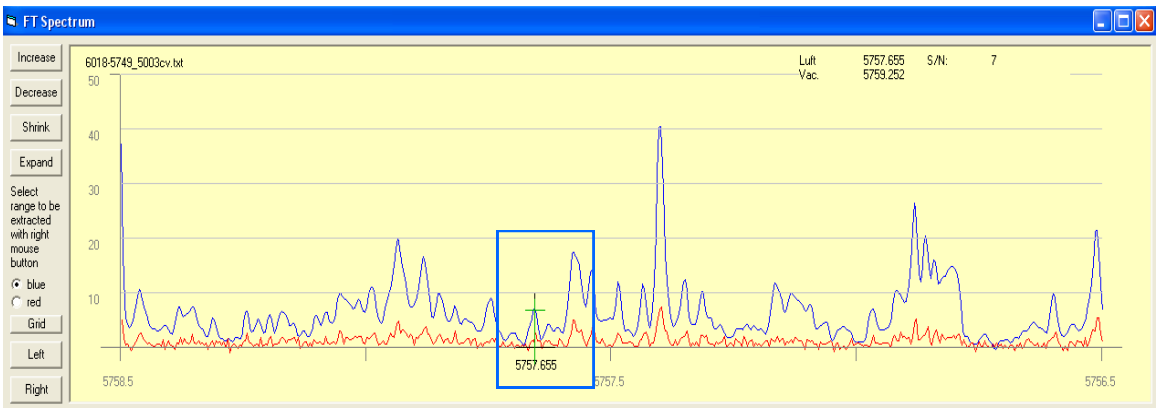

Figure 6.9: FT spectrum of line 5757.65 Å

The laser wavelength was set to 5757.65 Å and LIF signals were searched by tuning the transmission wavelength of the monochromator. LIF signals were observed on a number of fluorescence wavelengths, 4197 Å, 4412 Å, 4491 Å, 4847 Å, 4863 Å, 4979 Å, 5142 Å, 5263 Å and 5486 Å, the strongest LIF signal was observed on 4412 Å. The suggestion list was again inspected but none of the listed suggestions in the classification program showed any coincidence. The hyperfine structure of the line (figure 6.10) was then recorded on all observed fluorescence lines by scanning the laser frequency across the investigated region and successively setting the monochromator to each of the observed fluorescence lines.

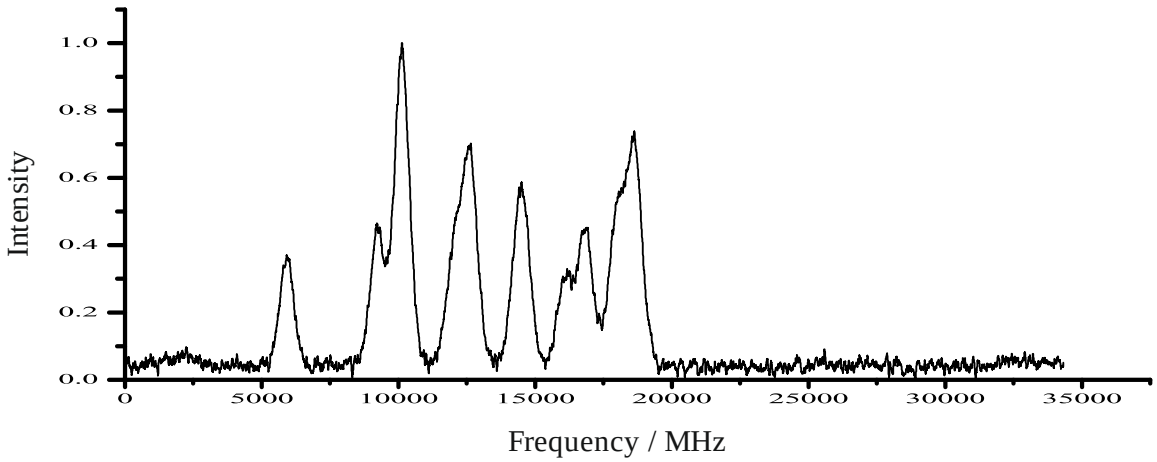

Figure 6.10: Recorded hf structure of line at cg wavelength 5757.620 Å.

Contrary to the expected a single peak structure an extended hf structure was recorded on all observed fluorescence wavelengths. The possible values of spectral parameters were suggested by analyzing the relative intensity and hf component positions of the recorded structure. A sharp decrease in the strength of the diagonal components was noticed indicating a small value of angular momentum of the combining fine structure levels. Moreover the off-diagonal components appear on both sides so $\Delta J = Jo - Ju = 0$. With these assumptions the recorded hf structure was simulated and the obtained J and A values of the upper and lower levels were given to the fitter program as start values. The best fit of the recorded hf structure with minimum SSE was obtained for spectral values Jo = Ju = 5/2, Ao = 845.15 MHz and Au = 1341.18 MHz (figure 6.11).

In the usual manner assuming that the upper level of the investigated line is unknown, a known lower level was searched in the data base of known levels based on A and J values. The search routine displayed a number of suggestions for possible new upper levels. One of the odd parity suggestions explained all the observed fluorescence lines. Using the energy of the known lower level and the cg wave number obtained from the fitting process, the energy of the upper level was calculated i.e. 30270.493 cm^{-1}, odd parity, Jo = 5/2, Ao = 845.15 MHz. The level was introduced in the data base of known levels and was uploaded in the classification program.

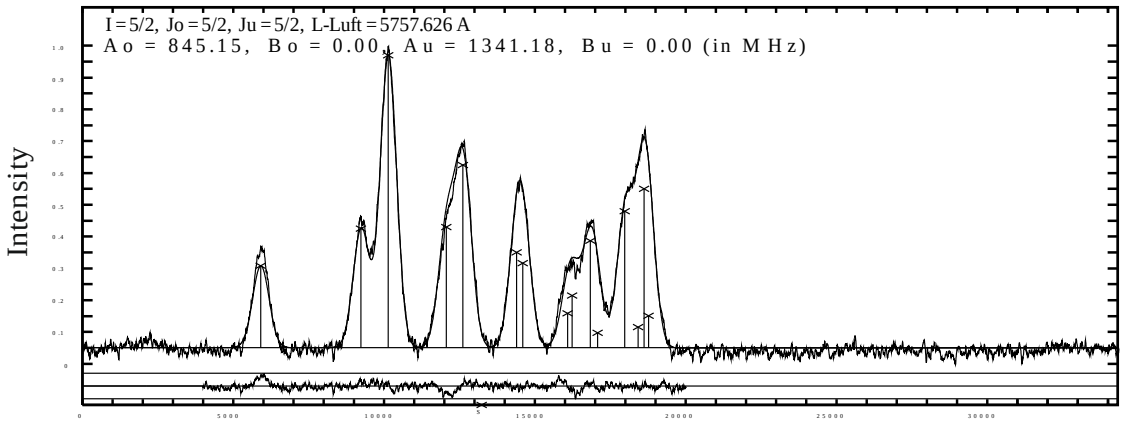

Figure 6.11: Best fit of the recorded hf structure of line 5757.62 Å.

All the observed fluorescence lines were explained by the generated transition list for the new found upper level. Furthermore, at 5262.719 Å, which is one of the observed fluorescence lines, the predicted hf structure of the line is in good agreement with the hf structure profile of a line in the FT spectrum (figure 6.12). At this line since the cg wave number can be determined precisely and the energy of the lower level was also known accurately, therefore the energy of the newly determined level was corrected, i.e. 30270.526 cm^{-1}.

In order to confirm experimentally the existence of the new found level, a second laser excitation from another known lower level (13032.634 cm^{-1}) was performed at one of the line 5799.576 Å taken from the transition list. Although the hf components of the line in FT spectrum are not completely visible, on excitation of this line LIF signals were observed on all previously found fluorescence wavelengths. The recorded hf structure of the line (figure 6.13) is in good agreement both in terms of shape and hf components positions with the hf structure predicted by classification program (figure 6.14).

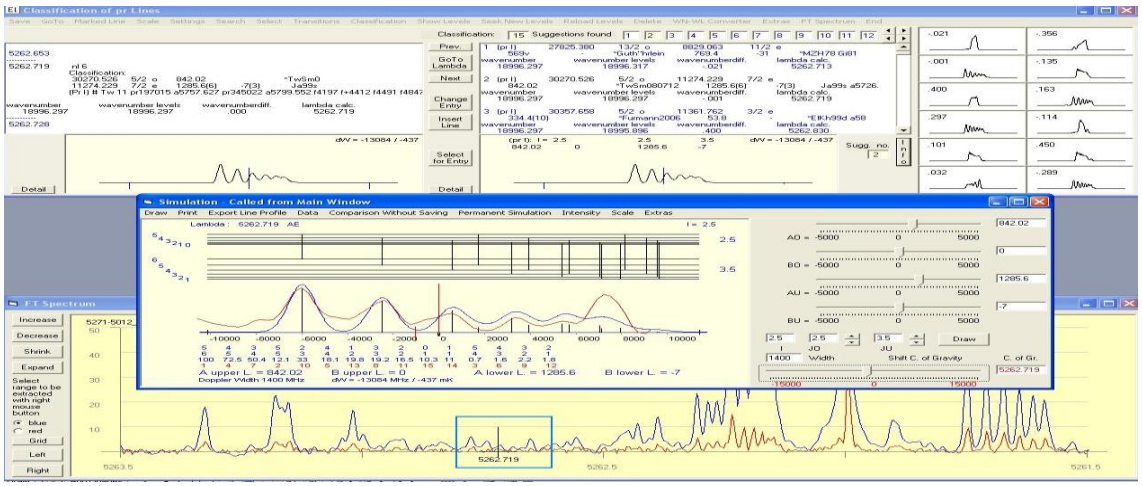

Figure 6.12: A good agreement between hf predicted by classification program and FT spectrum at 5262.719 Å.

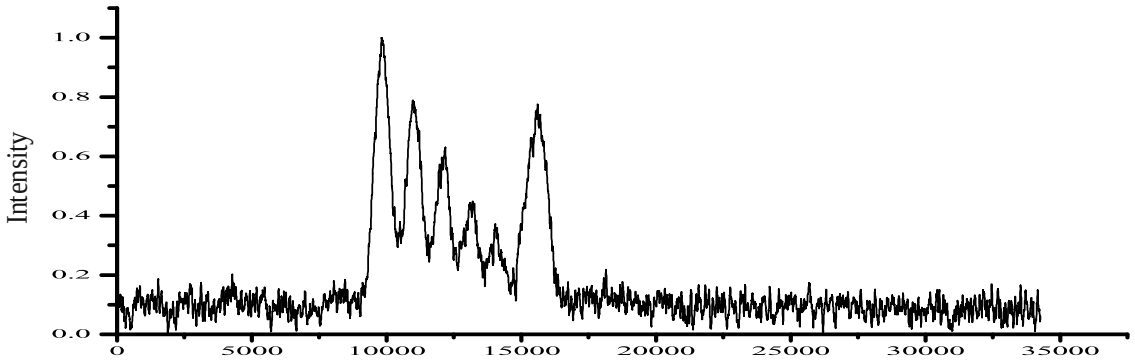

Figure 6.13: Recorded hf structure of line 5799.56 Å.

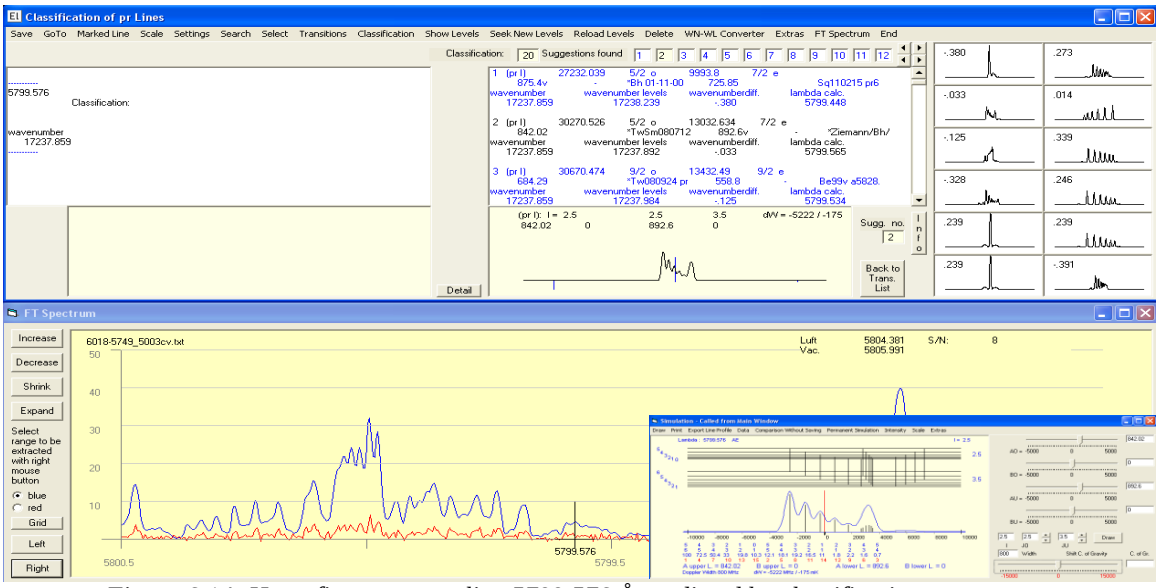

Figure 6.14: Hyperfine structure line 5799.576 Å predicted by classification program.

This confirmed the existence and energy of the newly discovered level. By using several recorded files for both excitations the statistical average of the A value of the newly determined level was calculated. The Newly determined level 30270.526(20) cm^{-1}, odd parity, J = 5/2, A = 844(5) MHz explained 10 lines (excitations and fluorescence lines). The excitation and fluorescence lines were classified. The level scheme for the newly discovered level is shown in figure 6.15.

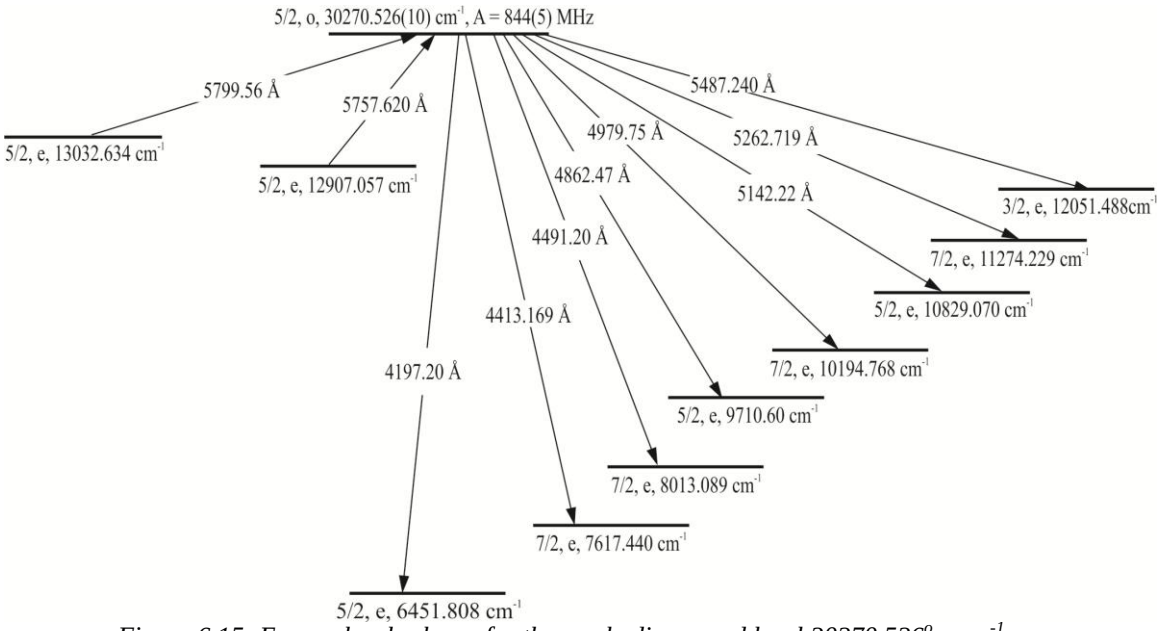

Figure 6.15: Energy level scheme for the newly discovered level 30270.526$^{o}_{5/2}$ cm^{-1}.

6.3 Discovery of a new energy level $28513.764^{o}_{5/2}$ cm^{-1}

The line 5828.608 Å in the FT spectrum shows clearly resolved hf components but the line could not be explained by any of the listed suggestions. This implies that either one or both the combining levels were not known and yet to be discovered. Laser excitation of the line was performed which resulted in a discovery of a new energy level. The investigated line has a good SNR of 24 (figure 6.16).

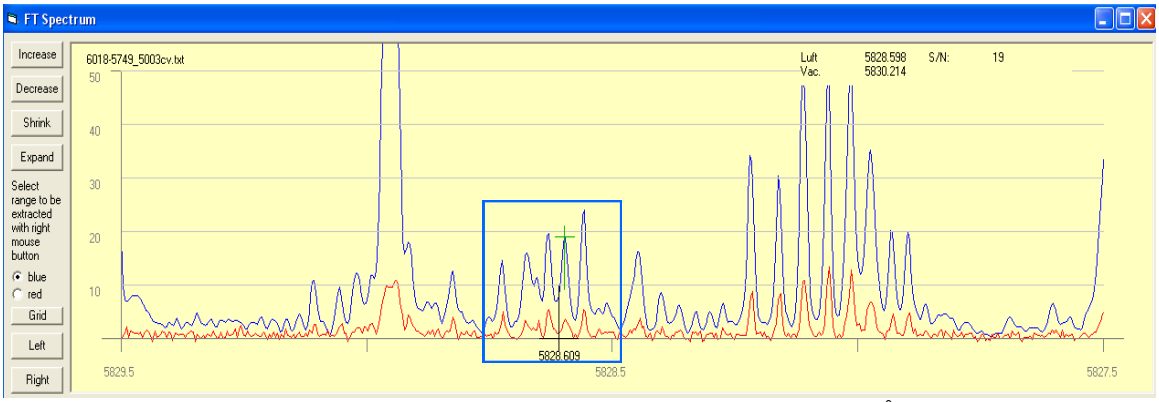

Figure 6.16: A section of FT spectrum for the line 5828.608 Å.

Excitation wavelength was set to 5828.56 Å and fluorescence signals were searched by varying the transmission wavelength of the monochromator. LIF signals were observed on a number of fluorescence wavelengths, 4548 Å, 4876 Å, 5055 Å, 5300 Å, 5316 Å and 5457 Å. The hyperfine structure was then recorded on all observed fluorescence wavelengths and as expected a hf structure profile was recorded (figure 6.17) similar in shape as appearing in the FT spectrum. On all observed fluorescence wavelengths same hf structure was observed indicating that all these lines belong to the excitation of the same upper level.

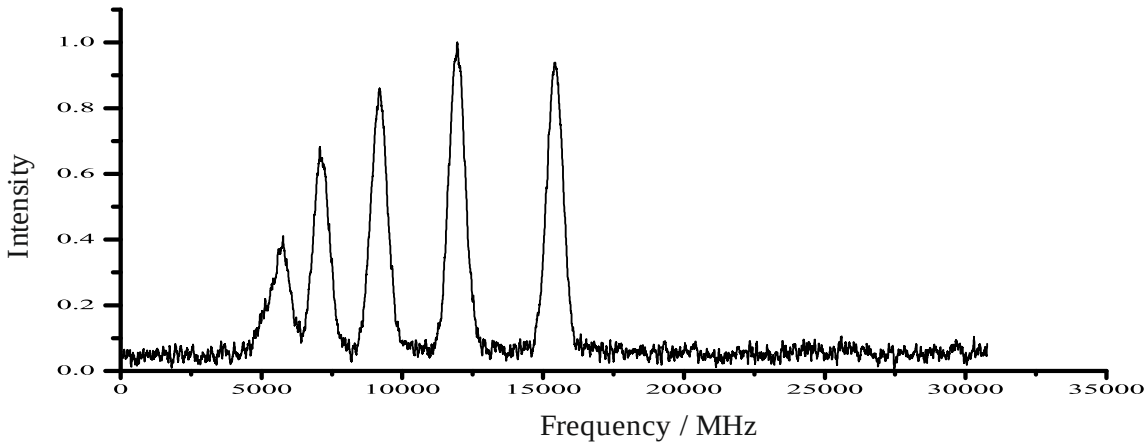

Figure 6.17: Recorded hf structure of the line 5828.607 Å.

In the recorded hf structure five diagonal hf components were visible instead of six. Moreover, the separation between the diagonal components suggested that combining levels have an angular momentum which may be less than 7/2. Furthermore the strongest diagonal component is on the higher frequency side and the off-diagonal components are not seen separated from diagonal components or lying underneath the diagonal components. The former observation suggested that the hf splitting of the upper level is larger than that of lower level which means that A constant of upper level is greater than that of the lower level The later observation suggested that one of the combining levels had a very small hf splitting compared to the other which means a very small A constant.

Using these assumptions the recorded hf structure was initially simulated to obtain possible spectral parameters of the combining levels. Then using these possible spectral values the recorded structure was fitted and a best fit with minimum SSE was obtained for spectral values Jo = 5/2, Ao = 708.61 MHz, Ju = 3/2 and Au = 30.27 MHz, figure 6.18.

As usual it was assumed the upper level is unknown in the combination. A search for a known lower level was performed with J = 3/2 and A value close to 30 MHz. The searching routine listed a number of suggestions; one of the listed suggestions for the possible new upper level explained all the observed fluorescence lines.

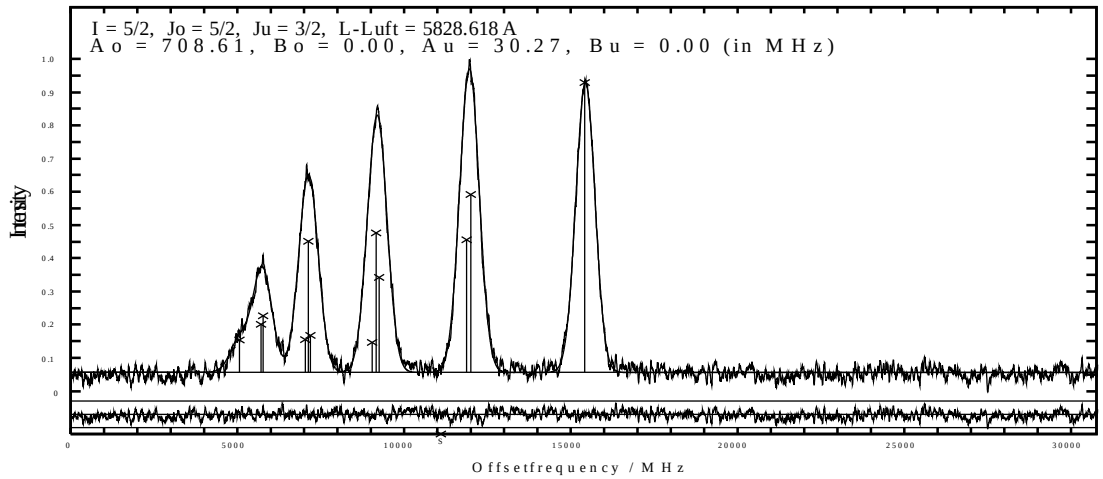

Figure 6.18: Best fit of the recorded hf structure of line 5828.608 Å.

The known lower level of the combination was 11361.762 cm^{-1}, even parity, Ju = 3/2 and Au = 53.8 MHz. The energy of the possible new upper level was calculated by adding the energy of the known lower level and the cg wave number of the line. Since the energy of the lower level was already corrected and in order to have a better accuracy in the energy of the upper level, the cg wave number of the line is taken from FT spectrum which shows clearly visible hf structure profile of the investigated line. The energy of the new upper level is 28513.764 cm^{-1}, odd parity, Jo = 5/2 and Ao = 723.89 MHz. The new found upper level was introduced in the data base of known levels and was uploaded in the classification program. The program generated a transition list which explained all the observed fluorescence lines. The hf structures predicted by the classification program for the lines 4876.526 Å, 5055.159 Å and 5316.776 Å are in good agreement with hf structure profiles in FT spectrum both in terms of shape and hf component positions (figure 6.19). This was a good confirmation of the existence and energy of the newly found level.

In order to further confirm the newly discovered level a second laser excitation was performed from another known lower level. The line 5743.532 Å present in the transition list appear in a blend or mixture of two or more lines in FT spectrum. Nevertheless, laser excitation was performed and an LIF was observed on all previously found fluorescence wavelengths suggesting that same upper level was excited but now from another lower level. Hyperfine structure of the line was recorded

(figure 6.20), on the observed fluorescence lines, which is in good agreement with hf structure predicted by the classification program both in terms of shape and hf components (figure 6.21).

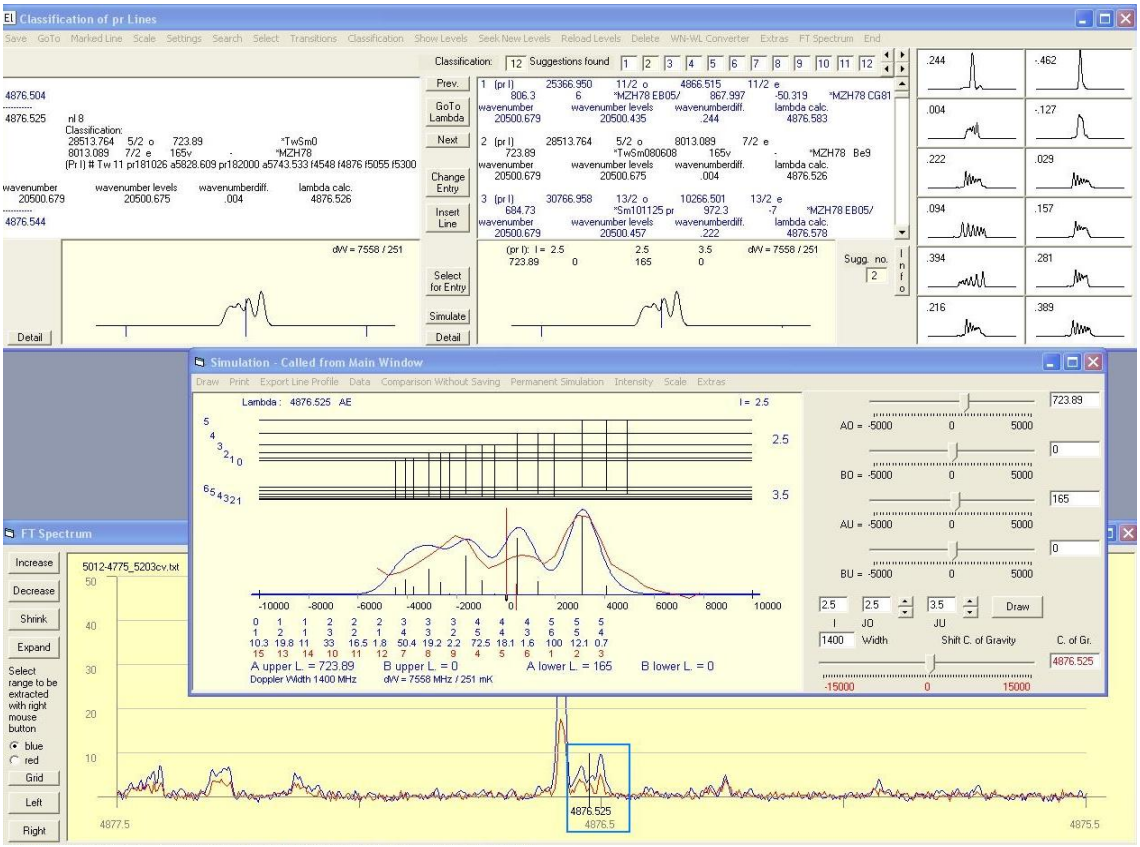

Figure 6.19: A good agreement between hf predicted by classification program and FT spectrum at 4876.525 Å.

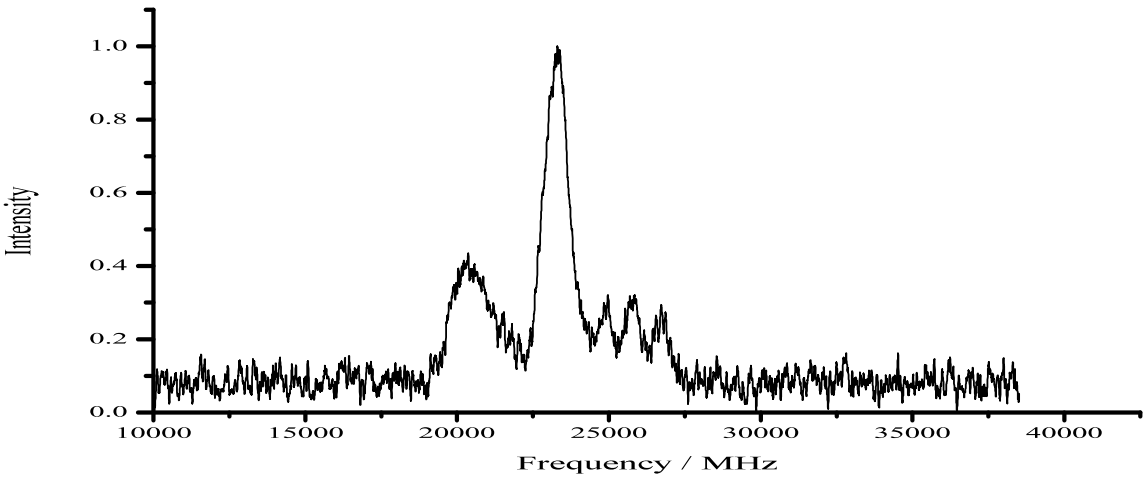

Figure 6.20: Recorded hf structure of line 5743.53 Å.

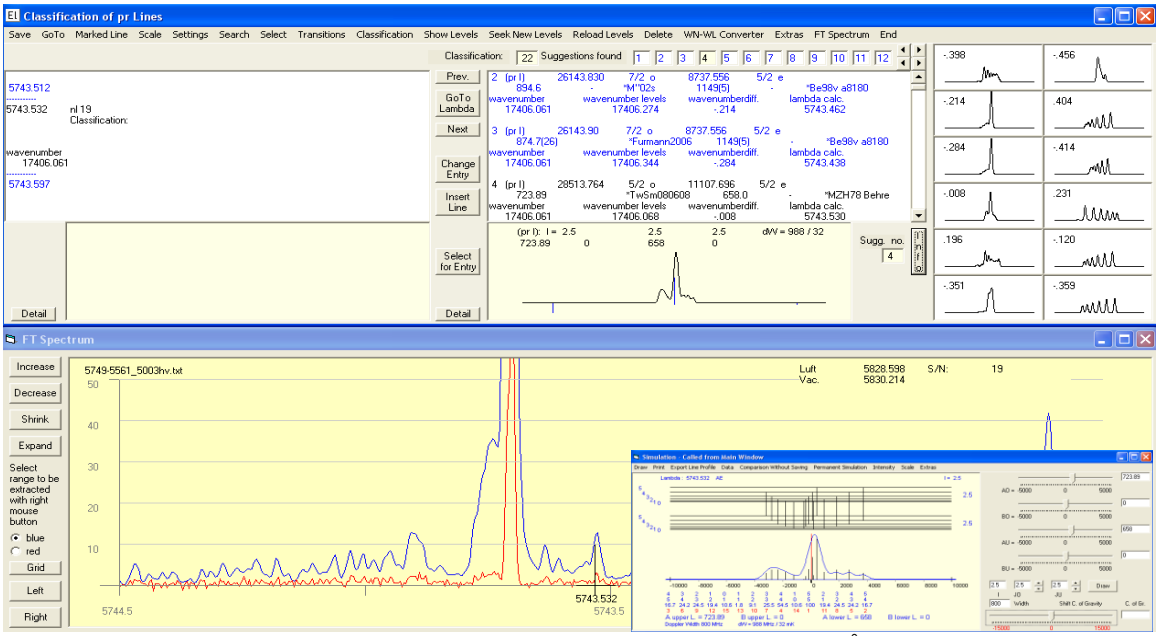

Figure 6.21: Predicted hf structure of the line 5743.53 Å.

By using several recorded files for both excitations the statistical average of the A value of the newly determined level was calculated. The newly discovered level 28513.765(10) cm^{-1}, odd parity, J = 5/2, A = 734(10) MHz explained 8 lines. The excitation and fluorescence lines were then classified. Level scheme for the newly found upper level is shown in figure 6.22.

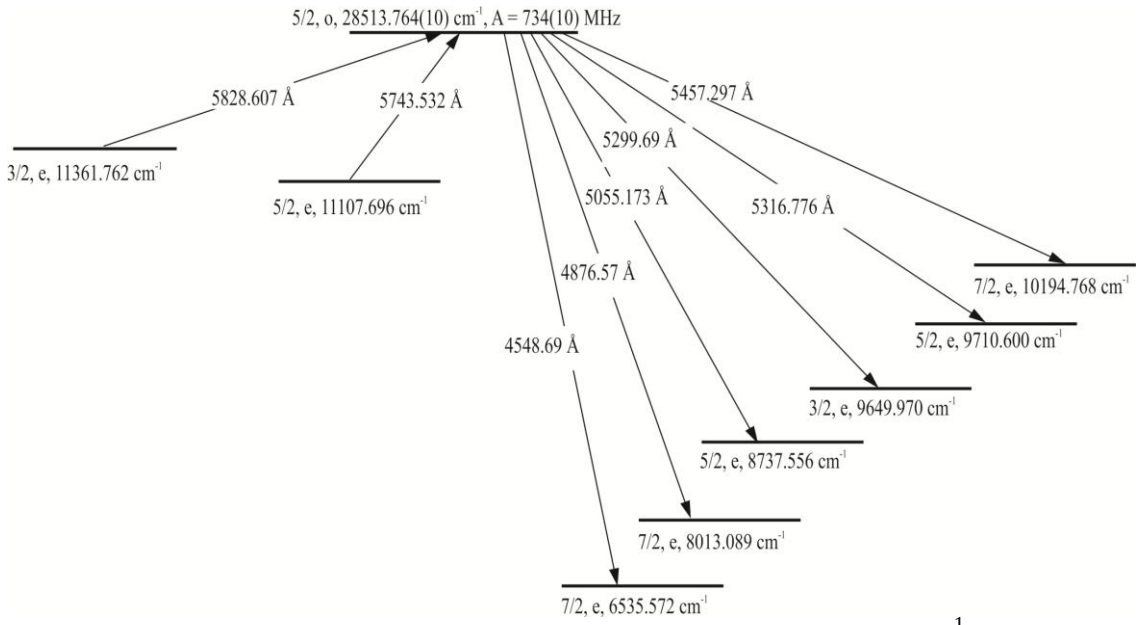

Figure 6.22: Energy level scheme for the newly discovered level 28513.764$^{o}_{5/2}$ cm^{-1}.

6.4 Discovery of a new energy level $29563.401^{o}_{5/2}$ cm^{-1}

A line 4341.35 Å in FT spectrum has a very weak SNR with a relative strength of 2 (Figure 6.23). Because of the weak SNR, the hf components of the line in FT spectrum are not visible and so the line could not be explained by any of the suggestions listed in the classification program. In any case the line was experimentally investigated using laser excitation.

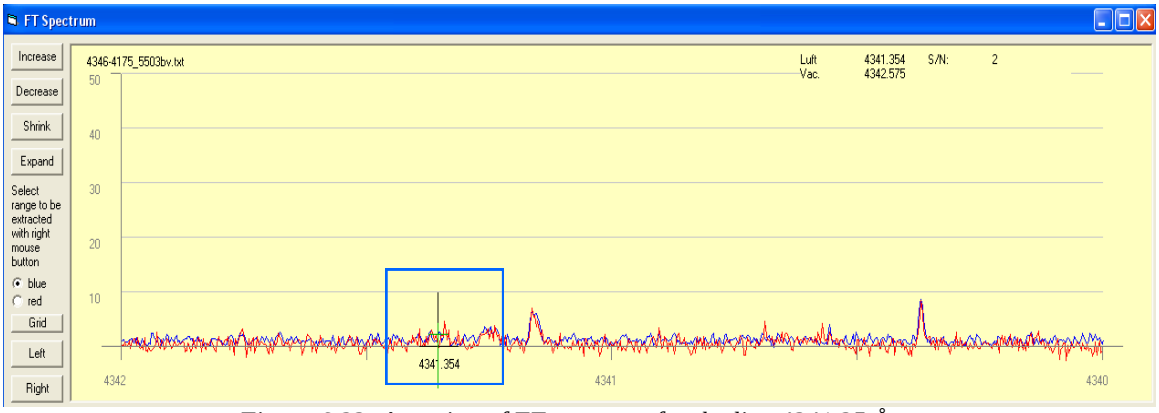

Figure 6.23: A section of FT spectrum for the line 4341.35 Å.

A LIF signal was searched by varying the transmission wavelength of the monochromator and setting the laser excitation wavelength to 4341.35 Å. LIF signal was observed on 4554 Å, 5019 Å, 5089 Å, 5335 Å and 5709 Å and subsequently the hf structure was recorded on all observed fluorescence wavelengths by scanning the laser excitation frequency across the investigated region within a width of 45 GHz. Hyperfine structure was recorded with good SNR on all observed fluorescence wavelengths (figure 6.24). The recorded hf structure was again inspected for a possible match in the suggestion list for line which proved unsuccessful.

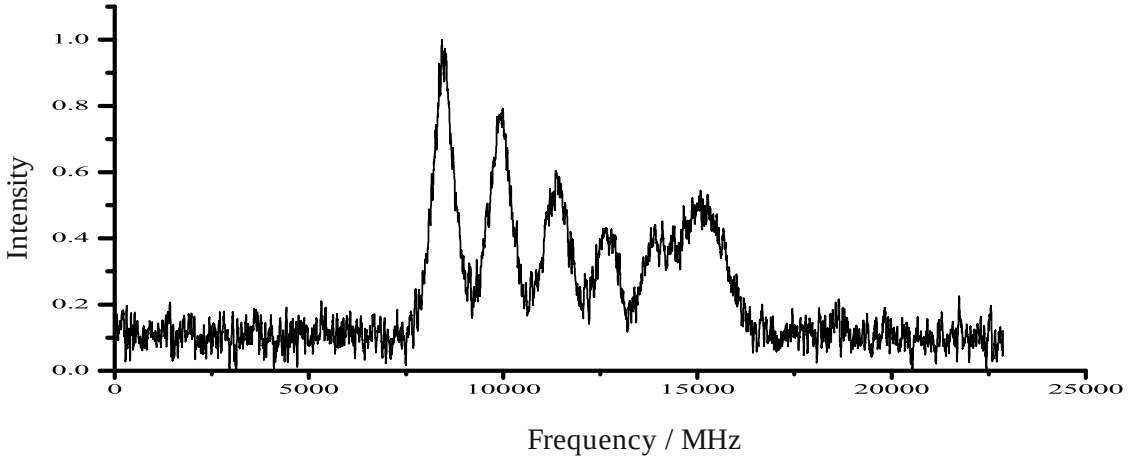

Figure 6.24: Recorded hf structure of the line 4341.35 Å.

The recorded hf structure was simulated to obtain possible spectral parameters of the combining levels. Taking these possible values as start values the hf structure was fitted using the fitter program. A best fit situation with minimum SSE was obtained for spectral values Jo = 5/2, Ao = 835.54 MHz, Ju = 7/2 and Au = 944.39 MHz (figure 6.25).

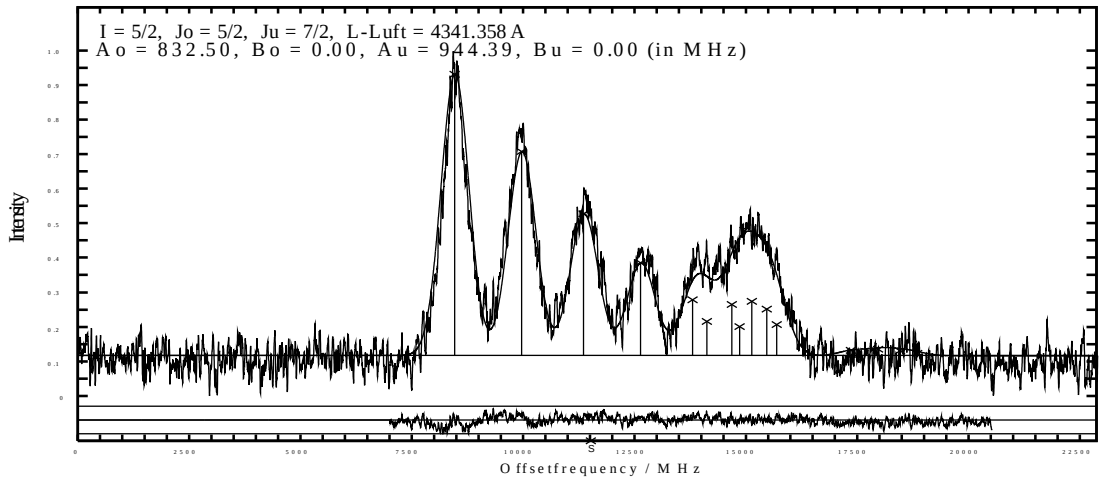

Figure 6.25: Best fit of recorded hf structure of line 4341.35 Å.

Assuming an unknown upper level, a known lower level was searched in the data base of known levels with J = 7/2 and A value close to 944 MHz. The searching routine generates a number of suggestions for possible new upper levels and lower levels which match the searching criteria within the specified searching range of A value of lower level. The transition list of one of the suggestions explained all the observed fluorescence lines, this upper level was considered as a possible new upper level. The

known lower level in the combination for this suggestion is 6535.572 cm^{-1}, even parity, Ju = 7/2 and Au = 979 MHz, Bu = 26 MHz. The energy of upper level was calculated from the energy of the lower level and cg wave number of the line obtained fitting procedure. Thus the possibly new upper level is 29563.321 cm^{-1}, odd parity, Jo = 5/2 and Ao = 871.13 MHz.

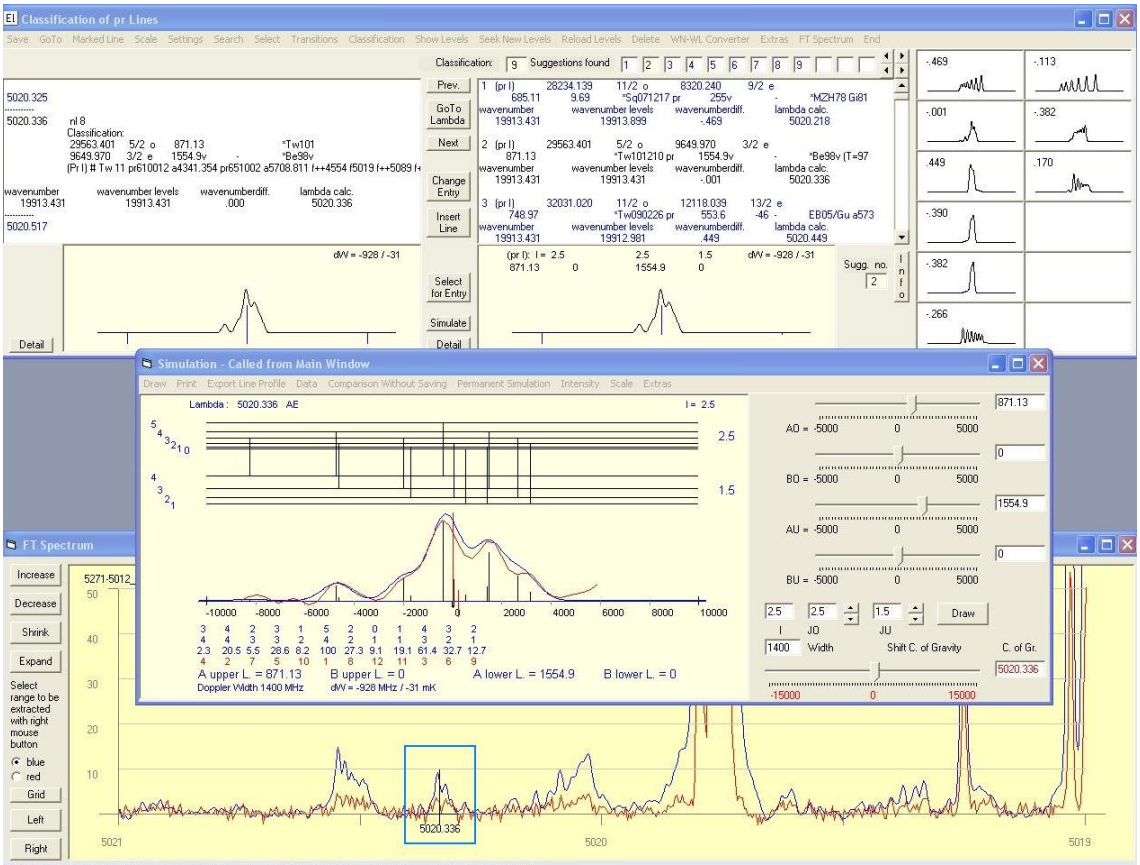

Figure 6.26: Confirmation of the existence of the newly found level from FT spectrum at fluorescence line 5020.336Å.

The newly found level was introduced in the data base of known levels and was then uploaded in the classification program. The generated transition list for the newly found upper level explained all the observed fluorescence lines and the hf structure patterns predicted by classification program for the lines 5020.337 Å, 5088.882 Å and 5336.340 Å which are the observed fluorescence lines are in good agreement not only in terms of shape but also in terms of hf component positions with the hf structure profile in the FT spectrum of the respective lines (figure 6.26). This confirms the existence and energy

of the newly found upper level. A second laser excitation from another known lower level was also performed at the line 5708.813 Å which is present in the transition list of the newly found level.

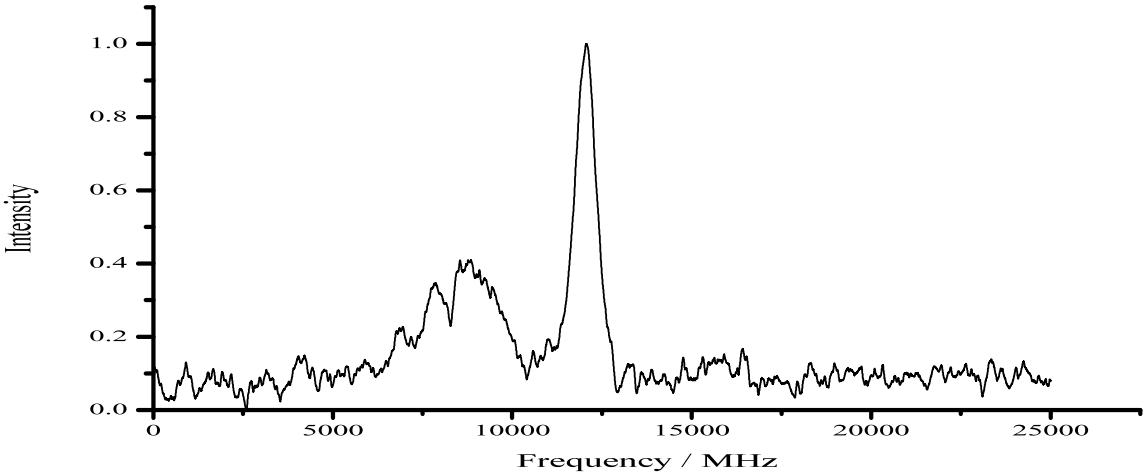

Figure 6.27: Recorded hf structure of the line 5708.813 Å.

Figure 6.28: Predicted hf structure of the line 5708.813 Å.

The hf structure of the line 5708.813 Å was recorded on all previously observed fluorescence. The recorded hf structure of the line (figure 6.27) is in good agreement both in terms of shape and hf components positions with the hf structure predicted by

classification program (figure 28). Since the hf structures at lines 5020.337 Å, 5088.882 Å, 5336.340 Å are in good agreement with the hf structure profile in FT spectrum of the respective lines, the energy of the newly discovered upper level was corrected by obtaining cg wave number from the FT spectrum and energies of the already corrected lower levels at these lines respectively. The corrected energy is 29563.401 cm^{-1}. By using more than one recorded file for both excitations the statistical average of the A value of the newly determined level was calculated. Finally newly determined level is 29563.401(10) cm^{-1}, odd parity, J = 5/2, A = 869(8) MHz. Both excitation and all the fluorescence lines were then classified. The level scheme for the newly discovered level is shown in figure 6.29.

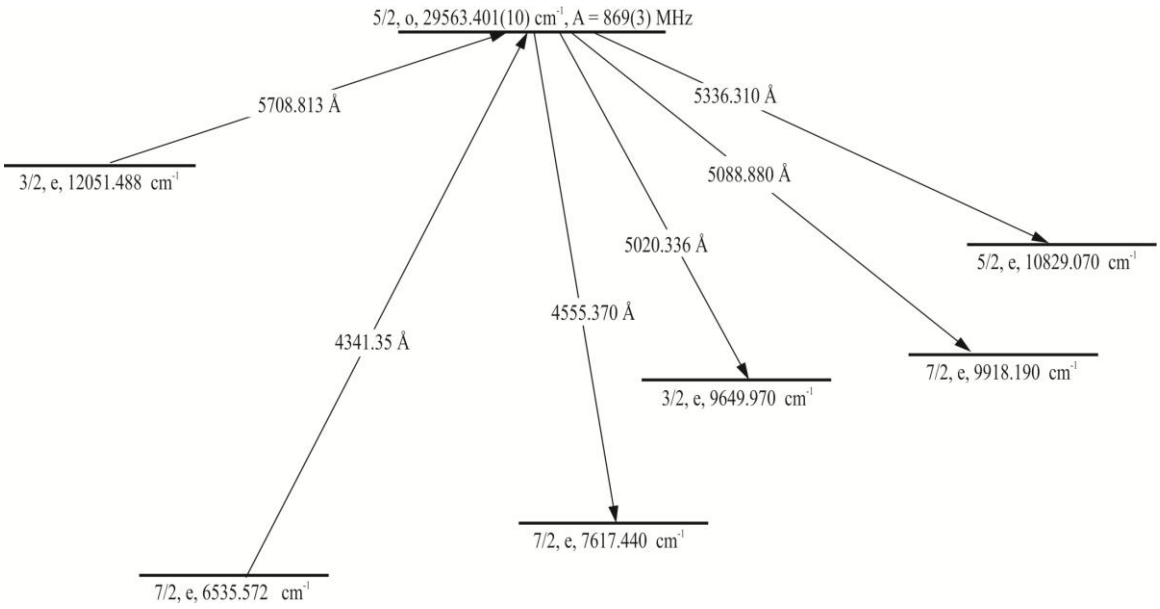

Figure 6.29: Energy level scheme for the newly discovered level 29563.401$^{o}_{5/2}$ cm^{-1}.

6.5 Discovery of a new energy level $27336.479^{e}_{7/2}$ cm^{-1}

A prominent unclassified line at an estimated cg wavelength 5992.67 Å with the good SNR of 24 (figure 6.30) was investigated. The diagonal components of the line are visible in FT spectrum but the line could not be explained by any of the suggestions listed in the classification program. For the identification of the combining levels involved in the formation of the line, laser excitation was performed.

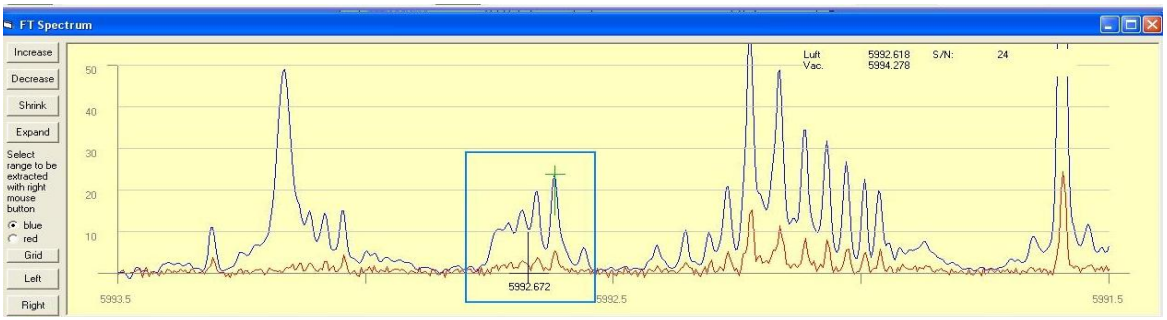

Figure 6.30: FT spectrum of the line 5992.67 Å.

Laser excitation wavelength was set to the strongest diagonal component of the investigated line and LIF signals were detected by tuning the transmission wavelength of the monochromator. Strong LIF signals were observed on 5236 Å, 6094 Å, 6172 Å and 6405 Å. Then on each of the observed fluorescence signals the hf structure of the investigated line was recorded by scanning laser frequency across the hf components of the line visible in FT spectrum. On all observed fluorescence wavelengths a same hf

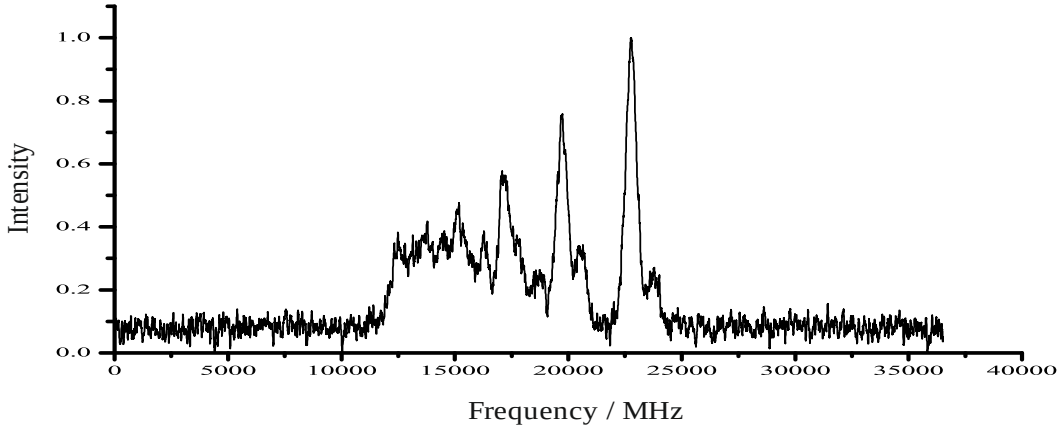

Figure 6.31: Recorded hf structure of the line 5992.67 Å.

structure was recorded with good SNR (figure 6.31). This means that all observed fluorescence lines come from the same excited upper level.

By the analysis of the intensity profile and hf component positions of the recorded hf structure probable spectral parameters of the combining levels were suggested. The off-diagonal components appear on both sides of the diagonal components indicating that $\Delta J = Jo - Ju = 0$. The strongest diagonal component appear on the high frequency side suggesting that Ao > Au. The intensity of the diagonal components decreases sharply indicating low values of angular momentum of the lower and upper combining levels. With these assumptions the recorded hf structure was simulated and the simulated values were taken as start values for fitting the recorded profile to a mathematical function. The best fit was obtained (figure 6.32) with lowest SSE for Jo = Ju = 7/2, Ao = 678.38 MHz and Au = 169 MHz.

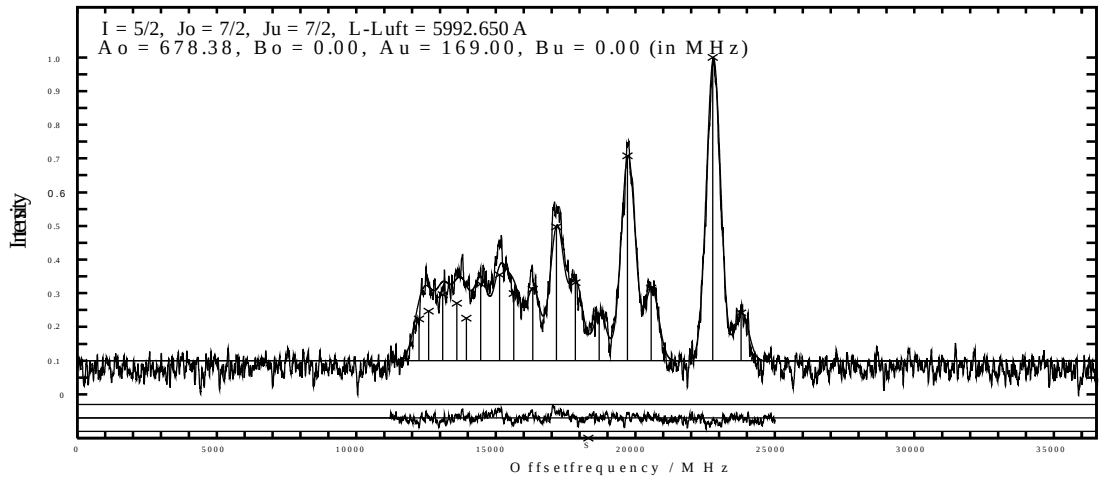

Figure 6.32: Best fit situation of the recorded hf structure of line 5992.67Å.

Assuming an unknown upper level, a known lower level is searched in the data base of known levels having J = 7/2 and A value close to 164 MHz. An odd parity level 10654.070 cm^{-1}, Ju = 7/2, Au = 169(2) MHz was found. The recorded hf structure was again fitted but keeping fixed the A value of the known lower level. Using the cg wave number obtained the fitting process and the energy of the lower level, the energy of the possible new upper level was calculated.

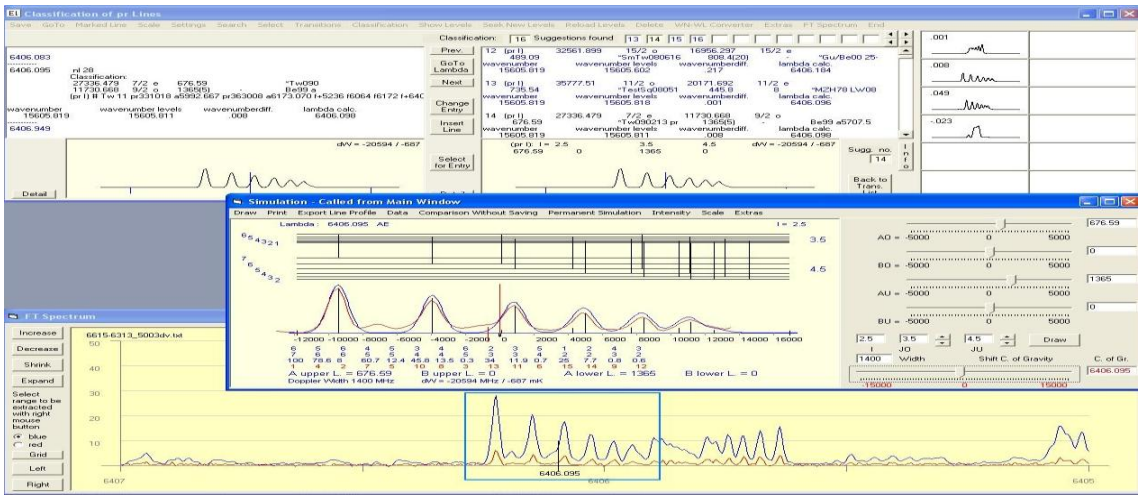

Figure 6.33: Confirmation of the existence of the newly found level from FT spectrum at fluorescence line 6406.095 Å.

The calculated new upper level 27336.556 cm^{-1}, even parity, Jo = 7/2 and Ao = 678.38 MHz explained all the observed fluorescence lines (figure 6.33). In addition to the observed fluorescence lines, two more lines 6274.359 Å and 6565.201 Å present in the

transition list of the this level are also in good agreement both in terms of shape and component positions with the hf structure profile of the respective lines appearing in the FT spectrum. In order to confirm experimentally the existence and energy of the newly found level another laser excitation at 6173.073 Å (which was one of its observed fluorescence lines) was performed. The recorded hf structure of this line has a good SNR (figure 6.34) and is in good agreement with the hf structure of the investigated line predicted by classification program (figure 6.35).

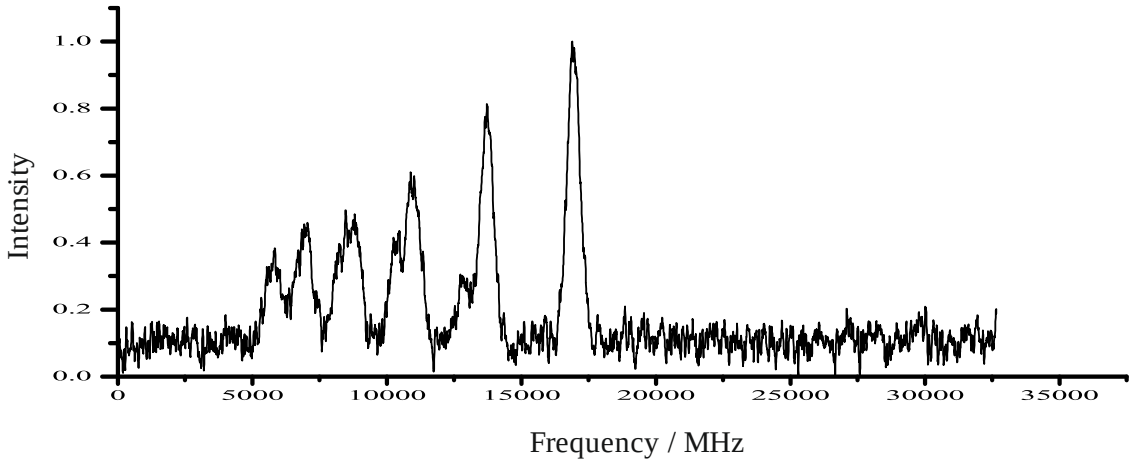

Figure 6.34: Recorded hf structure of line 6173.073 Å.

At several lines (5992.672 Å, 6095.934 Å, 6173.073 Å, 6406.099 Å, 6274.359 Å and 6565.840 Å) the cg wave number could be determined more precisely and the energy of the lower levels is also known precisely so the energy of the upper level was determined with higher accuracy. Furthermore, the accuracy of the A value of the newly discovered upper level was also improved by taking the statistical average of all the recorded files at the two excited lines.

Figure 6.35: Predicted hf structure of the line 6173.073 Å.

The newly discovered upper level 27336.479(10) cm^{-1}, even parity, J = 7/2 and A = 678(3) MHz explained all the observed fluorescence lines (figure 6.36).

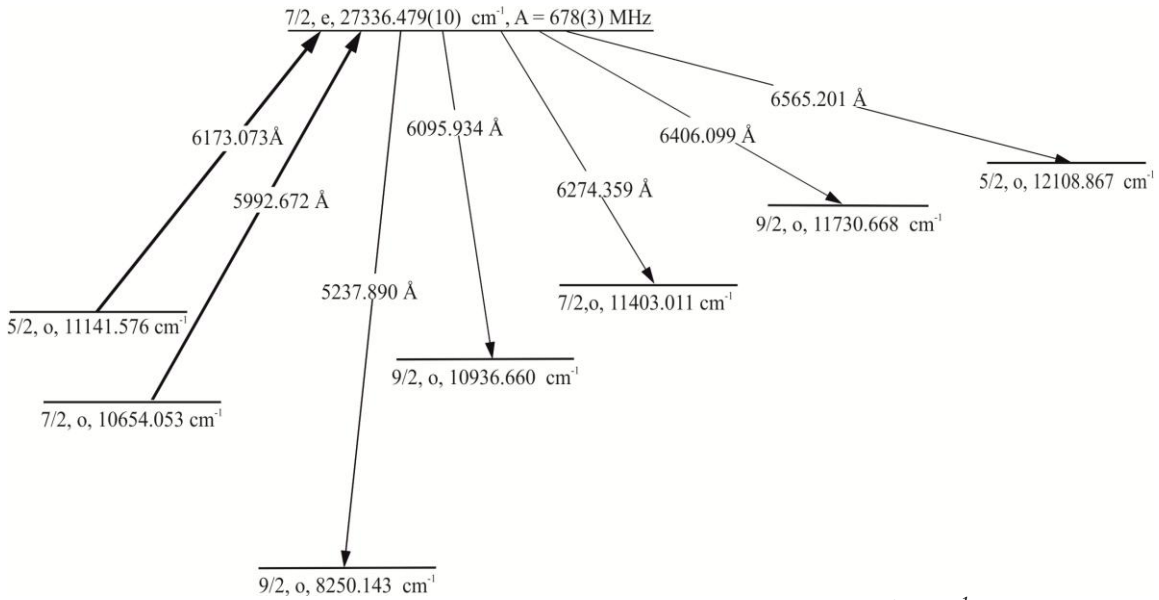

Figure 6.36: Level scheme for the newly discovered level 27336.479$^{e}_{7/2}$ cm^{-1}.

6.6 Discovery of a new energy level $24058.128^{o}_{9/2}$ cm^{-1}

A line with an estimated cg wavelength 5633.86 Å was experimentally investigated. The line at 5633.86 Å in FT-Spectrum (figure 6.37) could not be classified using any of the suggestions listed in classification program. The relative intensity of the line in FT spectrum is 12 and the hyperfine components are not resolved.

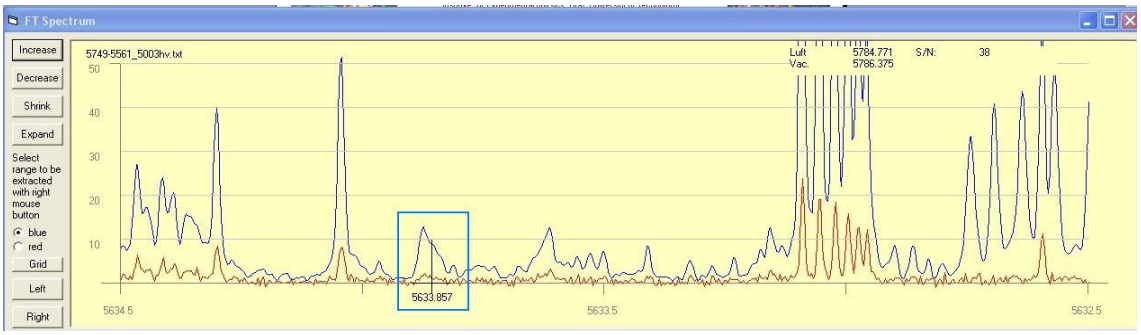

Figure 6.37: FT spectrum of line 5633.86 Å.

The laser wavelength was set to the strongest diagonal hf structure component of this line (5711.39 Å) and LIF signals at 5092 Å and 5482 Å were observed by tuning the transmission wavelength of the monochromator. The hf structure of the investigated line was then recorded by scanning the laser frequency across the investigated region and setting the monocromator transmission wavelength to each of the observed fluorescence wavelengths. The same hf structure (figure 6.38) was recorded on all observed fluorescence wavelengths which means that all the observed fluorescence wavelengths were the decay lines from the same upper level. The recorded hf structure profile was again inspected for a possible match but no coincidence was found. This means that either one or both combining levels are not known.

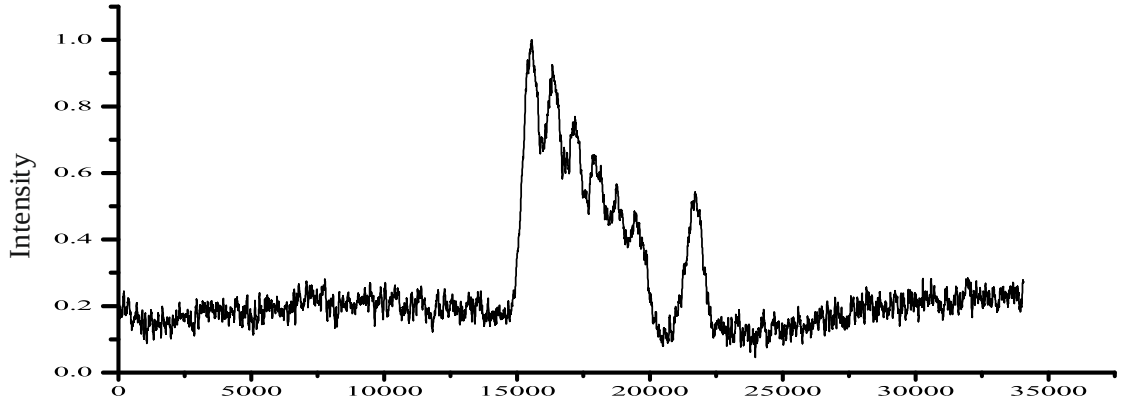

Figure 6.38: Recorded hf structure of line 5633.86 Å.

The intensity profile and the hf component positions of the recorded hf structure suggested that the change in angular momentum is -1 i.e. $\Delta J = Jo - Ju = -1$. Strongest diagonal component is on lower frequency side which meant that Au > Ao. The recorded hf structure was then simulated to obtain the possible values and angular momentum J and magnetic hf constant A of the combining lower and upper levels involved in the formation of the investigated line. Using the simulated values the recorded hf structure was fitted and a best fit situation obtained (figure 6.39) with minimum SSE for spectral values Jo = 9/2, Ao = 544 MHz, Ju = 11/2 and Au = 755 MHz.

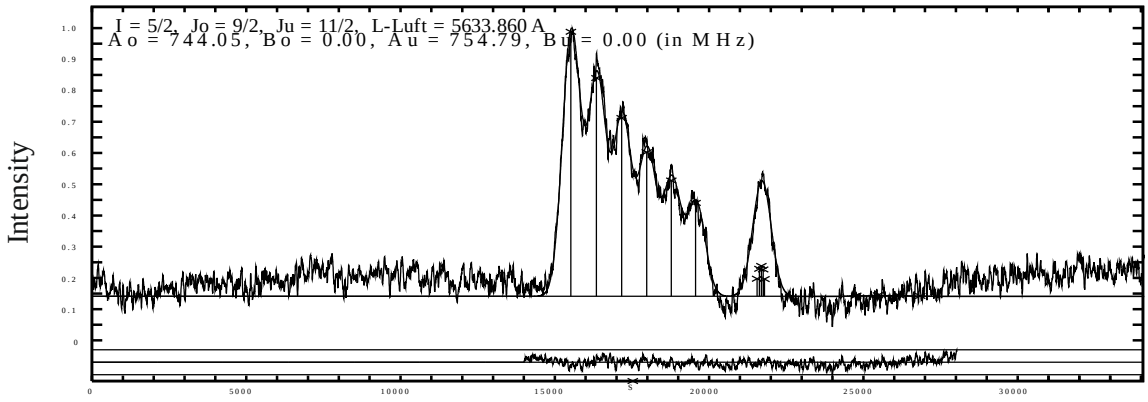

Figure 6.39: Fitted hf structure of line 5633.86 Å.

Assuming that the upper level is unknown, a lower level was searched in the data base of known levels having J = 11/2 and A value close to 755 MHz. An even parity known

lower level was found in the data base having the parameters 6313.224 cm^{-1}, Ju = 11/2 and Au = 756.4 MHz. The recorded hf structure was again fitted with fixed the A value of the known lower level, the A value of the upper level was allowed to change during the fitting process. The energy of the upper level was determined by adding the cg wave number of the investigated line obtained from the fit of the recorded structure to the energy of the known lower level. The calculated new upper level 24058.118 cm^{-1}, even parity, J = 9/2 and Ao = 747.45 MHz was introduced in the data base of known levels which was then uploaded in the classification program. The transition list of the newly determined upper level generated by the classification program explained all the observed fluorescence lines (for example figure 6.40 which explains the fluorescence line at 5093.887 Å). In addition to the observed fluorescence line the existence of the newly found level could also be confirmed at 5958.725 Å, 7564.089 Å, 7600.104 Å, 8252.693 Å and 8252.693 Å via FT spectrum. The predicted hf structure of the line 5958.725 Å taken from transition list is in good agreement both in terms of shape and hf component positions with the hf structure profile of the line 5705.346 Å (figure 6.41). In order to further confirm the existence and energy of the newly found level one more laser excitation was performed at the line 5705.346 Å. The recorded hf structure (figure 6.42) of the excited line is completely agreement with the predicted hf structure of the line. This confirmed the existence and energy of the newly discovered odd parity energy level. Since the cg wave number of the line could accurately be determined from FT spectrum at the line 5093.887 Å and also the energy of the lower level (4432.225 cm^{-1}) with high accuracy, therefore the energy of the newly discovered level was determined with higher accuracy.

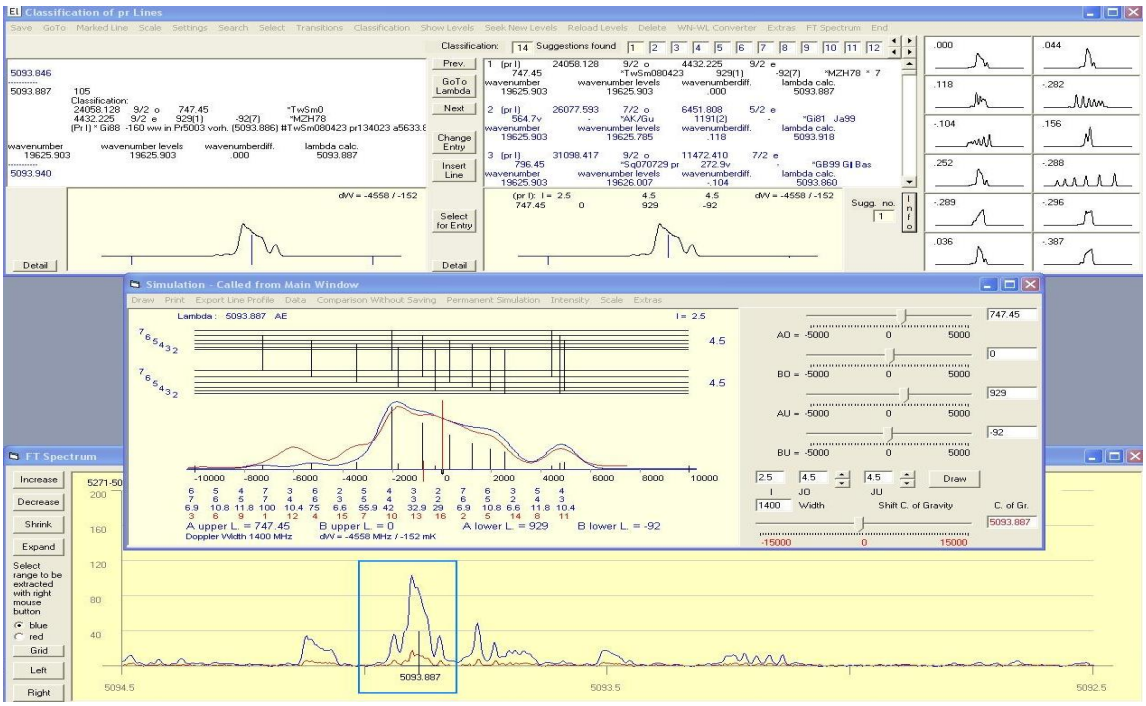

Figure 6.40: Confirmation of the existence of the newly found level from FT spectrum at fluorescence line 5093.887 Å.

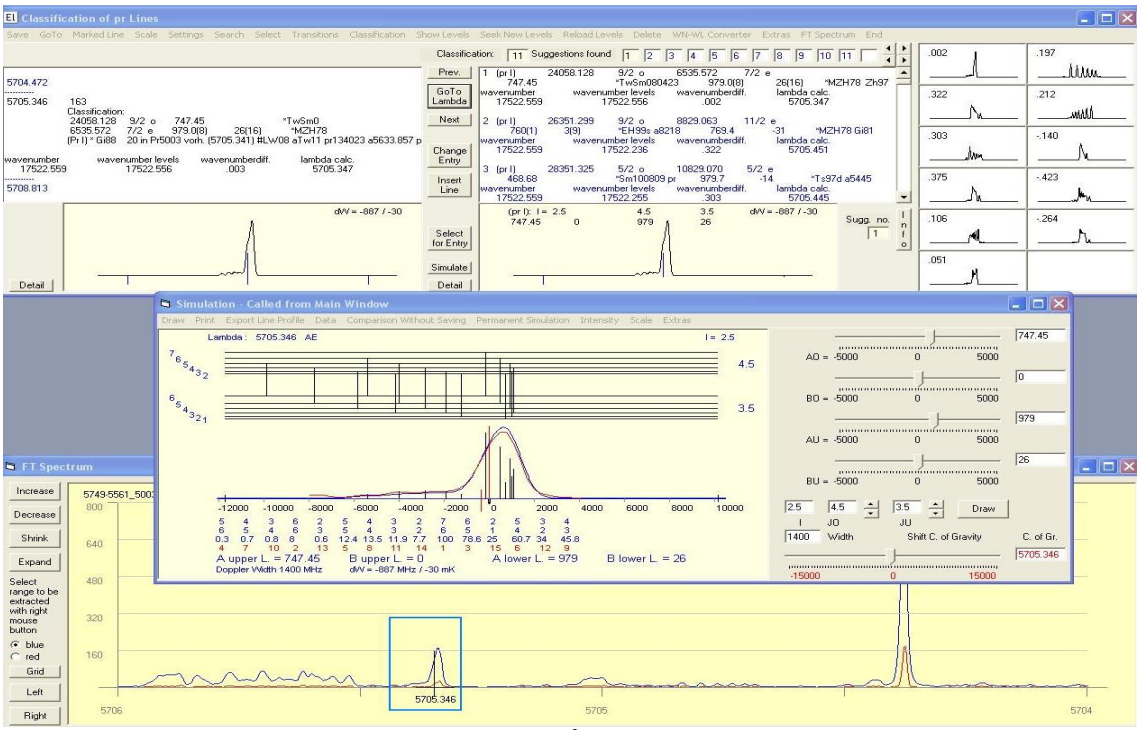

Figure 6.41: Predicted hf structure of line 5705.346 Å (blue profile) overlapped by the hf structure of the investigated line in FT spectrum.

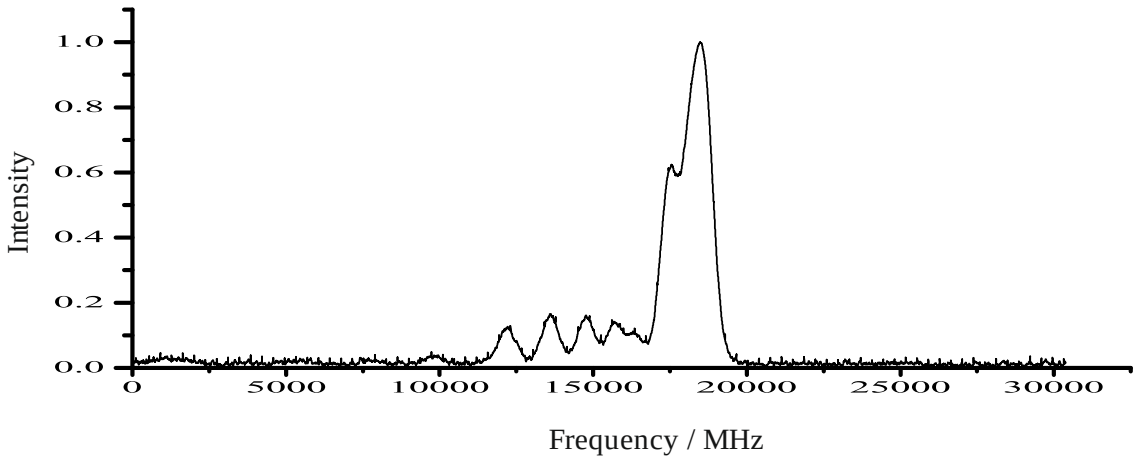

Figure 6.42: Recorded hf structure of the line 5958.730 Å.

By using several recorded files for both excitations the statistical average of the A value of the newly determined level was calculated. Finally newly determined level 24058.128(10) cm^{-1}, odd parity, J = 9/2 and A = 751(5) MHz explained 4 lines in the visible region and 4 lines in the far infrared region (Figure 6. 43). All eight lines were then classified.

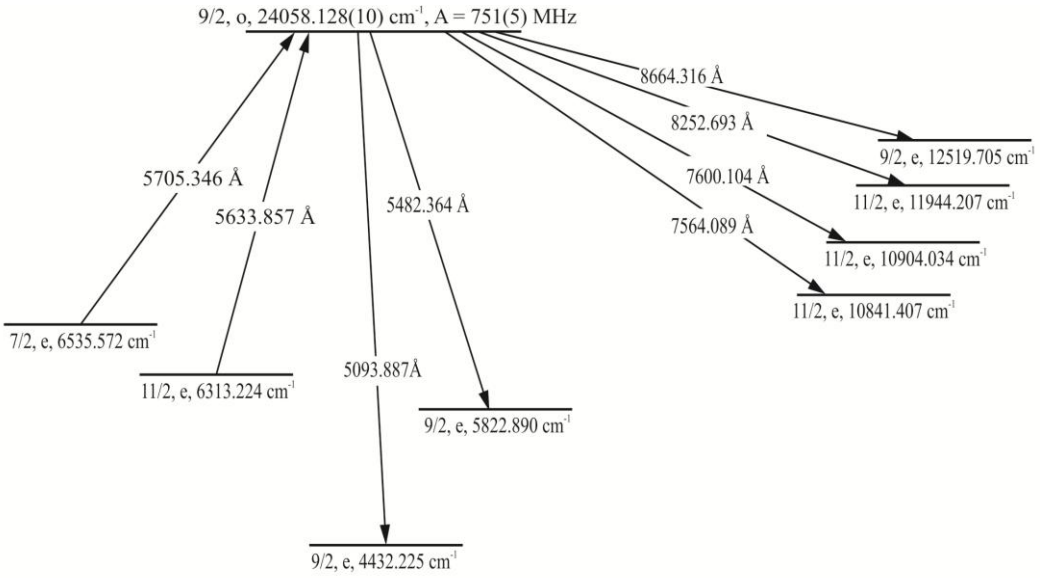

Figure 6.43: Energy level scheme for newly discovered level 24058.128$^{o}_{9/2}$ cm^{-1}.

6.7 Discovery of a new energy level $23403.929^{e}_{11/2}$ cm^{-1}

An unclassified line 6597.188 Å was experimentally investigated using laser spectroscopy. Although the line has a very good signal-to-noise ratio (SNR) of 47 as can be seen Fourier transform spectrum of praseodymium (figure 6. 44) but could not be explained by any of the suggestions for the combining known lower and upper levels listed in the classification program. Therefore in order to classify the line, laser excitation was performed.

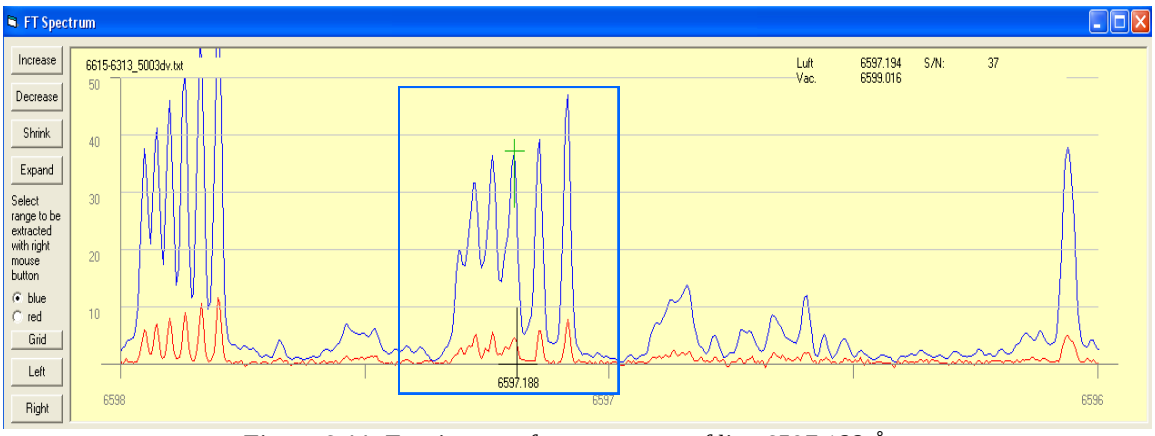

Figure 6.44: Fourier transform spectrum of line 6597.188 Å.

The laser wavelength for excitation was precisely set to the strongest (diagonal) hyperfine (hf) component of the investigated line which is extracted from FT spectrum. Then the transmission wavelength of the monochromator is varied in the range from 3000 Å to 7000 Å (which are the sensitive range of our monochromator and photomultiplier tube) to search for laser induced fluorescence (LIF) signals. LIF signals were observed at 4539 Å, 4862 Å, 4926 Å, 4940 Å and 5359 Å, the strongest being at 4862 Å. In order to record the hf structure of the investigated line, the monochromator was set to one of the observed fluorescence wavelengths, having a good SNR (in this case to 4862 Å) and then the laser frequency was scanned across the hf structure of the investigated line.

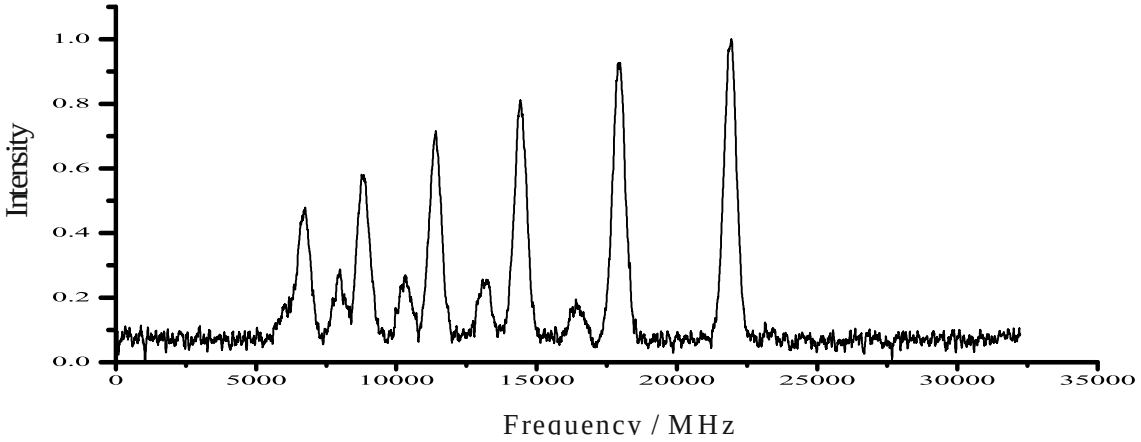

Figure 6.45: Recorded hf structure of the investigated line 6597.188 Å.

As expected a hf structure with widely separated hf components was recorded with a very good SNR, figure 6.45.

Once again the suggestion list generated by classification program for the investigated line was inspected for a possible match but none of the listed suggestion had any coincidence with recorded hf structure, neither in terms of shape of the hf structure nor in terms of component positions. It was concluded that either one or both of the combining levels for the investigated line were yet to be discovered. Further more on all observed fluorescence lines the same hf structure pattern was observed.

The recorded hf structure pattern of the investigated line was inspected for possible values of spectral parameters of the combining levels. The possible values of the spectral parameters (angular momentum J and hyperfine constants A of the upper and lower combining level of the line) are estimated by analyzing the relative intensity and hf component positions of the recorded hf structure. The strength of the diagonal components degrades towards longer wavelength which implies that the splitting of the upper combining level is larger as compared to the lower combining levels which in turn gives the information that magnetic hf structure constant A of the upper level is larger than that of the lower level. One visible group of off-diagonal components lies on the lower frequency side and no off-diagonal components on the other frequency side, suggesting that the change in angular momentum in going from lower to upper level is +1 ($\Delta J = +1$). With these assumptions the recorded hf structure was simulated

for probable values of the angular momentum and magnetic hf structure constants of the combining lower and upper levels. The best simulation was obtained for angular momentum values of the upper and lower levels with half integer values. This is specific to atomic levels for the case of praseodymium, having a nuclear spin quantum number I = 5/2. Using these probable values the recorded hf structure was fitted by letting the A values of the lower and upper level to change during the fitting process. This best fit with minimum sum of the squared errors (SSE) was obtained for values Jo = 11/2, Ao = 684.49 MHz, Ju = 9/2 and Au = 214.48 MHz, the best fit situation is depicted in figure 6.46.

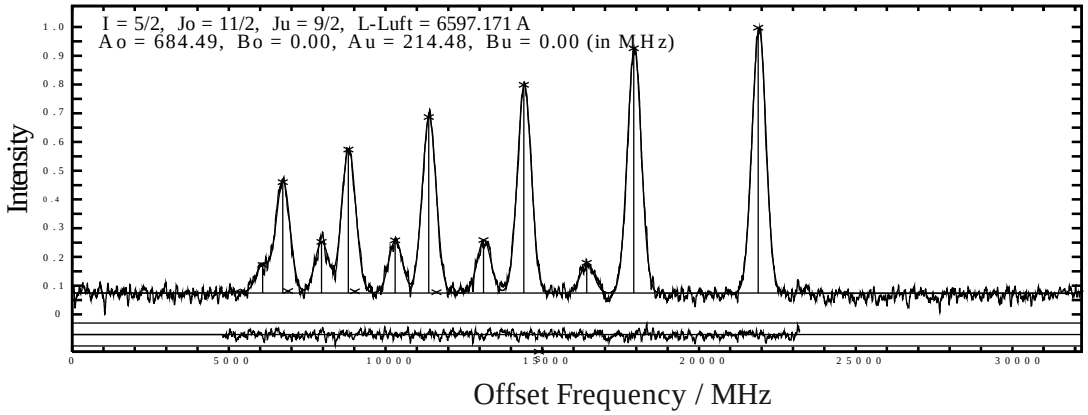

Figure 6.46: Best fit situation of the recorded hf structure of line 6597.188 Å.

Using these best fit spectral values (hf constants and J values) of the combining levels and assuming that only one of the involved levels is unknown i.e. the upper combining level, a known lower level was searched in our data base of known Pr I levels. The searching routine generates a number of suggestions for possible new upper levels and known lower levels having J = 11/2 and A value close to 214.48 MHz. For each possible suggestion the searching routine also builds a transition list. A known lower level with spectral parameters 8250.141 cm^{-1}, odd parity, Ju = 9/2, Au = 213.531 MHz and Bu = -4.136 MHz (with close agreement with the fitted A value) was found. The transition list generated for the possible new upper level explained only two observed fluorescence lines 4539 Å and 4862 Å. None of the other listed suggestions for possible new upper levels explained the observed fluorescence lines. Despite of the fact that only two observed fluorescence lines were seen in the transition list of the calculated

suggestion, nevertheless the calculated upper level was assumed to be the new upper combining level of the excited transition. The recorded hf structure was again fitted but now keeping fix the A and B values of the known lower level. Since the both A and B [25] values for lower level are accurately known to three decimal places, therefore while refitting the recorded hf structure the B value of the upper level was also allowed to change. This resulted in Ao = 683.85 MHz and Bo = -25.77 MHz for the upper level. Now by adding the cg wave number obtained from the fit process and the energy of the lower level, the energy of the upper level was calculated. Therefore with respect to the odd parity lower level an even parity possible new upper level 23403.967 cm^{-1}, Jo = 11/2, Ao = 684.49 MHz and Bo = -25.77 MHz was determined.

Figure 6.47: Inclusion of newly discovered level in the classiication program and its transition list.

The probable new upper level was introduced in the data base of known Pr I levels and is uploaded in the classification program which generated a transition list (figure 6.47). Since the energy of the lower level was accurately known, the level energy of the upper level was more accurately calculated by determining the cg wave number of the investigated line with the help from FT spectrum. The corrected level energy is

23403.929 cm^{-1}. The predicted hf structure at the observed fluorescence line 4862.120 Å is in good agreement with the hf structure of the line in FT spectrum both in terms of shape and the component positions (figure 6.48).

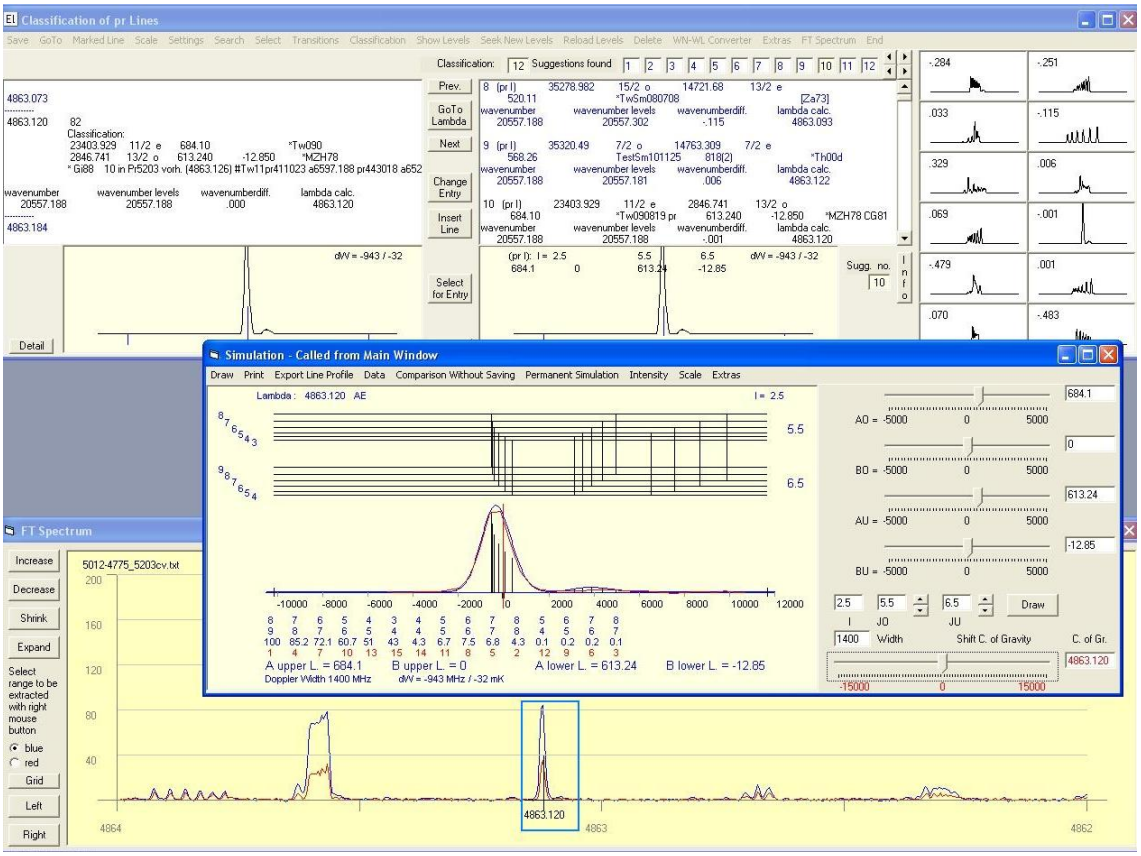

Figure 6.48: Confirmation of the existence of the newly found level from FT spectrum at fluorescence line 4863.120 Å.

In addition to the observed fluorescence line the existence of the newly found level could also be confirmed at 7286.760 Å via FT spectrum. The other three observed fluorescence lines viz. 4926 Å, 4940 Å, 5359 Å are indirect fluorescence lines and might have occurred as a result of collisional coupling. It may happen that an atom in the excited state may collide with an atom which incidentally has approximately the same excitation energy as the energy of the atom in excited state. This results in the transfer of energy to the other atom which decays from the collisionally populated energy state which decays subsequently at its fluorescence lines.

In order to further consolidate the energy and existence of newly discovered energy level one more laser excitation was performed from another known lower level to the newly discovered upper level. The line 6524.111 Å in the transition list of the newly discovered upper level appears in a blend of more than one line in the FT spectrum (figure 6.49). Laser wavelength was set to 6524.02 Å (strongest diagonalt component) and transmission wavelength of the monochromator was set to 4539 Å and 4862 Å. LIF signals were observed which were recorded by scanning the laser frequency across the hf components of the line. A hf structure with same shape and component positions as predicted by the classification program was recorded (figure 6.50).

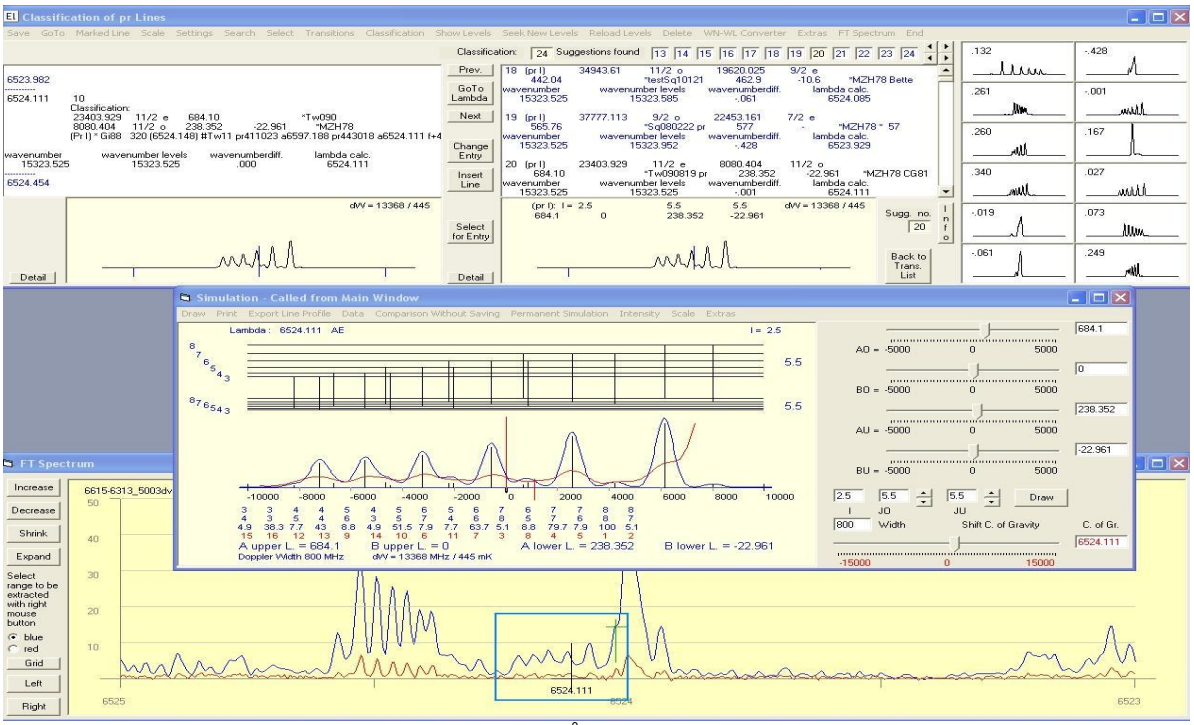

Figure 6.49: Predicted hf structure of line 6524.111 Å (blue profile) overlapped by the hf structure of the investigated line in FT spectrum.

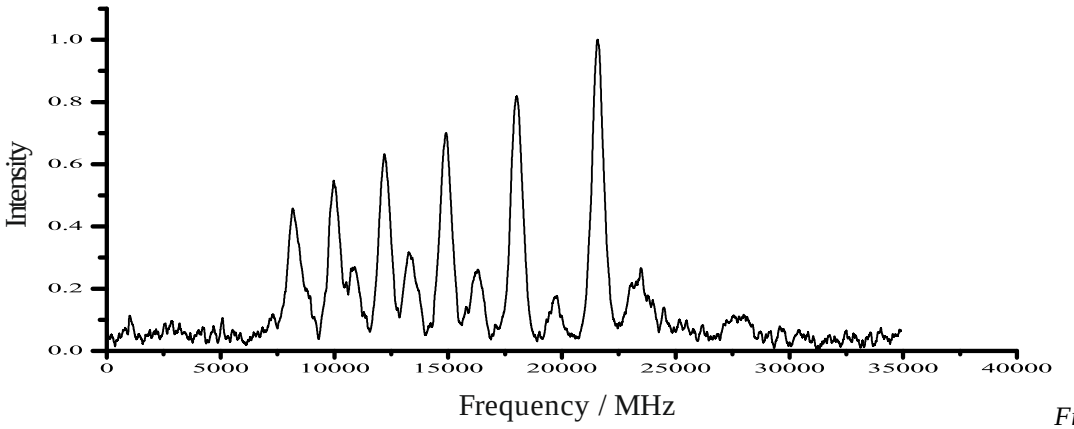

Figure 6.50: Recorded hf structure of line 6524.111 Å.

This confirmed the energy and existence of the newly discovered upper level. By using several recorded files for both excitations the statistical average of the A and B values of the newly determined level was calculated. Finally the newly determined level 23403.929(10) cm^{-1}, even parity, J = 11/2, A = 684(3) MHz and B = -32(10) MHz explained 4 lines in the visible region and 1 line in the far infrared region (Figure 6.51). All five lines (excitation and fluorescence lines and additional lines from FT spectrum) were then classified.

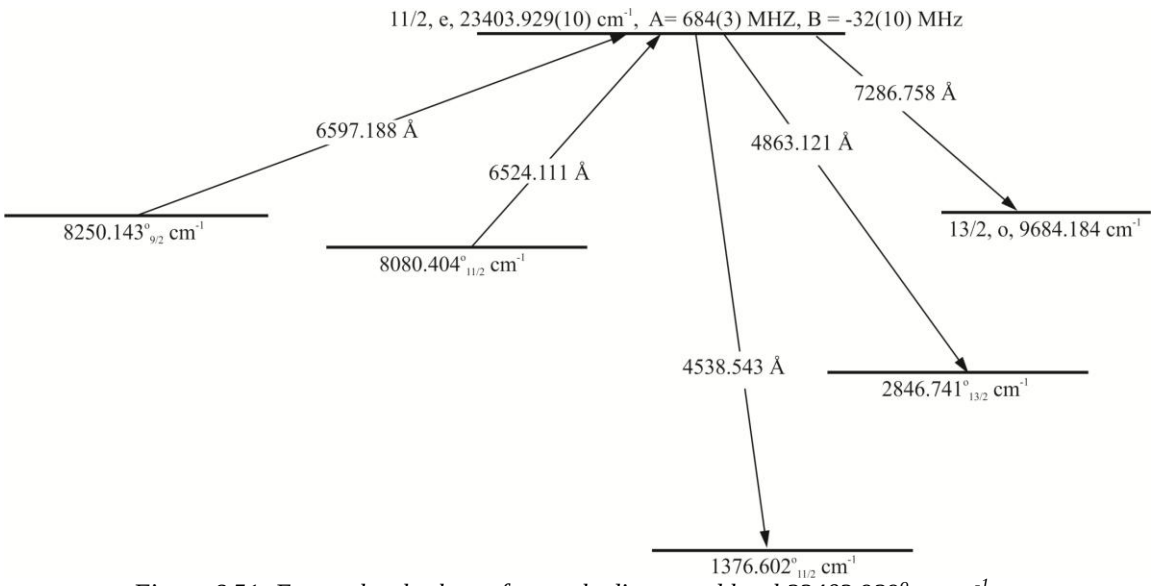

Figure 6.51: Energy level scheme for newly discovered level 23403.929$^{o}_{11/2}$ cm^{-1}.

6.8 Discovery of a level 19011.607$^{o}_{11/2}$ cm^{-1}

A line at an estimated cg wavelength 7202.51 Å was investigated. The line appears in a blend of one or more lines and none of the lines in the blend has clearly visible hf components as can be seen in FT spectrum (figure 6.52). The SNR at the investigated position is good having a relative strength of 21.

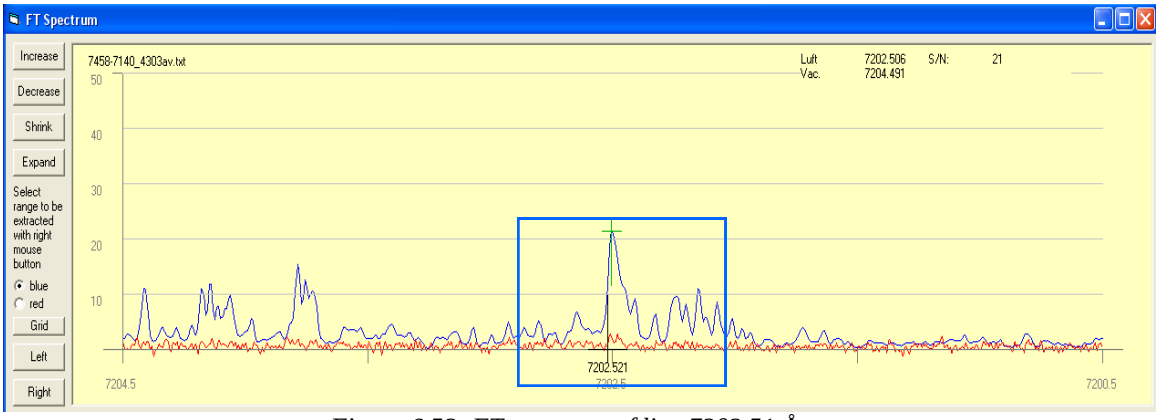

Figure 6.52: FT spectrum of line 7202.51 Å.

The laser wavelength was set at 7202.51 Å and fluorescence signals were searched by varying the transmission wavelength of the monochromator. Fluorescence signals were detected at lines 4784 Å, 5715 Å and 5592 Å and on all three fluorescence lines hf structure of the excited line was recorded by scanning the laser frequency around 7202.51 Å with a scan width of 30 GHz. An extended hf structure with widely separated diagonal components was recorded on all three fluorescence lines. It was noticed that the total width of the hf structure of the investigated line is larger than the total scan width (30 GHz) of our dye laser system. This compelled us to record the complete structure as lower and higher frequency parts separately in two data files. Using a computer program called Merge (figure 6.53) the low and high frequency parts in separate files were merged together to form a single file containing the complete LIF spectrum of the investigated line (figure 6.54).

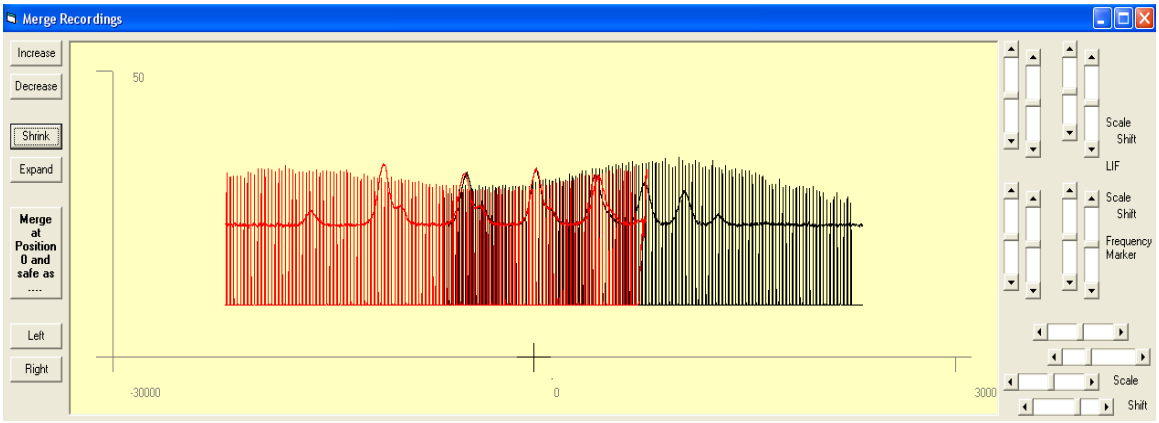

Figure 6.53: Merging two recorded LIF spectrum of line 7202.51 Å.

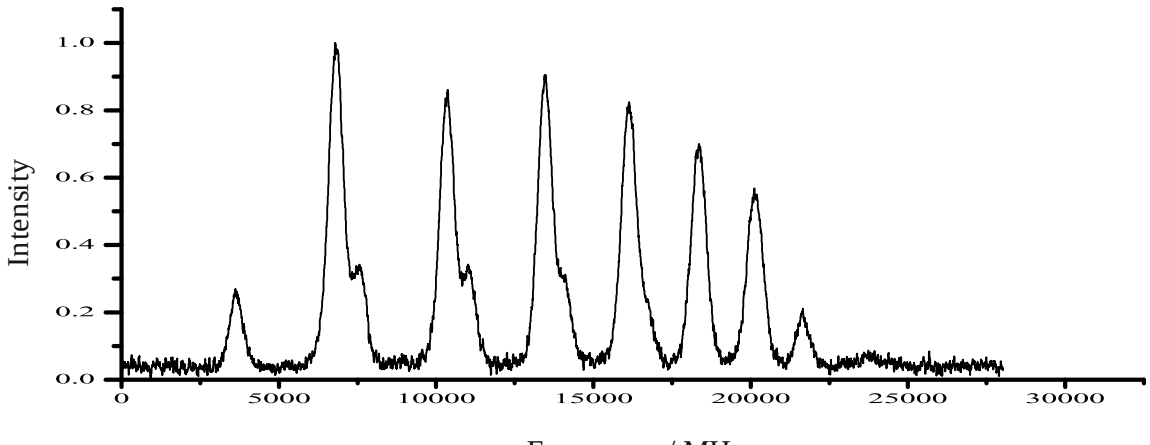

Figure 6.54: Recorded LIF spectrum of line 7202.51 Å.

The recorded LIF spectrum was again inspected but none of the existing suggestions match with recorded hf structure. This implied that either one or both of the combining levels were not known. The relative intensities of the diagonal components in the merged LIF spectrum of the investigated line do not show a normal decreasing behavior to one side. This is only because of the different scale factors of the two separate files which were merged together to form a single file. Nevertheless, by analyzing the intensity profile and component separations of the diagonal components, the J and A values of the combining levels can be predicted. Since the off-diagonal components appears on both sides of the diagonal components so $\Delta J = Jo - Ju = 0$. A very gradual decrease in the relative intensity of the diagonal components indicates a high angular momentum of the combining levels. The strongest diagonal component is

on the low frequency side suggesting Au > Ao. Using these assumptions the recorded hf structure was simulated and best simulation was obtained at spectral values Jo = Ju = 11/2, Ao = 400 MHz and Au = 845 MHz.

In the usual manner, by assuming that the upper level in the combination was not known a lower level was searched in the data base of known levels having J = 11/2 and A values close to 845 MHz. No level in the data base matches the searching criteria. This means that rather an unknown upper level, possibly the lower level in the combination is not known and it may be that the upper level is known. Now the upper level is searched in the data base of known levels having J = 11/2 and A value close to 400 MHz. A known even parity upper level 32891.473 cm^{-1}, Jo = 11/2 and Ao = 399.37 MHz was found whose transition list explained all the observed fluorescence lines. The energy of the lower level in the combination of the investigated line found done by subtracting the cg wave number from the energy of the known upper level. This gives 19011.3 cm^{-1}, odd parity, Ju = 11/2 and Au = 845 MHz. The newly found lower level was introduced in the data base of known levels and was then uploaded in the classification program.

The newly discovered level was confirmed by a second laser excitation to another known upper level at the line 7126.08 Å. The line appears in a blend situation and hf components as predicted by the classification program are not visible in the FT spectrum (figure 6.55).

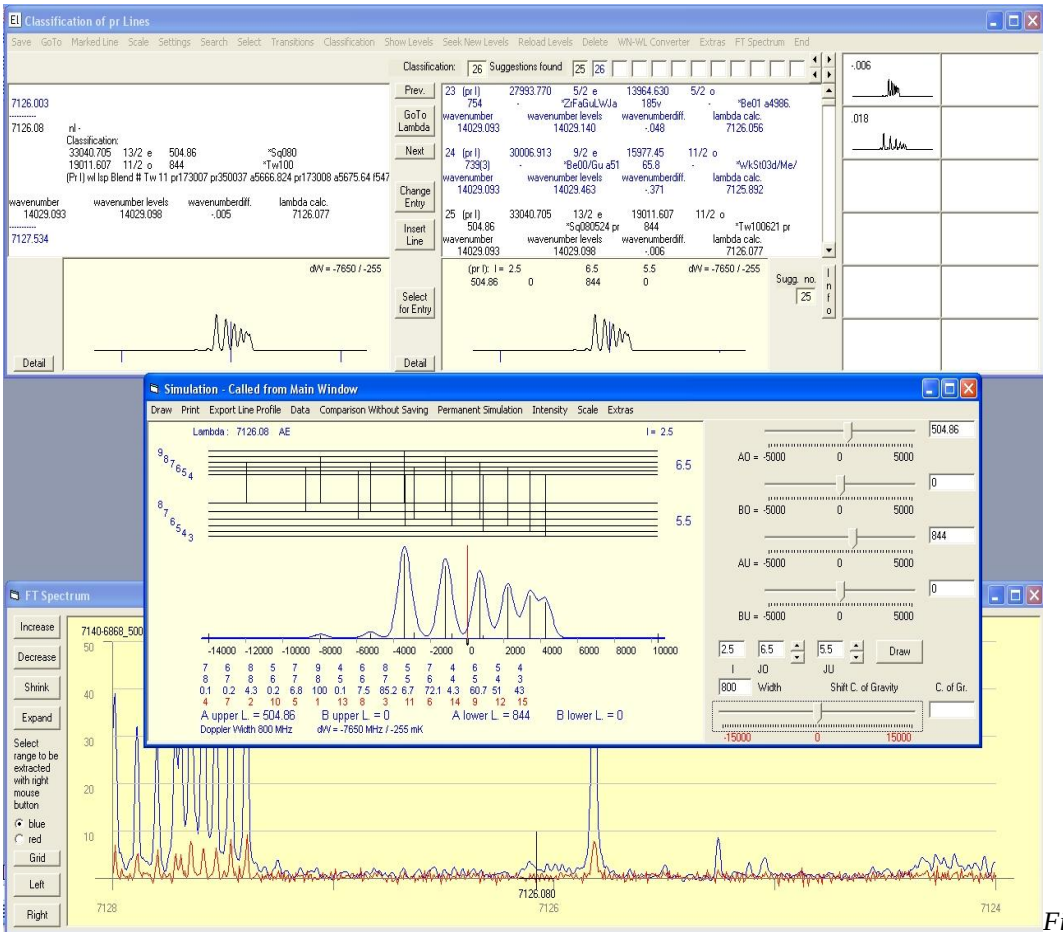

Figure 6.55: Predicted hf structure of line 7126.08 Å and its FT spectrum.

The newly discovered level combines with an already known upper level 33040.705 cm^{-1}, even parity, Jo = 13/2 and Ao = 504.86 MHz, having experimentally recorded fluorescence lines 5666.838 Å, 5675.64 Å, 5471.585 Å, 4750.716 Å.

Excitation wavelength is set to 7126.08 Å and LIF signal was checked by setting successively the transmission wavelength of the monochromator to each of observed fluorescence lines originating from the known upper level. At all the observed fluorescence wavelengths LIF signal was observed indicating that the same upper level is excited from the new lower. The hf structure of the line was recorded at each fluorescence wavelength by scanning the laser frequency and setting the monochromator transmission wavelength fix to one of the observed fluorescence lines. The recorded hf structure (figure 6.56) is in good agreement both in terms of shape and

component positions with the predicted hf structure of the investigated line. This confirms the existence and energy of the newly discovered lower level.

The recorded hf structure was simulated and using simulated J and A values of the combining levels the recorded hf structure was fitted to a mathematical function. The best fit with lowest SSE was obtained (figure 6.57) for Jo = 13/2, Ao = 504.86 MHz, Ju = 11/2 and Au = 843.44 MHz. The energy of the newly discovered level and its value were corrected and finally the level data base was updated. By using several recorded files for both excitations the statistical average of the A value of the newly determined level was calculated. Finally newly determined lower level is 19011.607(20) cm^{-1}, odd

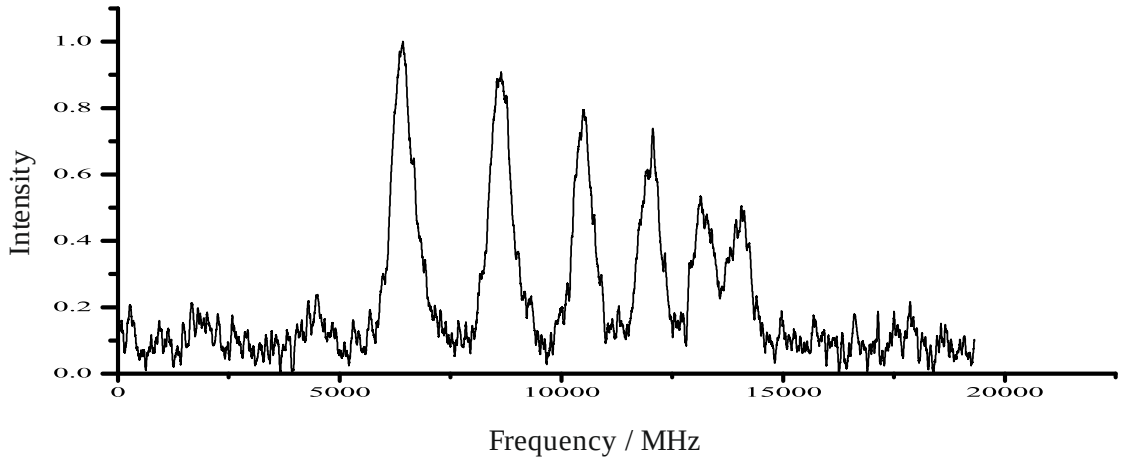

Figure 6.56: Recorded hf structure of line 7126.08 Å.

parity, J = 5/2, A = 845(10) MHz. Both excitation lines were then classified. The level scheme is shown in figure 6.58.

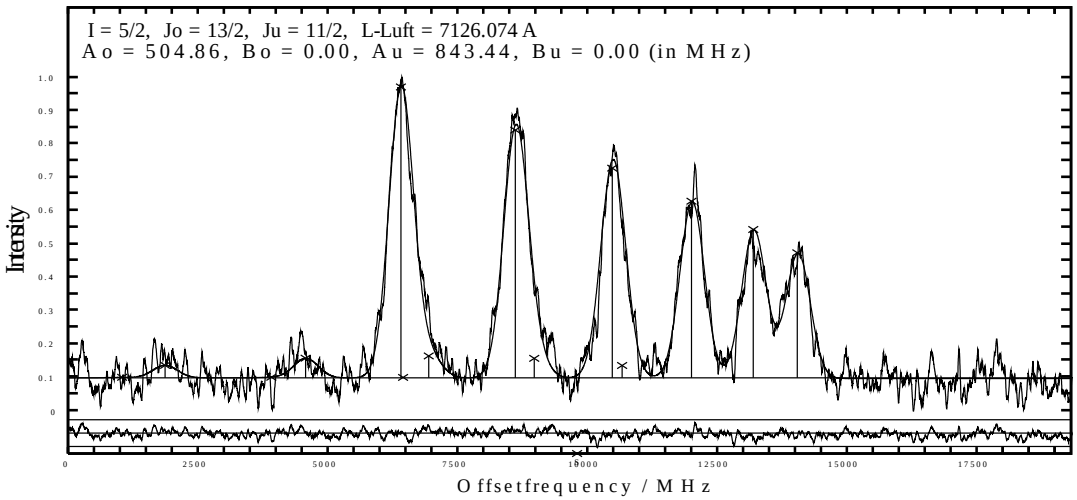

Figure 6.57: Fitted hf structure of line 7126.08 Å.

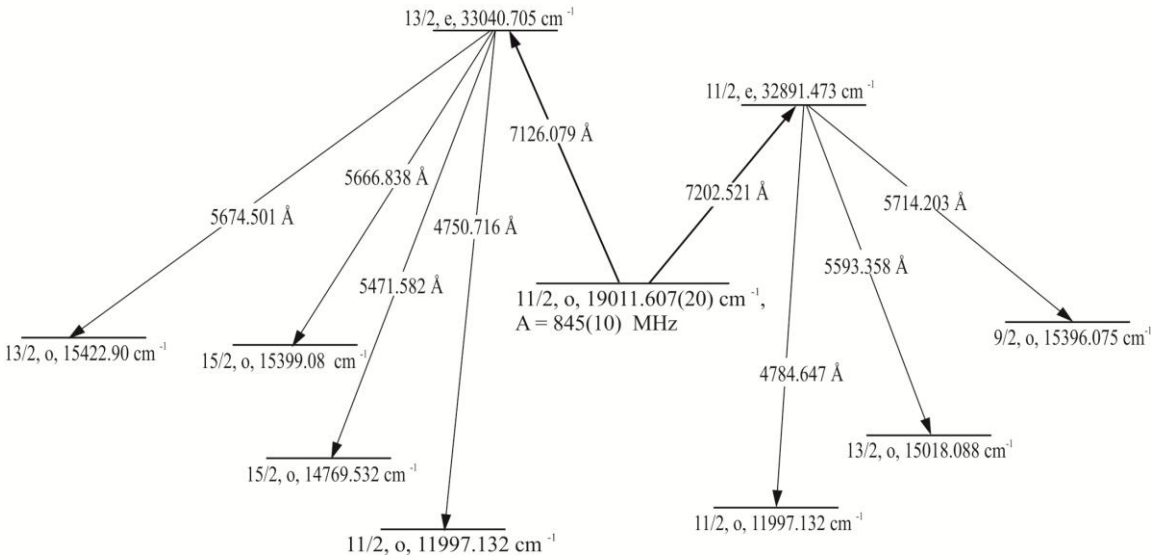

Figure 6.58: Energy level diagram for the newly discovered lower level 19011.607$^{o}_{11/2}$ cm^{-1}.

6.9 Discovery of a new energy level $26036.404^{o}_{13/2}$ cm^{-1}

An unclassified line with estimated cg wavelength 6032.62 Å having SNR of 45 in the FT spectrum (figure 6.59) was laser spectroscopically investigated.

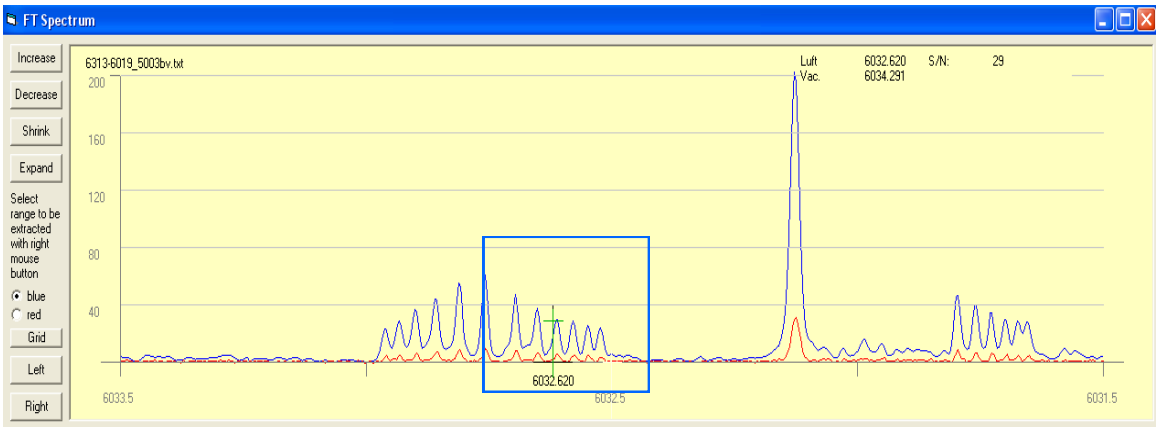

Figure 6.59: FT spectrum of the line 6032.62 Å.

The laser wavelength was set to the strongest (diagonal) hf structure component of the line i.e. 6032.69 Å and fluorescence signals at 4723 Å, 5068 Å, 5144 Å, 5810 Å, 5962 Å, 6039 Å, 6110 Å, 6339 Å and 6404 Å were detected by scanning the transmission wavelength of the grating monochromator. Then the hf structure of the excited line was recorded by scanning the laser wavelength over the hf structure of the line, setting the monochromator transmission wavelength successively to all nine observed fluorescence lines. On all observed fluorescence signals, the same hf structure was observed indicating that these nine lines originate from the same excitation (figure 6.60).

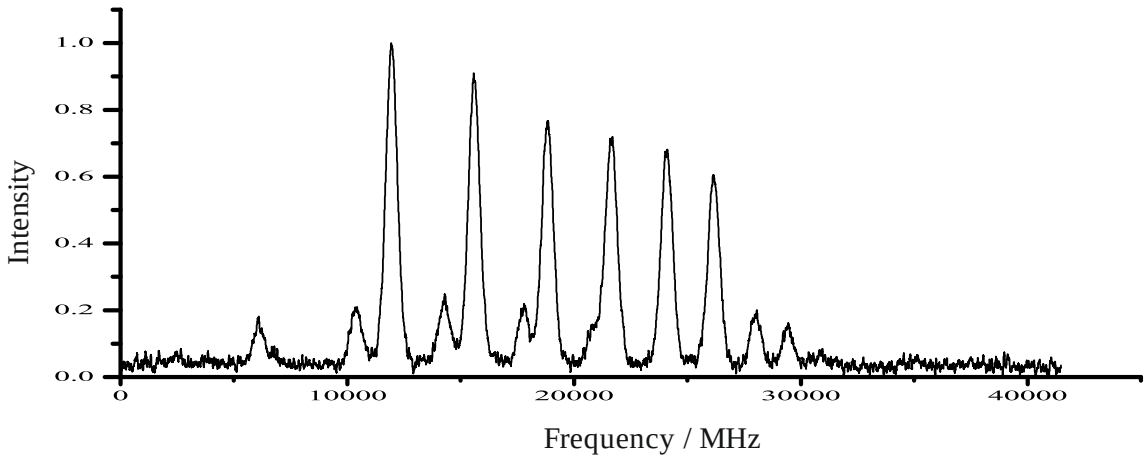

Figure 6.60: Recorded hf structure of line 6032.62 Å.

By analyzing the relative intensity and position of the components of the recorded hf structure, it was concluded that the transition is taking place between levels with the same J value ($\Delta J = 0$) and with a large difference of the values of the hf A constants upper and lower combining level, since the hf structure is widely splitted (Ao >Au). Using a fit program, the recorded hyperfine structure was fitted with different J values of upper and lower levels (always assuming $\Delta J = 0$). The best fit result with minimum SSE was obtained for angular momentum values J =13/2 (figure 6.61). The best fit values of the hyperfine constants of upper and lower levels are Ao = 651 MHz and Au = 1056 MHz, respectively.

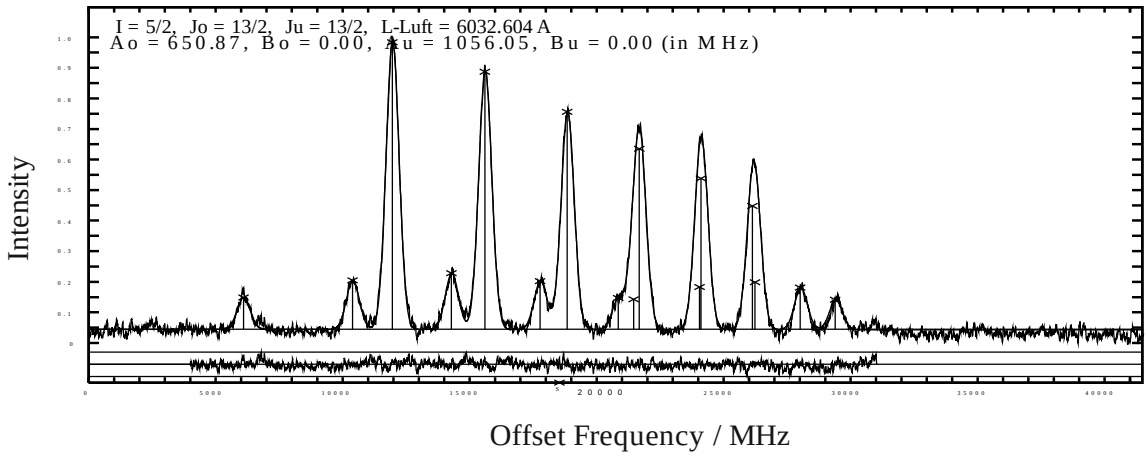

Figure 6.61: Best fit situation of the recorded hf structure of line 6032.62. Å

Assuming that an unknown upper level is involved in the excitation of this line, we searched for a known lower level having J = 13/2 and A value close to 1056 MHz,

contained in the database of known levels. An even parity lower level with energy 9464.440 cm^{-1}, Au = 1056.3(1) MHz, Bu = 0 and Ju = 13/2 was found. The new upper level was determined by adding the cg wave number of the investigated line to the energy of the lower level. This newly discovered level with energy 26036.40 cm^{-1}, odd parity, J = 13/2 and A = 651 MHz was introduced into our level data base. This newly discovered level explains all nine observed fluorescence signals (figure 6.62).

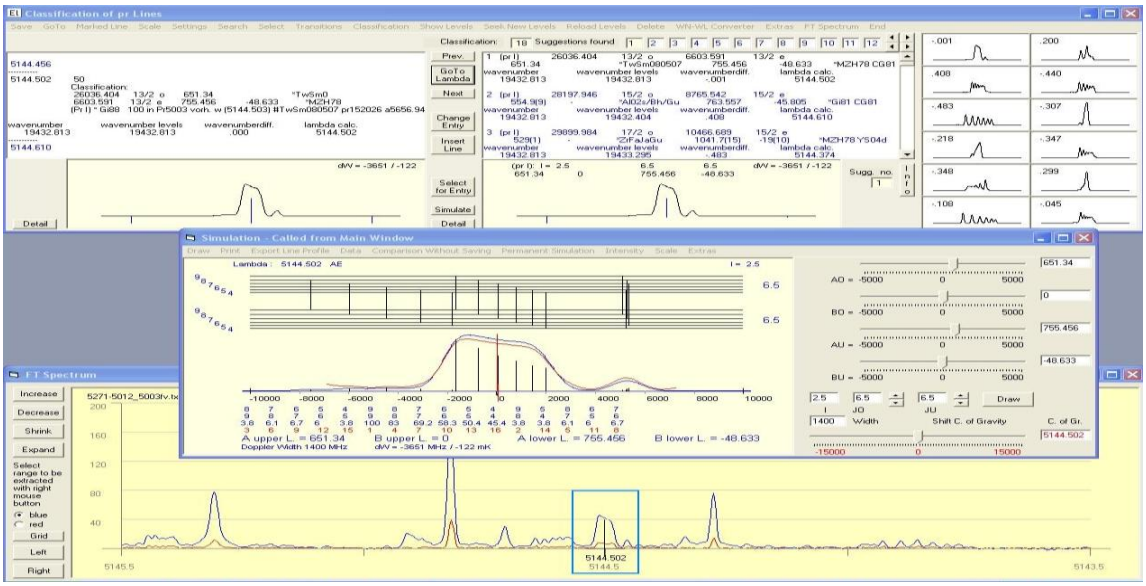

Figure 6.62: Confirmation of the existence of the newly found level from FT spectrum at fluorescence line 5144.502Å.

The new level was then confirmed by two more laser excitations from other known levels, one at line 5809.862 Å from the lower level 8829.063 cm^{-1} and another at line 5656.94 Å from the lower level 8363.901 cm^{-1} [25]. The recorded hf structures of lines 5656.94 Å and 5809.862 Å along with predicted hf patterns by classification program are shown in figures 6.63, 6.64, 6.65 and 6.66 respectively. This confirms the existence and energy of the newly discovered level.

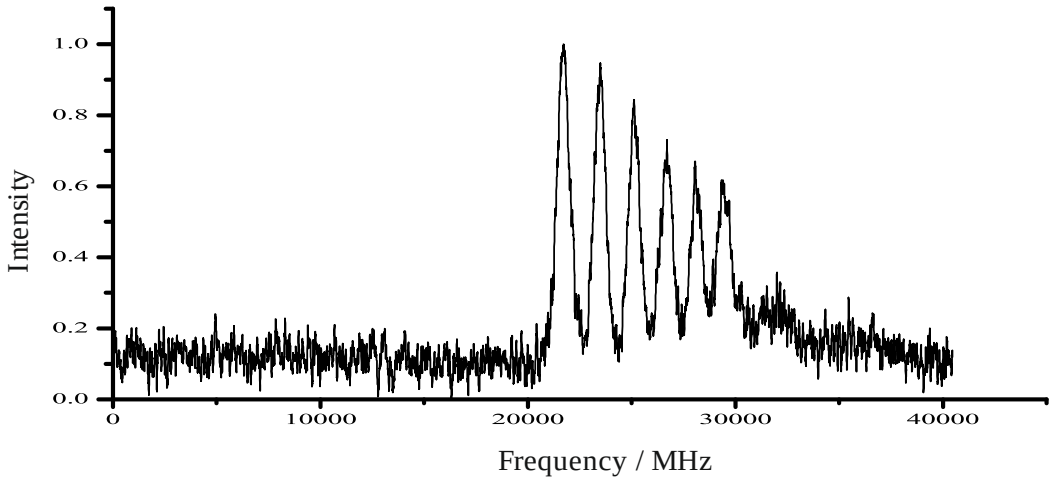

Figure 6.63: Recorded hf structure of line 5656.94 Å.

Figure 6.64: Predicted hf pattern of the line 5656.94 Å.

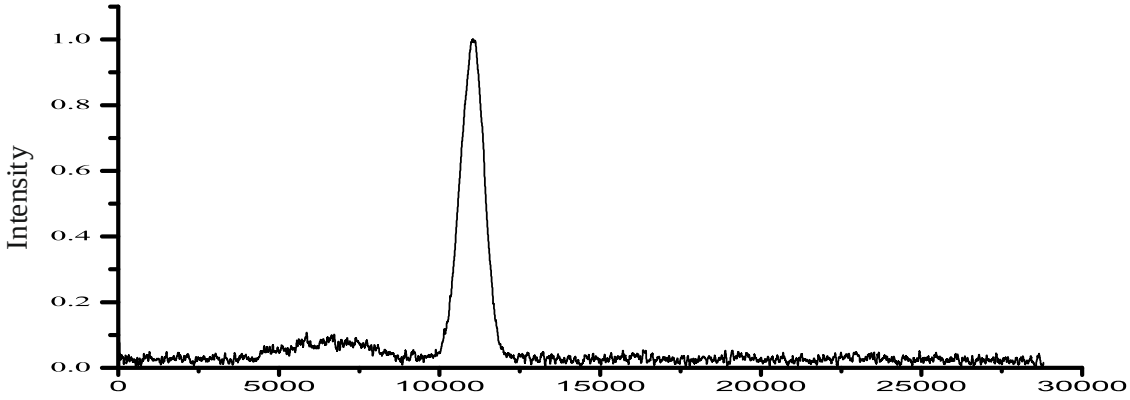

Figure 6.65: Recorded hf structure of the line 5809.848

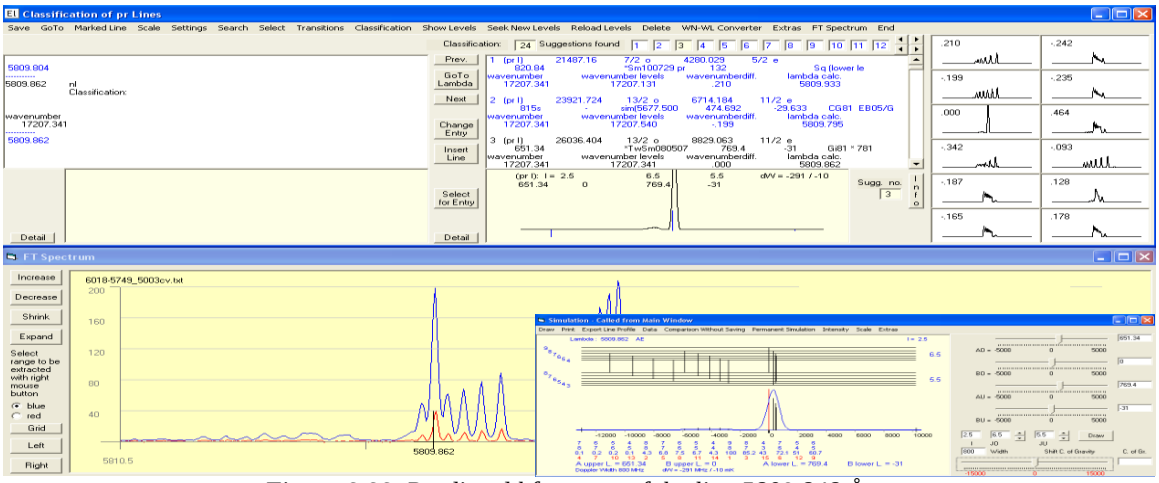

Figure 6.66: Predicted hf pattern of the line 5809.848 Å.

Those lines having a combination with the newly discovered level were then selected for the accurate determination of the cg wavelength. This allows consequently a more accurate determination of the energy of the newly discovered level. Finally, the newly discovered level with odd parity, J = 13/2, A = 650(3) MHz and B = 0(20) MHz and energy 26036.404(10) cm^{-1} explains 11 lines in the visible region (figure 6.67). All the excitation and fluorescence lines were then classified.

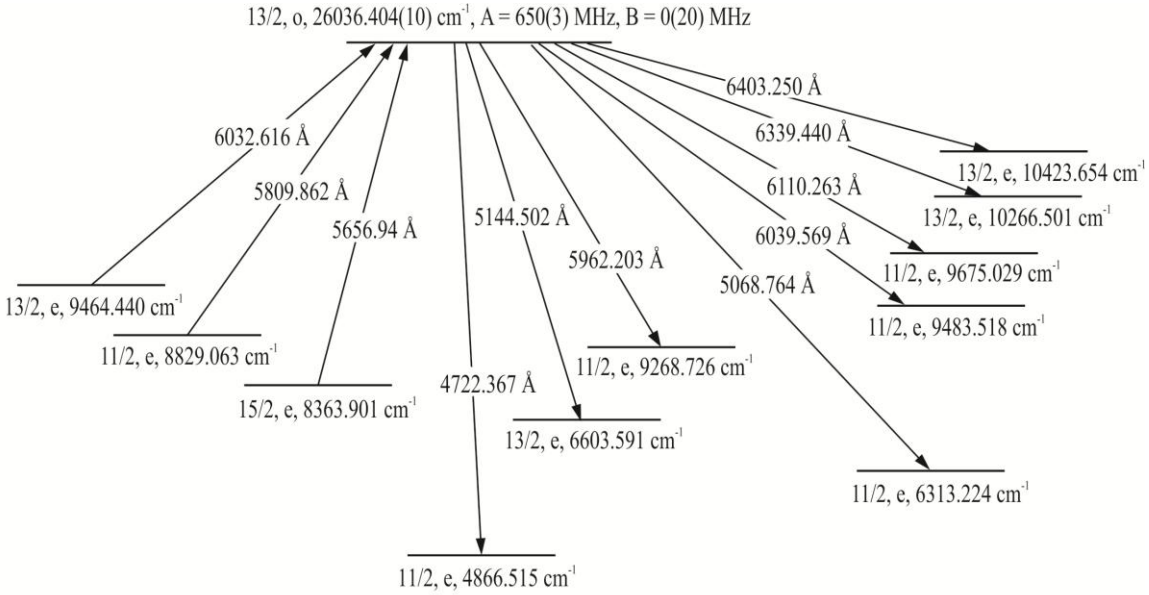

Figure 6.67: Energy level scheme for the newly discovered level 26036.404$^{o}_{13/2}$ cm^{-1}.

6.10 Discovery of a new energy level $31011.904^{o}_{15/2}\,cm^{-1}$

The spectral line 5907.006 Å has a very good SNR of 47 as can be seen in FT spectrum (figure 6.68). The suggestions for the line listed in the classification program were inspected for a possible agreement but none of them could explain both in terms of shape or component positions of the hf structure of the line. Therefore the line was experimentally investigated.

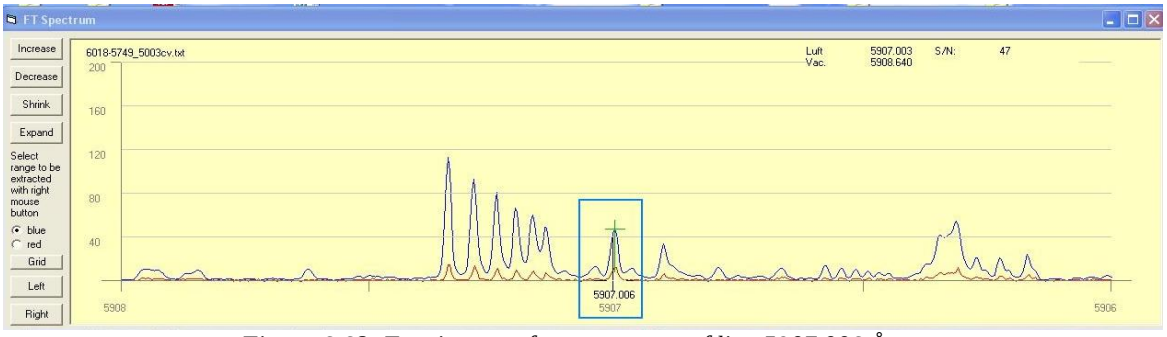

Figure 6.68: Fourier transform spectrum of line 5907.006 Å

The laser wavelength for the excitation of the line was set to 5907.64 Å and LIF signals were searched by varying the monochromator transmission wavelength.

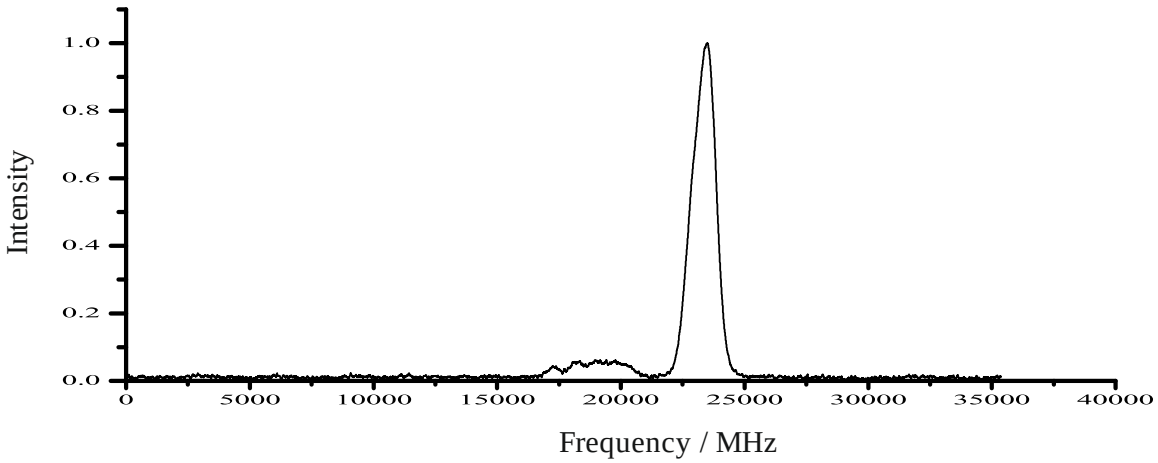

Figure 6.69: Recorded hf structure of line 5907.006 Å.

A very long list of fluorescence lines were observed viz. 4096 Å, 4337 Å, 4414 Å, 4494 Å, 4706 Å, 4819Å, 4866 Å, 5118 Å, 5139 Å, 5180 Å, 5291 Å, 5490 Å, 5594 Å and

5759 Å. The line at 4866 Å has the best SNR. After this the LIF signal was recorded by scanning the laser frequency across the hf components of the line. On all observed fluorescence lines a similar hf structure was recorded revealing all diagonal hf components being bunched together forming a single peak hf structure and one visible group of off-diagonal not completely resolved hf components on the lower frequency side (figure 6.69).

Since all observed LIF signals have same hf structure, we concluded that only one upper level was excited by laser light which decays to different lower levels. The appearance off-diagonal components on the lower frequency side suggests $\Delta J = +1$. From the shape of the single peak group of diagonal components one could guess that magnitude of the A constant for the lower combining level is a little bit larger than that of the upper combining level. Once again the recorded hf structure pattern was compared with the listed suggestions for a possible match but no match observed. It was then concluded that possibly both or one of the combining levels for the investigated line were yet be discovered.

In order to determine the spectral parameters of the combining levels of the investigated line, the recorded hf structure having good SNR was fitted to a mathematical function.

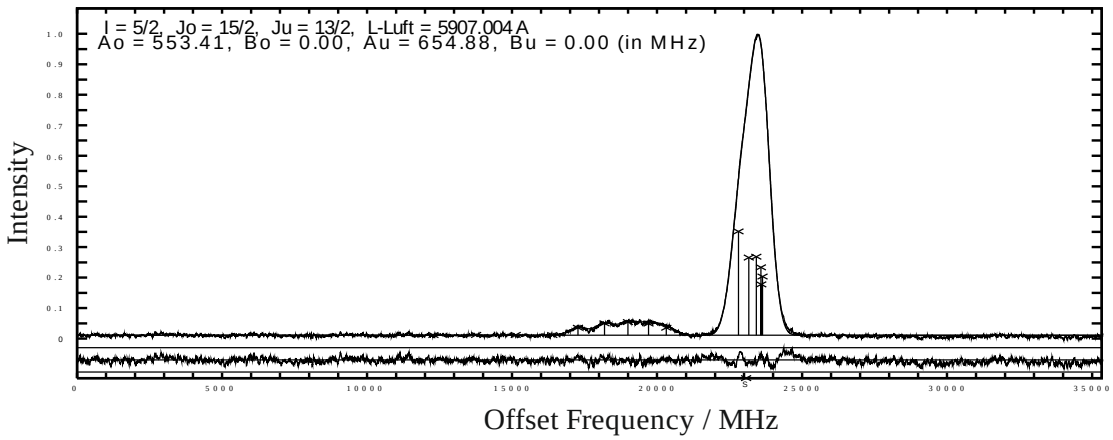

Figure 6.70: Best fit situation of the recorded hf structure of line 5907.005 Å.

A best fit with minimum SSE was obtained (figure 6.70) for spectral values Jo = 15/2, Ao = 553.41 MHz, Ju = 13/2 and Au = 654.88 MHz. Assuming an unknown upper

combining level of the investigated line, a known lower level was searched based on hf constant and J value using the searching routine in the classification program. A number of suggestions for possible new upper levels were displayed; one of them explained all the observed fluorescence lines. The known lower combining level in the suggestion for the new upper level explaining the fluorescence lines was 14087.545 cm^{-1}, even parity, Ju = 13/2, Au = 656.6 MHz. In order to have a better estimate of the A value of possibly new upper level, the recorded hf structure was again fitted now keeping fixed the A value of the known lower level. Using the cg wave number from the fitting process and the energy of the lower level, the energy of the possibly new upper level was calculated, i.e. 31011.91 cm^{-1}, odd parity, Jo = 15/2, Ao = 554.90 MHz. The newly found level was introduced in the data base of known Pr I levels and was uploaded in the classification program. All the observed fluorescence lines were explained by the transition list of the newly found level and the predicted hf structure of most of the fluorescence lines by the classification program are in agreement both in terms of shape and position of hf components in the FT spectrum. This confirms the existence of the newly found upper level of the investigated line. In order to further consolidate the energy and existence of the newly discovered level, three more laser excitations from three other known lower levels (7951.323 cm^{-1}, 13467.373 cm^{-1} and 14328.241 cm^{-1}, respectively) were performed at lines 4335.184 Å, 5698.204 Å and 5992.227 Å. On all these the lines previously observed fluorescence lines were again observed, suggesting that in each case the same upper level was excited. The hf structure of these lines was recorded by scanning the laser frequency across the hf components of the respective lines (figures 6.71, 6.72 and 6.73). The hf structures for all these lines are in good agreement with the hf structures of lines predicted by the classification program. Since the level energies of the lower combining levels were already corrected so the energy of newly discovered level was also corrected using those fluorescence lines whose hf structure is clearly visible in FT spectrum so that the cg wave number could be determined precisely.

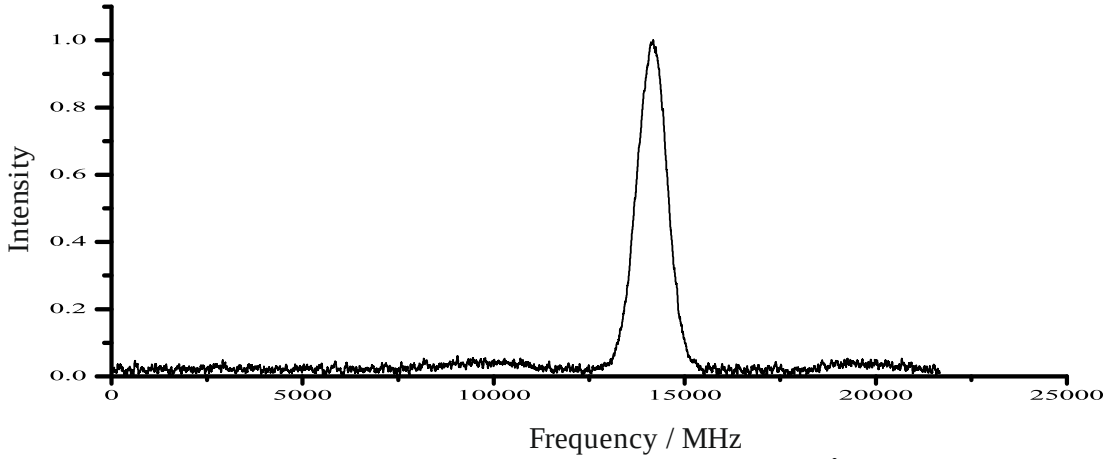

Figure 6.71: Recorded hf structure of line 4335.184 Å.

The corrected energy of the newly discovered levels is 31011.904 cm^{-1}. By using more than one recorded file for all excitations the statistical average of the A value of the newly determined level was calculated. In last newly found level 31011.904(25) cm^{-1}, odd parity, J = 11/2 , A = 553(3) MHz explained 17 lines in the visible region. The excitation and fluorescence lines were then classified. The energy level scheme for the newly discovered upper level is shown in figure 6.74.

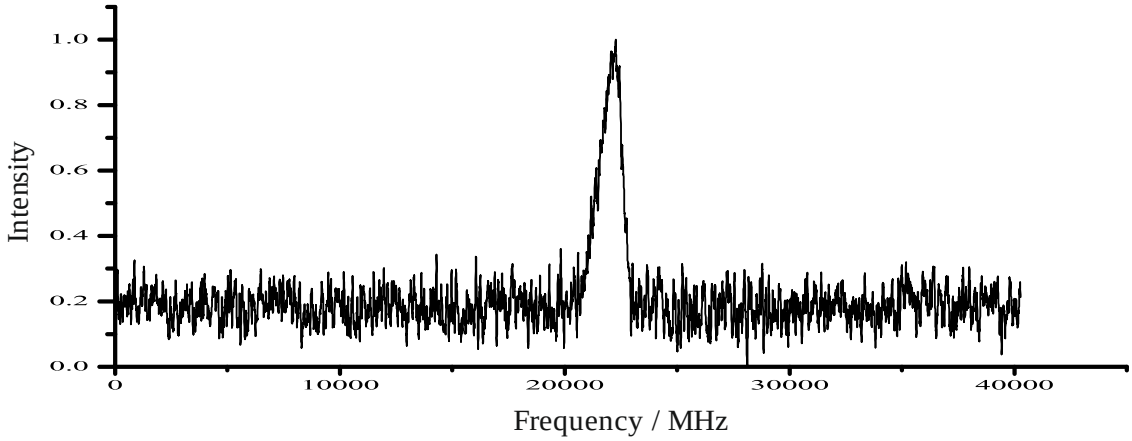

Figure 6.72: Recorded hf structure of line 5698.204 Å.

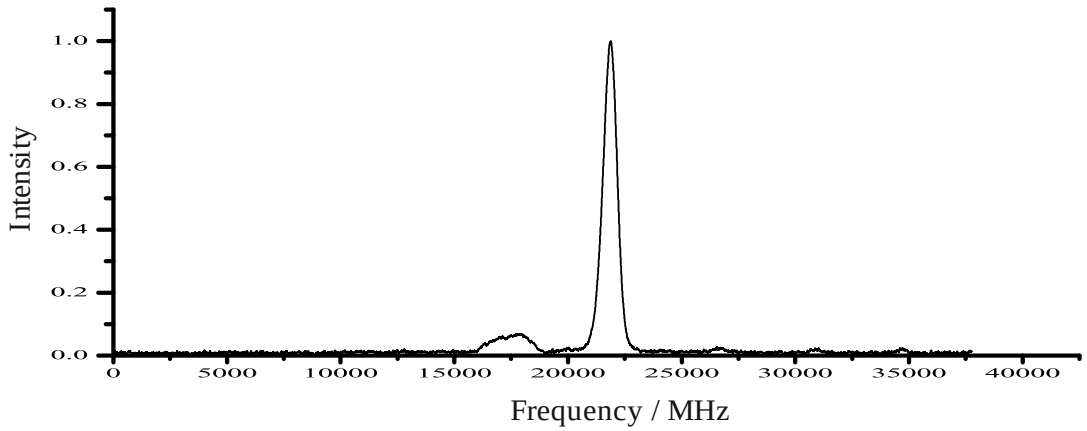

Figure 6.73: Recorded hf structure of line 5992.227Å.

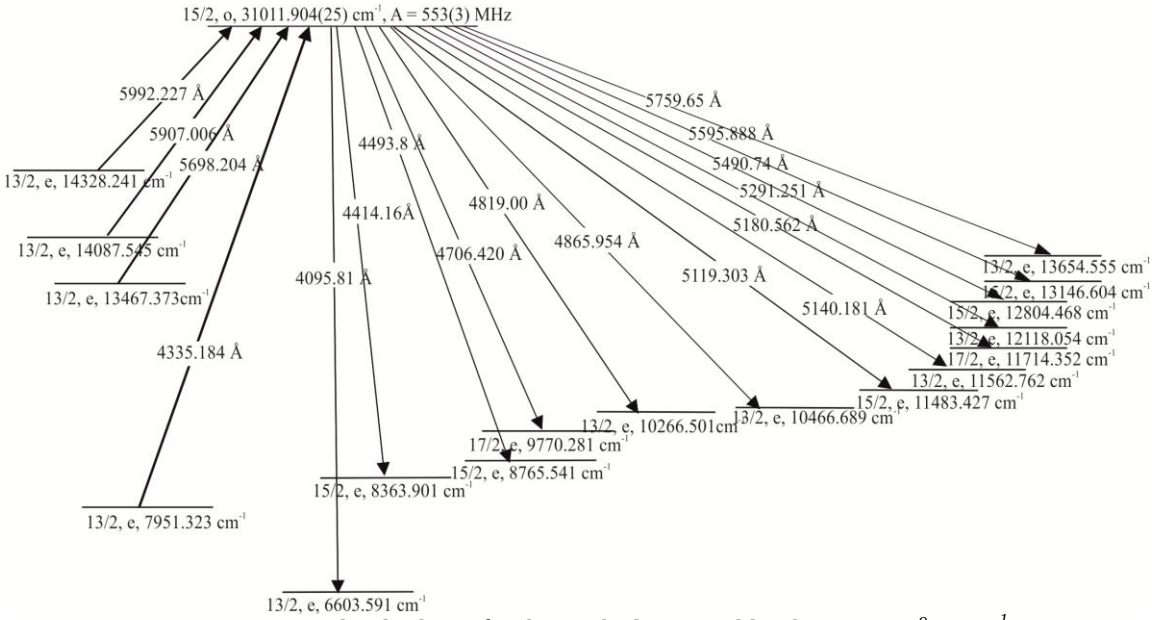

Figure 6.74: Energy level scheme for the newly discovered level 31011.904$^{o}_{15/2}$ cm^{-1}.

6.11 Discovery of a new energy level $32171.486^{o}_{17/2}$ cm^{-1}

An IR line 7249.013 Å with good SNR of 19 in the FT spectrum (figure 6.75) could not be classified by any of the suggestions listed in the classification program. This means that one or both levels involved in the formation of the line were yet to be discovered which led to the experimental investigation of the line.

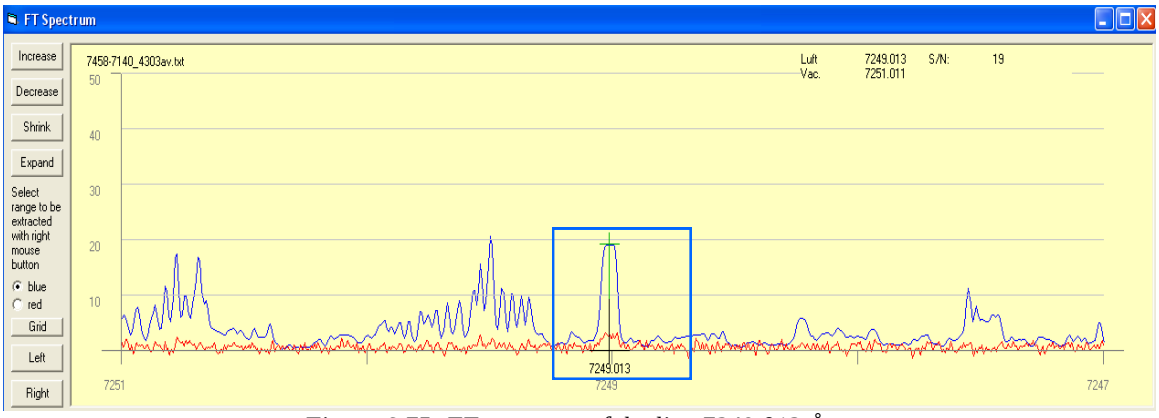

Figure 6.75: FT spectrum of the line 7249.013 Å.

The laser wavelength was set to strong peak of the investigated line at 7249.01 Å and fluorescence lines were searched by varying the transmission wavelength of the monochromator. A LIF signal was observed at 5505 Å, 5592 Å, 5682 Å, 5749 Å and 6569 Å with the strongest seen on 5682 Å. The hyperfine structure of the line was then recorded by scanning the laser frequency across the hf components of the investigated line. A hyperfine structure with narrowly spaced diagonal components and two groups of off-diagonal components appearing on both sides of the diagonal components was recorded on all observed fluorescence lines (figure 6.76). The suggestions listed by classification program for the investigated line were again inspected for a possible match but no coincidence was observed.

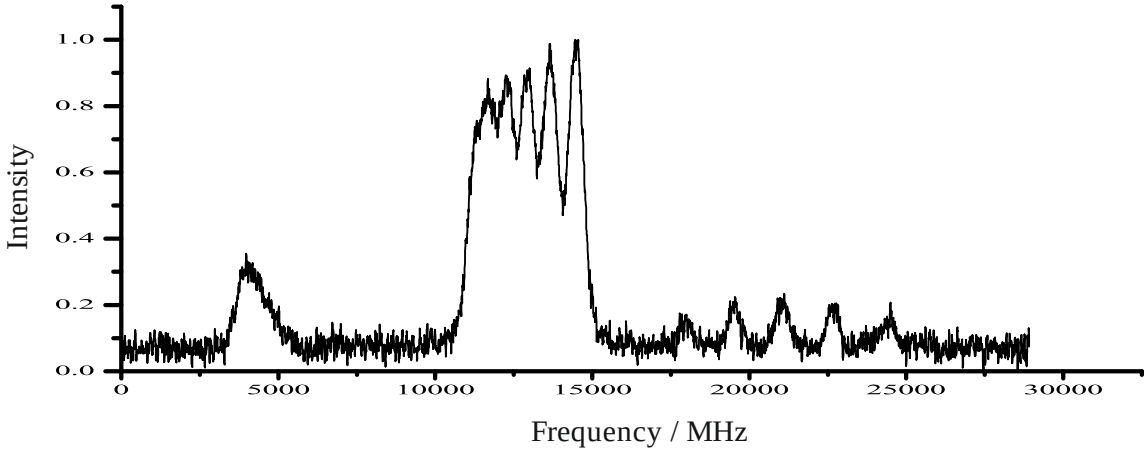

Figure 6.76: Recorded hf structure of the investigated line 7249.013 Å.

In the recorded hf structure the two off-diagonal groups of hf components are present on both sides of diagonal components; this means that the combining levels have the same angular momentum i.e. $\Delta J = 0$. In addition to this one could see that in the recorded hf structure the two groups of off-diagonal components are appreciably separated from diagonal components. This implies that both combining fine structure levels have large but comparable splitting which means that value of the A constants of upper and lower levels are large but comparable (Ao ~ Au). Since the off-diagonal components on higher frequency side are more resolved than the components on lower frequency side and the strongest diagonal component is appearing on higher frequency side, the splitting of upper level is little larger than splitting of lower level (Ao > Au). With these assumptions the recorded hf structure was simulated to obtain approximate spectral parameters (J and A values) of the combining levels. The recorded hf structure was then fitted to a mathematical function using the fitter program taking the simulated J and A values of the combining levels as input. A best fit with minimum SSE was obtained (figure 6.77) for values Jo = 17/2, Ao = 972.98 MHz, Ju = 17/2 and Au = 901.07 MHz.

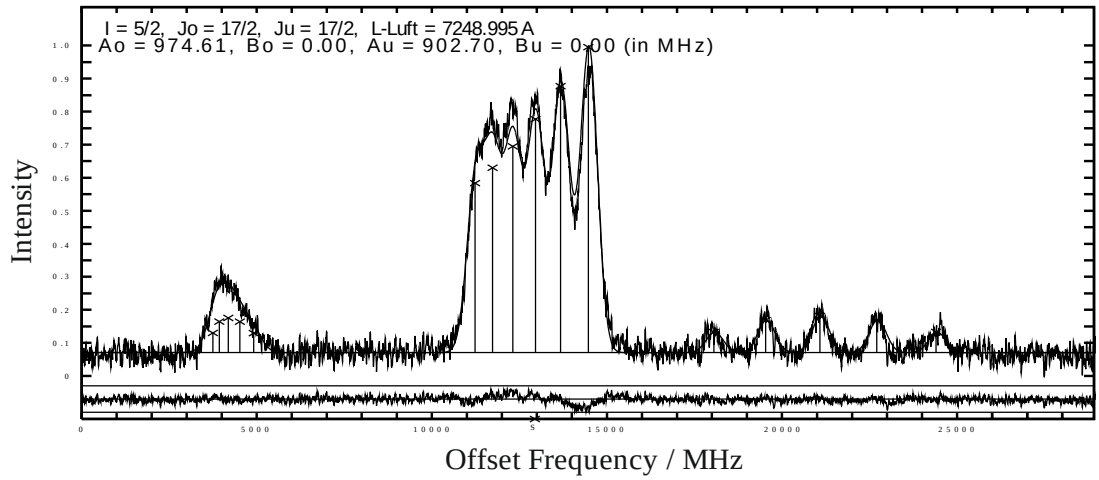

Figure 6.77: Best situation of the recorded hyperfine structure of line 7249.013 Å.

Assuming that the upper level in the investigated transition is unknown and by using the best fit J and A values for the upper and lower levels along with cg wavelength of experimentally investigated line and the fluorescence information, a possibly new upper level was found explaining all the observed fluorescence lines. The known lower combining level in the investigated transition is an even parity level with parameters 18380.305 cm^{-1}, Ju = 17/2 and Au = 902.7 MHz. To obtain better A value of the upper level the recorded hf structure was again fitted keeping fix the A value of the known lower level. The energy of the possibly new upper level was calculated by using the energy of known lower level and the cg wave number of the investigated line. This gives 32171.507 cm^{-1}, odd parity, Jo = 17/2 and Ao = 974.61 MHz. Since the energy of the known lower level is already corrected, the energy of the newly found level was corrected by accurately determining the cg of the investigated line with the help of FT spectrum. After correction the energy of the newly found level becomes 32171.486 cm^{-1}. The newly found level was introduced in the data base of known Pr I levels and was uploaded in the classification program. The newly found level could be confirmed from FT spectrum at 7343.114 Å both in terms of shape and component positions. Nevertheless to consolidate the existence of the newly found level a second laser excitation at the line 7343.114 Å was carried out. The recorded hf structure was in full agreement both in terms of shape and component positions with the hf structure

predicted by classification program (figures 6.78 and 6.79). This confirmed the energy and the existence of the newly discovered level.

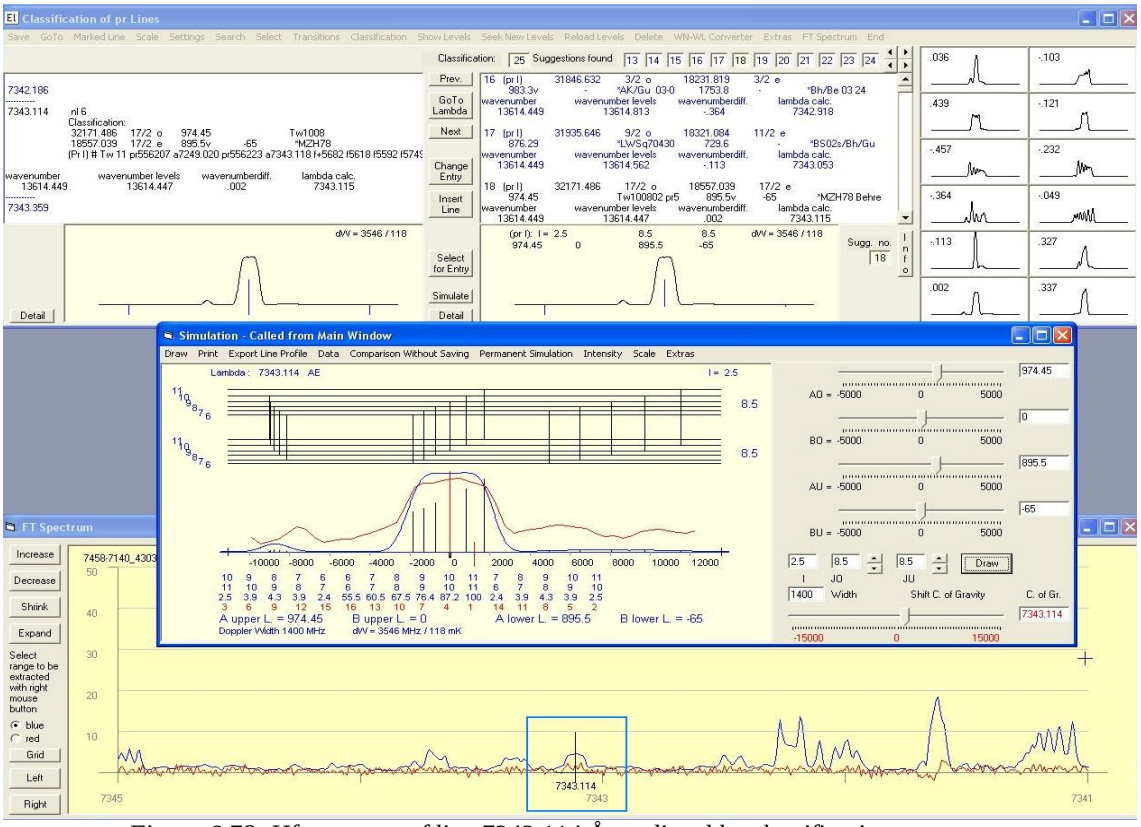

Figure 6.78: Hf structure of line 7343.114 Å predicted by classification program.

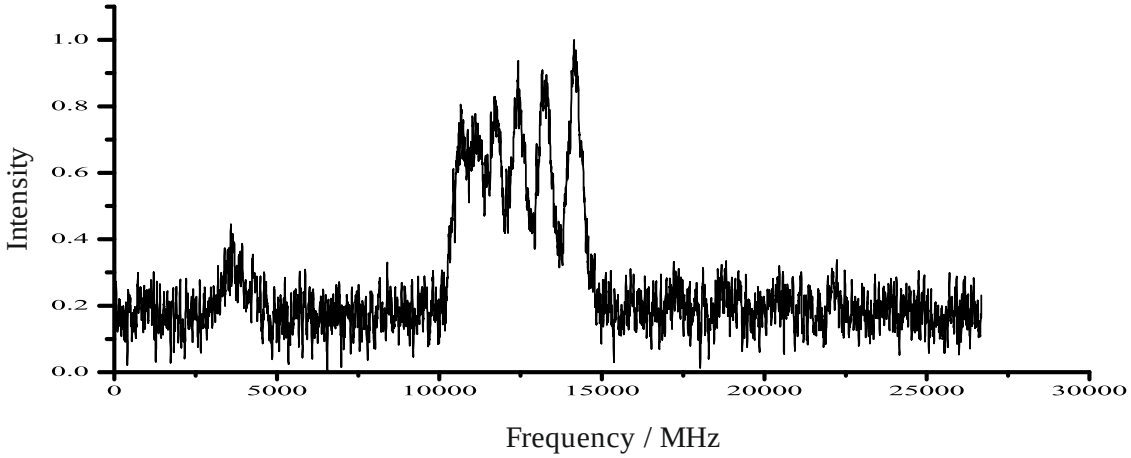

Figure 6.79: Recorded hf structure of line 7343.131 Å.

By using several recorded file for both excitations the statistical average of the A value of the newly determined level was calculated. The newly discovered upper level 32171.486(15) cm^{-1}, odd parity, J = 17/2, A = 973(5) MHz explained 4 lines in the visible region and 2 lines in far infrared region. The energy level diagram is depicted in figure 6.80. Both excitation lines and all the observed fluorescence lines were then classified.

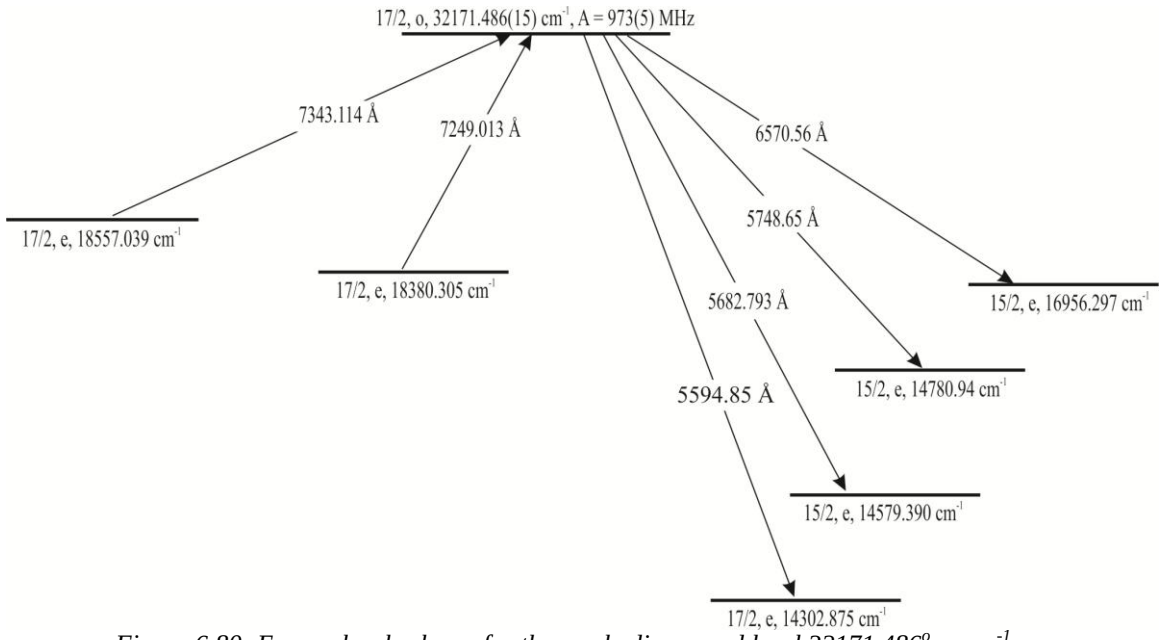

Figure 6.80: Energy level scheme for the newly discovered level 32171.486$^{o}_{17/2}$ cm^{-1}.

Table 6.1. Parity, J - value, energy and hf constants of the newly discovered Pr I levels. Excitation and fluorescence wavelengths are given in columns 5 and 6, respectively. Additionally, lines appearing in the FT spectrum classified by means of their hf patterns and wave numbers involving the new levels are given in column 7.

J	Energy cm^{-1}	A MHz	B MHz	λ_{exc} Å (in air)	λ_{LIF} Å (in air)	λ_{FT} Å (in air)
Even						
3/2	29557.116(20)	490(10)		5691.778, 5729.64	4859.93	
5/2	27976.873(20)	815(10)	-	5703.95, 6791.238	5264.343	6031.926
5/2	30799.760(20)	733(4)	-	5698.48, 5819.67	4748.267, 5591.15	
7/2	25391.496(10)	620(3)	-2(15)	5832.226, 6783.565	5832.226, 6783.565	
7/2	27336.479(10)	678(3)	-	5992.672, 6173.073	5237.890, 6095.935 6406.095	6274.359, 6565.201
7/2	27635.199(15)	536(5)	-	5986.887, 6158.90	3617.54, 5157.18, 6285.778, 6414.543	7810.656
7/2	28578.627(20)	545(5)	-	5666.73, 5733.324	4917.83, 5577.38, 5733.324	
7/2	29146.201(10)	495(7)	-	5740.408, 5847.609	5109.385, 5490.098,	5634.406
7/2	30582.777(20)	627(6)	-	5802.65, 5894.12	4759.905, 4797.715, 4965.638, 5894.12	
7/2	32011.634(20)	738(10)	-	5820.48, 5845.93	4636.565, 4833.786	
9/2	28314.791(10)	641(2)	-	5883.371, 6146.525	5883.371, 5911.399	
9/2	29053.224(10)	726(3)	-	5664.082, 5771.22	4944.744, 5133.78, 5518.275, 5664.082, 6645.334	
9/2	30021.169(15)	725(15)	-	5845.699, 5998.18	3490.06, 4890.68 5108.129, 5348.546 5611.100, 5634.39 6455.34	
9/2	30096.765(15)	698(5)	-	5805.90, 6214.271	5088.473, 5587.389	
9/2	30485.194(20)	684(3)	-	5659.61, 5677.81, 5837.903, 5928.218	4782.121, 4989.82, 5468.668, 5837.903	
9/2	30902.769(15)	732(7)	-	5696.833, 5698.936	3235.022	5917.780
9/2	31506.29(3)	531(5)	-	5711.395, 5958.731	3173.04, 5507.43, 5958.731	
9/2	31962.229(20)	502(4)	-	5636.68, 5736.361	4647.214, 5566.403, 5736.361	

11/2	23403.929(10)	684(3)	-32(10)	6524.111, 6597.188	4538.543, 4863.120	7286.758
11/2	23582.910(10)	518(4)	-7(42)	4821.144, 6520.178	4821.144, 6520.178	
11/2	24519.749(10)	556(7)	-12(12)	6081.284, 6144.730	4612.742, 6332.852	8545.611
11/2	26147.987(10)	778(3)	54(20)	5740.733, 6072.250	3823.301, 6352.596	7169.725, 7818.003
11/2	29363.384(10)	738(5)	-	5669.702, 5774.254	3404.625, 5053.292, 5274.842, 6064.185	
11/2	30401.686(15)	642(4)	-	5686.50, 5864.283, 6453.49	3444.308, 5241.833, 5493.764, 5499.144, 5686.50	
11/2	30465.360(15)	688(3)	-	5665.975, 5844.67	5222.41, 5474.61, 5844.67, 6072.52, 6494.352	
11/2	30895.062(10)	593(5)	-	5693.443, 5699.34, 5915.827	4690.167, 4880.42 5109.65, 6110.527	
11/2	32587.30(3)	460(12)	-	5746.82, 6144.89, 6184.50	3203.10, 4702.88, 4855.331	
13/2	25092.537(10)	492(6)	-	6809.278, 6819.019	4493.97, 5876.529, 6111.114, 6488.196	7260.116, 7756.874
13/2	27851.627(15)	320(12)	-	6207.419, 7218.57	3776.07, 5491.532	
13/2	28238.557(10)	591(3)	-	5909.89, 6061.783, 6561.359	3721.679, 6241.848, 6561.359	
13/2	29278.395(20)	590(5)	-	5702.25, 5855.201	3582.977, 3782.27, 5092.418, 5855.201, 6095.611	
13/2	29335.781(20)	583(7)	-	5683.646, 6248.303, 6519.87	3575.622, 5355.604, 6248.303	6863.288
13/2	29753.559(15)	631(3)	-	6098.455, 6175.675	3522.979, 5238.37, 5551.78, 5572.924, 6344.377	
13/2	30076.595(10)	520(6)	-	6531.124, 6638.931	5474.348	
13/2	30211.355(10)	650(3)	15(20)	6167.678, 6254.09	3467.045, 5054.294, 5115.650, 5414.138, 5434.245, 5932.775	

13/2	30345.528(15)	825(4)	-	6114.666, 6117.040	5025.03, 5448.55, 5723.217, 5885.910, 5957.810, 6522.444	
13/2	30679.356(20)	561(4)	-	5992.313, 6267.65	5299.423, 5351.187, 5411.19, 5615.888, 5841.60	
13/2	32115.075(25)	593(5)	-	5678.67, 5847.363	3415.682	
13/2	32512.919(25)	595(15)	-	5771.50, 5771.73, 5771.79, 5824.04	4872.94, 5123.928, 5398.944, 5466.936, 5621.43	
13/2	32870.250(15)	569(2)	-	5806.935, 6039.844	5031.76, 5918.09	
13/2	33155.831(20)	555(3)	-	5712.18, 5819.656	3298.39, 4724.866, 4960.46, 5511.832, 5613.768, 5889.16, 5937.40	
13/2	34180.492(20)	667(5)	-	5746.96, 6503.351	5746.96, 6503.351, 6557.45	
15/2	30242.928(25)	462(5)	-	5798.548, 5893.711, 5994.46, 6711.57	3649.103, 5120.85, 5913.047, 6153.280, 6286.476, 6460.92	
15/2	33563.160(10)	503(5)	-	5751.162, 5759.40	3254.649, 5247.066, 6034.149	8768.915
15/2	33858.230(20)	467(5)	-	5663.129, 5855.44	3391.48, 5491.775	
17/2	29834.920(10)	421(10)	-	6452.017, 6713.571	5547.764	6925.214, 8814.272
Odd						
3/2	28465.851(20)	1274(6)	-	5668.40, 5759.38	4541.28, 5313.181	8549.249, 9499.659
5/2	26144.239(15)	935(6)	-	6083.395, 6161.22	5076.678, 6268.066	
5/2	26593.333(10)	657(10)	-	6563.497, 6789.742	4963.482, 5268.378, 5919.519, 5921.56	
5/2	27870.595(20)	900(6)		6161.906, 6170.45	5034.475, 5505.078	
5/2	28513.764(20)	734(10)	-	5743.531, 5828.607	4548.69, 4876.525, 5055.173, 5299.69, 5316.776, 5457.297	

5/2	28658.247(15)	1230(5)	-	5696.243, 5876.597	4501.936, 4842.394	
5/2	29563.401(10)	869(8)	-	4341.35, 5708.813	4555.37, 5020.336, 5088.880, 5336.310	
5/2	30270.526(20)	844(5)	-	5757.620, 5799.56	4197.20, 4413.169, 4491.62, 4848.18, 4979.75, 5142.22, 5262.719, 5487.240	
5/2	31789.286(20)	835(13)	-	5755.693, 5758.692, 5911.49	3945.61, 4336.850, 5177.876, 5493.32	
7/2	26253.598(10)	923(5)	-	7279.253, 7490.52	4581.379, 5364.42, 5574.654	
7/2	28264.916(20)	720(3)	-	5763.90, 5826.84, 5980.87	4454.67, 4841.854, 4936.450,5119.594, 5388.084	7405.025
7/2	*29855.058(15)	1080(4)	-	4271.71, 5701.93	4580.454, 5084.977, 5332.60, 5380.394	
7/2	30828.528(15)	813(4)	-	5647.89, 5848.65	5185.567, 5217.826	
7/2	31282.953(20)	935(5)	-	5712.18, 5847.51	3926.61, 4507.722, 4633.01, 5091.10, 5108.512	
9/2	22641.351(10)	645(8)	55(40)	5944.198, 6207.232	5944.198, 6207.232	7237.935, 7475.903, 7597.941, 7710.162, 8725.926
9/2	23817.594(10)	633(4)	-	5784.756, 6669.926	5157.092, 6171.073, 6325.561, 6669.926	7338.599, 7741.667, 7913.475, 9029.698, 9575.362
9/2	24058.128(10)	751(5)	-	5633.857, 5705.346	5093.887, 5482.364	7564.089, 7600.104, 8252.693, 8664.316
9/2	26497.094(15)	986(3)	-	5748.153, 5802.773	4530.822, 4621.790, 4953.065, 5053.46, 5295.234, 5942.927, 6385.686, 6418.058	

9/2	28215.971(20)	780(6)	-	5869.820, 6057.924, 6190.94	4203.37, 4281.547, 4564.358, 4649.474, 4688.451, 5107.879, 5156.68, 5336.84, 5391.971, 5463.626, 5597.792, 5869.820, 5970.79, 6255.56	
9/2	29742.537(20)	777(8)	-	5837.850, 7224.682	4018.80, 4266.956, 4341.250, 4375.214, 4934.694, 5289.215, 5386.97	
9/2	29921.796(15)	756(13)	-	4341.155, 5788.714, 6173.30	4802.481, 4891.413, 5418.728	
9/2	30670.529(10)	682(5)	-	4336.594, 5746.23, 5780.904, 5904.748	4336.594, 4577.16, 4635.735, 4671.20, 4882.459, 5130.423, 5154.188, 5251.214, 5338.59, 5422.688, 5537.760	
9/2	31279.329(20)	696(8)	-	5699.771, 5846.00, 5870.38, 5971.917	3784.966, 4508.46, 4541.99, 4680.09, 5170.49	
9/2	31713.237(20)	508(5)	-	5732.24, 5797.196	3723.79, 4148.93, 4421.93, 4497.220, 4808.00, 4891.24, 5057.007	
9/2	32503.025(20)	393(6)	-	5748.05, 5890.62	3617.370, 4379.35, 4481.39, 4845.08, 4862.73, 5198.65, 5248.211,5290.27, 5339.92, 5416.45	
9/2	34116.595(20)	620(7)	-	5692.49, 5802.637	3533.34, 4980.99, 5106.43	
11/2	19011.607(20)	845(10)	-	7126.08, 7202.695		
11/2	26026.626(10)	732(3)	-	5751.22, 5813.165, 6036.177	4629.533, 4724.551, 4948.198, 5071.277, 5176.568, 5554.831	7474.555
11/2	28313.508(10)	1137(7)	-	5836.396, 5963.546, 7072.613	4628.478, 4667.103, 5130.871, 6383.150, 6543.633, 6693.156	8021.533, 8165.278

11/2	28798.703(15)	657(4)	-	5675.627, 5800.22, 5993.306	4722.663, 5006.203, 5118.909, 5175.835, 5420.91	6841.638
11/2	30688.191(20)	575(10)	-63(30)	5740.39, 5852.32	3807.58, 3871.62, 4714.621, 4933.35, 5151.789	
11/2	31562.535(20)	665(8)	-	5635.399, 5651.25, 5684.19	3744.812, 3883.956, 4005.45, 4995.38, 5288.374	
11/2	31650.07(3)	648(5)	-	5771.455, 6742.92	3945.70, 4549.322, 5098.43, 5134.690	
11/2	33212.554(15)	510(10)	-	5806.27, 6654.468	3473.60, 3716.507, 3757.06, 4617.69, 5008.15, 5013.66, 5278.45, 5561.92, 5594.496, 5619.98	
7/2	33695.84(3)	568(12)	-	5647.75, 5754.21, 5765.36	4065.41, 5008.49, 5251.96, 5300.80	
13/2	26036.404(10)	650(3)	0(20)	5656.94, 5809.862, 6032.616	4722.367, 5068.764, 5144.502, 5809.862, 5962.203, 6039.569, 6110.263, 6339.440, 6403.250	
13/2	27334.898(20)	730(3)	-	5660.985, 5911.59	4755.665, 4848.138, 4890.532, 5073.499, 5157.572, 5533.671	
13/2	30509.700(25)	715(5)	-	5721.200, 5792.457, 5866.11	3898.567, 4597.65, 4754.644, 4814.61, 5248.764	
13/2	32704.514(20)	639(2)	-	5767.997, 5783.97	3788.053, 4038.742, 5369.949	
13/2	32758.666(20)	560(10)	-	5665.059, 5750.03	3780.296, 4098.08, 4858.077, 5158.08, 5182.25, 5380.550, 5476.85	
13/2	32772.769(25)	556(5)	-	5701.416, 5919.09	3820.205, 4695.87, 4871.40	
15/2	27982.287(10)	680(5)	-	7164.644, 7321.819	4990.88, 5095.839, 5202.346	

15/2	30726.768(15)	1000(3)	-	7102.249, 7271.913	4770.457, 5189.617, 5258.26, 5372.33, 5686.64, 5782.836, 6820.852	
15/2	30850.254(20)	722(3)	-	5741.820, 5751.20	4365.79, 4736.915, 5156.56	7485.282
15/2	31011.904(25)	553(3)	-	4335.184, 5698.204, 5907.006, 5992.227	4095.81, 4335.184, 4414.16, 4493.86, 4706.420, 4819.00, 4865.954, 5119.303, 5140.18, 5180.56, 5291.25, 5490.74, 5759.65	
15/2	31699.958(25)	515(8)	-	5754.887, 5802.25, 6122.872	3983.514, 4284.01, 4359.03, 4558.75, 4940.05, 5002.21, 5290.796, 5388.36, 5540.040, 6042.859, 6122.872, 6140.87	
15/2	32784.476(25)	465(5)	-	5757.32, 6187.32	3818.49,4162.20, 5003.59,5090.777, 5167.730	
15/2	33168.727(20)	773(4)	-	5746.789, 5846.73	4605.77, 5123.05, 5346.484, 5550.110	
15/2	35103.018(25)	522(3)	-	5656.74, 6140.09	3681.963, 3942.469, 4743.786, 5143.34	
17/2	27405.036(15)	652(3)	-30(30)	5669.049, 6596.873	5250.329, 5363.464, 5669.049	7473.841
17/2	32171.486(15)	973(5)	-	7249.013, 7343.114	5594.85, 5682.793, 5748.65, 6570.56	
17/2	32925.302(10)	428(5)	-	5904.856, 6142.81	5368.378, 5449.293, 5555.43	
17/2	33124.424(10)	472(8)	-	5726.239, 5836.23	5078.486, 5235.319, 5311.581, 5390.78	
17/2	35343.001(25)	460(15)	-	5664.82, 5886.059	3905.506, 5080.605, 5127.374, 5374.847, 5529.176	

* This energy level was introduced by the Guthöhrlein group as test level in 2003 but they were not sure about it.

Table 6.2. Lines classified via laser excitation involving the new levels. For hf patterns not visible in the FT spectrum or masked in blend situations "–" is given in column 3. For such lines, the cg wavelengths are determined by our lambdameter. 'nl' means 'new line' not listed in commonly used wavelength tables, e.g. [95].

λ_{exc} / Å (in air)	Comment	SNR	Even Levels		Odd Levels	
			J	Energy / cm^{-1}	J	Energy / cm^{-1}
4271.71	nl	-	5/2	6451.808	7/2	29855.058
4335.184	nl	5	13/2	7951.323	15/2	31011.904
4336.594	nl	8	9/2	7617.440	9/2	30670.529
4341.155	nl	6	11/2	6892.949	9/2	29921.796
4341.35	nl	-	7/2	6535.572	5/2	29563.401
4821.144	nl	24	11/2	23582.910	13/2	2846.741
5633.857	nl	12	11/2	6313.224	9/2	24058.128
5635.399	nl	7	9/2	13822.494	11/2	31562.535
5636.68	nl	-	9/2	31962.229	11/2	14226.22
5647.75	nl	-	9/2	15994.584	7/2	33695.84
5647.89	nl	-	5/2	13127.722	7/2	30828.528
5651.25	nl	-	11/2	13872.266	11/2	31562.535
5656.74	nl	-	15/2	17429.924	15/2	35103.018
5656.94	nl	-	15/2	8363.901	13/2	26036.404
5659.61	nl	-	9/2	30485.194	9/2	12821.044
5660.985	nl	12	11/2	9675.029	13/2	27334.898
5663.129	nl	8	15/2	33858.230	13/2	16205.05
5664.082		42	9/2	29053.224	7/2	11403.011
5664.82	nl	-	17/2	17695.09	17/2	35343.001
5665.059	nl	15	11/2	15111.49	13/2	32758.666
5665.975	nl	17	11/2	30465.360	9/2	12821.044
5666.73	nl	-	7/2	28578.627	9/2	10936.647
5668.40	nl	-	5/2	10829.07	3/2	28465.851
5669.049	nl	14	17/2	9770.281	17/2	27405.036
5669.702	nl	8	11/2	29363.384	9/2	11730.67
5675.627		30	9/2	11184.396	11/2	28798.703
5677.81	nl	-	9/2	30485.194	11/2	12877.682
5678.67	nl	-	13/2	32115.075	13/2	14510.209

5683.646	nl	17	13/2	29335.781	13/2	11746.328
5684.19	nl	-	9/2	13974.732	11/2	31562.535
5686.50	nl	-	11/2	30401.686	9/2	12821.044
5691.778	nl	13	3/2	29557.116	3/2	11992.79
5692.49	nl	-	9/2	16554.39	9/2	34116.595
5693.443	nl	10	11/2	30895.062	13/2	13335.87
5696.243	nl	10	5/2	11107.7	5/2	28658.247
5696.833	nl	5	9/2	30902.769	9/2	13354.04
5698.204	nl	7	13/2	13467.373	15/2	31011.904
5698.48	nl	-	5/2	30799.760	5/2	13256.082
5698.936	nl	4	9/2	30902.769	11/2	13360.5
5699.34	nl	-	11/2	30895.062	9/2	13354.04
5699.771	nl	8	7/2	13739.71	9/2	31279.329
5701.416	nl	6	11/2	15238.14	13/2	32772.769
5701.93	nl	-	7/2	12321.99	7/2	29855.058
5702.25	nl	-	13/2	29278.395	13/2	11746.328
5703.95	nl	-	5/2	27976.873	7/2	10450
5705.346		162	7/2	6535.572	9/2	24058.128
5708.813	nl	15	3/2	12051.49	5/2	29563.401
5711.395	nl	10	9/2	31506.29	11/2	14002.294
5712.18	nl	-	13/2	33155.831	13/2	15654.24
5712.18	nl	-	7/2	13781.37	7/2	31282.953
5721.200	nl	8	11/2	13035.697	13/2	30509.700
5726.239	nl	10	17/2	15665.8	17/2	33124.424
5729.64	nl	1	3/2	29557.116	5/2	12108.87
5732.24	nl	-	9/2	14272.877	9/2	31713.237
5733.324	nl	20	7/2	28578.627	5/2	11141.576
5736.361	nl	8	9/2	31962.229	9/2	14534.39
5740.39	nl	-	9/2	13272.61	11/2	30688.191
5740.39	nl	-	9/2	13272.61	11/2	30688.191
5740.408	nl	13	7/2	29146.201.2	9/2	11730.67
5740.733	nl	15	11/2	26147.987	13/2	8733.440

5741.820	nl	5	15/2	13439.009	15/2	30850.254
5743.531	nl	12	5/2	11107.7	5/2	28513.764
5746.23	nl	-	9/2	13272.613	9/2	30670.529
5746.789	nl	20	13/2	15772.55	15/2	33168.727
5746.82	nl	-	11/2	32587.30	13/2	15191.22
5746.96	nl	-	13/2	34180.492	15/2	16784.800
5748.05	nl	-	7/2	15110.661	9/2	32503.025
5748.153	nl	12	9/2	9105.020	9/2	26497.094
5750.03	nl	1	13/2	15372.27	13/2	32758.666
5751.162	nl	15	15/2	33563.160	15/2	16180.2
5751.20	nl	-	13/2	13467.373	15/2	30850.254
5751.22	nl	-	9/2	8643.824	11/2	26026.626
5754.21	nl	-	9/2	16322.122	7/2	33695.84
5754.887		36	13/2	14328.241	15/2	31699.958
5755.693	nl	5	3/2	14420	5/2	31789.286
5757.32	nl	-	13/2	15420.12	15/2	32784.476
5757.620	nl	8	5/2	12907.06	5/2	30270.526
5758.692	nl	13	7/2	14429.05	5/2	31789.286
5759.38	nl	-	5/2	11107.7	3/2	28465.851
5759.40	nl	-	15/2	33563.160	13/2	16205.05
5763.90	nl	-	9/2	10920.365	7/2	28264.916
5765.36	nl	-	5/2	16355.699	7/2	33695.84
5767.997	nl	18	13/2	15372.271	13/2	32704.514
5771.22	nl	-	9/2	29053.224	9/2	11730.668
5771.455	nl	10	13/2	14328.24	11/2	31650.07
5771.50	nl	-	13/2	15191.218	13/2	32512.919
5771.73	nl	-	13/2	15191.891	13/2	32512.919
5771.79	nl	-	15/2	15192.075	13/2	32512.919
5774.254	nl	8	11/2	29363.384	9/2	12049.94
5780.904	nl	5	11/2	13376.992	9/2	30670.529
5783.97	nl	-	13/2	15420.120	13/2	32704.514
5784.756		38	7/2	6535.572	9/2	23817.594

5788.714	nl	5	9/2	12651.59	9/2	29921.796
5792.457	nl	4	11/2	13250.673	13/2	30509.700
5797.196	nl	8	9/2	14468.303	9/2	31713.237
5798.548	nl	11	15/2	30242.928	15/2	13002.020
5799.56	nl	-	7/2	13032.63	5/2	30270.526
5800.22	nl	-	13/2	11562.762	11/2	28798.703
5802.25	nl	-	13/2	14470.047	15/2	31699.958
5802.637	nl	9	9/2	16887.83	9/2	34116.595
5802.65	nl	-	7/2	30582.777	9/2	13354.04
5802.773	nl	15	11/2	9268.726	9/2	26497.094
5805.90	nl	-	9/2	30096.765	11/2	12877.68
5806.27	nl	-	9/2	15994.62	11/2	33212.554
5806.935	nl	17	13/2	32870.250	13/2	15654.24
5809.862		200	11/2	8829.063	13/2	26036.404
5813.165	nl	3	11/2	8829.063	11/2	26026.626
5819.656	nl	5	13/2	33155.831	11/2	15977.45
5819.67	nl	-	5/2	30799.760	7/2	13621.400
5820.48	nl	-	7/2	32011.634	5/2	14835.7
5824.04	nl	8	13/2	32512.919	13/2	15347.43
5826.84	nl	-	5/2	11107.696	7/2	28264.916
5828.607	nl	12	3/2	11361.76	5/2	28513.764
5832.226		122	7/2	25391.496	9/2	8250.143
5836.23	nl	-	15/2	15994.78	17/2	33124.424
5836.396	nl	13	9/2	11184.396	11/2	28313.508
5837.850		15	7/2	12617.700	9/2	29742.537
5837.903	nl	12	9/2	30485.194	11/2	13360.502
5844.67	nl	-	11/2	30465.360	11/2	13360.502
5845.699	nl	22	9/2	30021.169	7/2	12919.32
5845.93	nl	-	7/2	32011.634	9/2	14910.48
5846.00	nl	-	11/2	14178.37	9/2	31279.329
5846.73	nl	-	13/2	16069.89	15/2	33168.727
5847.363	nl	8	13/2	32115.075	13/2	15018.088

5847.51	nl	-	9/2	14186.35	7/2	31282.953
5847.609		22	7/2	29146.201	9/2	12049.94
5848.65	nl	-	5/2	13735.298	7/2	30828.528
5852.32	nl	-	9/2	13605.67	11/2	30688.191
5855.201	nl	12	13/2	29278.395	11/2	12204.286
5855.44	nl	-	15/2	33858.230	15/2	16784.83
5864.283	nl	6	11/2	30401.686	9/2	13354.04
5866.11	nl	-	13/2	13467.373	13/2	30509.700
5869.820	nl	18	9/2	11184.4	9/2	28215.971
5870.38	nl	-	7/2	14249.4	9/2	31279.329
5876.597	nl	12	5/2	11646.31	5/2	28658.247
5883.371		15	9/2	28314.791	11/2	11322.44
5886.059	nl	15	15/2	18358.41	17/2	35343.001
5890.62	nl	-	9/2	15531.574	9/2	32503.025
5893.711		15	15/2	30242.928	17/2	13280.404
5894.12	nl	-	7/2	30582.777	7/2	13621.400
5904.748	nl	6	7/2	13739.706	9/2	30670.529
5904.856	nl	7	15/2	15994.78	17/2	32925.302
5907.006		43	13/2	14087.545	15/2	31011.904
5909.89	nl	-	13/2	28238.557	11/2	11322.443
5911.49	nl	-	3/2	14877.86	5/2	31789.286
5911.59	nl	-	13/2	10423.654	13/2	27334.898
5915.827	nl	10	11/2	30895.062	13/2	13995.93
5919.09	nl	-	11/2	15882.93	13/2	32772.769
5928.218	nl	10	9/2	30485.194	7/2	13621.400
5944.198		57	9/2	5822.89	9/2	22641.351
5958.731		12	9/2	31506.29	11/2	14728.843
5963.546	nl	6	9/2	11549.602	11/2	28313.508
5971.917	nl	4	7/2	14538.93	9/2	31279.329
5980.87	nl	-	9/2	11549.602	7/2	28264.916
5986.887	nl	10	7/2	27635.199	9/2	10936.65
5992.227		60	13/2	14328.241	15/2	31011.904

5992.313	nl	16	13/2	30679.356	13/2	13995.93
5992.672	nl	23	7/2	27336.479	7/2	10654.05
5993.306		10	13/2	12118.039	11/2	28798.703
5994.46	nl	-	15/2	30242.928	15/2	13565.490
5998.18	nl	-	9/2	30021.169	9/2	13354.04
6032.616		47	13/2	9464.440	13/2	26036.404
6036.177		20	13/2	9464.440	11/2	26026.626
6039.844		15	13/2	32870.250	13/2	16318.12
6057.924	nl	52	9/2	11713.24	9/2	28215.971
6061.783		14	13/2	28238.557	13/2	11746.328
6072.250	nl	8	11/2	26147.987	13/2	9684.184
6081.284		54	11/2	24519.749	11/2	8080.404
6083.395	nl	15	5/2	9710.600	5/2	26144.239
6098.455	nl	12	13/2	29753.559	11/2	13360.5
6114.666		22	13/2	30345.528	13/2	13995.93
6117.040	nl	22	13/2	30345.528	11/2	14002.29
6122.872		20	13/2	15372.271	15/2	31699.958
6140.09	nl	-	15/2	18821.135	15/2	35103.018
6142.81	nl	-	15/2	16650.6	17/2	32925.302
6144.730		62	11/2	24519.749	9/2	8250.143
6144.89	nl		11/2	32587.30	13/2	16318.12
6146.525	nl	10	9/2	28314.791	9/2	12049.94
6158.90	nl	-	7/2	27635.199	7/2	11403.01
6161.22	nl	-	7/2	9918.190	5/2	26144.239
6161.906	nl	8	5/2	11646.31	5/2	27870.595
6167.678		12	13/2	30211.355	11/2	14002.29
6170.45	nl	-	7/2	11668.79	5/2	27870.595
6173.073	nl	25	7/2	27336.479	5/2	11141.58
6173.30	nl	-	11/2	13727.48	9/2	29921.796
6175.675	nl	12	13/2	29753.559	15/2	13565.49
6184.50	nl	-	11/2	32587.30	11/2	16422.28

6187.32	nl	-	13/2	16626.88	15/2	32784.476
6190.94	nl	-	9/2	12068.17	9/2	28215.971
6207.232		57	7/2	6535.572	9/2	22641.351
6207.419	nl	9	13/2	27851.627	13/2	11746.33
6214.271	nl	3	9/2	30096.765	7/2	14009.23
6248.303		16	13/2	29335.781	13/2	13335.870
6254.09	nl	-	13/2	30211.355	11/2	14226.22
6267.65	nl	-	13/2	30679.356	11/2	14728.84
6452.017		15	17/2	2934.920	17/2	14340.17
6453.49	nl	-	11/2	30401.686	9/2	14910.476
6503.351	nl	6	13/2	34180.492	11/2	18808.052
6519.87	nl	-	13/2	29335.781	11/2	14002.294
6520.178	nl	16	11/2	23582.910	9/2	8250.143
6524.111		10	11/2	23403.929	11/2	8080.404
6531.124		5	13/2	30076.595	15/2	14769.53
6561.359		25	13/2	28238.557	15/2	13002.02
6563.497	nl	5	3/2	11361.76	5/2	26593.333
6596.873		12	15/2	12250.519	17/2	27405.036
6597.188		47	11/2	23403.929	9/2	8250.143
6638.931		10	13/2	30076.595	13/2	15018.09
6654.468	nl	3	9/2	18189.21	11/2	33212.554
6669.926		24	11/2	8829.063	9/2	23817.594
6711.57	nl	-	15/2	30242.928	13/2	15347.425
6713.571		6	17/2	2934.920	17/2	14943.83
6742.92	nl	5	13/2	16823.79	11/2	31650.07
6783.565		8	7/2	25391.496	7/2	10654.053
6789.742	nl	6	7/2	11869.29	5/2	26593.333
6791.238	nl	8	5/2	27976.873	5/2	13256.08
6809.278		20	13/2	25092.537	13/2	10410.745
6819.019		52	13/2	25092.537	11/2	10431.716
7072.613		12	11/2	14178.365	11/2	28313.508

7102.249		8	15/2	16650.6	15/2	30726.768
7126.08	nl	-	13/2	33040.71	11/2	19011.607
7164.644	nl	6	17/2	14028.71	15/2	27982.287
7202.695	nl	4	11/2	32891.47	11/2	19011.607
7218.57	nl	-	13/2	27851.627	11/2	14002.29
7224.682	nl	8	11/2	15904.915	9/2	29742.537
7249.013		18	17/2	18380.31	17/2	32171.486
7271.913	nl	5	13/2	16979.02	15/2	30726.768
7279.253	nl	10	9/2	12519.71	7/2	26253.598
7321.819	nl	6	13/2	14328.24	15/2	27982.287
7343.114	nl	6	17/2	18557.04	17/2	32171.486
7490.52	nl	-	5/2	12907.06	7/2	26253.598

Table 6.3. Lines classified via laser-induced fluorescence. For hf patterns not visible in the FT spectrum or masked in blend situations "–" is given in column 3. The calculated cg wavelength for such lines is given in column 1 (number of figures after decimal point depends on energy accuracy, see table 6.1). nl means new line not listed in commonly used wavelength tables, e.g. [95].

λ_{LIF} / Å (in air)	Comment	SNR	Even Levels		Odd Levels	
			J	Energy / cm^{-1}	J	Energy / cm^{-1}
3173.04	nl	-	9/2	31506.29	9/2	0.000
3203.10	nl	-	11/2	32587.30	11/2	1376.602
3235.022		5	9/2	30902.769	9/2	0
3254.649	nl	15	15/2	33563.160	13/2	2846.741
3298.39	nl	-	13/2	33155.831	13/2	2846.741
3391.48	nl	-	15/2	33858.230	15/2	4381.072
3404.625	nl	15	11/2	29363.384	9/2	0
3415.682	nl	19	13/2	32115.075	13/2	2846.741
3444.308	nl	9	11/2	30401.686	11/2	1376.602
3467.045	nl	12	13/2	30211.355	11/2	1376.602
3473.60	nl	-	9/2	4432.225	11/2	33212.554
3490.06	nl	-	9/2	30021.169	11/2	1376.602
3522.979	nl	28	13/2	29753.559	11/2	1376.602
3533.34	nl	-	9/2	5822.89	9/2	34116.595
3575.622	nl	11	13/2	29335.781	11/2	1376.602
3582.977	nl	19	13/2	29278.395	11/2	1376.602
3617.370	nl	5	11/2	4866.515	9/2	32503.025
3617.54	nl	-	7/2	27635.199	9/2	0
3649.103	nl	9	15/2	30242.928	13/2	2846.741
3681.963	nl	7	13/2	7951.323	15/2	35103.018
3716.507	nl	5	11/2	6313.224	11/2	33212.5544
3721.679	nl	14	13/2	28238.557	11/2	1376.602
3723.79	nl	-	11/2	4866.515	9/2	31713.237
3744.812	nl	12	11/2	4866.515	11/2	31562.535
3757.06	nl	-	13/2	6603.591	11/2	33212.554
3776.07	nl	-	13/2	27851.627	11/2	1376.602
3780.296	nl	4	11/2	6313.224	13/2	32758.666
3782.27	nl	-	13/2	29278.395	13/2	2846.741

3784.966		4	11/2	4866.515	9/2	31270.329
3788.053	nl	10	11/2	6313.224	13/2	32704.514
3807.58	nl	-	9/2	4432.225	11/2	30688.191
3818.49	nl	-	13/2	6603.591	15/2	32784.476
3820.205	nl	6	13/2	6603.591	13/2	32772.769
3823.301	nl	21	11/2	26147.987	9/2	0.000
3871.62	nl	-	11/2	4866.515	11/2	30688.191
3883.956	nl	10	9/2	5822.890	11/2	31562.535
3898.567	nl	12	11/2	4866.515	13/2	30509.700
3905.506	nl	8	15/2	9745.376	17/2	35343.001
3926.61	nl	-	9/2	5822.89	7/2	31282.953
3942.469	nl	5	15/2	9745.376	15/2	35103.018
3945.61	nl	-	5/2	6451.808	5/2	31789.286
3945.70	nl	-	11/2	6313.224	11/2	31650.07
3983.514	nl	5	13/2	6603.591	15/2	31699.958
4005.45	nl	-	13/2	6603.591	11/2	31562.535
4018.80	nl	-	11/2	4866.515	9/2	29742.537
4038.742	nl	5	13/2	7951.323	13/2	32704.514
4065.41	nl	-	9/2	9105.021	7/2	33695.84
4095.81	nl	-	13/2	6603.591	15/2	31011.904
4098.08	nl	-	15/2	8363.901	13/2	32758.666
4148.93	nl	-	7/2	7617.440	9/2	31713.237
4162.20	nl	-	15/2	8765.542	15/2	32784.476
4197.20	nl	-	5/2	6451.808	5/2	30270.526
4203.37	nl	-	9/2	4432.225	9/2	28215.971
4266.956	nl	8	11/2	6313.224	9/2	29742.537
4281.547	nl	3	11/2	4866.515	9/2	28215.971
4284.01	nl	-	15/2	8363.901	15/2	31699.958
4336.850	nl	2	5/2	8737.556	5/2	31789.286
4341.250	nl	4	11/2	6714.184	9/2	29742.537
4359.03	nl	-	15/2	8765.542	15/2	31699.958
4365.79	nl	-	13/2	7951.323	15/2	30850.254

4375.214	nl	7	11/2	6892.949	9/2	29742.537
4379.35	nl	-	11/2	9675.029	9/2	32503.025
4413.169	nl	3	7/2	7617.44	5/2	30270.526
4414.16	nl	-	15/2	8363.901	15/2	31011.904
4421.93	nl	-	9/2	9105.020	9/2	31713.237
4454.67	nl	-	9/2	5822.890	7/2	28264.916
4481.39	nl	-	7/2	10194.768	9/2	32503.025
4491.62	nl	-	7/2	8013.089	5/2	30270.526
4493.86	nl	-	15/2	8765.542	15/2	31011.904
4493.97	nl	-	13/2	25092.537	13/2	2846.741
4497.220	nl	2	11/2	9483.518	9/2	31713.237
4501.936	nl	3	5/2	6451.808	5/2	28658.247
4507.722	nl	8	9/2	9105.021	7/2	31282.953
4508.46	nl	-	9/2	9105.02	9/2	31270.329
4530.822	nl	4	9/2	4432.225	9/2	26497.094
4538.543	nl	7	11/2	23403.929	11/2	1376.602
4541.28	nl	-	5/2	6451.808	3/2	28465.851
4541.99	nl	-	11/2	9268.726	9/2	31270.329
4548.69	nl	-	7/2	6535.572	5/2	28513.764
4549.322	nl	13	11/2	9675.029	11/2	31650.07
4555.37	nl	-	7/2	7617.44	5/2	29563.401
4558.75	nl	-	17/2	9770.281	15/2	31699.958
4564.358	nl	11	11/2	6313.224	9/2	28215.971
4577.16	nl	-	11/2	8829.063	9/2	30670.529
4580.454	nl	3	9/2	8029.275	7/2	29855.058
4581.379	nl	14	9/2	4432.225	7/2	26253.598
4597.65	nl	-	15/2	8765.542	13/2	30509.700
4605.77	nl	-	13/2	11462.9	15/2	33168.727
4612.742	nl	18	11/2	24519.749	13/2	2846.741
4617.69	nl	-	13/2	11562.76	11/2	33212.554
4621.790	nl	9	11/2	4866.515	9/2	26497.094
4628.478	nl	10	11/2	6714.184	11/2	28313.508

4629.533	nl	12	9/2	4432.225	11/2	26026.626
4633.01	nl	-	7/2	9704.744	7/2	31282.953
4635.735	nl	15	9/2	9105.021	9/2	30670.529
4636.565	nl	3	7/2	32011.634	7/2	10450
4647.214	nl	4	9/2	31962.229	7/2	10450
4649.474	nl	5	11/2	6714.184	9/2	28215.971
4667.103	nl	8	11/2	6892.949	11/2	28313.508
4671.20	nl	-	11/2	9268.726	9/2	30670.529
4680.09	nl	-	7/2	9918.19	9/2	31270.329
4688.451	nl	8	11/2	6892.949	9/2	28215.971
4690.167		6	11/2	30895.062	9/2	9579.82
4695.87	nl	-	15/2	11483.43	13/2	32772.769
4702.88	nl	-	11/2	32587.30	9/2	11329.7
4706.420		3	17/2	9770.281	15/2	31011.904
4714.621	nl	4	11/2	9483.518	11/2	30688.191
4722.367	nl	6	11/2	4866.515	13/2	26036.404
4722.663		9	13/2	7630.132	11/2	28798.703
4724.551		6	11/2	4866.515	11/2	26026.626
4724.866	nl	3	13/2	33155.831	11/2	11997.14
4736.915	nl	2	15/2	9745.376	15/2	30850.254
4743.786	nl	4	17/2	14028.706	15/2	35103.018
4748.267		8	5/2	30799.760	5/2	9745.334
4754.644	nl	6	11/2	9483.518	13/2	30509.700
4755.665		30	11/2	6313.224	13/2	27334.898
4759.905	nl	6	7/2	30582.777	9/2	9579.820
4770.457	nl	15	17/2	9770.281	15/2	30726.768
4782.121		10	9/2	30485.194	9/2	9579.820
4797.715	nl	4	7/2	30582.777	5/2	9745.334
4802.481		5	9/2	9105.035	9/2	29921.796
4808.00	nl	-	9/2	10920.365	9/2	31713.237
4814.61	nl	-	15/2	9745.376	13/2	30509.700
4819.00	nl	-	13/2	10266.501	15/2	31011.904

4833.786	nl	8	7/2	32011.634	9/2	11329.7
4841.854	nl	9	7/2	7617.440	7/2	28264.916
4842.394	nl	4	7/2	8013.089	5/2	28658.247
4845.08	nl	-	7/2	11869.290	9/2	32503.025
4848.138	nl	11	11/2	6714.184	13/2	27334.898
4848.18	nl	-	3/2	9649.97	5/2	30270.526
4855.331	nl	8	11/2	32587.30	11/2	11997.14
4858.077		5	11/2	12180.13	13/2	32758.666
4859.93	nl	-	3/2	29557.116	3/2	8986.443
4862.73	nl	-	11/2	11944.207	9/2	32503.025
4863.120		82	11/2	23403.929	13/2	2846.741
4865.954		6	15/2	10466.689	15/2	31011.904
4871.40	nl	-	15/2	12250.52	13/2	32772.769
4872.94	nl	-	13/2	32512.919	11/2	11997.14
4876.525	nl	8	7/2	8013.089	5/2	28513.764
4880.42	nl	-	11/2	30895.062	13/2	10410.75
4882.459	nl	5	7/2	10194.768	9/2	30670.529
4890.532	nl	7	11/2	6892.949	13/2	27334.898
4890.68	nl	-	9/2	30021.169	9/2	9579.82
4891.24	nl	-	7/2	11274.229	9/2	31713.237
4891.413		8	11/2	9483.518	9/2	29921.796
4917.83	nl	-	7/2	28578.627	9/2	8250.143
4933.35	nl	-	13/2	10423.65	11/2	30688.191
4934.694		12	11/2	9483.518	9/2	29742.537
4936.450	nl	3	7/2	8013.089	7/2	28264.916
4940.05	nl	-	13/2	11462.895	15/2	31699.958
4944.744		3	9/2	29053.224	11/2	8835.383
4948.198		140	9/2	5822.890	11/2	26026.626
4953.065	nl	3	11/2	6313.224	9/2	26497.094
4960.46	nl	-	13/2	33155.831	15/2	13002.02
4963.482	nl	26	5/2	6451.808	5/2	26593.333
4965.638		14	7/2	30582.777	7/2	10449.997

4979.75	nl	-	7/2	10194.77	5/2	30270.526
4980.99	nl	-	7/2	14045.88	9/2	34116.595
4989.82	nl	-	9/2	30485.194	7/2	10449.997
4990.88	nl	-	13/2	7951.323	15/2	27982.287
4995.38	nl	-	9/2	11549.602	11/2	31562.535
5002.21	nl	-	17/2	11714.352	15/2	31699.958
5003.59	nl	-	15/2	12804.47	15/2	32784.476
5006.203		6	11/2	8829.063	11/2	28798.703
5008.15	nl	-	11/2	13250.673	11/2	33212.5544
5008.49	nl	-	5/2	13735.298	7/2	33695.84
5013.66	nl	-	9/2	13272.61	11/2	33212.554
5020.336	nl	8	3/2	9649.97	5/2	29563.401
5025.03	nl	-	13/2	30345.528	15/2	10450.68
5031.76	nl	-	13/2	32870.250	15/2	13002.02
5034.475	nl	42	7/2	8013.089	5/2	27870.595
5053.292	nl	78	11/2	29363.384	9/2	9579.82
5053.46	nl	-	11/2	6714.184	9/2	26497.094
5054.294	nl	12	13/2	30211.355	11/2	10431.716
5055.173	nl	8	5/2	8737.556	5/2	28513.764
5057.007	nl	6	11/2	11944.207	9/2	31713.237
5068.764	nl	23	11/2	6313.224	13/2	26036.404
5071.277		135	11/2	6313.224	11/2	26026.626
5073.499	nl	24	13/2	7630.132	13/2	27334.898
5076.678	nl	9	5/2	6451.808	5/2	26144.239
5078.486	nl	7	15/2	13439.01	17/2	33124.424
5080.605	nl	8	17/2	15665.796	17/2	35343.001
5084.977		15	7/2	10194.77	7/2	29855.058
5088.473	nl	14	9/2	30096.765	7/2	10450
5088.880	nl	10	7/2	9918.19	5/2	29563.401
5090.777		15	13/2	13146.58	15/2	32784.476
5091.10	nl	-	5/2	11646.31	7/2	31282.953
5092.418	nl	7	13/2	29278.395	15/2	9646.830

5093.887		100	9/2	4432.225	9/2	24058.128
5095.839		45	15/2	8363.901	15/2	27982.287
5098.43	nl	-	13/2	12041.66	11/2	31650.07
5106.43	nl	-	7/2	14538.93	9/2	34116.595
5107.879	nl	21	9/2	8643.824	9/2	28215.971
5108.129	nl	4	9/2	30021.169	7/2	10450
5108.512	nl	15	9/2	11713.24	7/2	31282.953
5109.385	nl	8	7/2	29146.201	9/2	9579.82
5109.65	nl	-	11/2	30895.062	9/2	11329.7
5115.65	nl	5	13/2	30211.355	15/2	10668.950
5118.909	nl	10	11/2	9268.726	11/2	28798.703
5119.303	nl	4	15/2	11483.427	15/2	31011.904
5119.594	nl	25	5/2	8737.556	7/2	28264.916
5120.85	nl	-	15/2	30242.928	17/2	10720.359
5123.05	nl	-	13/2	13654.56	15/2	33168.727
5123.928	nl	8	13/2	32512.919	15/2	13002.02
5127.374	nl	5	9.5	15845.28	17/2	35343.001
5130.423	nl	10	9/2	11184.396	9/2	30670.529
5130.871	nl	4	11/2	8829.063	11/2	28313.508
5133.78	nl	-	9/2	29053.224	9/2	9579.820
5134.690	nl	75	11/2	12180.21	11/2	31650.07
5140.18	nl	-	13/2	11562.762	15/2	31011.904
5142.22	nl	-	5/2	10829.07	5/2	30270.526
5143.34	nl	-	17/2	15665.802	15/2	35103.018
5144.502		50	13/2	6603.591	13/2	26036.404
5151.789	nl	12	11/2	11282.87	11/2	30688.191
5154.188	nl	12	7/2	11274.229	9/2	30670.529
5156.56		-	13/2	11462.895	15/2	30850.254
5156.68	nl	-	11/2	8829.063	9/2	28215.971
5157.092	nl	47	9/2	4432.225	9/2	23817.594
5157.18	nl	-	7/2	27635.199	9/2	8250.143
5157.572		33	13/2	7951.323	13/2	27334.898

5158.08	nl	-	11/2	13376.99	13/2	32758.666
5167.730	nl	5	15/2	13439.01	15/2	32784.476
5170.49	nl	-	11/2	11944.21	9/2	31270.329
5175.835		22	11/2	9483.518	11/2	28798.703
5176.568	nl	12	11/2	6714.184	11/2	26026.626
5177.876	nl	3	5/2	12481.71	5/2	31789.286
5180.56	nl	-	17/2	11714.352	15/2	31011.904
5182.25	nl	-	13/2	13467.37	13/2	32758.666
5185.567	nl	4	9/2	11549.602	7/2	30828.528
5189.617		5	13/2	11462.9	15/2	30726.768
5198.65	nl	-	9/2	13272.613	9/2	32503.025
5202.346		80	15/2	8765.542	15/2	27982.287
5217.826		25	7/2	11668.794	7/2	30828.528
5222.41	nl	-	11/2	30465.360	11/2	11322.443
5235.319	nl	4	17/2	14028.71	17/2	33124.424
5237.890	nl	22	7/2	27336.479	9/2	8250.143
5238.37	nl	-	13/2	29753.559	15/2	10668.950
5241.833		16	11/2	30401.686	9/2	11329.696
5247.066	nl	3	15/2	33563.160	13/2	14510.21
5248.211		12	7/2	13454.218	9/2	32503.025
5248.764	nl	9	13/2	11462.895	13/2	30509.700
5250.329		40	15/2	8363.901	17/2	27405.036
5251.96	nl	-	9/2	14600.622	7/2	33695.84
5258.26	nl	-	17/2	11714.37	15/2	30726.768
5261.214	nl	11	7/2	11668.794		30670.529
5262.719	nl	6	7/2	11274.23	5/2	30270.526
5264.343	nl	22	5/2	27976.873	3/2	8986.443
5268.378	nl	20	7/2	7617.44	5/2	26593.333
5274.842	nl	25	11/2	29363.384	13/2	10410.75
5278.45	nl	-	9/2	14272.88	11/2	33212.554
5288.374	nl	20	11/2	12658.401	11/2	31562.535
5289.215		12	11/2	10841.407	9/2	29742.537

5290.27	nl	-	9/2	13605.665	9/2	32503.025
5290.796	nl	22	15/2	12804.468	15/2	31699.958
5291.25	nl	-	13/2	12118.039	15/2	31011.904
5295.234	nl	10	7/2	7617.440	9/2	26497.094
5299.423	nl	8	13/2	30679.356	15/2	11814.65
5299.69	nl	-	3/2	9649.97	5/2	28513.764
5300.80	nl	-	5/2	14836.016	7/2	33695.84
5311.581		17	17/2	14302.88	17/2	33124.424
5313.181	nl	25	3/2	9649.97	3/2	28465.851
5316.776	nl	18	5/2	9710.6	5/2	28513.764
5332.60	nl	-	5/2	11107.7	7/2	29855.058
5336.310	nl	15	5/2	10829.07	5/2	29563.401
5336.84	nl	-	11/2	9483.518	9/2	28215.971
5338.59	nl	-	7/2	11944.207	9/2	30670.529
5339.92	nl	-	7/2	13781.374	9/2	32503.025
5346.484	nl	25	13/2	14470.05	15/2	33168.727
5348.546	nl	6	9/2	30021.169	9/2	11329.7
5351.187		32	13/2	30679.356	11/2	11997.14
5355.604		18	13/2	29335.781	15/2	10668.950
5363.464		240	15/2	8765.542	17/2	27405.036
5364.42	nl	-	7/2	7617.44	7/2	26253.598
5368.378	nl	12	17/2	14302.88	17/2	32925.302
5369.949		46	13/2	14087.545	13/2	32704.514
5372.33	nl	-	13/2	12118.05	15/2	30726.768
5374.847	nl	22	17/2	16742.8	17/2	35343.001
5380.394	nl	6	7/2	11274.23	7/2	29855.058
5380.550	nl	20	11/2	14178.37	13/2	32758.666
5386.97	nl	-	9/2	11184.396	9/2	29742.537
5388.084	nl	26	5/2	9710.600	7/2	28264.916
5388.36	nl	-	13/2	13146.584	15/2	31699.958
5390.78	nl	-	15/2	14579.39	17/2	33124.424
5391.971	nl	28	11/2	9675.029	9/2	28215.971

5398.944	nl	5	13/2	32512.919	13/2	13995.93
5411.19	nl	-	13/2	30679.356	11/2	12204.29
5414.138	nl	12	13/2	30211.355	13/2	11746.328
5416.45	nl	-	7/2	14045.878	9/2	32503.025
5418.728	nl	14	7/2	11472.41	9/2	29921.796
5420.91	nl	-	9/2	10356.737	11/2	28798.703
5422.688	nl	12	11/2	12334.616	9/2	30670.529
5434.245	nl	15	13/2	30211.355	15/2	11814.647
5448.55	nl	-	13/2	30345.528	11/2	11997.14
5449.293	nl	11	15/2	14579.4	17/2	32925.302
5457.297	nl	10	7/2	10194.77	5/2	28513.764
5463.626	nl	18	7/2	9918.19	9/2	28215.971
5466.936	nl	15	13/2	32512.919	11/2	14226.22
5468.668	nl	10	9/2	30485.194	11/2	12204.286
5474.348	nl	18	13/2	30076.595	15/2	11814.65
5474.61	nl	-	11/2	30465.360	11/2	12204.286
5476.85	nl	-	11/2	14505.07	13/2	32758.666
5482.364		60	9/2	5822.890	9/2	24058.128
5487.240	nl	8	3/2	12051.49	5/2	30270.526
5490.098	nl	8	7/2	29146.201	9/2	10936.65
5490.74	nl	-	15/2	12804.468	15/2	31011.904
5491.532	nl	85	13/2	27851.627	15/2	9646.83
5491.775	nl	19	15/2	33858.230	13/2	15654.24
5493.32	nl	-	7/2	13590.35	5/2	31789.286
5493.764		30	11/2	30401.686	11/2	12204.286
5499.144	nl	11	11/2	30401.686	13/2	12222.091
5505.078	nl	20	5/2	9710.6	5/2	27870.595
5507.43	nl	-	9/2	31506.29	9/2	13354.04
5511.832	nl	12	13/2	33155.831	13/2	15018.09
5518.275	nl	27	9/2	29053.224	9/2	10936.647
5529.176	nl	4	15/2	17262.14	17/2	35343.001
5533.671	nl	16	11/2	9268.726	13/2	27334.898

5537.760	nl	11	7/2	12617.700	9/2	30670.529
5540.040		18	13/2	13654.555	15/2	31699.958
5547.764	nl	12	17/2	29834.920	15/2	11814.65
5550.110	nl	12	13/2	15156.07	15/2	33168.727
5551.78	nl	-	13/2	29753.559	13/2	11746.328
5554.831		67	9/2	8029.275	11/2	26026.626
5555.43	nl	18	15/2	14929.89	17/2	32925.302
5561.92	nl	-	11/2	15238.14	11/2	33212.554
5566.403	nl	18	9/2	31962.229	11/2	14002.29
5572.924	nl	15	13/2	29753.559	15/2	11874.647
5574.654	nl	15	9/2	8320.24	7/2	26253.598
5577.38	nl	-	7/2	28578.627	7/2	10654.053
5587.389	nl	20	9/2	30096.765	11/2	12204.29
5591.15	nl	-	5/2	30799.760	7/2	12919.316
5594.496	nl	5	9/2	15342.8	11/2	33212.554
5594.85	nl	-	17/2	14302.88	17/2	32171.486
5597.792	nl	5	9/2	10356.74	9/2	28215.971
5611.100	nl	6	9/2	30021.1	11/2	12204.29
5613.768	nl	6	13/2	33155.831	13/2	15347.43
5615.888	nl	8	13/2	30679.356	11/2	12877.67
5619.98	nl	-	9/2	15423.84	11/2	33212.554
5621.43	nl	12	13/2	32512.919	11/2	14728.84
5634.39	nl	-	9/2	30021.169	7/2	12277.94
5682.793	nl	12	15/2	14579.39	17/2	32171.486
5686.64	nl	-	13/2	13146.58	15/2	30726.768
5723.217	nl	6	13/2	30345.528	11/2	12877.68
5748.65	nl	-	15/2	14780.94	17/2	32171.486
5759.65	nl	-	13/2	13654.555	15/2	31011.904
5782.836	nl	12	15/2	13439.01	15/2	30726.768
5841.60	nl	-	13/2	30679.356	15/2	13565.49
5876.529	nl	10	13/2	25092.537	11/2	8080.404
5885.910	nl	5	13/2	30345.528	11/2	13360.5

5889.16	nl	-	13/2	33155.831	15/2	16180.2
5911.399	nl	18	9/2	28314.791	7/2	11403.01
5913.047		25	15/2	30242.928	13/2	13335.870
5918.09	nl	-	13/2	32870.250	11/2	15977.6
5919.519	nl	12	7/2	9704.744	5/2	26593.333
5921.56	nl	-	5/2	9710.6	5/2	26593.333
5932.775	nl	5	13/2	30211.355	11/2	13360.502
5937.40	nl	-	13/2	33155.831	13/2	16318.12
5942.927		10	11/2	9675.029	9/2	26497.094
5957.810	nl	5	13/2	30345.528	15/2	13565.49
5962.203		185	11/2	9268.726	13/2	26036.404
5970.79	nl	-	7/2	11472.41	9/2	28215.971
6034.149	nl	6	15/2	33563.160	17/2	16995.41
6039.569		10	11/2	9483.518	13/2	26036.404
6042.859	nl	10	13/2	15156.070	15/2	31699.958
6064.185	nl	12	11/2	29363.384	11/2	12877.68
6072.52	nl	-	11/2	30465.360	11/2	14002.294
6095.611	nl	6	13/2	29278.395	11/2	12877.682
6095.935	nl	15	7/2	27336.479	9/2	10936.65
6110.263	nl	18	11/2	9675.029	13/2	26036.404
6110.527	nl	4	11/2	30895.062	9/2	14534.39
6111.114		12	13/2	25092.537	13/2	8733.440
6140.87	nl	-	13/2	15420.120	15/2	31699.958
6153.280	nl	13	15/2	30242.928	13/2	13995.931
6171.073		24	7/2	7617.440	9/2	23817.594
6241.848		12	13/2	28238.557	13/2	12222.091
6255.56	nl	-	11/2	12234.62	9/2	28215.971
6268.066		11	7/2	10194.768	5/2	26144.239
6285.778	nl	8	7/2	27635.199	9/2	11730.67
6286.476		10	15/2	30242.928	17/2	14340.174
6325.561	nl	4	7/2	8013.089	9/2	23817.594
6332.852		20	11/2	24519.749	13/2	8733.440

6339.440		12	13/2	10266.501	13/2	26036.404
6344.377	nl	6	13/2	29753.559	13/2	13995.931
6352.596		32	11/2	26147.987	13/2	10410.745
6383.150	nl	4	9/2	12651.586	11/2	28313.508
6385.686		7	11/2	10841.407	9/2	26497.094
6403.250	nl	6	13/2	10423.654	13/2	26036.404
6406.095	nl	28	7/2	27336.479	9/2	11730.67
6414.543	nl	6	7/2	27635.199	9/2	12049.94
6418.058		10	9/2	10920.365	9/2	26497.094
6455.34	nl	-	9/2	30021.169	9/2	14534.39
6460.92	nl	-	15/2	30242.928	15/2	14769.529
6488.196	nl	4	13/2	25092.537	13/2	9684.184
6494.352		7	11/2	30465.360	9/2	15071.624
6522.444	nl	6	13/2	30345.528	13/2	15018.09
6543.633	nl	5	11/2	13035.697	11/2	28313.508
6557.45	nl	-	13/2	34180.492	11/2	18934.862
6570.56	nl	-	15/2	16956.3	17/2	32171.486
6645.334	nl	2	9/2	29053.224	7/2	14009.225
6693.156	nl	5	11/2	13376.992	11/2	28313.508
6820.852	nl	15	13/2	16069.89	15/2	30726.768

Table 6.4. Spectral lines appearing in the FT spectrum classified by means of their hf patterns and wave numbers involving the newly discovered energy levels given in table 6.1. 'nl' means 'new line' not listed in commonly used wavelength tables, e.g. [95].

λ_{FT} / Å (in air)	Comment	SNR	Even Levels		Odd Levels	
			J	Energy / cm^{-1}	J	Energy / cm^{-1}
5634.406	nl	250	7/2	29146.201	7/2	11403.01
5917.780	nl	8	9/2	30902.769	7/2	14009.23
6031.926	nl	15	5/2	27976.873	7/2	11403.01
6274.359	nl	15	7/2	27336.479	7/2	11403.01
6565.201	nl	11	7/2	27336.479	5/2	12108.87
6841.638	nl	3	9/2	14186.352	11/2	28798.703
6863.288	nl	2	13/2	29335.781	15/2	14769.529
6925.214	nl	8	17/2	29834.920	15/2	15398.92
7169.725	nl	5	11/2	26147.987	11/2	12204.286
7237.935	nl	35	11/2	8829.063	9/2	22641.351
7260.116	nl	4	13/2	25092.537	11/2	11322.443
7286.758	nl	4	11/2	23403.929	13/2	9684.184
7338.599	nl	19	7/2	10194.768	9/2	23817.594
7405.025	nl	4	9/2	14764.288	7/2	28264.916
7473.841	nl	6	17/2	14028.706	17/2	27405.036
7474.555	nl	7	9/2	12651.586	11/2	26026.626
7475.903	nl	17	11/2	9268.726	9/2	22641.351
7485.282	nl	4	17/2	17494.382	15/2	30850.254
7564.089	nl	4	11/2	10841.407	9/2	24058.128
7597.941	nl	8	11/2	9483.518	9/2	22641.351
7600.104	nl	8	11/2	10904.034	9/2	24058.128
7710.162	nl	12	11/2	9675.029	9/2	22641.351
7741.667	nl	15	11/2	10904.034	9/2	23817.594
7756.874	nl	4	13/2	25092.537	11/2	12204.286
7810.656	nl	9	7/2	27635.2	5/2	14835.7
7818.003	nl	3	11/2	26147.987	11/2	13360.502
7913.475		30	9/2	11184.396	9/2	23817.594
8021.533	nl	4	13/2	15850.483	11/2	28313.508

8165.278	nl	6	13/2	16069.885	11/2	28313.508
8252.693	nl	2	11/2	11944.207	9/2	24058.128
8545.611	nl	2	11/2	24519.749	9/2	12821.044
8549.249	nl	3	5/2	16772.15	3/2	28465.851
8664.316		30	9/2	12519.705	9/2	24058.128
8725.926	nl	11	9/2	11184.4	9/2	22641.351
8768.915	nl	2	15/2	33563.160	15/2	22162.41
8814.272	nl	3	17/2	29834.920	17/2	18492.8
9029.698	nl	2	9/2	12746.067	9/2	23817.594
9499.659	nl	8	3/2	17941.91	3/2	28465.851
9575.362	nl	2	11/2	13376.992	9/2	23817.594

Table 6.5. Spectral lines excited by laser light in order to determine more accurate hf constants of the involved levels. For hf patterns not visible in the FT spectrum or masked in blend situations "–" is given in column 3. nl means new line not listed in commonly used wavelength tables, e.g. [95].

λ_{exc} / Å (in air)	Comment	SNR	even Levels		odd Levels	
			J	energy / cm^{-1}	J	energy / cm^{-1}
5759.434		80	15/2	8363.901	17/2	25721.903
5807.212		365	15/2	8363.901	17/2	25579.095
5837.226		150	9/2	5822.890	11/2	22949.567
6518.24	nl	-	11/2	24172.708	11/2	8835.383
6697.471		11	15/2	8765.542	13/2	23692.429
6726.330		17	13/2	6603.591	13/2	21466.434
6727.645		20	13/2	7951.323	11/2	22811.263
6782.518		19	15/2	12250.519	17/2	26990.236
7162.662		155	11/2	8829.063	13/2	22786.511
7225.373		40	13/2	7630.132	13/2	21466.434
7446.560	nl	2	11/2	12658.401	9/2	26083.725
7453.699	nl	3	11/2	13035.697	13/2	26448.161
7476.88	nl	-	15/2	17907.819	13/2	31278.686

Table 6.6. Pr I hyperfine constants of known levels determined within this work in comparison with literature values.

Energy / cm^{-1}	J	Parity	This work		Previous work		Reference	λ_{exc} / Å (in air)
			A / MHz	B[a] / MHz	A / MHz	B / MHz		
25721.903	17/2	o	665(4)	0	672.9	0	[24]	5759.434
25579.095	17/2	o	648(6)	0	648	0	[24]	5807.212
22949.567	11/2	o	697(2)	0	699.5	0	[24]	5837.226
24172.708	11/2	e	473(2)	-26(20)	473	-47	[24]	6518.24
23692.429	13/2	o	637(3)	0	642.4	0	[24]	6697.471
21466.434	13/2	o	882(3)	0	882.2	0	[24]	6726.330, 7225.373
22811.263	11/2	o	919(2)	0	918.13	0	[24]	6727.645
26990.236	17/2	o	700(2)	0	699.5	0	[24]	6782.518
22786.511	13/2	o	731(2)	0	732	0	[24]	7162.662
26083.725	9/2	o	918(10)	0	929.4	0	[24]	7446.560
26448.161	13/2	o	963(2)	0	959.2	50	[96]	7453.699
31278.686	13/2	o	658(2)	0	659.4(20)	0	[45]	7476.88

[a] In some cases the value of the hyperfine constant B could not be determined because it was too small to be detectable within the accuracy of our fitting procedure. We have given an entry of 0 without error bars in these cases.

7 CONCLUSION

This thesis is focused on systematic experimental investigations of spectral lines extracted from a highly resolved FT spectrum of praseodymium atoms in the region from 4200 to 7600 Å using laser spectroscopy in a hollow cathode discharge lamp. The levels were found by analysis of the experimentally recorded hyperfine structure patterns of the investigated transitions. A total of 100 new energy levels of praseodymium atom were found, which included 99 upper levels and one lower level. 54 new levels are odd and 46 are even parity levels. The discovery of these new energy levels led to the classification of 631 spectral lines; 231 lines were classified via laser excitation and 400 lines via laser-induced fluorescence. Furthermore, 39 spectral lines, involving these newly discovered levels, have fully resolved hf structure in the FT spectrum. These lines were classified by means of their wave numbers and their hyperfine patterns. During these investigations, laser excitation of 12 known levels was also performed. The accuracy of their hf structure constants was improved. These excited lines connecting known levels were not investigated previously by the LIF technique, 13 spectral lines were classified as combinations with these levels.

The discovery of new levels will help in reducing the number of unclassified lines of Pr I. This work shows that along with a highly resolved FT spectrum, laser spectroscopy is a powerful technique to investigate the spectrum of all elements.

Measurements of the hf structure of praseodymium are very useful for astrophysics since Pr lines are found in the optical spectrum of many chemical peculiar (CP) stars. Laboratory measurements are helpful in giving the abundance of Pr in such stars. From the view of basic research, the study of the spectrum of Pr is helpful in further theoretical understanding of its electronic structure.

8 BIBLIOGRAPHY

8.1 Consulted Literature

- White H. E., Introduction to Atomic Spectra, McGraw-Hill Kogakusha, Ltd. (1934)
- Ramsey N.F., Nuclear Moments, John Wiley & Sons, New York (1953)
- Condon E. U. and Shortley G. H., The theory of atomic Spectra, Cambrige at the university press, 1959
- Kuhn H. G., Atomic Spectra, Academic Press, New york (1962)
- Sobel'man, I. I., An introduction to the theory of atomic spectra, Pergamon, Oxford (1972)
- Thorne, A. P., Spectrophysics, Chapman & Hall, London (1974)
- Martin W C, Zalubas R and Hagan L., 1978 Atomic Energy Levels - The Rare Earth Elements National Bureau of Standards, NSRDS-NBS 60, Washington, DC, p. 98 ff
- Mitchel Weissbluth, Atoms and Molecule, student edition, Academic press, Inc. (1978)
- Sobel'mann, I. I., Vanshtein, L. A., Yukov, E. A., Excitation of atoms and broadenings of spectral lines, Springer (1981)
- Demtröder, W., Laser Spectroscopy, Springer (1982)
- Bransden B H. and Joachain C. J., Physics of atoms and molecules, Longman Scientific and technical (1983)
- Haken and Wolf, Atomic and Quatum Physics, Spring- Verlag, (1987)
- Sune Svanberg, Atomic and Molecular Spectroscopy, Spring-Verlag, (1991)
- James M., Lord M. P., Macmillan's Chemical and Physical Data, Macmillan, London, UK, (1992)
- Wolfgang Demtröder, Laser Spectroscopy Basic Concepts and Instrumentation, Third Edition Springer (2002)

- Lide, David R., CRC Handbook of Chemistry and Physics, 83rd edition, CRC Press: Boca Raton, FL, 2002; p 4:24
- Radiant Dyes, cw-Ring Dye Laser Operation and Maintenance Manual Wermelskirchen, Germany
- William T. Silvast, Laser fundamental, second edition, Cambridge University press (2004)
- Halliday David, Robert Resnick and Kenneth S. Krane, Physics, fifth edition, Wiley (2002)

8.2 References

[1] Pauli, W., Naturwissenschaften., 1924. **12**: p. 741.

[2] Schüler, H. and T. Schmidt, Z Phys., 1936. **99**: p. 717

[3] Lide, D.R., *CRC Handbook of Chemistry and Physics*, ed. r. ed. 2002: CRC Press: Boca Raton FL.

[4] King, A.S., *Temperature Classification of the Stronger Lines of Cerium and Praseodymium.* Astrophysical Journal, 1928. **68**( ): p. 194.

[5] White, H.E., *Hyperfine Structure in Singly Ionized Praseodymium.* Physical Review, 1929. **34**(11): p. 1397.

[6] Rosen, N., G.R. Harrison., and J.R.J. McNally, *Zeeman Effect Data and Preliminary Classification of the Spark Spectrum of Praseodymium—Pr II.* Physical Review, 1941. **60**(10): p. 722.

[7] Lew, H., *The Hyperfine Structure and Nuclear Moments of Pr^{141}.* Physical Review, 1953. **91**(3): p. 619.

[8] Brix, P., *Nuclear Magnetic Moment of Pr^{141} from the Hyperfine Structure of Pr II.* Physical Review, 1953. **89**(6): p. 1245.

[9] Baker, J.M. and B. Bleaney, *Hyperfine Structure of Praseodymium.* Proceedings of the Physical Society. Section A, 1955. **68**(10): p. 936.

[10] Murakawa, K., *Hyperfine structure of the spectra of Pr I and Pr II.* Journal of the Physical Society of Japan, 1960. **15**(12): p. 2306-2309.

[11] Judd, B.R. and I. Lindgren, *Theory of Zeeman Effect in the Ground Multiplets of Rare-Earth Atoms.* Physical Review, 1961. **122**(6): p. 1802.

[12] Wybourne, B.G., *Nuclear Moments and Intermediate Coupling.* J. CHEM. PHYS., 1962. **37**(8): p. 1807.

[13] Amado, Y.C., et al., *Hyperfine Structure of Praseodymium-142.* Physical Review, 1962. **126**(3): p. 1004.

[14] Spector, N., *Configurations $4f^2 6s$ and $4f^2 6p$ in Doubly Inonized Pr.* J. Opt. Soc Am., 1964. **54**(11): p. 1359.

[15] Reader, J. and J. Sugar, *Nuclear Magnetic Moment of Pr^{141} from Hyperfine structure of Pr II.* Phys. Rev., 1965. **137**: p. B 784.

[16] Zalubas, R. and M. Wilson, J. Res. Nat. Bur. Stand. (U.S.), 1965. **69 A**: p. 59.

[17] Ginibre, A. and S. Gerstenkorn. 1970.

[18] Zalubas, R. and B.R. Borchardt, J. Opt. Soc. Am., 1973. **63**: p. 102.

[19] Blaise, J., et al. 1973.

[20] Blaise, J. and A. Ginibre. 1976.

[21] Wyart, J.F., *Progrès Récents dans l'Interprétation des Configurations $4 f^N (5 d + 6 s)$ des Lanthanides II. Etude Paramétrique des Configurations.* Phys. Scr., 1974. **9**(6): p. 325.

[22] Meggers, W.F., C.H. Corliss, and B.F. Scribner, *Tables of spectral line intensities, arranged by elements.* Nat. Bur. Stand, 1975. **part I**: p. 403.

[23] Martin, W.C., R. Zalubas, and L. Hagan, *Atomic Energy Levels-The Rare Earth Elements*. 1978: National Bureau of Standards, NSRDS-NBS 60, Washington, DC. 98.

[24] Ginibre, A., Phys. Scr., 1981. **23**(3): p. 260.

[25] Childs, W.J. and L.S. Goodman, Phys. Rev., 1981. **24**(3): p. 1342.

[26] Macfarlane, R.M., D.P. Burum, and R.M. Shelby, *New Determination of the Nuclear Magnetic Moment of ^{141}Pr.* Physical Review Letters, 1982. **49**(9): p. 636.
[27] Cheng, K.T. and W.J. Childs, *Ab initio calculation of $4f^N6s^2$ hyperfine structure in neutral rare-earth atoms.* Physical Review A, 1985. **31**(5): p. 2775.
[28] Reddy, M.N. and G.N. Rao, Physica, 1988. **150**(3): p. 457.
[29] Ginibre, A., Phys. Scr., 1989. **39**(6): p. 694.
[30] Ginibre, A., Phys. Scr., 1989. **39**(6): p. 710.
[31] Imura, H., et al., *Measurement of Hyperfine Structure of the $4f^35d\,^5G$-$4f^36p\,^5H$ in PrII by Collinear Laser-Ion-Beam Spectroscopy.* J. Phys. Soc. Jpn., 1990. **59** p. 4208-4210
[32] Kim, M.K. and R. Kachru, *Hyperfine structures of praseodymium ions in solids using stimulated-photon-echo modulation.* Physical Review B, 1991. **44**(18): p. 9826.
[33] Iimura, H., et al., *Nuclear moments of ^{143}Pr by laser spectroscopy.* Physical Review C, 1994. **50**(2): p. 661.
[34] Kuwamoto, T., et al., J. Phys. Soc. Japan, 1996. **65**(10): p. 3180.
[35] Krzykowski, A., et al., Opt. Commun., 1997. **140**(4-6): p. 216.
[36] Song, M., et al., Eur. Phys. J., 1998. **D 2**(2): p. 115.
[37] Li, M., et al., *Hyperfine-structure measurements in ^{141}Pr II and ^{143,145}Nd II by collinear laser-ion-beam spectroscopy.* PHYS. REV. A, 2000. **62**: p. 052504.
[38] Ivarsson, S., U. Litzen, and G.M. Wahlgren, Phys. Scr., 2001. **64**(5): p. 455.
[39] Furmann, B., et al., Eur. Phys. J., 2001. **D 17**(3): p. 275.
[40] Ma, H.L., *Hyperfine structure of singly ionized lanthanum and praseodymium.* Chinese Physics, 2002. **11**(9): p. 905.
[41] Rivest, R.C., et al., *Laser spectroscopic measurements of hyperfine structure in Pr II.* Can. J. Phys., 2002. **80**: p. 557.
[42] Glenn, M.W., *The Lanthanide Elements in Stellar and Laboratory Spectra.* Physica Scripta, 2002. **2002**(T100): p. 22.
[43] Ruczkowski, J., et al., Phys. Scr., 2003. **68**(2): p. 133.
[44] Furmann, B., et al., Phys. Scr., 2005. **72**(4): p. 300.
[45] Furmann, B., et al., *New levels and hyperfine structure evaluation in neutral praseodymium.* Physica Scripta, 2006. **74**(6): p. 658.
[46] Guthöhrlein, G.H. 1996, (Helmut-Schmidt-Universität, Universität der Bundeswehr, Holstenhofweg 85, D-22043 Hamburg, Germany)
[47] Uddin, Z., *PhD Thesis* 2006, Technische Universität Graz
[48] Oppel, S.G., et al., *Active laser frequency stabilization using neutral praseodymium (Pr).* Applied Physics B: Lasers and Optics, 2010. **101**(1): p. 33-44.
[49] Gamper, B., *Investigation of the hyperfine structure of Pr I and Pr II lines based on highly resolved Fourier transform spectra.* Journal of Physics B: Atomic, Molecular and Optical Physics, 2011. **44**(4): p. 045003.
[50] Kuhn, H.G., *Atomic Spectra* 1962: Academic press New york.
[51] Penning, F.M., Physica, 1928. **8**: p. 137.
[52] Kenty, C., Phys. Rev., 1950. **80**: p. 95.
[53] Meissner, K.W. and W.F. Miller, *Phys. Rev.*, 1953. **92**: p. 896.
[54] Green, B., et al., Appl. Phys. Lett., 1976 **29**: p. 727.
[55] Travis, J.C., *"Analytical optogalvanic spectroscopy in flames" In Analytical Laser, spectroscopy,* . 1985: edby S. Martellucci A. N. Chester (Plenum. New York.213).

[56] King, D., et al., Appl. Opt., 1977. **16**: p. 2617
[57] Lawler, J.E., et al., *Ser.Opt.Sci*, 1979. **21**: p. 188.
[58] Grandin, J.F. and X.J. Husson, Phys. B, 1981. **14**: p. 433.
[59] Caesar, T. and J.L. Huelly, J. Phys. C, 1983. **44,**: p. 216
[60] Skolnick, M.L., IEEE J Quantum Electron, 1970. **6**: p. 139.
[61] Thomason, W.H. and D.C. Elbers, Rev. Sci. Instrum, 1975. **46**: p. 409.
[62] Furmann, B., D. Stefańska, and J. Dembczyński, J. Phys. B: At. Mol. Opt. Phys., 2009. **42**(17): p. 175005.
[63] Furmann, B., D. Stefańska, and J. Dembczyński, J. Phys. B: At. Mol. Opt. Phys., 2010. **43**(1): p. 015001.
[64] Bennett, W.R.J., *Hole Burning Effects in a He-Ne Optical Maser.* Phys. Rev., 1962. **126**(2): p. 580.
[65] Lamb, W.E.J., *Phys. Rev. A*, 1964. **134**: p. 1429.
[66] Lee, P.H. and M.L. Skolnick, Appl. Phys. Lett., 1967. **10**: p. 303.
[67] Hänsch, T.W., Phys. Rev. Lett., 1971. **27**: p. 707.
[68] Levenson, M.D. and A.L. Schawlow, PHYS. REV. A, 1972. **6**: p. 10.
[69] Borde, C., *C. R. Acad. Sci. B* 1970. **271**: p. 371.
[70] Jackson, D.A. and H. Kuhn, *Proc. Roy. Soc. A* 1938. **167**: p. 205.
[71] H, J.D.A.a.K., *Proc. Roy. Soc. A* 1938. **167**: p. 205.
[72] Ezekiel, S. and R. Weiss, Phys. Rev. Lett., 1968. **20**: p. 91
[73] Duong, H.T., *C. R. Acad. Sci. B*, 1973. **276**: p. 909
[74] Brinkmann, U., et al., *App. Phys.*, 1974. **5**: p. 109.
[75] Frisch, R., *Z Physik*, 1933. **86**: p. 42
[76] Ashkin, S., Phys. Rev. Lett., 1971. **25**: p. 1321.
[77] Jacquinot, P., Opt. Comm., 1973. **8**: p. 163.
[78] Rabi, I.I., et al., Phys. Rev., 1938. **53**: p. 318.
[79] Rabi, I.I., *Phys. Rev.*, 1952. **87**: p. 379
[80] Marrus, R. and D. McColn, *Phys. Rev. Lett.* , 1965. **15**: p. 813.
[81] *Radiant Dyes cw- Ring Dye Laser "Operation and Maintenance Manual"* Wermelskirchen , Germany: Radiant Dyes Laser Accessories.
[82] Schüler, H., *Z Phys.*, 1926. **35**: p. 323.
[83] Schüler, H., Z Phys., 1930 **59**: p. 149.
[84] Paschen, F., Ann. Phys., 1933. **18**: p. 867.
[85] Feldmann, D., Opt. Comm., 1979 **29**: p. 67.
[86] Miyazaki, K., H. Scheingraber, and C.R. Vidal, Phys. Rev., 1983. **A 28** p. 2229.
[87] Behrens, H.O. and G.H. Guthöhrlein, J. Phys., 1983 **C7-44**: p. 149.
[88] Behrens, H.O., G.H. Guthöhrlein, and A. Kasper, J. Phys., 1983 **C7-44**: p. 239
[89] Shamim, K., I. Siddiqui, and L. Windholz, Eur. J. Phy. D, 2011.
[90] Windholz, L. and G.H. Guthöhrlein, Phys. Scr., 2003. **T105**(1): p. 55.
[91] Peck, E.R. and K. Reeder, J. Opt. Soc. Am., 1972. **62** p. 958.
[92] Ritz, W., Astrophys J, 1908. **28**: p. 237
[93] Guthöhrlein, G.H., *Program package ˝Fitter˝, developed by*. 1998, Helmut-Schmidt-Universität, Universität der Bundeswehr, Holstenhofweg 85, D-22043 Hamburg, Germany (unpublished).
[94] Imran, S., *PhD Thesis 2010, Technische Universität Graz* 2010.
[95] Harrison, G.R., *Wavelength Tables*. 1969, Cambridge MA: MIT Press.

[96] Guthöhrlein, G.H. 1996, Helmut-Schmidt-Universität, Universität der Bundeswehr, Holstenhofweg 85, D-22043 Hamburg, Germany (unpublished)